Reconstruction and study of plant hormone signaling pathways in plant and mammalian systems

Inaugural-Dissertation

zur Erlangung des Doktorgrades
der Mathematisch-Naturwissenschaftlichen Fakultät
der Heinrich-Heine-Universität Düsseldorf

vorgelegt von

Jennifer Andres
aus Düsseldorf

Düsseldorf, Dezember 2019

aus dem Institut für Synthetische Biologie
der Heinrich-Heine-Universität Düsseldorf

Gedruckt mit der Genehmigung der
Mathematisch-Naturwissenschaftlichen Fakultät der
Heinrich-Heine-Universität Düsseldorf

Berichterstatter:

1. Prof. Dr. Matias D. Zurbriggen

2. Prof. Dr. Ilka Maria Axmann

Tag der mündlichen Prüfung: 17.02.2020

EIDESSTATTLICHE ERKLÄRUNG

Ich versichere an Eides Statt, dass die Dissertation von mir selbständig und ohne unzulässige fremde Hilfe unter Beachtung der „Grundsätze zur Sicherung guter wissenschaftlicher Praxis an der Heinrich-Heine-Universität Düsseldorf“ erstellt worden ist.

_____ _____

Datum Unterschrift

Table of contents

DANKSAGUNG

Zunächst möchte ich mich bei Prof. Dr. Matias D. Zurbriggen für die Möglichkeit bedanken, meine Doktorarbeit in seinem Institut anzufertigen. Seine positive Einstellung motivierte mich stets, mich in neue Themen einzuarbeiten, weiterführende Forschungen anzustellen und aktuelle Hypothesen kritisch zu hinterfragen. Sein hohes Maß an Fachwissen im Bereich der synthetischen Biologie und allen angrenzenden Fachbereichen, ermöglichte viele produktive und konstruktive Diskussionen und Zusammenarbeiten mit diversen Kooperationspartnern. Für auftretende Probleme und Fragestellungen hatte er immer ein offenes Ohr und konnte mit wertvollen Vorschlägen zu deren Lösung beitragen. Sein Vertrauen in meine Fähigkeiten trug schon früh dazu bei, dass ich meine Experimente schon von Beginn an selbstständig planen, durchführen, optimieren und analysieren sowie neue Systeme designen und etablieren konnte. Weiterhin schätze ich es sehr, viele verschiedene Methoden und Systeme im Laufe meiner Doktorarbeit kennengelernt zu haben.

Des Weiteren bedanke ich mich bei meiner Mentorin Prof. Dr. Ilka M. Axmann für ihre Unterstützung und Betreuung sowie wertvolle Ratschläge.

Ich möchte mich auch bei unseren Kooperationspartnern Prof. Dr. Salim Al-Babili, Prof. Dr. Jorge Casal und Dr. Miguel Blázquez für die gute Zusammenarbeit, ertragreiche Diskussionen und einen regen Datenaustausch bedanken.

Ich bedanke mich bei Patrick Fischbach für eine sehr gute und vor allen Dingen freundschaftliche Zusammenarbeit während unserer Zeit im Labor (ganze 8 Jahre sind wir inzwischen schon befreundet!). Besonders in der Schreibphase (in der natürlich parallel auch sehr viele Experimente durchgeführt wurden) haben wir uns gegenseitig motiviert und hatten weiterhin Spaß an der Arbeit. Wir konnten uns immer auf die Unterstützung des Anderen verlassen, dafür vielen Dank! Meine Arbeit hätte bis zur Fertigstellung wesentlich länger gebraucht, hätten wir uns nicht gegenseitig vorangetrieben.

Ich bin sehr froh, dass Leonie-Alexa Koch und ich während unserer Zeit in der Synthetischen Biologie sehr gute Freunde geworden sind. Ich danke ihr für ihre Hilfe, Geduld, Unterstützung und das Korrekturlesen sämtlicher Texte. Die pflanzliche Zellkultur werden wir auch noch hochziehen - irgendwann.

Tim Blomeier und ich haben die Halloween-Nacht 2018 zum Tag gemacht. 26 h Review schreiben haben am Ende echt geschlaucht, aber ich bin froh, dass wir es zusammen geschafft haben. Danke für die Ruhe und Geduld während dieser Zeit und auch die sehr gute Zusammenarbeit von Beginn an – wir sind das ursprüngliche Team Reconstruction. Auch in Finnland hatten wir eine super Zeit; mit nur wenigen Kollegen (bzw. inzwischen Freunden) wäre das so möglich gewesen.

Ich danke allen meinen Studenten, besonders Lea Dahmen, Aljoscha von Papen, Julia Kapr und Gianni D´Apollonio, für ihr Engagement und ihre Unterstützung bei meinen Projekten. Auch wenn es ihre Daten leider nicht in meine Thesis geschafft haben, schätze ich jeden Einzelnen sehr und wünsche allen viel Glück für die Zukunft.

Ohne die Unterstützung von Reinhild Wurm und Michaela Gerads, wäre es mir nicht möglich gewesen, so viele Experimente innerhalb von 3 Jahren durchzuführen. Ich bin Beiden für ihre Hilfe und wertvollen Ratschläge unendlich dankbar und wünsche ihnen für ihre private und berufliche Zukunft nur das Beste. Weiterhin danke ich dem restlichen Labor für eine gute Zusammenarbeit.

Mein ganz besonderer Dank gilt meinen Eltern, meiner Schwester und meinem Freund. Wie auch in allen anderen Lebensbereichen standen sie mir während meiner Doktorarbeit (und auch während des gesamten Studiums) die ganze Zeit beratend und motivierend zur Seite. Sie hatten immer ein offenes Ohr für meine Probleme und waren stets geduldig.

Ein großer Dank geht auch an Sabine Erzmoneit, Vanessa Briem und Steffen Schindler für ihre Unterstützung und aufmunternden Worte.

Zum Schluss danke ich allen, die mich unterstützt haben, deren Namen ich hier leider vergessen haben.

FIGURES

ABBREVIATIONS

ABA	abscisic acid
AFB	auxin signaling F-box
AM	arbuscular mycorrhizal
ARF	AUXIN RESPONSE FACTOR
ARR	ARABIDOPSIS RESPONSE FACTOR
ASK1	ARABIDOPSIS SKP1-LIKE1
Aux1	AUXIN TRANSPORTER PROTEIN
Aux/IAA	auxin resistant/indole-3-acetic acid inducible
BR	brassinosteroids
CK	cytokinin
Co-R	co-receptor
D14	DWARF 14
D53	DWARF 53
DLK2	D14-LIKE 2
EAR	ETHYLENE-RESPONSE FACTOR-associated amphiphilic repression
ET	ethylene
FF	firefly luciferase
FRET	Förster resonance energy transfer
FUL	FRUITFULL
GA	gibberellins
GAI	GA-INSENSITIVE
GGPP	geranylgeranyldiphosphate
GID1	GIBBERELLIN INSENSITIVE DWARF1
GR24	synthetic strigolactone analog
GRAS	GAI, RGA, SCARECROW
HEK	human embryonic kidney
IAA	indole-3-acetic acid, auxin
JA	jasmonate
JAZ	jasmonate-ZIM-domain
KAI2	KARRIKIN INSENSITIVE 2
KAR	karrikin
MAX2	MORE AXILLARY GROWTH 2
NLS	nuclear localization signal
NO	nitric oxide
PB1	PHOX/BEM1p
phy	phytochrome
PIF	PHYTOCHROME INTERACTING FACTOR
PIN	PIN-FORMED
REN	renilla luciferase
RGA	REPRESSOR OF GA1-3
RHT	Reduced height
RGL1	RGA-LIKE1
RGL2	RGA-LIKE2
RGL3	RGA-LIKE3
SA	salicylic acid
SCF	Skp-1-Cullin-F-box
SEAP	secreted human placental alkaline phosphatase
SL	strigolactone
SM	sensor module
SMAX	SUPPRESSOR OF MAX2
SMXL	SMAX1-LIKE
SNE	SNEEZY
SPL	SQUAMOSA PROMOTER BINDING PROTEIN LIKE

TIR1	TRANSPORT INHIBITOR RESPONSE 1
TF	transcription factor
WT	wild type

SUMMARY

Synthetic biology, as an established but ever-growing discipline, bridges engineering with life sciences. Basic engineering principles are implemented for the logical design of novel tools and the modular and combinatorial assembly of biological parts into higher order complex signaling and metabolic structures. In the last years, numerous synthetic biology switches and even synthetic networks have been designed and implemented in bacteria, yeast and mammalian cells. As plant signaling networks are highly complex in terms of genetic redundancy, interconnectivity and shared components, the implementation of synthetic biology tools *in planta* lags behind. In this work, quantitative tools and platforms have been generated and implemented to study plant hormone signaling processes in plant cells and mammalian cells as an orthogonal system.

Genetically-encoded ratiometric, degradation-based biosensors for the plant hormones strigolactones, auxins and gibberellins were constructed and implemented to analyze hormone signaling at various levels. Substrate specificity and sensitivity screens were performed to characterize the degradation behavior of distinct regulators involved in phytohormone perception. Furthermore, experimental approaches in *Arabidopsis thaliana* signaling mutant protoplasts revealed the necessity and functionality of certain signaling components. The high sensitivity of the biosensor platform allowed for the answering of metabolic questions in a quantitative manner. In a combined approach of quantitative experimental data and mathematical modelling, new insights on mechanistic aspects were obtained.

Due to the high interconnectivity and redundancy of signaling components, the analysis of single components and their interplay with other related or unrelated components is particularly difficult to study in vivo *in planta*. In the course of this work, mammalian cells, which display reduced complexity and crosstalk with plant-specific components, were utilized as an orthogonal platform to reconstruct gibberellin perception and signaling. Towards this aim, a synthetic biology toolbox comprising Mammalian-Hybrid systems, ranging from M1H to M4H systems, was developed and successfully implemented. The binding of transcription factors to certain promoter regions as well as protein-protein interactions related to gibberellin signaling could be demonstrated and analyzed in M1H and M2H systems. In addition, the order of perception complex formation in response to gibberellin was revealed utilizing M3H and M4H systems.

This work illustrates the necessity of synthetic biology tools and approaches to quantitatively investigate plant signaling in plant and orthogonal systems. The combinations of these strategies together with traditional tools *in planta*, comprise a powerful platform with their application spectrum being far from exhausted.

1 Introduction

1.1 Plant Signaling

Plants, as sessile organisms, need to react and adapt their behavior towards different internal and external stimuli. Changing light conditions as well as temperature influence the plant´s life cycle. In order to meet these challenging demands, plants developed extremely complex and intertwined signaling pathways with extensive crosstalk, but also a high degree of redundancy increasing their robustness (Koornneef and Pieterse, 2008; Depuydt and Hardtke, 2011; Vanstraelen and Benková, 2012). However, this redundancy makes it also difficult to investigate plant signaling components separately. As many pathways share key signaling components or even mechanisms, there is a great need for molecular tools to quantitatively analyze them. The generation of mutant plants and their analysis, molecular cloning and genetic engineering, as well as ever-growing databases have led to major breakthroughs in the past decades (Sheen, 2010). Today, plant signaling research aims at applying molecular biology tools to quantitatively analyze specific, individual signaling components as well as crosstalk between pathways. Synthetic biology approaches comprising distinct techniques might help to overcome remaining challenges in plant signaling research. Obtained quantitative data can be integrated in computational tools and mathematical modeling to decipher plant signaling step by step and develop predictive models that could also be useful for agricultural sciences.

1.1.1 Phytohormones

In the 19th century, Julius von Sachs and Charles Darwin both described “substances” that moved throughout the plant to regulate numerous growth processes (von Sachs, 1880; Darwin and Darwin, 1880). These “substances”, later called phytohormones, are structurally unrelated, molecular compounds that comprehensively regulate processes of the plant lifecycle such as seed germination, vegetative growth, flowering, development and responses to biotic and abiotic stress factors (Bernier and Périlleux, 2005; Gazzarrini and Tsai, 2015; Verma et al., 2016). Phytohormones are typically present at very low concentrations and their biosynthesis, metabolism and distribution are strongly regulated in plants. They act either locally or in distant tissues mediated by passive or active transport, e.g. through specific transporters (Santner et al., 2009). To date, several phytohormones have been identified including auxins (IAAs), abscisic acid (ABA), brassinosteroids (BRs), cytokinins (CKs), ethylene (ET), gibberellins (GAs), jasmonate (JA), nitric oxide (NO), salicylic acid and strigolactones (SLs) (Santner and Estelle, 2009). Additionally, plants make use of peptide hormones to regulate growth responses (Jun et al., 2008).

During the last years, many proteins involved in hormone signaling, for instance hormone receptors and regulator proteins, have been identified through genetic screens in plants and have led to major breakthroughs in phytohormone research (Santner and Estelle, 2009). These new insights have led to the conclusion that the phytohormones auxin, jasmonate, gibberellin and strigolactone are perceived through similar mechanisms. Target gene expression is regulated through de-repression. The phytohormone binds to either a F-box/receptor or to an additional specific co-receptor and thus initiates complex formation with specific hormone response regulator proteins. Auxins and jasmonates are perceived over a “two component”-mechanism (F-Box and regulator proteins) while gibberellins and strigolactones are perceived over a “three component”-mechanism (F-Box, co-receptor and regulator protein). The subsequent polyubiquitination of the regulator proteins is mediated by the conserved Skp (Arabidopsis SKP1-related (ASK1))-1-Cullin-F-box (SCF) E3 ubiquitin ligase complex. Finally, the polyubiquitinated regulator proteins become degraded by the 26S proteasome (**Figure 1,** Vierstra, 2009). As a result of this degradation process, hormone regulator proteins no longer physically interact with transcription factors (TFs) and other regulators. This leads to an activation of the hormone response, mostly by de-repression of target gene expression. Finally, even small changes in hormone concentrations can result in major alterations in transcription. Details about the investigated hormone signaling pathways during this work are discussed in the following sections.

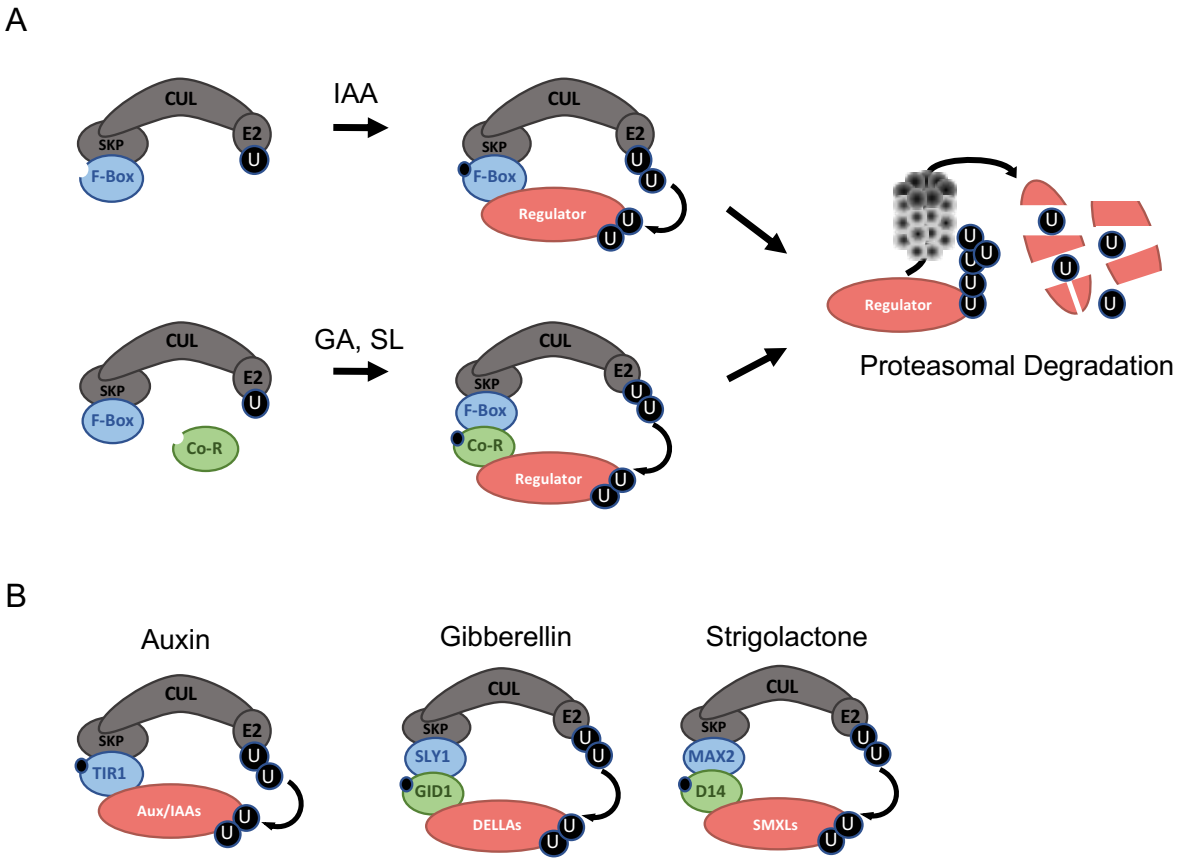

Figure 1: Phytohormone perception mechanism. (A) General phytohormone perception complex formation through either a two or three-component perception complex. Both mechanisms are formed with a SCF perception complex comprising SKP/ASK (rice/*Arabidopsis*), Cullin (CUL), and an E3 ubiquitin ligase (containing an E2 ubiquitin-conjugating enzyme loaded with ubiquitin residues (U)). In the two-component perception complex, the F-Box is at the same time the phytohormone receptor, for instance for auxin, whereas in the three-component mechanism an additional Co-Receptor (Co-R) for phytohormone perception is needed that binds the hormone and associates to the complex via the F-Box protein. As a consequence of hormone binding, specific response regulators (Regulator) can associate to this $SCF^{F\text{-}Box}$ complex and become polyubiquitinated and thereby targeted for degradation by the 26S proteasome. (B) Specific phytohormone perception complexes for auxin, gibberellin and strigolactone. The phytohormone auxin is perceived through a two-component complex with TIR1 as a F-Box and hormone receptor and Aux/IAAs as regulator proteins. Gibberellin and strigolactone both denote the necessity of a co-receptor for hormone perception, GID1 and D14 respectively, in addition to the F-Box, SLY1 and MAX2. Regulators for gibberellin signaling are called DELLA proteins and for strigolactone SMXLs (figure elements are adapted from the manuscript of Andres et al. and modified from Samodelov et al., 2016.).

1.1.1.1 Strigolactones

Strigolactones (SLs) are carotenoid-derived lactones that affect diverse growth-related and developmental processes in plants by acting as endogenous phytohormones as well as exogenous signals in the rhizosphere (Al-Babili and Bouwmeester, 2015; Soundappan et al., 2015). They fulfil a plethora of tasks within plants regarding adaptations to nutrient availability, drought and stress tolerance, shoot branching and gravitropism, leaf shape and senescence as well as root architecture (Ha et al., 2014; Sang et al., 2014; Yamada et al., 2014; Al-Babili and Bouwmeester, 2015; Ueda and Kusaba, 2015). In addition, they support the plant by promoting symbiosis with arbuscular mycorrhizal fungi and thereby provide the plant with minerals (Akiyama et al., 2005; Besserer et al., 2008). However, SLs also display a huge drawback in plants by conveying the recognition of host roots by parasitic weeds of the genera *Striga* or *Orobanche* (Samodelov et al., 2016; Waters et al., 2017). This leads to enormous crop yield losses in Africa, Asia as well as in Europe and thus increases the research interest in this important endogenous phytohormone and exogenous signaling molecule (Parker, 2009).

In the last years, the first proteins in *A. thaliana* were identified and described as essential to SL perception and signaling. These signaling components comprise MORE AXILLARY GROWTH2 (MAX2) engaged in a SKP1-Cullin-F-box E3 ubiquitin ligase protein complex and belonging to the leucine-rich repeat F-box protein family, DWARF14 (AtD14 in *A. thaliana*) being a member of the α/β hydrolase superfamily and the regulators of SL response SMAX1-LIKE 6,7 and 8 (SMXL6,7 and 8) (Stirnberg et al., 2007; Umehara et al., 2008; Arite et al., 2009; Jiang et al., 2013; Soundappan et al., 2015).

After SLs are recognized by the co-receptor D14, they are hydrolyzed and form a covalently linked bridge with the catalytic sites of D14 (Hu et al., 2017). This leads to a conformational change of D14 enabling a complex formation between D14, SCF^{MAX2} and SMXL6/7 or 8. As a consequence, the D53-like SMXLs are polyubiquitinated by the E3 ubiquitin ligase SKP1-Cullin-F-box (SCF^{MAX2}) and thereby targeted for degradation through the 26S proteasome (Zhou et al., 2013; Wang et al., 2015). Furthermore, there are evidences that the co-receptor D14 also undergoes SL dependent degradation, however, with slower dynamics (Chevalier et al., 2014; Hu et al., 2017). This receptor degradation mechanism, functioning as a negative feedback loop in response to hormone treatment, could also be observed as a fine-tuning mechanism for other phytohormones such as abscisic acid (ABA), jasmonic acid (JA) and ethylene (Kevany et al., 2007; Wu et al., 2011; Kong et al., 2015).

The genome of *A. thaliana* encodes three paralogs/family members of the D14 α/β hydrolase protein family: the already mentioned DWARF14 (D14), KARRIKIN INSENSITIVE2 (KAI2) and DWARF 14-LIKE2 (DLK2) (Waters et al., 2012). While the function of DLK2 still remains unknown, D14 and KAI2 are associated with SL and karrikin signaling (Guo et al., 2013; Hu et

al., 2017; Végh et al., 2017). Karrikins are smoke-derived compounds in plant smoke that stimulate seed germination and are homologous to SLs (Bythell-Douglas et al., 2017). In addition, there are eight D53-like SMXLs in *A. thaliana*, of which only three (SMXL6,7 and 8) are associated with SL signaling (Soundappan et al., 2015). SMXL3, 4 and 5 are central regulators of phloem formation (Wallner et al., 2017), whereas SMAX1 and SMXL2 are involved in karrikin signaling (Waters et al., 2014). The proposed perception mechanism of karrikins involves also MAX2 as a F-box as well as the receptor KAI2 and the regulators SMAX1 and SMXL2 (Meng et al., 2016). Similar to SL perception, karrikins bind to the co-receptor KAI2 and induce a conformational change. This might yield to a complex formation between KAI2, SCF^{MAX2} and SMAX1 (Soundappan et al., 2015; Stanga et al., 2016). As a consequence, SMAX1 becomes polyubiquitinated and degraded by the 26S proteasome (**Figure 2**). In response to karrikin and GR24 induction, KAI2 becomes degraded. Nevertheless, compared to D14, this degradation does not depend on MAX2 and the 26S proteasome (Waters et al., 2015).

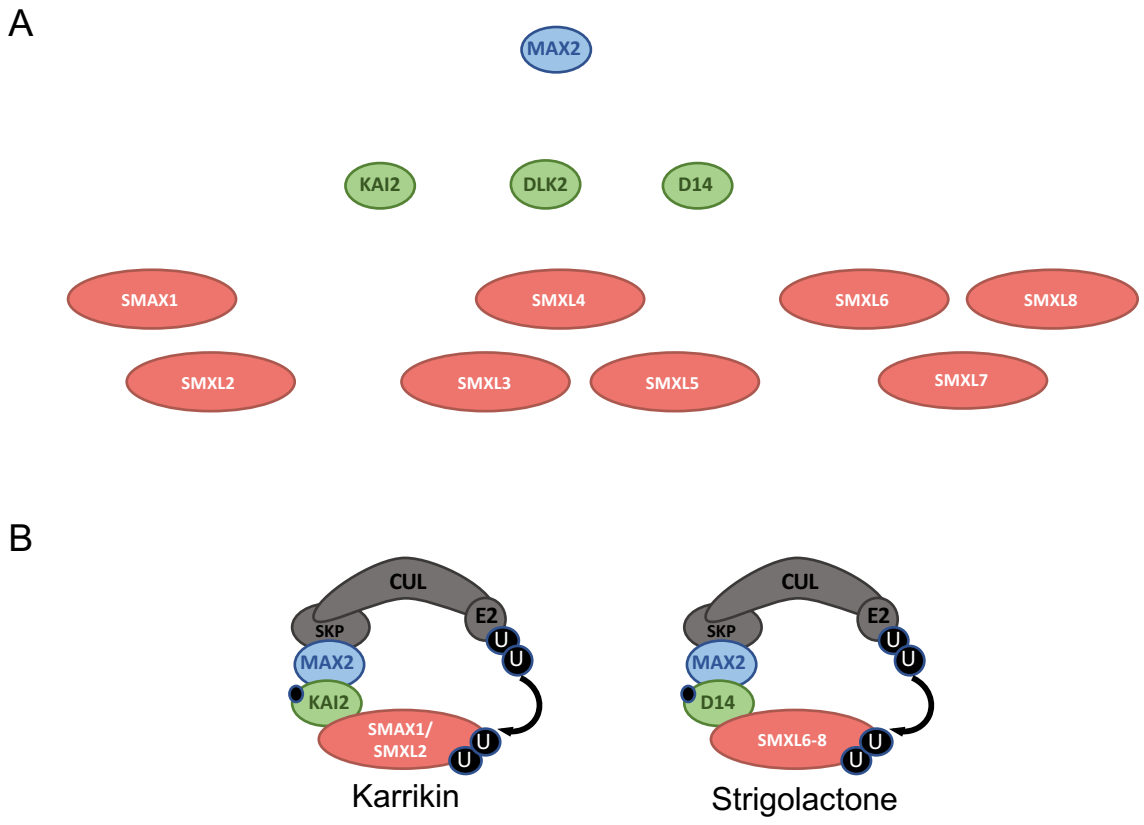

Figure 2: Strigolactone and karrikin signaling components and perception. (A) Putative strigolactone and karrikin signaling components. *A. thaliana* encodes one F-Box protein associated with strigolactone/karrikin signaling, MAX2, three homologous receptors, D14, KAI2 and DLK2, as well as 8 SMXL proteins. The function of DLK2 is yet unknown, while SMXL3-5 have recently been associated with strigolactone-independent phloem formation. (B) Current karrikin and strigolactone perception hypotheses. Both perception complexes utilize MAX2 as a F-Box, whereas D14 and KAI2 function as strigolactone and karrikin-specific receptors. Upon karrikin binding to the receptor, the perception complex is formed and SMAX1 or SMXL2 becomes polyubiquitinated by the SCF^{MAX2} E3 ubiquitin ligase complex and subsequently degraded. Upon strigolactone binding, SMXL6-8 become polyubiquitinated and thus degraded by the 26S proteasome.

Although strigolactone research still represents a relatively young field, a lot of progress has been made in the last years to uncover hormone perception and signaling mechanism. However, there still remains a multitude of open questions especially concerning the roles of SMAX1 and SMXL2 in strigolactone and karrikin signaling. In this work, all SMXLs were constructed and implemented as biosensors for their characterization. In addition, SMAX1 and SMXL2 sensors were used in *A. thaliana* wildtype (wt) and mutant backgrounds to quantitatively analyze their function within a perception complex. Furthermore, dynamic analyses were conducted and then integrated into mathematical models.

1.1.1.2 Auxins

Auxins are by far the most studied phytohormones with more than a century of research since their discovery as growth regulators in 1880 by Charles Darwin and his son (Darwin and Darwin, 1880). However, almost fifty years later, in 1926, these growth regulators were extensively studied and isolated (Went, 1926). The growth regulators, later called auxins, are essential in plants regulating a multitude of developmental and growth processes including cell division, differentiation, and elongation, gravitropism and phototropism as well as root and shoot development (Overvoorde et al., 2010; Fankhauser and Christie, 2015; Velasquez et al., 2016; Di Mambro et al., 2017; Su et al., 2017). As auxins are involved in that many developmental processes at different stages in the plant´s life cycle, the regulatory auxin effect depends on its cellular concentration and spatial distribution (cellular and tissue polarity, gradients).

The biosynthesis of auxins, including indole-3-acetic acid as the most abundant form and main auxin in higher plants, is highly complex with multiple pathways, primarily starting with tryptophan as a common precursor (Zhao, 2010). However, there are also tryptophan-independent pathways for auxin biosynthesis (Korasick et al., 2013).

Auxin transporters, like efflux transporters of the PIN-FORMED (PIN) family and influx transporters such as AUX1 (AUXIN TRANSPORTER PROTEIN 1), have been identified to distribute auxin and establish gradients throughout the plant (Swarup et al., 2001; Swarup et al., 2004; Blilou et al., 2005; Grunewald and Friml, 2010).

Intracellular auxin perception and transcriptional regulation requires three main components: i) TIR1/AFB F-box proteins (TRANSPORT INHIBITOR RESISTANT1/AUXIN SIGNALING F-BOX) engaged in a SCF protein complex ii) Aux/IAA (AUXIN/INDOLE ACETIC ACID) transcriptional repressors and iii) ARF (AUXIN RESPONSE FACTOR) transcription factors (Salehin et al., 2015). Normally, at low auxin concentration, Aux/IAAs and ARFs form multimers which results in the repression of ARF activity. When auxin is present, it is bound by TIR1/AFB and enhances the formation of a co-receptor complex between TIR1/AFB and an Aux/IAA (Calderón Villalobos et al., 2012). Consequently, the Aux/IAA becomes polyubiquitinated by the $SCF^{TIR1/AFB}$ complex and subsequently degraded by the 26S proteasome. This leads to a de-repression of the ARFs and the activation of target gene expression (Salehin et al., 2015).

The genome of *A. thaliana* encodes 6 TIR1/AFB proteins involved in auxin signaling with distinct biochemical properties (Parry et al., 2009). TIR1 and its five homologs AFB1-5 display different affinities towards Aux/IAAs which also depend on the stability of the Aux/IAA itself. Aux/IAA 7, which has a low stability in response to auxin, interacts strongly with TIR1, whereas Aux/IAA31 interacts poorly with TIR1 and is relatively stable in response to auxin treatment (Calderón Villalobos et al., 2012).

In addition to 6 TIR1/AFBs, 29 Aux/IAAs arose from gene duplication events in *A. thaliana* (**Figure 3C**, Wu et al., 2017). These Aux/IAAs contain typically 4 different domains (**Figure 3A**). Domain I mediates the binding to TOPLESS corepressors as well as other downstream interacting partners through an ethylene-responsive element binding factor-associated amphiphilic repression (EAR) motif, LxLxL (Szemenyei et al., 2008). Domain II is the TIR1-binding domain containing a highly conserved degron motif of 13 amino acids (QVVGWPPVRSYRK). This core sequence is responsible for the degradation of Aux/IAAs in response to auxin. However, the 13 amino acids of this consensus sequence exhibit variations among the Aux/IAA family members leading to differential affinities for the receptors as described below (Ramos et al., 2001; Calderón Villalobos et al., 2012). Additionally, regions outside this binding domain can also contribute to the binding and the degradation process of Aux/IAAs (Shimizu-Mitao and Kakimoto, 2014; Winkler et al., 2017). Depending on the composition of this DII core domain, Aux/IAAs can be divided into canonical and non-canonical Aux/IAAs. Canonical Aux/IAAs contain all 4 domains, i.e. an (almost) complete DII 13 aa core sequence, whereas non-canonical Aux/IAAs deviate slightly from this DII core consensus sequence or show no similarities at all. 23 Aux/IAAs possess a complete, conserved DII domain. Aux/IAA20, 30, 32, 33 and 34 are non-canonical Aux/IAAs with strong deviations from this DII core sequence, while Aux/IAA 31 contains only a small part of the DII consensus sequence (Shimizu-Mitao and Kakimoto, 2014). The presence or absence of this conserved DII consensus domain as well as its composition are responsible for the binding affinity towards TIR1/AFBs and the degradation rate of the Aux/IAAs themselves (Calderón Villalobos et al., 2012; Havens et al., 2012).

Finally, domain III and IV together form a PB1 (PHOX and BEM1) domain, conferring interaction with Aux/IAAs and ARFs (Guilfoyle, 2015).

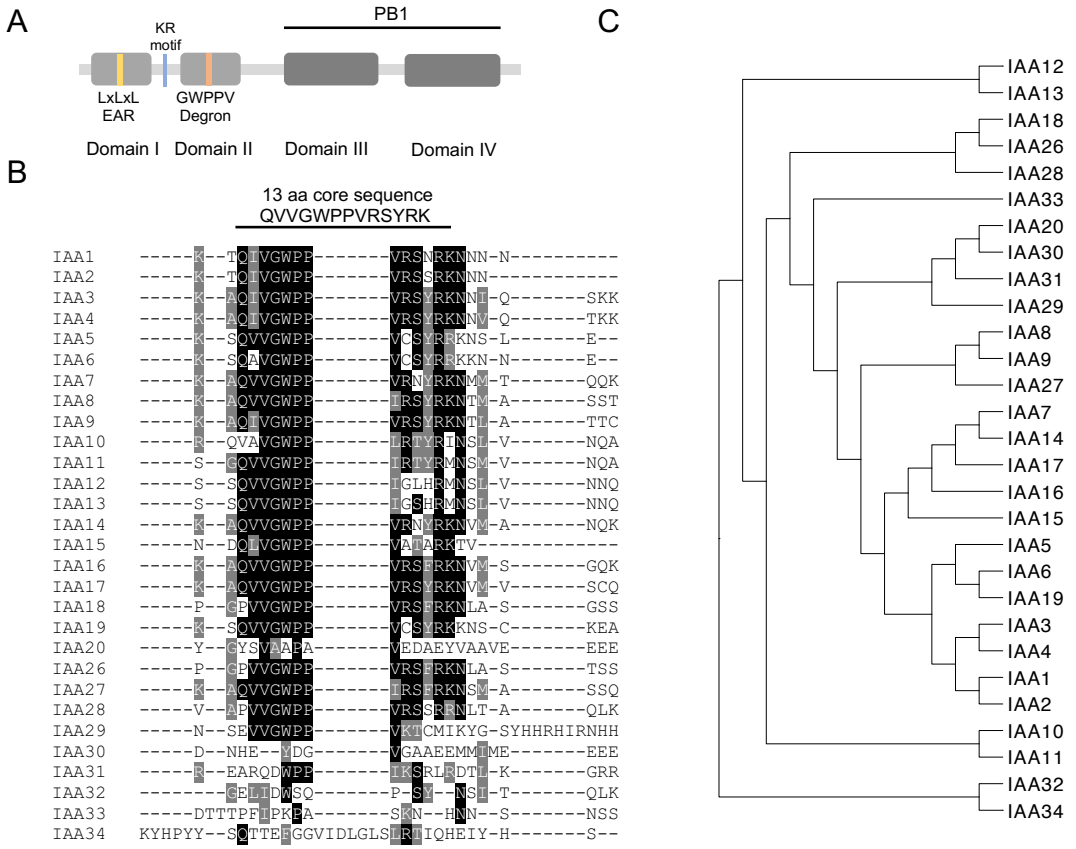

Figure 3: Aux/IAA structure and phylogenetic relationships. (A) Canonical Aux/IAA structure. Aux/IAAs comprise 4 domains. Domain I contains an EAR motif which mediates interactions with TOPLESS and other regulators. The GWPPV core degron in domain II is the TIR1 binding domain and responsible for Aux/IAA degradation in response to auxin. Domain III and IV form the PB1 domain mediating interactions with Aux/IAAs and ARFs. (B) Domain II core degron comparison of all Aux/IAAs. All Aux/IAAs except from Aux/IAA 20,30, 32-34 contain a (mostly) complete core sequence. Aux/IAA31 possesses a partial core degron. The multiple alignments were performed with TCoffee (Notredame et al., 2000) and then visualized with BoxShade. (C) *A. thaliana* Aux/IAA protein family phylogeny tree. The tree was created with the program iq-tree (Nguyen et al., 2015).

At the end point of this auxin perception and signaling process, Aux/IAAs are degraded and thus release distinct ARFs which can bind to auxin response DNA elements (AuxRE) in promoter regions, thereby either activate or repress target gene expression. ARFs are typically consisting of two regions: i) an N-terminal B3-type DNA binding domain, which functions as either activation domain or repression domain, and ii) a C-terminal dimerization domain involved in protein-protein interactions with Aux/IAAs and ARFs. As *A. thaliana* encodes 23 ARFs, there is a multiplicity of putative targets and thus signaling responses adding up to a high combinatorial complexity (Li et al., 2016).

To gain a deeper understanding of the great number of Aux/IAAs and their distinct functions in *A. thaliana*, we constructed and utilized biosensors and analyzed their behavior towards IAA. As this is particularly complicated to analyze *in planta*, we used *A. thaliana* wildtype protoplasts as a minimal system.

1.1.1.3 Gibberellins

Gibberellins are diterpene phytohormones that control diverse aspects of developmental and growth processes in plants such as seed germination, vegetative growth and flowering (Yamaguchi, 2008; Davière and Achard, 2013). In addition, they are also found in fungi and bacteria, being first isolated in 1938 from the fungal rice pathogen *Gibberella fujikuroi* (Yabuta and Sumiku, 1938).

By the 1960s, the world population had been steadily grown leading to an increased food demand, e.g. for wheat and rice in the developing countries. The breeding of dwarfing traits into these plants resulted in higher yields and more stable plants contributing to the so-called green revolution. These dwarfing traits were achieved by mutations in the REDUCED HEIGHT (*Rht*) gene which caused a reduced response to gibberellin and is an ortholog to one of the regulators of gibberellin response in *A. thaliana* (Hedden, 2003).

The biosynthesis and rapid deactivation of GAs in response to environmental cues as well as part of the development process are crucial to plants. Starting with trans-geranylgeranyl diphosphate (GGPP), many enzymes, intermediate steps, distinct cellular compartments and GAs as intermediate products are required to biosynthesize bioactive GAs. More than 130 gibberellin family members have been identified so far, but only a few are biologically active (Yamaguchi, 2008). In *A. thaliana*, the main bioactive GAs comprise GA_1, GA_3, GA_4 and GA_7 (Davière and Achard, 2013). The common precursor of all bioactive GAs in plants which is specific for the GA biosynthesis pathway is GA_{12}. This in turn is further metabolized by several GA oxidases until its final conversion, namely a 3-β-hydroxylation, mediated by GA3-oxidases, of GA_9 and GA_{20} into the bioactive form GA_4 and GA_1, respectively (Hedden and Thomas, 2012). To biosynthesize GA_3 or GA_7, a further conversion step with another intermediate is needed. For the biosynthesis of GA_3, GA_{20} is first converted to GA_5 and then 3-β-hydrolyzed into the bioactive GA_3. For the production of GA_7, GA_9 is first metabolized into 2,3-Didehydro GA_9 and then converted by a GA3-oxidase into bioactive GA_7 (**Figure 4**, Farrow and Facchini, 2014).

To be able to respond to environmental changes, plants need to rapidly adapt their GA content. The main inactivation pathway is the 2-β-hydroxylation mediated by GA2-oxidases which can act either on C20-GAs, containing only intermediates with 20 carbons such as GA_{12}, or C19-GAs with 19 carbons like the bioactive GA_1 and GA_4 and convert them to GA_8 and GA_{34}, respectively (Sun, 2011).

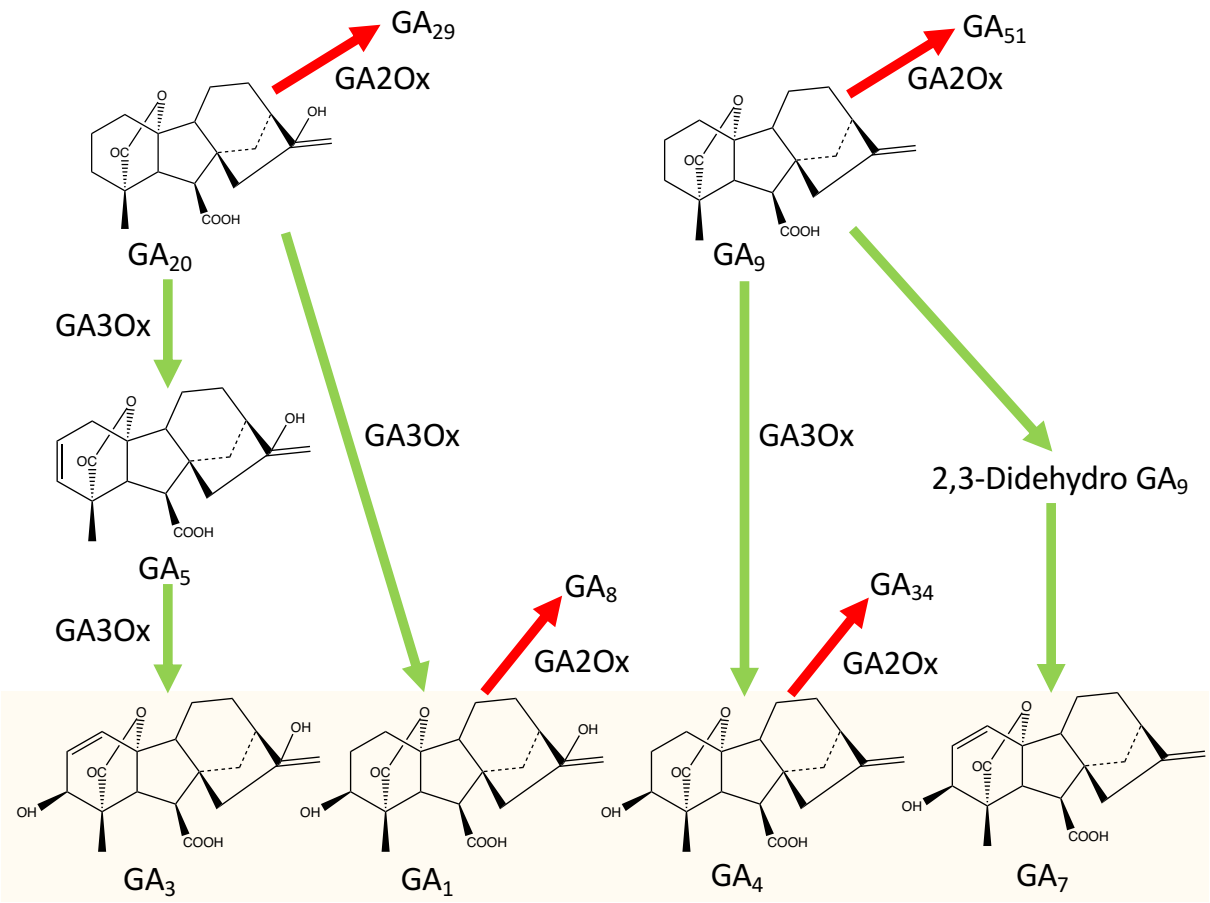

Figure 4: Biosynthesis and inactivation of bioactive GAs in *A. thaliana*. The bioactive GA_1 and GA_3 are metabolized from their common precursor GA_{20}. Additionally, the bioactive GAs GA_4 and GA_7 are biosynthesized from their common precursor GA_9. GA3oxidases catalyze these reactions, namely 3-β-hydroxylations (indicated with green arrows). GA_1 and GA_4 as well as their precursors are biologically inactivated by GA2oxidases (indicated with red arrows).

Similar to strigolactones, gibberellins are also perceived through a 3-component receptor complex. The genome of *A. thaliana* encodes the F-Box protein SLEEPY1 (SLY1) which is engaged in the E3 ubiquitin ligase SKP1-Cullin-F-box protein complex, three GA receptors (GIBBERELLIN INSENSITIVE DWARF1 (GID1) -a, -b and -c, and 5 regulators of gibberellin response proteins (DELLA proteins: GA-INSENSITIVE, GAI; REPRESSOR-of-ga1-3,RGA; RGA-LIKE1, RGL1; RGL2 and RGL3) (Dill et al., 2004; Griffiths et al., 2006; Murase et al., 2008). Upon binding of (bioactive) GAs, DELLA proteins associate with the GID1s and SCF^{SLY1} and are subsequently polyubiquitinated and thereby targeted for degradation by the 26S proteasome (**Figure 5B**, Davière and Achard, 2013). This leads to a GA-mediated change of regulation in target gene expression. The identification of the GID1 as a soluble nuclear GA receptor in GA-insensitive dwarf rice mutants marked a breakthrough in gibberellin research (Ueguchi-Tanaka et al., 2005; Sun, 2011).

In *A. thaliana*, GID1 and DELLA have undergone gene-duplication events leading to an additional degree of complexity in terms of possible interactions. The existence of three GID1s

and five DELLAs results in fifteen GID1/DELLA protein combinations (Nakajima et al., 2006). To make GA signaling in *A. thaliana* even a bit more complex, there is a second F-box protein, SNEEZY (SNE), which is a homologue of SLY1. Nonetheless, SLY1 is considered as the major F-box mediating gibberellin signaling. Experimental results in mutant plants revealed that SNE could only partially rescue GA-related phenotypes, whereas SLY1 is able to fully rescue them. SNE seems to only have partly functional overlaps regulating only a subset of DELLAs (Ariizumi et al., 2011).

This high degree of redundancy generates robust GA signaling with partially overlapping functions as shown in multiple knock-out mutant plants. However, it also enables different expression patterns and affinities of GID1s towards DELLAs and GA that lead to adaptations to specific growth or developmental processes (Suzuki et al., 2009).

Crystal structure data in *A. thaliana* revealed details about the GA-induced DELLA/GID1 binding mechanism (Murase et al., 2008; Shimada et al., 2008). The binding of GA to its specific pocket in the receptor GID1 induces a conformational change of the flexible N-terminal GID1 extension, thereby covering the pocket with the bound GA. As a result of this conformational change, DELLAs are able to associate to the GA-GID1 complex (Murase et al., 2008). DELLAs belong to the plant-specific family of GRAS transcriptional regulators (named after the first identified members GAI, RGA and SCARECROW) containing a conserved C-terminal GRAS-domain which is responsible for transcriptional regulation. The N-terminal part is DELLA-specific and comprises two important, conserved domains: the DELLA and the TVHYNP domain. These domains are involved in GA signaling by mediating the interaction with the N-terminal GID1 lid of the GA-GID1 complex (**Figure 5A**, Peng et al., 1997; Silverstone et al., 1998; Davière and Achard, 2013). First Yeast-3-Hybrid evidence demonstrated that the GID1-GA complex promotes the interaction of DELLAs with the SCF^{SLY1} complex (Griffiths et al., 2006). As a consequence of GA perception, DELLAs become degraded and thus no longer physically interact with diverse transcriptions factors (TFs).

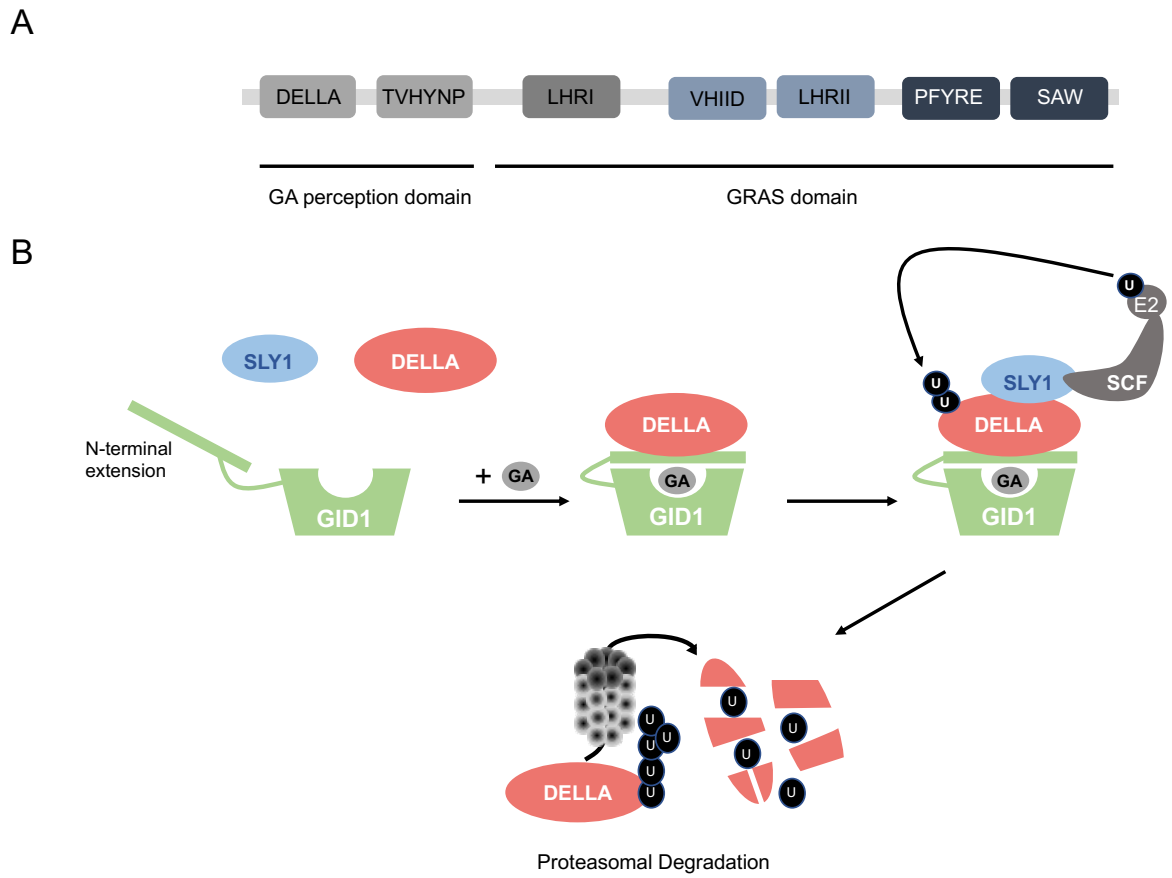

Figure 5: Gibberellin perception mechanism. (A) General scheme of DELLA protein domains showing the functional bisection. The GA perception domain comprises two important motifs: the DELLA and the TVHYNP motif mediating the physical interaction with the N-terminal GID1 extension of the GA-GID1 complex. The conserved C-terminal GRAS domain contains several motifs responsible for the transcriptional regulation. (B) GA perception mechanism. The binding of GA to the GID1-GA-binding pocket induces a conformational change in the GID1 N-terminal extension which then covers the pocket with the bound GA. DELLAs associate to this N-terminal extension via the DELLA and the TVHYNP domains. Next, the SCF^{SLY1} protein complex recruits the GA-GID1-DELLA complex. Consequently, the DELLA becomes polyubiquitinated by the SCF^{SLY1} complex and subsequently degraded by the 26S proteasome (modified from Davière and Achard, 2013).

DELLAs are central hubs in transcriptional regulation of GA-mediated signaling. However, they are also involved in other phytohormone signaling pathways such as jasmonic acid (JA), cytokinin and auxin as well as light signaling (Hou et al., 2010; Oh et al., 2014; Dolgikh et al., 2019). The interactions with these diverse classes of TFs and regulatory proteins, block their DNA-binding capacity or simply inhibit their activity (Davière and Achard, 2013). One of the numerous DELLA downstream targets is the plant-specific SQUAMOSA PROMOTER BINDING PROTEIN LIKE (SPL) family which is involved in floral initiation in *A. thaliana*. Distinct members of the SPL family such as SPL3, SPL9 and SPL15 regulate gene expression of those genes involved in floral initiation and development by binding to the corresponding promoter regions. In the presence of GA, the SPL is released from the DELLA and binds to its DNA target regions, for instance to the FRUITFULL promoter (P_{FUL}) (Hyun et al., 2016). In addition, DELLAs also participate in light signaling by blocking the transcriptional activity of PHYTOCHROME INTERACTING FACTORS (PIFs) through their bHLH DNA recognition

domain (Alabadí et al., 2007; de Lucas et al., 2008). In the presence of GA, the DELLAs become degraded so that PIF-mediated target gene expression in hypocotyl elongation can proceed. Furthermore, DELLAs are also intertwined in various hormone signaling pathways additional to GA signaling. They contribute to plant defense by interacting with JASMONATE ZIM-DOMAIN (JAZ) proteins and interact with ARABIDOPSIS RESPONSE REGULATORS (ARR) and thereby mediate cytokinin signaling (Hou et al., 2010; Davière and Achard, 2013; Marín-de la Rosa et al., 2015).

A deeper understanding on the regulatory mechanisms is limited by the functional redundancy of various GA signaling components in *A. thaliana*, and therefore new theoretical-experimental approaches to tackle these constraints are needed. Many studies have been performed in mutant plants or Y2H/Y3H systems. In this work, different synthetic biology approaches are introduced in protoplasts and for the first time in mammalian cells as orthogonal minimal systems to unveil novel aspects of GA perception and signaling.

1.2 Synthetic biology tools for the analysis and reconstruction of plant signaling pathways

Synthetic biology still represents a relatively new discipline integrating engineering with life sciences. Basic engineering principles are applied for the modular and combinatorial assembly of biological parts into higher order complex signaling and metabolic structures (Andres et al., 2019). Towards the reconstruction of plant signaling pathways, several biosynthetic tools have been engineered and utilized in the course of this work to generate a platform in plant as well as in mammalian cells. All applied tools aim at studying plant signaling in a quantitative manner and thus several readout systems such as luminescence and absorbance-based systems were developed. The obtained quantitative data were integrated in mathematical modeling approaches to gain more insights about the dynamics of the systems. The implementation of mathematical modeling represents one key strategy for the design and quantitative functional characterization of newly developed systems as well as optimization of the individual modules and networks (Ellis et al., 2009; Lim, 2010; Andres et al., 2019).

As platforms, we chose protoplasts and mammalian cells as minimal systems. Mammalian cells, as an orthogonal platform, were used to study interactions of plant signaling components, complex formation and downstream transcriptional regulation. They represent a good alternative platform to analyze plant-specific bindings and interactions without any crosstalk with other plant signaling components.

In addition, biosensors in protoplasts have been developed for the quantification of intracellular phytohormone amounts with a multiplicity of applications. While other methods like mass spectrometry and chromatography suffer from the limitation of tissue disruption, protoplasts as well as mammalian cells allow dynamic analyses of living cells (Okamoto et al., 2009; Urbanová et al., 2013).

1.2.1 Quantitative ratiometric phytohormone biosensors

Biosensors combine the sensing of a specific small molecule or biological process of interest with a quantifiable readout (Walia et al., 2018). They should ideally display a high selectivity and specificity, a quantitative readout, a high signal-to-noise ratio as well as no inference with biological processes/systems (Samodelov and Zurbriggen, 2017; Walia et al., 2018). To analyze plant signaling, transcriptional-, degradation- and Förster resonance energy transfer (FRET)-based genetically encoded biosensors have been developed (Brunoud et al., 2012; Wells et al., 2013; Larrieu et al., 2015; Rizza et al., 2017). In this work, luminescent, degradation-based genetically encoded biosensors were constructed and employed to analyze phytohormone signaling following the design principle of Wend et al. (2013). These biosensors, first developed for auxin, take advantage of the targeted degradation of regulator proteins during phytohormone perception. They comprise a specific regulator protein as a

sensor module (SM), here Aux/IAA domain II sequences, C-terminally fused to a firefly luciferase from *Photinus pyralis*. A second luciferase as an internal normalization element, renilla luciferase from *Renilla reniformis*, is N-terminally connected via a 2A peptide to the SM. The 2A peptide leads to the stoichiometric co-expression of the renilla luciferase on one hand and the SM-firefly fusion on the other hand by autocatalytic cleavage of the whole mRNA transcript during translation (**Figure 6**, Wend et al., 2013; Samodelov et al., 2016). The modular sensor design allows for the incorporation of any protein of interest as a SM. For instance, the StrigoQuant sensor was built comprising SMXL6 as one of the regulators of strigolactone signaling (Samodelov et al., 2016). In the frame of this work, a multiplicity of biosensors was developed for the analysis of the phytohormones auxin, gibberellin as well as strigolactone which all follow the same degradation-based perception mechanism. As these biosensors are able to monitor the specific regulator degradation in response to exogenous phytohormone treatment, they can be seen as proxies to study phytohormone signaling on various levels in protoplasts. The sensitivity and specificity towards distinct phytohormones as well as synthetic analogs or precursors were determined during this work as well as transporter analyses. On the perception complex formation level, different regulators for each hormone as well as co-receptors and F-boxes were tested. In addition, this biosensor system allows for instance mutations and domain swaps to be explored for the deeper analysis of regulator proteins in terms of their recognition and binding.

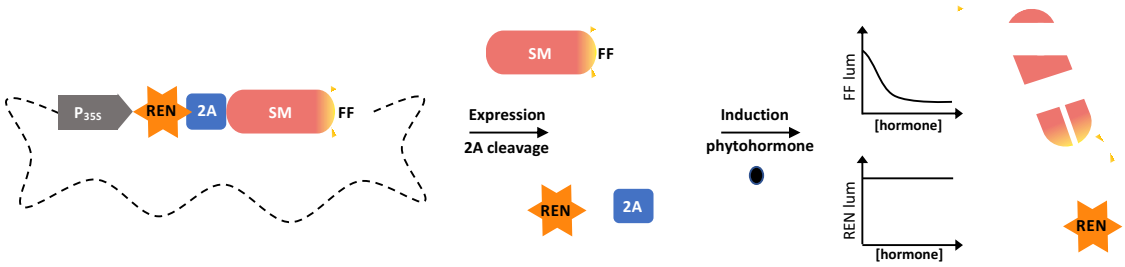

Figure 6: General genetically encoded, ratiometric, degradation-based phytohormone biosensor design. The biosensor construct expresses a renilla luciferase (REN) connected via a 2A peptide to a sensor module (SM) fused to a firefly luciferase (FF). The 2A peptide leads to the stoichiometric co-expression of the renilla luciferase, as a normalization element, and the SM-FF fusion. Upon hormone induction, the SM-FF becomes polyubiquitinated and degraded by the 26S proteasome whereas REN expression remains constant resulting in a decrease in FF/REN ratio (modified from Samodelov et al., 2016).

1.2.2 Reconstruction of phytohormone signaling pathways in mammalian cells

Plants, as sessile organisms, have evolved complex interactions of diverse signaling processes which are mostly intertwined. This high degree of crosstalk between signaling pathways makes it difficult to functionally analyze single components and their interplay. In addition to traditional and valuable research *in planta*, especially concerning the biological context, orthogonal systems are needed to investigate proteins of interest isolated from possible influences from other signaling pathways or crosstalk partners. Orthogonal platforms which are established in the field of plant research are for instance protoplasts and Y2H

systems for the investigation of protein-protein interactions (Ochoa-Fernandez et al., 2016; Matiolli and Melotto, 2018). However, especially Y2H systems show drawbacks concerning false positive and negative results as well as the limitations in terms of the protein fusion site (Mehla et al., 2017). More recently, mammalian cells as a new orthogonal platform for the analysis of plant signaling pathways, gained momentum due to the development of many different tools (Weber and Fussenegger, 2010). Mammalian cells allow for a fast, cheap and systematic analysis of plant signaling components in a high-throughput manner. The possibility of protein fusions on either the C- or N-terminal end make the system flexible and less prone to false positive or negative results. Additionally, numerous reporter systems enable a quantitative analysis to identify the components which are minimally required for specific plant signaling pathways. In combination with mathematical modeling, the obtained quantitative data in mammalian cells give new insights into plant signaling.

In summary, mammalian cells represent a good alternative platform to already existing methods and thereby expand the toolbox to analyze plant signaling pathways.

In this work, several synthetic tools like Mammalian-X-Hybrid and split-transcription factor systems were engineered and developed to reconstruct GA signaling for the first time in an orthogonal mammalian cell-based system.

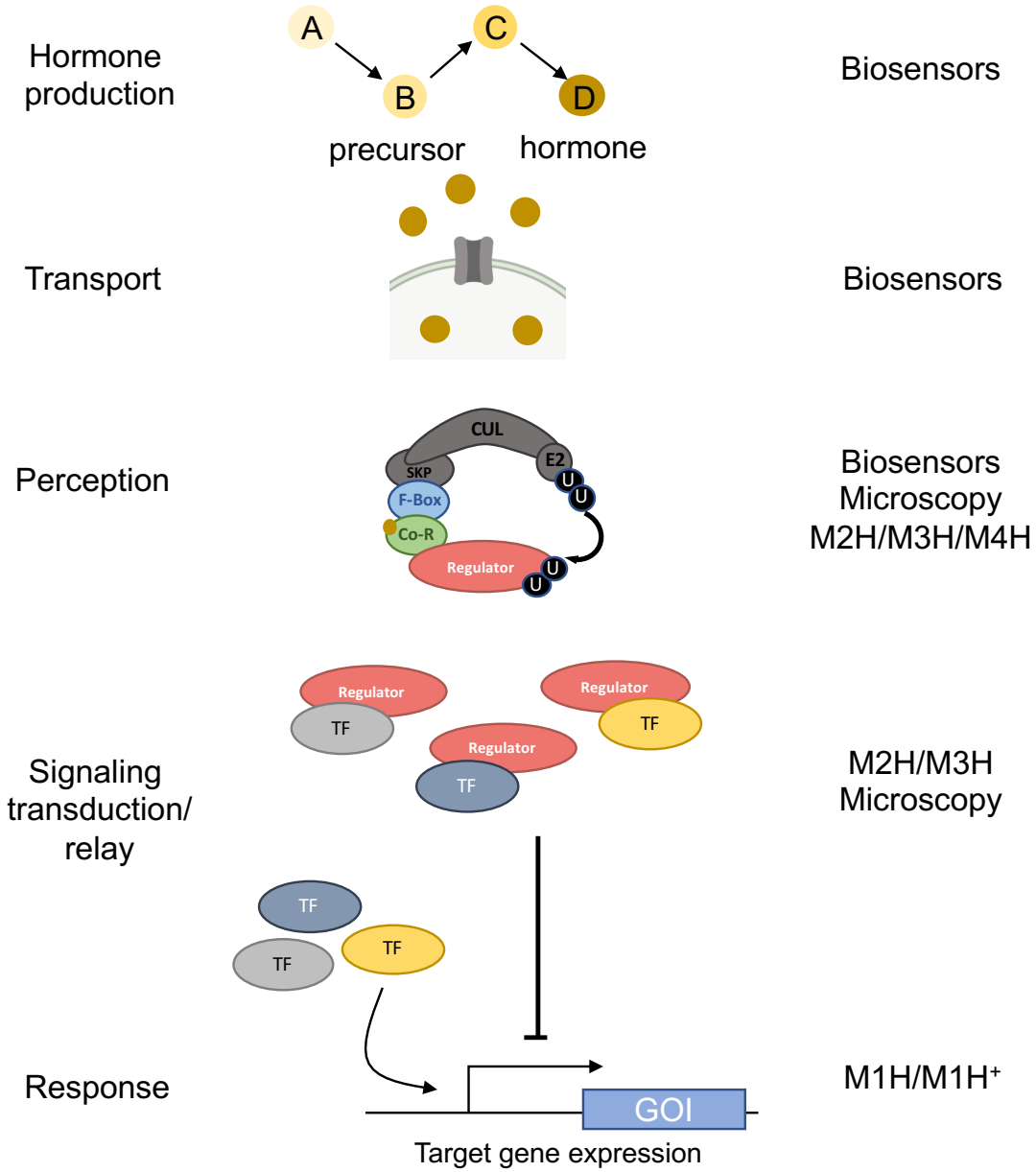

Figure 7: Phytohormone signaling and quantitative tools for the reconstruction in protoplasts and mammalian cells. Biosensors enable the analysis of phytohormone production, their transport and perception. On the perception complex formation level, (quantitative) microscopy as well as our M2H/M3H and M4H systems have been established to investigate phytohormone signaling. These methods can also be used to study signaling transduction/relay. The here described novel M1H/M1H$^+$ systems allow the analysis of target gene expression.

2 Aims

In this work, quantitative synthetic biology tools were designed, constructed, characterized and implemented to analyze and reconstruct phytohormone signaling.

The aims and thus this work, can be separated into two big parts. In a first chapter, ratiometric, luminescent biosensors were implemented based on the specific regulator degradation mechanism to study phytohormone perception and dynamics. The principles were adapted from the work of Wend et al. (2013) and Samodelov et al. (2016) developing the first biosensors for auxin as well as strigolactone. Numerous sensors for strigolactone, auxin as well as gibberellin were designed in this work containing all 8 SMXLs, 29 Aux/IAAs and 5 DELLAs. The distinct biosensors were first characterized and then implemented for several applications namely the analysis and identification of minimally required components for the specific phytohormone pathways as well as metabolic analyses. Additionally, kinetic analyses in combination with mathematical modeling were performed to gain deeper insights into the phytohormone perception mechanism.

The second objective was to answer remaining open phytohormone signaling questions in mammalian cells as an orthogonal system. For this, a platform for the reconstruction of gibberellin signaling was developed to facilitate the study of phytohormone signaling components. Different aspects such as gibberellin perception complex formation as well as downstream signaling were tackled with the establishment of several Mammalian-X-Hybrid systems (M1H-M4H). All systems allow for a high-throughput analysis in a quantitative manner.

In total, this work aimed at developing powerful synthetic biology tools in protoplasts and mammalian cells as a new approach to answer phytohormone-related questions in orthogonal minimal systems.

3 Results and Discussion

The following sections contain the most relevant data regarding plant signaling studies obtained during the course of this PhD thesis. A more detailed view on synthetic biology approaches in plants can be found in the attached review (Andres et al., 2019).

3.1 Quantitative analysis of phytohormone perception and signaling via biosensors

3.1.1 Strigolactones

3.1.1.1 Analysis of StrigoQuant dynamics

This chapter is based on a manuscript in preparation, Andres and Saadat et al., in cooperation with the lab of Oliver Ebenhöh (Institute of Quantitative and Theoretical Biology, Heinrich-Heine-Universität Düsseldorf, Germany) in **Appendix 7.2**.

The research interest in the phytohormone strigolactone has increased rapidly in the last years. Strigolactones regulate i.a. various adaptations to changes in the environment such as nutrient availability and convey the recognition of host roots by parasitic weeds of the genera *Striga* or *Orobanche* leading to enormous yield losses in crops and other cereals primarily in Africa and Asia (Parker, 2009). First synthetic biology tools were engineered to gain more knowledge about this important phytohormone. One of these tools is the ratiometric, degradation-based luminescent strigolactone biosensor StrigoQuant (Samodelov et al., 2016).

To obtain insights into mechanistic and regulatory aspects of SL signaling, we utilized the already established StrigoQuant sensor to generate a quantitative description of kinetic responses (Samodelov et al., 2016). Briefly, the biosensor comprises SMXL6 as a sensor module fused to a firefly luciferase (FF) connected via a 2A peptide to a renilla luciferase (REN) as a normalization element. It is worth noting that the expression is driven by the CaMV35S constitutive promoter (P_{35S}). The biosensor is predicated on the degradation-based SL perception mechanism: the binding of SLs to the receptor D14 leads to the formation of a co-receptor complex with MAX2 and the SMXL regulators (Samodelov et al., 2016). This results in the ubiquitylation and proteolysis of the regulators and thus triggers SL signaling (**Figure 8A**).

For quantitative kinetic description, we used an interdisciplinary approach integrating quantitative experimental data and mathematical modelling. First, quantitative kinetic data on SMXL6 degradation were obtained by transforming *A. thaliana* col-0 wt protoplasts with the StrigoQuant biosensor. 20 h after protoplast transformation, the samples were induced with the indicated concentrations of the synthetic strigol-like SL analog racemic GR24 (*rac*-GR24) for 15 min, 30 min, 1,5 h, 3 h, 6 h and 9 h and luciferase activity was determined (**Figure**

8B+C). After 15 min, up to 50 % SMXL6-FF degradation could be observed at high concentrations (1 µM) demonstrating the fast response of the sensor. Over the course of this kinetic measurement, significant degradation even at low *rac*-GR24 concentrations (up to 100 pM) was monitored depicting the high sensitivity. After 9 h, almost 90 % of SMXL6-FF was degraded at higher concentrations (100 nM – 1 µM).

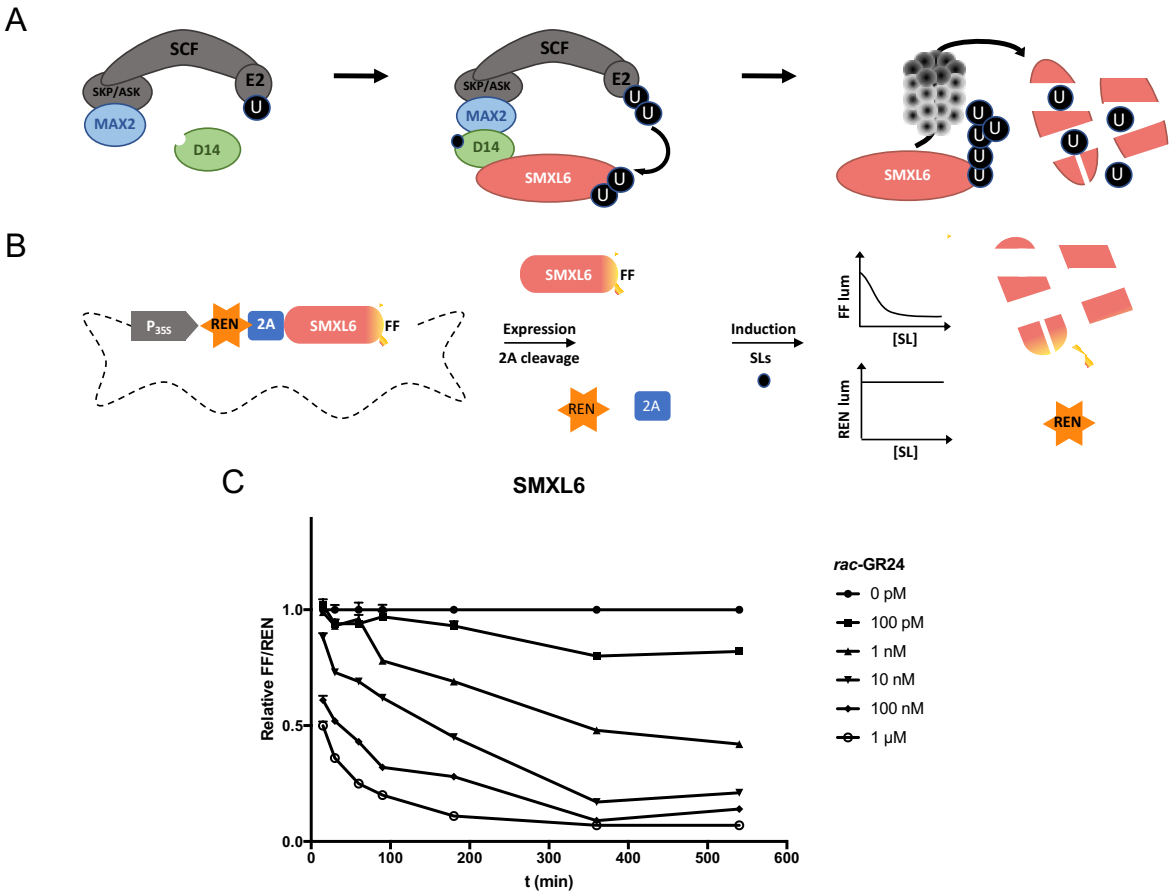

Figure 8: SL perception mechanism, StrigoQuant design and quantitative data on StrigoQuant dynamics. (A) Scheme of the SL perception machinery in *A. thaliana*. Upon binding of SLs to the receptor D14, SMXL6 is recruited to the perception machinery complex with MAX2 and SKP1/CUL1/F-box E2 ubiquitin ligase complex (SCF^{MAX2}). As a consequence, SMXL6 becomes polyubiquitinated (U) and thereby targeted for degradation by the 26S proteasome. (B) StrigoQuant biosensor design. StrigoQuant expresses a renilla luciferase (REN) connected via a 2A peptide to SMXL6 (as a sensor module) fused to a firefly (FF) luciferase, under the control of a P_{35S} promoter. The 2A peptide leads to the stoichiometric co-expression of REN (as a normalization element) and the SMXL6-FF fusion. In the presence of SLs, SMXL6-FF becomes polyubiquitinated and degraded by the 26S proteasome, whereas REN expression remains constant leading to a decrease in FF/REN ratio. (C) Quantitative kinetic data on the StrigoQuant behavior upon induction with *rac*-GR24. StrigoQuant was transiently expressed in *A. thaliana* mesenchymal protoplasts and 20 h post transformation induced with *rac*-GR24 (concentrations ranging from 100 pM to 1 µM) for 15 min, 30 min, 1 h, 1.5 h, 3 h, 6 h and 9 h. Luciferase activity was determined and the averaged FF/REN ratios were calculated. The data shown in this graph correspond to one representative experiment of three independent technical replicates. The error bars represent the SEM for this individual experiment with *n*=6. This figure is modified from Andres et al. (**Appendix 7.2**) with figure elements modified from Samodelov et al. (2016).

The quantitative kinetic data was then integrated into an ad-hoc developed theoretical computational modelling to enable a better quantitative description of the process. The modelled data led to the prediction that D14 might also undergo degradation triggered by *rac*-

GR24. Subsequently, a quantitative degradation-based, ratiometric sensor was engineered based on the receptor D14. The sensor follows the same modular composition as the StrigoQuant sensor incorporating D14 instead of SMXL6 as a sensor module (**Figure 9B**). To analyze the behavior and the degradation mechanism of D14, kinetics experiments with the same experimental setup were performed. These kinetic experiments were able to point out that D14 is indeed degraded up to almost 30 % after 9 h of *rac*-GR24 induction (**Figure 9C**). However, the D14 receptor degradation is only detectable at high *rac*-GR24 concentrations (100 nM – 1 µM) with slower kinetics than SMXL6, first arising around 3 h after hormone induction, and a reduced dynamic range.

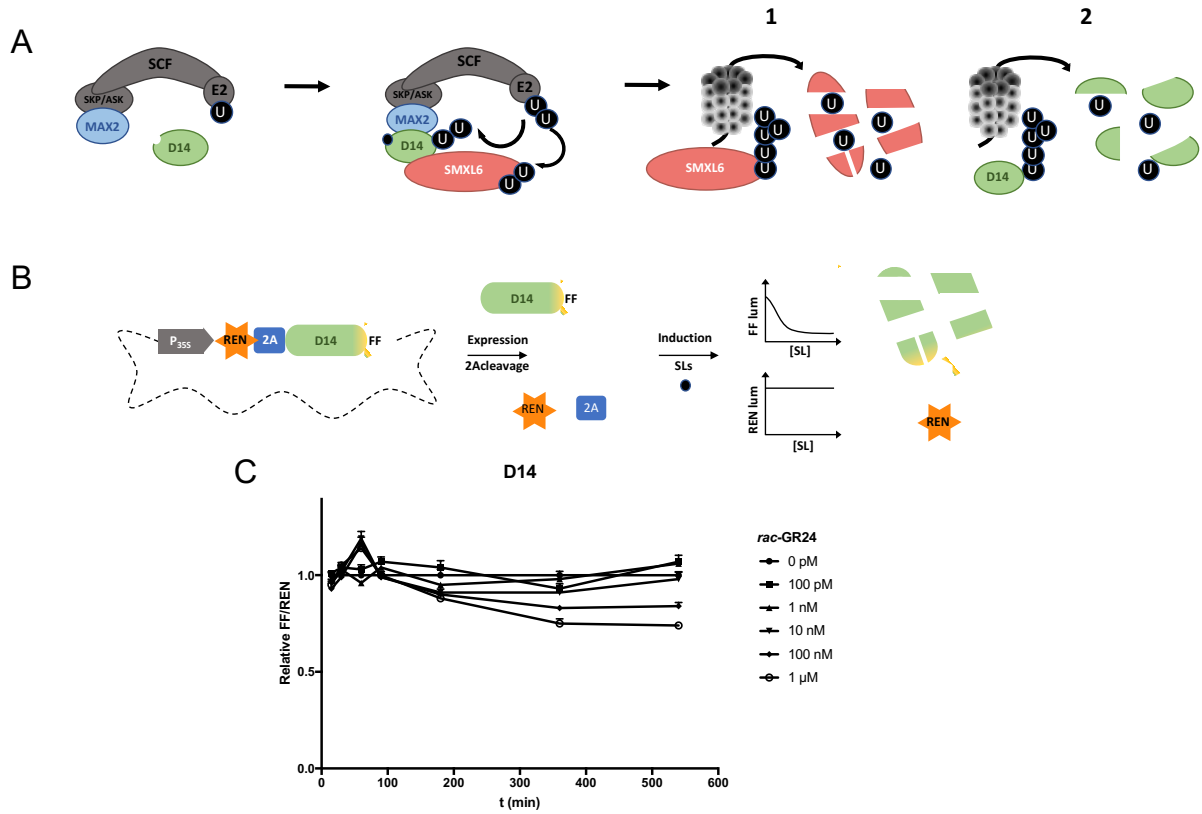

Figure 9: SL perception mechanism, D14-receptor sensor design and quantitative data on D14-receptor sensor dynamics. (A) Scheme of the SL perception machinery in *A. thaliana*. Upon binding of SLs to the receptor D14, SMXL6 is recruited to the perception machinery complex with MAX2 and SKP1/CUL1/F-box E3 ubiquitin ligase complex (SCF^{MAX2}). As a result, SMXL6 becomes polyubiquitinated (U) and thereby targeted for degradation by the 26S proteasome (1). In a negative feedback loop, D14 becomes also polyubiquitinated and thus degraded by the 26S proteasome, but with slower kinetics. (B) D14-receptor biosensor design. The D14-receptor biosensor expresses a renilla luciferase (REN) connected via a 2A peptide to D14 (as a sensor module) fused to a firefly (FF) luciferase, under the control of a P_{35S} promoter. The 2A peptide leads to the stoichiometric co-expression of REN (as a normalization element) and the D14-FF fusion. In the presence of SLs, D14-FF becomes polyubiquitinated and degraded by the 26S proteasome, whereas REN expression remains constant leading to a decrease in FF/REN ratio. (C) Quantitative kinetic data on the D14-receptor sensor behavior upon induction with *rac*-GR24. D14-receptor sensor was transiently expressed in *A. thaliana* mesenchymal protoplasts and 20 h post transformation induced with *rac*-GR24 (concentrations ranging from 100 pM to 1 µM) for 15 min, 30 min, 1 h, 1.5 h, 3 h, 6 h and 9 h. Luciferase activity was determined and the averaged FF/REN ratios were calculated. The data shown in this graph correspond to one representative experiment of three independent technical replicates. The error bars represent the SEM for this individual experiment with *n*=6. This figure is modified from Andres et al. (**Appendix 7.2**).

For this project, an already established strigolactone biosensor (StrigoQuant, Samodelov et al., 2016) comprising the negative regulator SMXL6 as a sensor module, was utilized to perform kinetic analyses. The data was then used to parameterize a mathematical model. This mathematical model yielded a new hypothesis, namely that D14 – as a part of the receptor complex – might also be degraded. We tested this experimentally by building a D14-receptor sensor confirming that D14 is indeed degraded. This interdisciplinary approach between experimental synthetic biology and mathematical modeling gave us insight on mechanistic aspects of strigolactone perception dynamics (**Figure 10**).

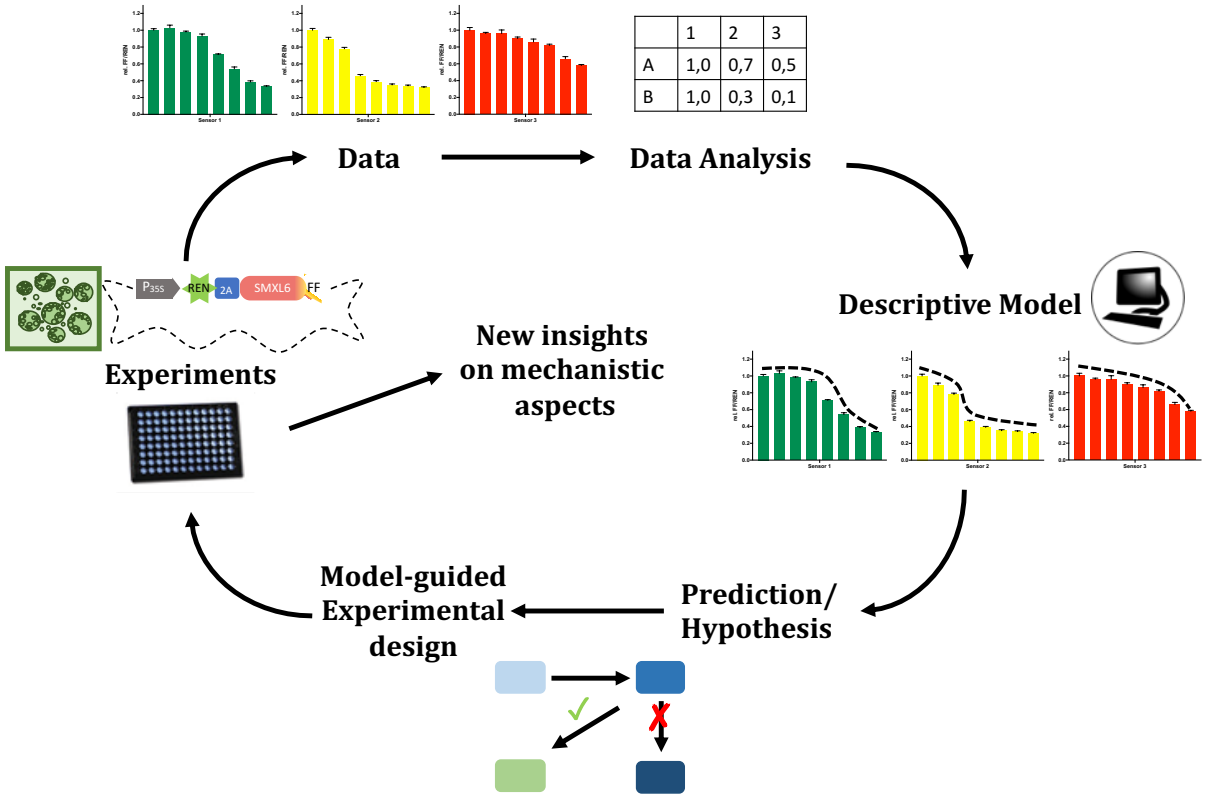

Figure 10: Experimental workflow of an exemplary interdisciplinary research project. An already established quantitative biosensor (StrigoQuant) was implemented to gain kinetic data, and these data where utilized to generate a mathematical model. From this descriptive model, a new prediction/hypothesis arose, namely that the D14 receptor might also be degraded. This in turn led to a new model-guided experimental design and further biosensor experiments which gave us new insights on mechanistic aspects of the strigolactone perception kinetic. This figure is adapted from Andres et al. (**Appendix 7.2**)

3.1.1.2 Sensitivity and specificity of SL/Kar-induced degradation among SMXL family members

The genome of *A. thaliana* does not only encode SMXL6 as a regulator for strigolactone signaling, but actually eight SMXLs in total. These can be divided into three subgroups: i) SMAX1 and SMXL2 are supposedly involved in karrikin signaling mediated by KAI2 (Guo et al., 2013; Waters et al., 2013), ii) SMXL3, 4 and 5 are strigolactone-independent central regulators of phloem development (Wallner et al., 2017), and iii) SMXL6, 7 and 8 are involved in strigolactone-mediated developmental and growth processes (Zhou et al., 2013; Wang et al., 2015). This combinatorial complexity makes it particularly difficult to analyze their individual roles in *A. thaliana*. As there is still little knowledge about the influence of strigolactones as well as karrikins (SL homologs derived from smoke) on all SMXL subgroups in *A. thaliana*, we cloned all eight SMXLs as biosensors and analyzed their behavior towards a racemic mixture of the synthetic strigolactone analog, *rac*-GR24, karrikin 1 (Kar1) and karrikin 2 (Kar2). To establish these biosensors as new quantitative tools for phytohormone assays, it is indispensable to have a good dynamic range to observe and analyze significant reductions in expression levels. This depends on the general expression level of the sensor constructs as well as their sensitivity towards endogenous hormones which are already present in the protoplasts. *A. thaliana* wt protoplasts were transiently transformed with the sensor constructs and 20 h post transformation, induced with the above-mentioned hormones. 4 h after *rac*-GR24 or karrikin induction, luciferase activity was determined. As depicted in **Figure 11**, different expression levels between the distinct SMXLs could be observed. While SMAX1, SMXL2, SMXL7 and SMXL8 are expressed with low FF absolute values, the expression for SMXL3, 4, 5 and 6 is generally higher in all experiments. REN, as a normalization element, is expressed at high levels (all above 2500 RLU) indicating that all sensors are properly transcribed. The overall REN expression is stable within every construct, but varies slightly among them. When induced with *rac*-GR24, SMXL6 and SMXL8 show a strong degradation curve with up to almost 90 % degradation for SMXL6 (**Figure 11A**). For SMXL7, which is expressed close to the background level, no hormone-dependent degradation could be detected. In general, SMXL7 is more unstable than SMXL6 and 8 indicating that it might be degraded by low endogenous hormone concentrations present in the protoplasts. It might also be possible that SMXL7 becomes unstable or non-functional when fused C-terminally, for instance with a firefly luciferase in this case. Instability and fast degradation in response to hormone treatment have already been reported before for SMXL7 (Soundappan et al., 2015; Liang et al., 2016). In future experiments, SMXL7 could be fused N-terminally to test its stability in protoplasts and plants. In addition, biosensors could be built where SMXL7 is fused N-terminally with a firefly luciferase and C-terminally connected via a 2A peptide to a renilla luciferase.

Subgroup 1, containing SMAX1 and SMXL2, is generally low expressed in wt protoplasts. After *rac*-GR24 induction, a slight degradation at high concentrations can be observed. SMXL3, 4 and 5, which form subgroup 2, do not show a clear degradation curve when induced with increasing concentrations of *rac*-GR24.

The screenings with karrikin 1 and karrikin 2 (**Figure 11B+C**) did not show any clear degradation curve. Karrikin 1 induction leads to a slight decrease in SMXL6 and SMXL8 abundance at high concentrations (1 µM). However, induction with karrikin 2 did not lead to any SMXL degradation at all, indicating that even SMAX1 and SMXL2, which are supposedly involved in karrikin signaling, are not influenced by karrikins in *A. thaliana* wt protoplasts. This could be due to the fact that they are either not responding to Kar1 and Kar2 at all or that they are already degraded down to a minimum in the wt (in response to endogenous compounds like SL) that no more degradation is possible. To check this, we tested these two biosensors in different *A. thaliana* mutant protoplasts involved in SL as well as Kar perception (next chapter).

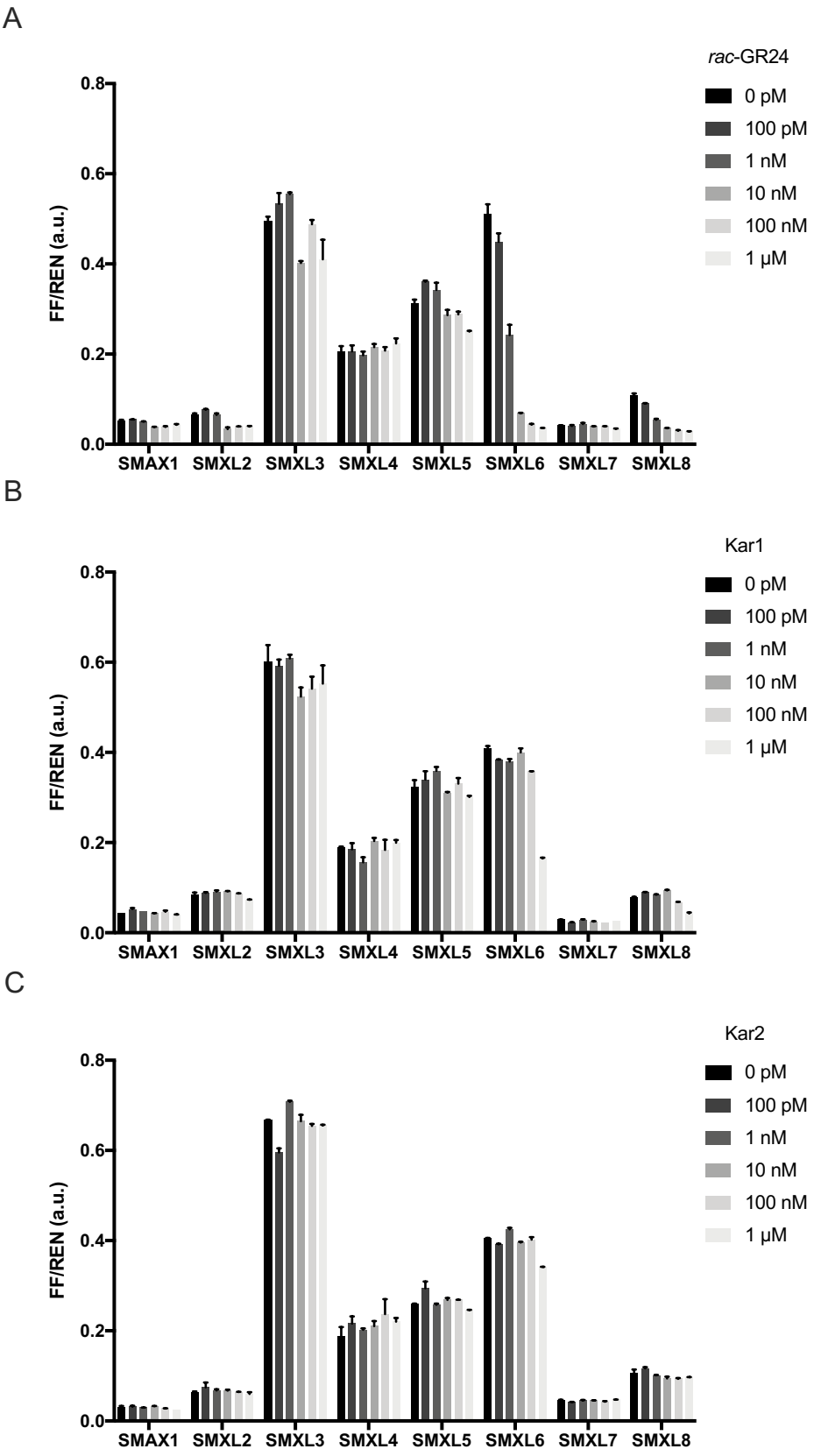

Figure 11: SMXL stability in *A. thaliana* wt protoplasts. Biosensors incorporating SMAX1/SMXL2-8 as sensor modules were transiently expressed in *A. thaliana* mesenchymal protoplasts and 20 h post transformation induced with either (A) *rac*-GR24, (B) Kar1 or (C) Kar2 (concentrations ranging from 100 pM to 1 µM) for 4 h. Luciferase activity was determined and the averaged FF/REN ratios were calculated. The data shown in this graph correspond to one representative experiment of three independent technical replicates. The error bars represent the SEM for this individual experiment with *n*=6.

3.1.1.3 SMAX1 and SMXL2 stability in various SL/Kar signaling mutants

In *A. thaliana* wt protoplasts, the SMAX1 and SMXL2 biosensors had a low expression level and thus did not show any degradation upon *rac*-GR24 or karrikin induction. Up to date, only a little is known about the roles of SMAX1 and SMXL2 in karrikin as well as SL signaling. To analyze the roles of SMAX1 and SMXL2 regarding strigolactone and karrikin perception, we transformed different *A. thaliana* mutants with these two biosensors and induced with *rac*-GR24. For this, we chose components either being involved in SL biosynthesis or in the strigolactone/karrikin perception complex formation. SLs are biosynthesized from a common precursor named carlactone which is converted into carlactonic acid by MAX1 (MORE AXILLARY GROWTH1) (Abe et al., 2014; Yoneyama et al., 2018). Therefore, we selected a *max1* mutant to investigate if the general SMAX1/SMXL2 biosensor expression level would be higher without endogenous SLs like Orobanchol present. As shown in **Figure 12**, the expression level in this *max1* mutant is slightly higher compared to the wt when transformed with SMAX1. This could not be observed for SMXL2. However, no degradation curve after *rac*-GR24 induction could be observed for both. Future mutant experiments should include an enzyme which is involved earlier in the SL biosynthesis pathway, for instance MAX4 which produces carlactone from a precursor (9-cis-β-apo-10'-carotenal) for which the exact enzymatic mechanism is still not understood (Al-Babili and Bouwmeester, 2015). This would prevent the biosynthesis of any kind of SLs. Next, we investigated the influence of different (proposed) perception complex components for SL as well as karrikin signaling. The current hypotheses for SL as well as karrikin perception includes MAX2 as a F-Box protein involved in both signaling pathways (Nelson et al., 2011). Therefore, *max2* mutant protoplasts (provided by the group of S. Al-Babili) were transformed with the SMAX1/SMXL2 biosensors and induced with *rac*-GR24. The FF expression levels for both sensors were strongly increased in this mutant compared to the wt (**Figure 12**) indicating that MAX2 is indeed somehow connected to SMAX1/SMXL2 stability in *A. thaliana*. As expected for the F-Box *max2* mutant, no degradation after *rac*-GR24 induction could be observed, only some fluctuations for SMXL2. Since high expression levels, but no degradation could be observed in the *max2* mutant, the biosensors were transformed into mutants of the three paralogous receptors D14, KAI2 and DLK2 (provided by the group of S. Al-Babili). The expression level in the *dlk2* mutant is even lower than the wt indicating that DLK2 does not play any role in the stability as well as the degradation of SMAX1 and SMXL2. The expression level in the *d14* mutant is slightly increased/comparable to the wt, but no degradation was observed. However, high expression as well as a strong degradation curve could be monitored for both biosensors in the *kai2* mutant. Furthermore, a *kai2d14* double mutant was transformed with the two biosensors leading to high expression, but no *rac*-GR24-dependent degradation.

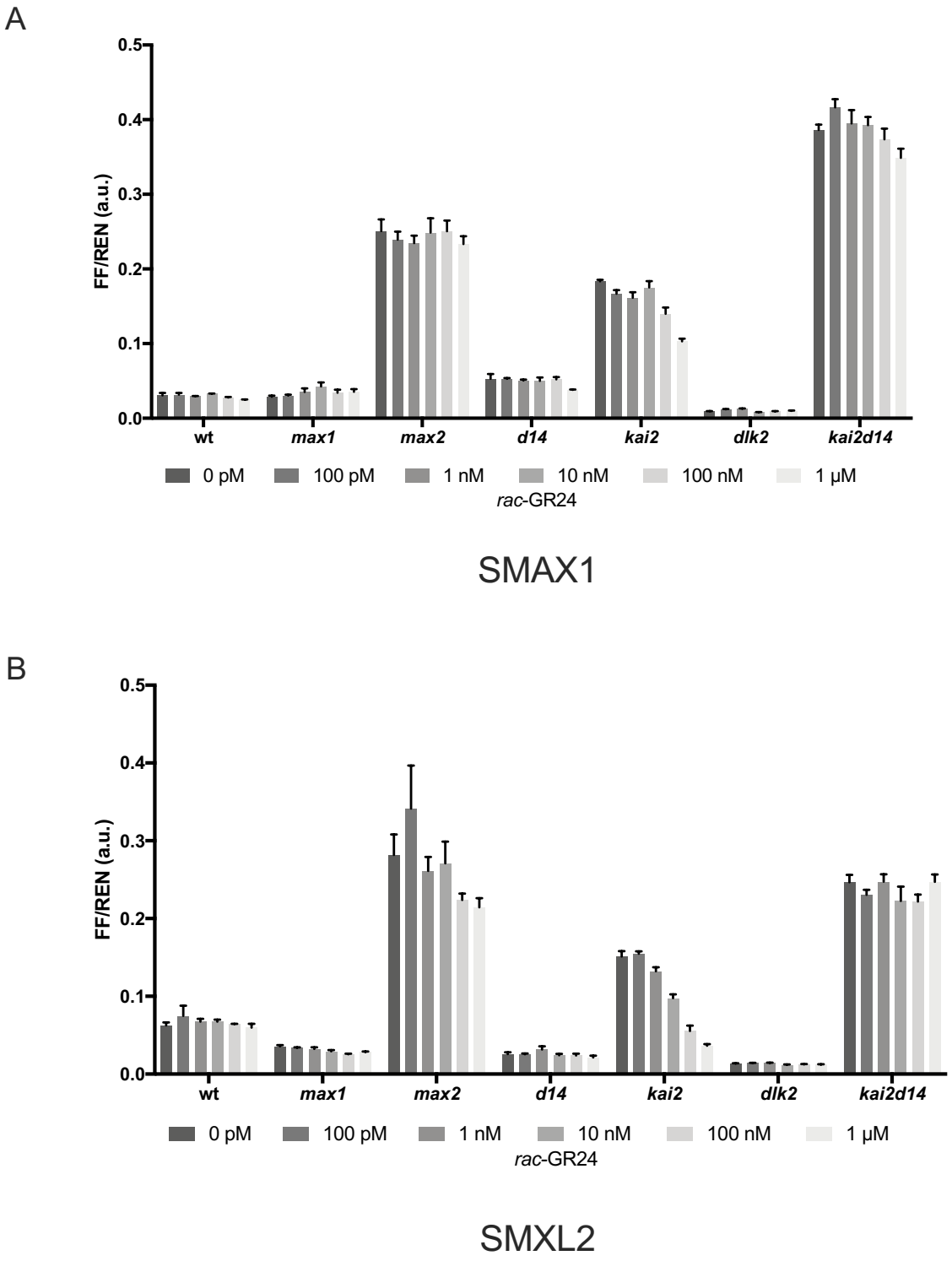

Figure 12: SMAX1 and SMXL2 stability in *A. thaliana* wt and signaling mutant-derived protoplasts. *A. thaliana* wt, *max1*, *max2*, *d14*, *kai2*, *dlk2* and *kai2d14* mutant protoplasts were transformed with either the SMAX1 or the SMXL2 biosensor and induced with *rac*-GR24 20 h post transformation. After hormone incubation for 4 h, luciferase activity and subsequently the FF/REN ratios were determined. The data shown in this graph correspond to one representative experiment of two independent technical replicates. The error bars represent the SEM for this individual experiment with *n*=6.

The conducted experiments in the course of this work in *A. thaliana* protoplasts provide the first clear indications that SMAX1 and SMXL2 are indeed degraded in response to *rac*-GR24 induction in a *kai2* mutant background. D14 might be involved as a receptor to perceive *rac*-GR24, as it is also true for SL signaling mediated by the SL-D14-SMXL6-8 complex. Nevertheless, KAI2 appears to be connected to SMAX1 and SMXL2 stability, too. Only the high expression level in the *kai2* mutant enables the SMAX1/SMXL2 degradation curve in response to *rac*-GR24.

Future experiments in mutant backgrounds with karrikins could explain the connection between KAI2 and SMAX1 and SMXL2. In addition, different SLs should be tested to further investigate the role of SMAX1/SMXL2 in SL signaling.

In summary, a connection between SMAX1/SMXL2 stability and MAX2 as well as KAI2 could be shown for the first time. Moreover, SMAX1 and SMXL2 degradation could be shown upon induction with *rac*-GR24 leading to a new hypothesis for the roles of SMAX1 and SMXL2 in strigolactone signaling (**Figure 13**).

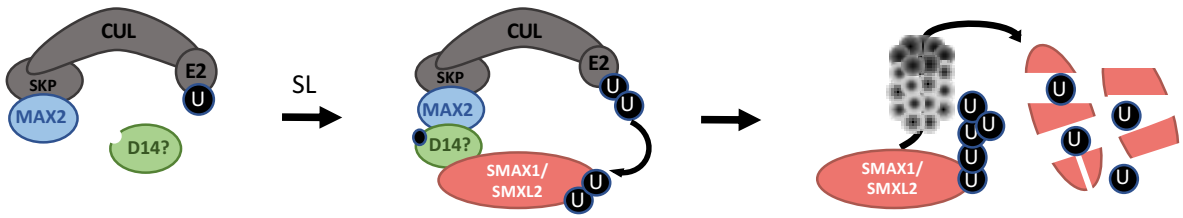

kai2 mutant background

Figure 13: The role of SMAX1 and SMXL2 in SL signaling in *A. thaliana kai2* mutant protoplasts. In this hypothesis, developed in the course of this work, *rac*-GR24 is perceived through a receptor, probably D14, and SMAX1 or SMXL2 and subsequently SCF^{MAX2} associate to this complex. SMAX1/SMXL2 becomes polyubiquitinated and targeted for degradation by the 26S proteasome.

3.1.2 Aux/IAA protein stability in response to IAA and temperature

The first part of this chapter is based on an accepted manuscript, Andres *et al.*, in **Appendix 7.3**.

The phytohormone auxin mediates a multitude of developmental and physiological processes in plants (Luo et al., 2018). Its perception mechanism is similar to that of gibberellins and strigolactones, but without being mediated by a second co-receptor. Bioactive IAAs bind to TIR1/AFB enabling the interaction between regulators of auxin response (Aux/IAAs) and TIR1/AFB-IAA. This leads to the polyubiquitination of the Aux/IAAs by the $SCF^{TIR1/AFB}$ complex and the subsequent degradation by the 26S proteasome. The Aux/IAA protein family in *A. thaliana* comprises 29 family members which all share highly conserved domains (Shimizu-Mitao and Kakimoto, 2014). Although they are involved in different responses in development, the number, i.e. 29, of Aux/IAAs as regulators for auxin response seems to be surprisingly high. In our studies, we aimed at investigating the signification of having that many Aux/IAA family members. First, as a proof of principle, we cloned three Aux/IAAs with a structurally different domain II core sequence as sensor modules in our ratiometric luminescent biosensor platform, and performed kinetic analyses. Towards this aim, we chose the following full-length Aux/IAAs: i) Aux/IAA34, which has no sequence homology with the domain II core consensus sequence, ii) Aux/IAA31 containing only a part of this consensus sequence, and iii) Aux/IAA17 comprising the full consensus sequence (**Figure 14**). *A. thaliana* wt protoplasts were transformed with the three different biosensor constructs and induced 20 h post transformation with a serial dilution of IAA (from 100 pM to 1 µM) for 2, 4 and 6 h. Afterwards, luminescence was measured in microplate readers.

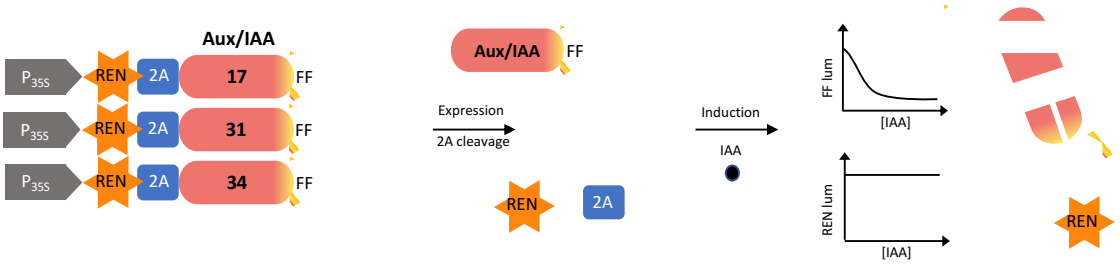

Figure 14: Aux/IAA biosensor design. The Aux/IAA biosensors express a renilla luciferase (REN) connected via a 2A peptide to an Aux/IAA (as a sensor module) fused to a firefly (FF) luciferase, under the control of a P_{35S} promoter. The 2A peptide leads to the stoichiometric co-expression of REN (as a normalization element) and the Aux/IAA-FF fusion. In the presence of IAA, Aux/IAA-FF becomes polyubiquitinated and degraded by the 26S proteasome, whereas REN expression remains constant leading to a decrease in FF/REN ratio. The figure is adapted from the manuscript of Andres et al. (**Appendix 7.3**).

The Aux/IAAs displayed different degradation behaviors in response to the auxin treatment (**Figure 15**). Whereas, Aux/IAA17 was strongly degraded up to 80 % (at high nM concentrations) already after 2 h, Aux/IAA34 was not degraded at all. Aux/IAA31 showed a slight decrease after 2h (at high auxin concentrations), but a strong degradation (up to 80 %)

only after 4 h and 6 h. These first proof of principle experiments indicated that the Aux/IAA degradation behavior depends on the composition of the Aux/IAA domain II.

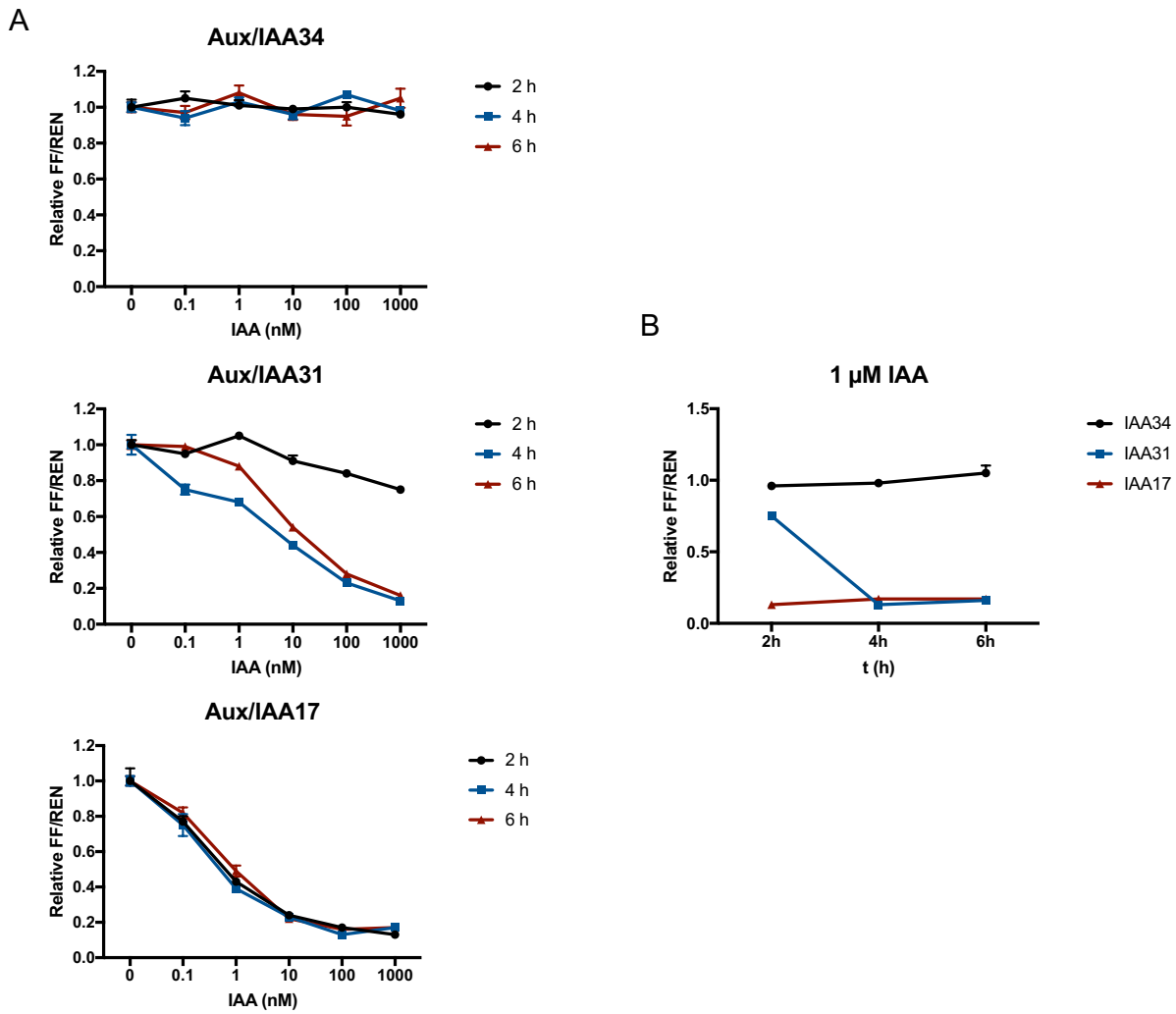

Figure 15: Sensitivity of auxin-induced degradation among three Aux/IAA family members. Biosensors incorporating Aux/IAA17, 31 and 34 as sensor modules were transiently expressed in *A. thaliana* mesenchymal protoplasts and 20 h post transformation induced with IAA (concentrations ranging from 100 pM to 1 µM) for 2 h, 4 h and 6 h. Firefly and renilla luciferase activities were determined and the averaged FF/REN ratios were calculated. The error bars represent the SEM for this individual experiment with *n*=6. (A) Degradation curves for Aux/IAA 17, 31 and 34 after 2 h, 4 h and 6 h IAA induction (concentrations ranging from 100 pM to 1 µM). (B) Degradation curves for Aux/IAA 17, 31 and 34 induced with 1 µM IAA for 2 h, 4 h and 6 h. This figure and the figure legend are adapted from Andres et al. (**Appendix 7.3**).

As the suitability of the biosensor system for comparative analyses of Aux/IAA stability in response to auxin was already shown, we cloned all 29 Aux/IAAs as sensor modules in our ratiometric luminescent biosensor platform and transformed them into protoplasts. 20 h post transformation, the protoplasts were supplemented with increasing concentrations of IAA (100 pM to 1 µM) for 2 h and luminescence was determined in micro plate readers. As depicted in **Figure 16**, several Aux/IAAs display a high sensitivity towards IAA. However, 5 Aux/IAAs, namely Aux/IAA20, 30, 32, 33 and 34, are not degraded by auxin at all, whereas Aux/IAA31 only shows a slight decrease in FF/REN ratio. In addition, different sensitivities towards IAA could be observed. Some Aux/IAAs, such as Aux/IAA13 and 17, display a high sensitivity

towards IAA even at low concentrations (pM-range), while Aux/IAA15 and 26 are less sensitive towards IAA (nM-range). For all Aux/IAAs, the proteasome-dependency of their degradation was shown by supplementing the proteasomal inhibitor MG132 2 h prior to hormone induction (data not shown).

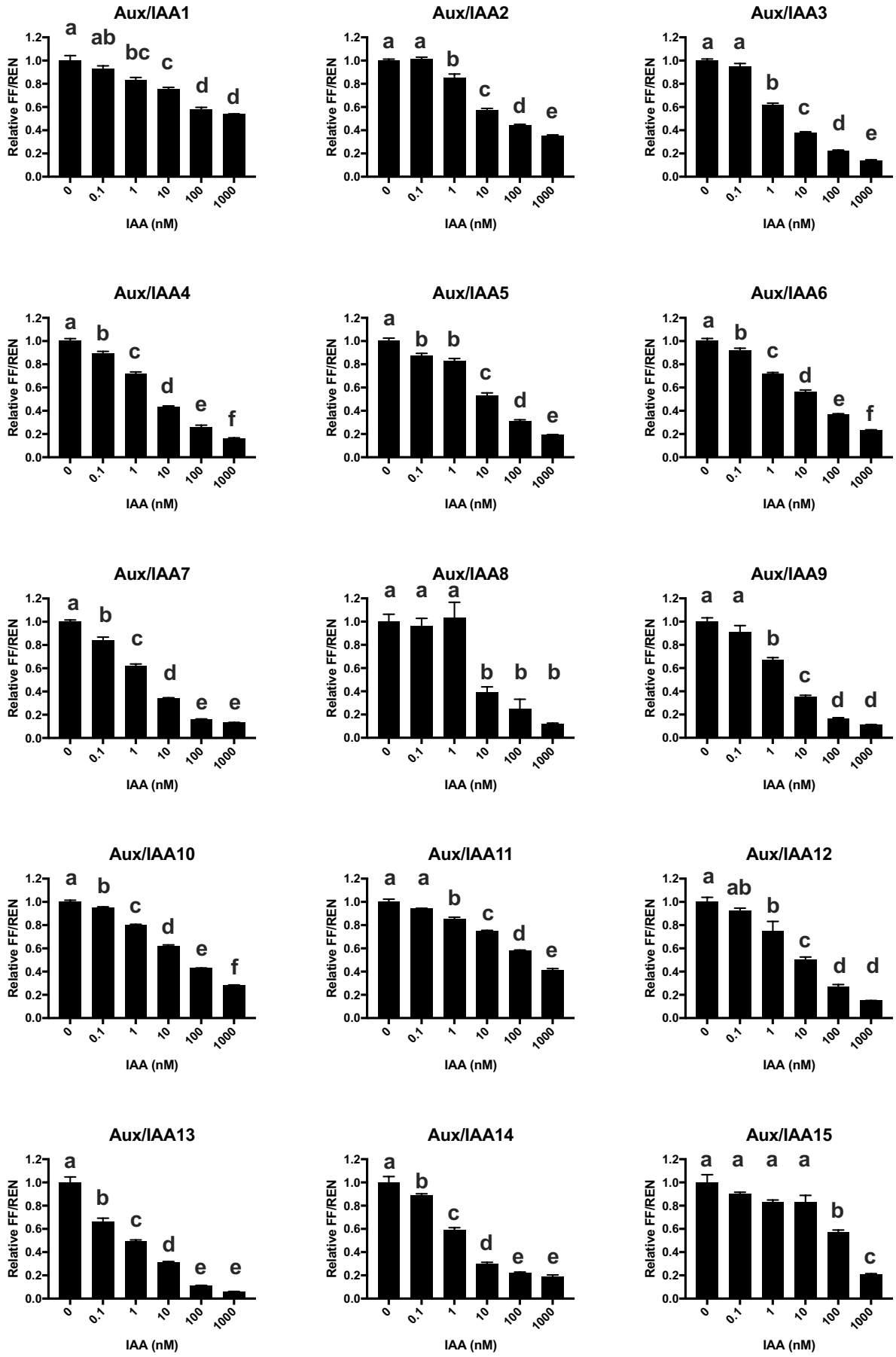
Aux/IAA1
a ab bc c d d
Aux/IAA2
a a b c d e
Aux/IAA3
a a b c d e
Aux/IAA4
a b c d e f
Aux/IAA5
a b b c d e
Aux/IAA6
a b c d e f
Aux/IAA7
a b c d e e
Aux/IAA8
a a a b b b
Aux/IAA9
a a b c d d
Aux/IAA10
a b c d e f
Aux/IAA11
a a b c d e
Aux/IAA12
a ab b c d d
Aux/IAA13
a b c d e e
Aux/IAA14
a b c d e e
Aux/IAA15
a a a a b c
Relative FF/REN
0.0 0.2 0.4 0.6 0.8 1.0 1.2
0 0.1 1 10 100 1000
IAA (nM)

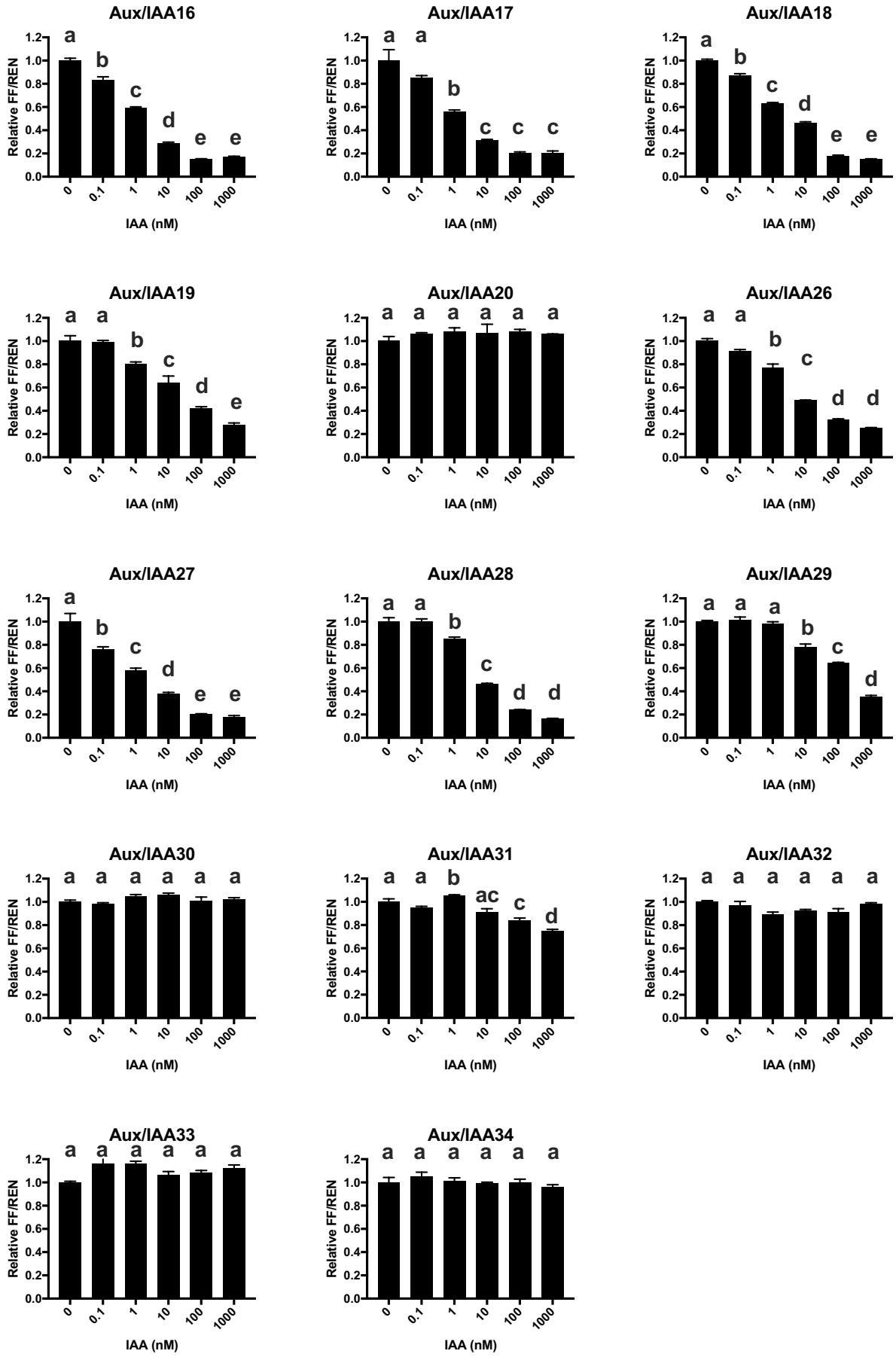
Aux/IAA16
a b c d e e
Aux/IAA17
a a b c c c
Aux/IAA18
a b c d e e
Aux/IAA19
a a b c d e
Aux/IAA20
a a a a a a
Aux/IAA26
a a b c d d
Aux/IAA27
a b c d e e
Aux/IAA28
a a b c d d
Aux/IAA29
a a a b c d
Aux/IAA30
a a a a a a
Aux/IAA31
a a b ac c d
Aux/IAA32
a a a a a a
Aux/IAA33
a a a a a a
Aux/IAA34
a a a a a a
Relative FF/REN
0.0 0.2 0.4 0.6 0.8 1.0 1.2
0 0.1 1 10 100 1000
IAA (nM)

Figure 16: Sensitivity of auxin-induced degradation among all Aux/IAA family members. Biosensors incorporating Aux/IAA1-20 as well as 26-34 as sensor modules were transiently expressed in *A. thaliana* mesenchymal protoplasts and 20 h post transformation induced with IAA (concentrations ranging from 100 pM to 1 µM) for 2 h. Luciferase activity was determined and the averaged FF/REN ratios were calculated. The data shown in this graph correspond to one representative experiment of three independent technical replicates. The statistical significance between the different IAA concentrations is indicated in lower case letters, where "a" significantly differs from "b", "b" from "c" and so on. One-way analysis of variance (ANOVA) were performed with $p < 0.05$. The error bars represent the SEM for this individual experiment with n=6.

As already explained earlier, Aux/IAAs possess four domains. Domain II contains the auxin degron which comprises a conserved "GWPPV" motif. This motif can interact with SCF^{TIR1} (Luo et al., 2018). All Aux/IAAs which have a fragmentary or no auxin degron are not degraded by IAA (**Figure 16**). Considering that these Aux/IAAs are also grouped with the other 24 Aux/IAAs, which are sensitive towards IAA, into a group of negative regulators of auxin response based on their structural similarity, this is remarkable.

What is the point of having Aux/IAAs which are not reacting to auxin? To answer this question, we examined putative factors influencing Aux/IAA stability. Light stimuli and the influence of temperature are of immense importance to plants as sessile organisms to adjust their metabolism, physiology and development. There is evidence that the photoreceptor PhyB is also involved in temperature perception by integrating light and temperature signals (Legris et al., 2017; Song et al., 2017). As PhyB and auxin signaling are intertwined *in planta* (Legris et al., 2017), we analyzed whether high temperature might also affect Aux/IAA stability. To test this hypothesis, we developed an experimental setup: 20 h post transformation, the protoplasts were transferred into darkness (to prevent any light stimuli) at 22 °C or 28 °C for 6 h. Additionally, samples were first incubated at 22 °C and after 1 h and 3 h transferred to 28 °C. The results indicated that some Aux/IAAs are strongly degraded by high temperature and some are not affected at all. By analyzing the data of both screenings, we could form groups where Aux/IAAs are i) degraded by auxin and temperature ii) only degraded by auxin iii) only degraded by temperature, and iv) neither degraded by auxin nor by temperature (**Figure 17**). Most Aux/IAAs are degraded by auxin and high temperature. However, there are two Aux/IAAs which are only degraded by temperature, namely Aux/IAA32 and 34. As these two Aux/IAAs display strong deviations from the 13aa consensus sequence in domain II, which confers binding to TIR1/AFB and subsequent degradation of the Aux/IAAs by the 26S proteasome, the mechanism of temperature-dependent Aux/IAA degradation does not seem to rely on the SCF^{TIR1} complex mediated degradation mechanism. Additionally, Aux/IAA20, 30 and 33, which either do not contain the domain II consensus sequence or only a strongly deviated version of it, are neither degraded by auxin nor by temperature. These results imply that not all Aux/IAAs that lack the 13aa consensus sequence in domain II are degraded by temperature. Additionally, the influence of light on this temperature-dependent degradation was tested, because the temperature perception of PhyB is also influenced by light. Experiments

conducted in dark as well as light caused no significant difference to the temperature treatment. This indicates that light does not seem to influence the temperature-dependent degradation of Aux/IAAs (data not shown). To evaluate the 26S proteasome dependency of the temperature-dependent Aux/IAA degradation, experiments with the proteasomal inhibitor MG132 were conducted (data not shown). These experiments demonstrated that the above-mentioned degradation is not mediated by the 26S proteasome.

These two large quantitative screenings were done for the first time in plant cells. This constitutes a pioneering approach for the study of the correlation between Aux/IAA stability and temperature changes. A direct influence of temperature on Aux/IAA stability was demonstrated for the first time. Until now, these screenings remain rather descriptive. Future goals would be to unveil the mechanism of temperature-dependent degradation of Aux/IAAs, since our results indicate an alternative, 26S proteasome-independent degradation pathway. For this, further sequence analyses as well as engineering of Aux/IAA chimeras will be needed. Moreover, different degradation pathways, such as plant vacuolar degradation related to natural and stress-induced senescence as well as plasma membrane components, should be investigated (Scheuring et al., 2012; Otegui, 2018). Further screenings could reveal if low temperature might have a stabilizing effect on Aux/IAAs. The discovery of the Aux/IAA temperature-dependent degradation in the course of this work in combination with the future revelation of the corresponding degradation mechanism will be of great value and interest in the field of auxin research and could help to unveil the complexity of auxin perception and signaling.

A

Group 1 Degradation by Auxin and high temperature	Group 2 Degradation by Auxin	Group 3 Degradation by high temperature	Group 4 No degradation
Aux/IAA1 Aux/IAA10 Aux/IAA28	Aux/IAA11	Aux/IAA32	Aux/IAA20
Aux/IAA2 Aux/IAA12 Aux/IAA29	Aux/AA16	Aux/IAA34	Aux/IAA30
Aux/IAA3 Aux/IAA13 Aux/IAA31	Aux/IAA19		Aux/IAA33
Aux/IAA4 Aux/IAA14			
Aux/IAA5 Aux/IAA15			
Aux/IAA6 Aux/IAA17			
Aux/IAA7 Aux/IAA18			
Aux/IAA8 Aux/IAA26			
Aux/IAA9 Aux/IAA27			

B

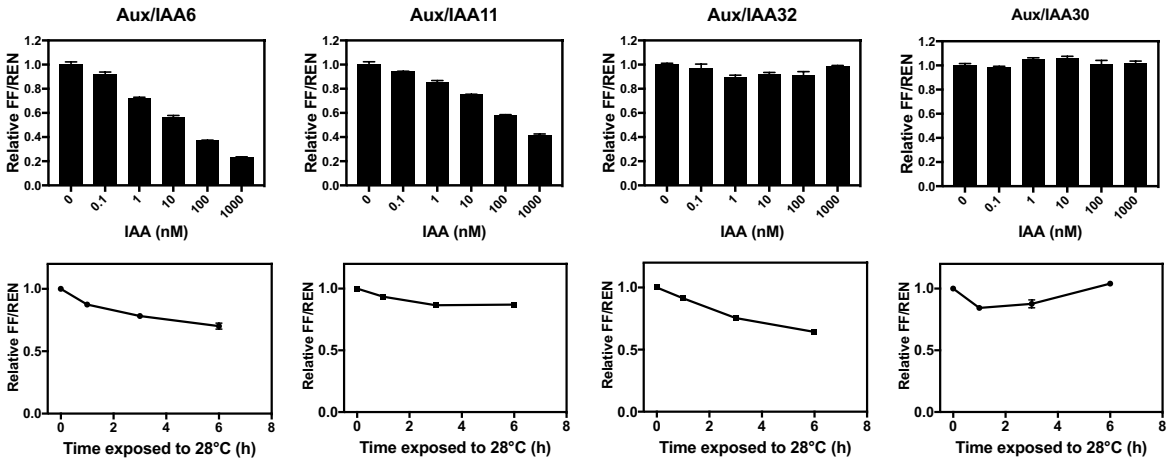

Figure 17: Auxin- and temperature-dependent degradation among all Aux/IAA family members. (A) Classification of all Aux/IAAs into groups. Group 1 contains all Aux/IAAs being degraded by auxin and high temperature (28 °C), group 2 the ones which are only degraded by auxin, group 3 the Aux/IAAs which are only degraded by high temperature, and group 4 the ones which are not degraded at all. (B) Selected examples for the four different degradation groups.

3.1.3 Quantitative ratiometric biosensors for the analysis of gibberellin signaling dynamics and metabolism

This chapter is based on the Andres et al. manuscript (**Appendix 7.1**) and contains selected results thereof.

The phytohormone gibberellin controls diverse aspects of developmental and growth processes such as seed germination, vegetative growth and flowering (Davière and Achard, 2013). As major regulators of developmental and growth processes, they are of great importance to plants. To analyze GA dynamics, sensitivity and specificity towards distinct GAs as well as certain GA metabolism aspects, we constructed gibberellin biosensors with all five DELLA proteins (RGA, GAI, RGL1-3), following the same modular design as the auxin and strigolactone biosensor (Wend et al., 2013; Samodelov et al., 2016). A RGA biosensor with a 17 amino acid deletion in the DELLA sequence (RGAΔ17) which should not react to GA induction was included as a control (Dill et al., 2001). We aimed at providing quantifications of the phytohormone gibberellin at high temporal resolution and a highly sensitive system to analyze gibberellin dynamics. To investigate the specificity and sensitivity of the distinct DELLAs towards known bioactive GAs, we transformed *A. thaliana* protoplasts transiently with these biosensors. 20 h later, the samples were induced with either GA_1, GA_3, GA_4 or GA_7 for 5 h. Afterwards, the luciferase activity was determined and the FF/REN ratios were analyzed. All five biosensors showed the highest sensitivity towards GA_4 and GA_7 with sensitivities below 10 pM (**Figure 18**) which makes them more sensitive than other established GA biosensors in *Xenopus* and *S. cerevisiae* (Khakhar et al.; Rizza et al., 2017). Especially the RGA-biosensor displays a high sensitivity towards GA_3, GA_4 and GA_7 with up to 70 % degradation at higher GA concentrations (more than 100 nM). The CtrlQuant sensor, containing a repetitive GA sequence instead of a sensor module, as well as the RGAΔ17 biosensor showed no degradation. Additional experiments with the proteasomal inhibitor MG132 demonstrated the dependency on the 26S proteasome (**Appendix 7.1**).

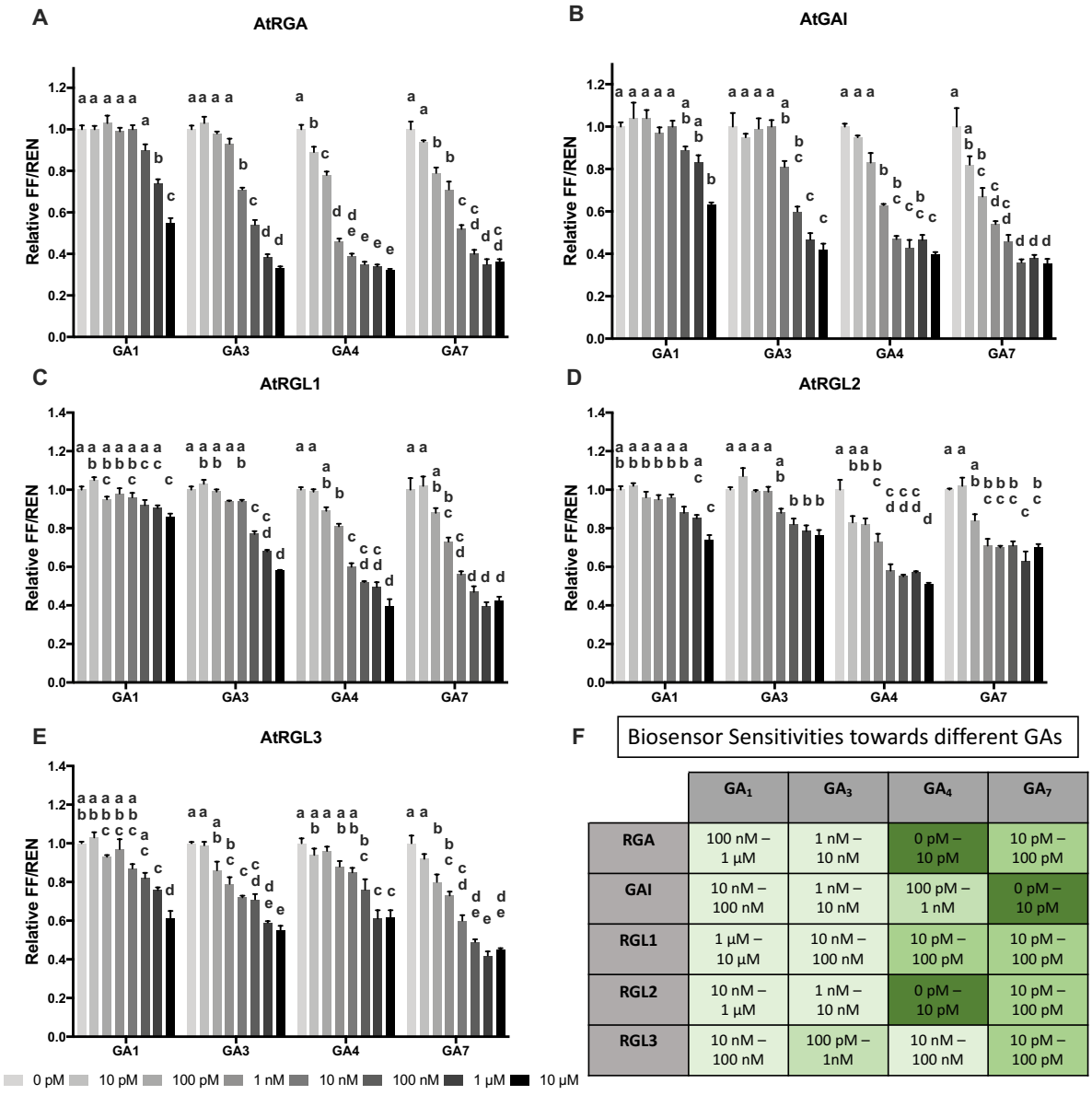

F Biosensor Sensitivities towards different GAs

	GA_1	GA_3	GA_4	GA_7
RGA	100 nM – 1 µM	1 nM – 10 nM	0 pM – 10 pM	10 pM – 100 pM
GAI	10 nM – 100 nM	1 nM – 10 nM	100 pM – 1 nM	0 pM – 10 pM
RGL1	1 µM – 10 µM	10 nM – 100 nM	10 pM – 100 pM	10 pM – 100 pM
RGL2	10 nM – 1 µM	1 nM – 10 nM	0 pM – 10 pM	10 pM – 100 pM
RGL3	10 nM – 100 nM	100 pM – 1nM	10 nM – 100 nM	10 pM – 100 pM

Figure 18: Sensitivity and specificity of RGA-, GAI-, RGL1-, RGL2- and RGL3-based biosensors towards the bioactive gibberellins GA_1, GA_3, GA_4 and GA_7. *A. thaliana* wildtype protoplasts were transformed with the different sensor constructs containing either **A)** RGA, **B)** GAI, **C)** RGL1, **D)** RGL2 or **E)** RGL3 as a sensor module (SM). 20h after transformation, the protoplasts were supplemented with serial dilutions ranging from 10 pM to 10 µM of either GA_1, GA_3, GA_4 or GA_7 for 5h. Afterwards, the luciferase activity was determined. The error bars represent the SEM (n = 6). The statistical significance between the different GA concentrations is indicated in lower case letters, where "a" significantly differs from "b", "b" from "c" and so on. One-way analysis of variance (ANOVA) were performed with $p < 0.05$ (for RGL1,2 and 3 with GA_1) or $p < 0.01$ (for RGA and GAI). **F)** Table summarizing the biosensor sensitivities towards the different bioactive gibberellins (dark green: sensitivity lower than 10 pM, green: sensitivity between 10 pM and 100 pM, lime-green: sensitivity between 100 pM and 1 nM, lime-green shade: sensitivity higher than 1 nM). This figure is adapted from the manuscript Andres et al. (**Appendix 7.1**).

After the characterization and further kinetic analyses of the RGA biosensor (**Appendix 7.1**), we chose this biosensor with the highest sensitivity to analyze selected metabolic aspects. For this, we co-transformed *A. thaliana* protoplasts with the RGA biosensor and three different GA2-oxidases which represent one main GA inactivation pathway. It has been shown for the GA2oxidases 1, 2, 3, 4 and 6 that they act specifically on C19-GAs including GA_1 and GA_4 by catalyzing the 2-β-hydroxylation of GA_4 to GA_{34} and GA_1 to GA_8 (**Figure 4**, Thomas et al., 1999; Rieu et al., 2008). On the contrary, GA2oxidase 7 and 8 catalyze the 2-β-hydroxylation of C20 GAs such as the common precursor GA_{12} (Schomburg et al., 2003). The RGA biosensor was applied to study the activity and specificity of GA2oxidase 1, 2 and 8 in protoplasts. 20 h post transformation, increasing concentrations of GA_1 and GA_4 from 1 nM to 10 µM were supplemented and luciferase activity was determined. Additionally, the RGA biosensor was co-transformed with a control vector that contains a small repeated GA sequence (GAGAGAGAGAGAGA) instead of a sensor module (Samodelov et al., 2016).

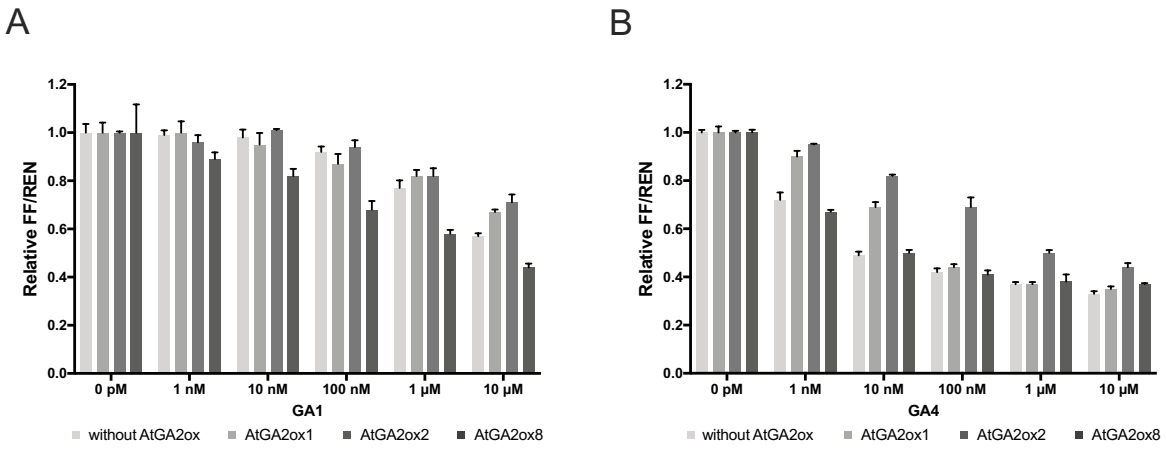

Figure 19: RGA biosensor as a tool to study the activity and specificity of GA oxidases in plant cells. *A. thaliana* wildtype protoplasts were transformed with the RGA biosensor construct and an additional GA2 oxidase (either GA2ox1, GA2ox2, GA2ox8 or a control). 20h after transformation, the protoplasts were supplemented with serial dilutions from 1 nM to 10 µM of GA_1 or GA_4 for 4h. Afterwards, luciferase activity was measured. The data shown in this graph correspond to one representative experiment of three independent technical replicates. The error bars represent the SEM (n = 6). This figure is adapted from Andres et al. (Appendix 7.1).

As depicted in **Figure 19A**, the dynamic range for degradation induced by GA_1 is not good enough to observe differences at low hormone concentrations. The first slight GA_1 inactivation by GA2Ox1 and 2 appears at 1 – 10 µM. However, the better dynamic range and high sensitivity of the RGA biosensor towards GA_4 allow to analyze the effect of GA2-oxidases on RGA-FF also at lower concentrations. The co-transformation of GA2ox1 and GA2ox2 with the RGA sensor led to less degradation compared to the control. Especially, GA2Ox2 has a huge effect on GA_4, whereas GA2ox1 displays only a moderate effect (**Figure 19B**). No effect could be observed for GA2Ox8 on GA_4. We could demonstrate by applying our novel, highly sensitive RGA biosensor that GA2Ox1 and GA2Ox2 inactivate bioactive C19 GAs such as GA_1 and GA_4

and convert them to non-bioactive catabolites. These non-bioactive catabolites are no longer able to induce degradation of RGA. Furthermore, we could not show any direct effect of GA2Ox8 on GA_4. This is in accordance with earlier results which indicate that GA2Ox8 only acts on C20 GAs (Schomburg et al., 2003). In summary, five biosensors comprising RGA, GAI, RGL1, RGL2 and RGL3 as sensor modules were built in the course of this work. The construct composition allows the highly sensitive analysis of intracellular changes upon exogenous application of GAs as well as their dynamic analysis. Therefore, the biosensors can be used as molecular proxies for the study of metabolic processes and the investigation of specificities and sensitivities towards different GAs and possible GA analogs. For the establishment of the GA biosensor system, we utilized proof of principle applications to demonstrate its applicability. However, the possible applications to study gibberellin perception and signaling are far from exhausted.

3.2 Reconstruction of Gibberellin signaling pathways in mammalian cells

The chapters 3.2.2, 3.2.3 and 3.2.4 contain experimental data being part of a collaborative project together with Tim Blomeier (Institute of Synthetic Biology, Heinrich-Heine University, Düsseldorf) who performed complementary microscopy experiments.

Up to date, there is a plethora of plant signaling-related open questions which cannot be answered with conventional analysis methods, such as plant breeding and mutant analysis. The complexity and the crosstalk between distinct signaling pathways *in planta* as well as the lack of quantitative methods require the implementation of new (synthetic biology) approaches to overcome these limitations and answer these questions in a quantitative manner. One of the approaches is the reconstruction of plant signaling pathways in mammalian cells. Phytohormone signaling related open questions comprise for instance i) binding of transcription factors to promoter regions and the influence of other transcription factors or transcriptional regulators on their binding affinities, ii) protein-protein interactions iii) the influence of exogenously applied phytohormones on protein-protein interactions as well as the necessity and the impact of additional proteins for these protein-protein interactions. To address these questions, we developed different orthogonal systems in mammalian cells in the course of this work. Mammalian cells as an orthogonal system provide reduced complexity, i.e. no crosstalk with other plant signaling pathways and components of the same pathway, and are therefore ideal to analyze single plant signaling components. For the establishment of the different systems, we decided to focus on gibberellin and gibberellin-associated signaling pathways. Dependent on the complexity of the interactions or bindings, we developed Mammalian-1-Hybrid (M1H) up to Mammalian-4-Hybrid (M4H) systems in human embryonic kidney (HEK) cells (**Figure 20**). All methods combined constitute a platform for the reconstruction of phytohormone signaling pathways.

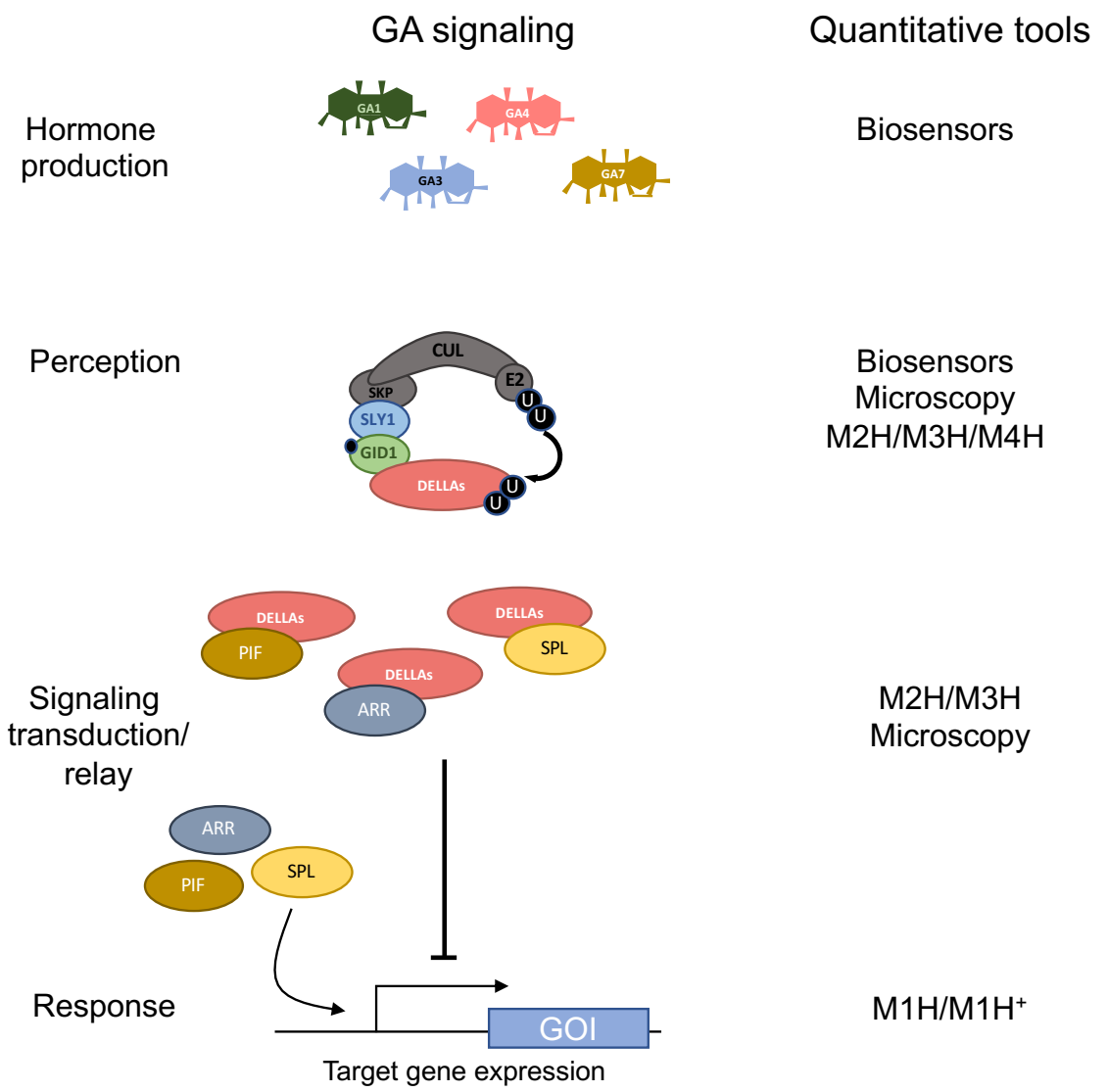

Figure 20: Gibberellin signaling scheme and quantitative tools for the study thereof. Our newly developed toolbox comprises quantitative approaches to study GA signaling on various level. Biosensors are utilized to investigate the hormone production as well as their perception. The perception complex formation level is also studied with M2H, M3H and M4H systems. In addition, microscopic analyses are applied to study perception complex formation as well as signaling transduction. To analyze signaling transduction/relay, we developed M2H and M3H systems. M1H and M1H$^+$ systems are employed to investigate downstream responses of GA signaling.

3.2.1 Development of a Mammalian-one-Hybrid system (M1H) for the investigation of transcription factor bindings to DNA-regions

The here presented experimental data are all obtained during the course of my PhD thesis and are part of a collaborative project with the group of Prof. Dr. G. Coupland (Max Planck Institute for plant breeding research).

Two of the numerous downstream targets of GA signaling are SPL9 and SPL15. These plant-specific transcription factors belong to the SQUAMOSA PROMOTER BINDING PROTEIN LIKE (SPL) family and are involved in the floral initiation in *A. thaliana* by directly activating transcription of floral regulators like FRUITFULL (FUL) (Wang et al., 2009; Hyun et al., 2016). SPL15 integrates external and internal cues including age (miRNA156 abundance) and GA signaling (DELLA abundance) to coordinate floral initiation (Hyun et al., 2016). Because of the immense importance of SPL9 and SPL15 in the flowering process we chose them for the establishment of a M1H system in HEK293T cells by i) studying whether they directly bind to the FRUITFULL promoter without any assistance of other plant-specific transcription factors and ii) investigating the binding site or the binding motif of SPL9 and SPL15.

To analyze the binding capacity of the SPLs to $P_{FRUITFULL}$ (P_{FUL}), we established an orthogonal M1H system. SPL9 and SPL15 were cloned with and without a C-terminal fusion of the transactivator Virus Protein 16 (VP16; Müller et al., 2013) and an additional nuclear localization sequence (NLS) under the control of P_{SV40}. The full length P_{FUL} version as well as two predicted binding regions (amplicon VII and X) were cloned upstream of a P_{CMV} minimal promoter controlling the expression of the secreted alkaline phosphatase (SEAP) as a reporter (**Figure 21**). Only upon binding of a transcription factor (here SPL9/SPL15) to the promoter region (here P_{FUL}) and the recruitment of the transcriptional machinery, SEAP will be expressed. Several transfection setups including different cell lines and temperature conditions were tested during this establishment process to guarantee optimal conditions. The synthetic constructs were co-transfected in HEK293T, HeLa and CHO-K1 cells to find a suitable one for the M1H experiments to enable good expression levels and a high dynamic range. In addition, different temperatures (30 °C and 37 °C) were tested to achieve an optimal environment for the plant transcription factors and promoters (data not shown). Finally, the best experimental setup constitutes co-transfection of both above-explained synthetic constructs in HEK293T cells at 37 °C. 24 h post transfection SEAP was measured.

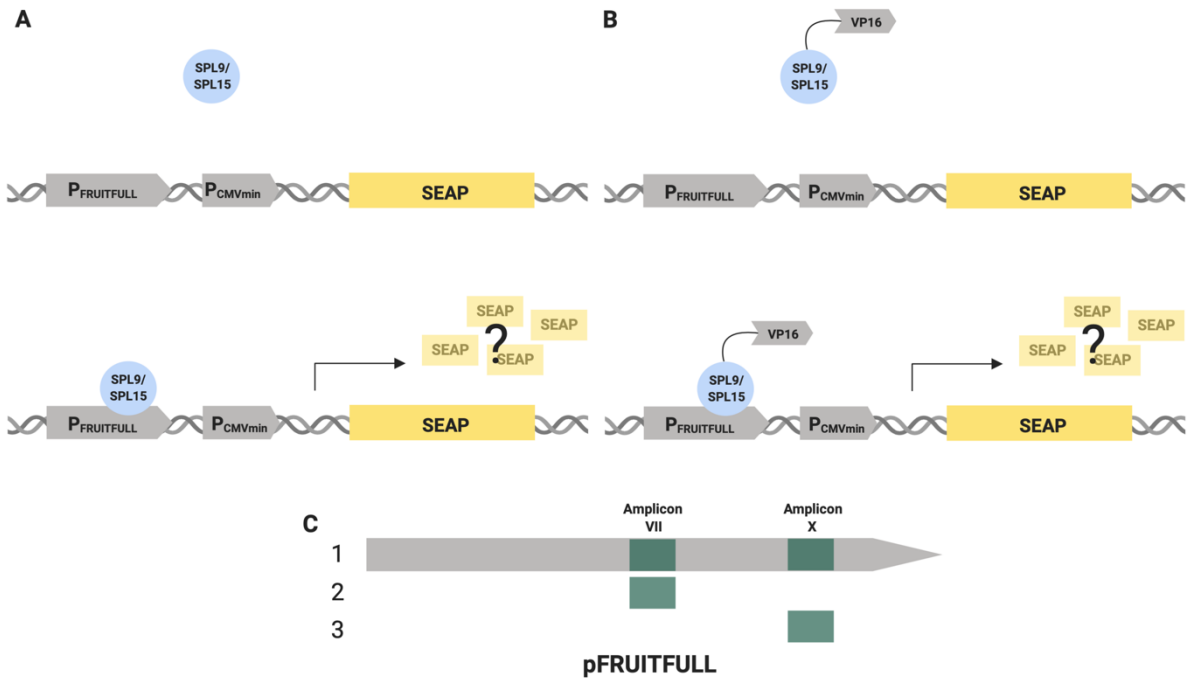

Figure 21: Schematic representation of tested M1H strategies. A plant transcription factor, here SPL9 or SPL15, is cloned under the control of a P_{SV40} promoter either without (A) or with (B) a VP16 transactivator C-terminally fused to it. A DNA-binding region of interest, here $P_{FRUITFULL}$, is cloned upstream of a P_{CMVmin} promoter controlling SEAP expression. If SPL9/SPL9-VP16 or SPL15/SPL15-VP16 bind to the $P_{FRUITFULL}$ promoter region and are able to recruit the transcriptional machinery, SEAP is expressed. (C) Schematic drawing of $P_{FRUITFULL}$. The full-length promoter with the amplicons VII and X annotated as possible SPL binding regions (1), as well as a short version with only amplicon VII (2) and amplicon X (3) are tested in this experimental setup. This figure was created with BioRender.

As depicted in **Figure 22A**, almost no basal activity was observed with the short amplicon versions of the P_{FUL} promoter. The basal activity or leakiness describes the basal expression of the reporter plasmid when transfected alone in absence of any additional plant transcription factor. The full-length version of the promoter alone showed a slightly increased leakiness (about 3 SEAP U/L) compared to the short version which was expected according to the size of the full-length promoter (more than 5 kB). The transfection of the P_{FUL} construct alone served as a negative control to exclude interference with endogenous transcriptional regulators in mammalian cells. Enhanced SEAP expression could only be observed when SPL9/SPL15-VP16 are co-transfected with the full-length version of the FRUITFULL promoter as well as with Amplicon X with induction folds of 13/8 (SPL9/SPL15-VP16 + P_{FUL} full length version) and 192/86 (SPL9/SPL15-VP16 + P_{FUL} amplicon X), respectively. To reduce the basal activity, especially of the large promoter constructs, the transfected reporter level was also decreased to ¼ of its originally transfected amount (**Figure 22B**). This caused an enormous increase in the dynamic range with a reduced basal activity for the P_{FUL} full length promoter version (approx. 1 U/L) with fold inductions of 27 (+SPL9-VP16) and 13 (+SPL15-VP16). For the short amplicon X, the fold inductions increased to more than 1,000 in combination with SPL9-VP15 and more than 500 for SPL15-VP16.

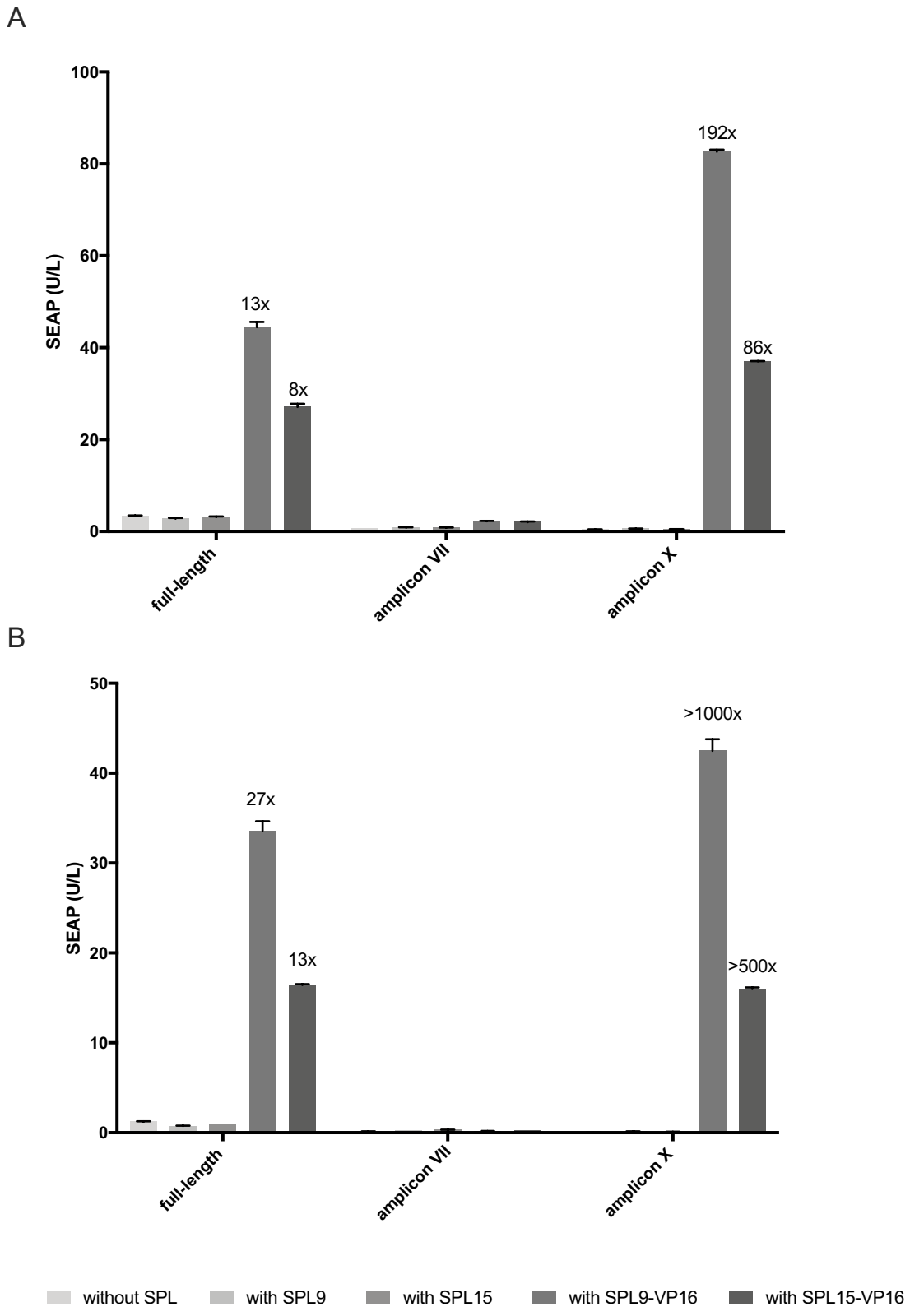

Figure 22: Establishment of a M1H system. (A) Experimental SEAP assay results. HEK293T cells were transfected with the indicated configurations and incubated for 24 h before the quantification of the SEAP reporter gene. (B) Experimental SEAP assay results with a reduced reporter plasmid amount. HEK293T cells were transfected with the same indicated configurations as in (A) and incubated for 24 h before the quantification of the SEAP reporter gene. To reduce the basal activity, the reporter plasmid amount is decreased to ¼ compared to (A). The data shown in these graphs correspond to one representative experiment of at least three independent technical replicates. The error bars represent the SEM for this individual experiment with *n*=4.

These results indicate that a transactivator domain (here: VP16) is necessary for the recruitment of the transcriptional machinery to promote SEAP expression. That does not necessarily imply that there is no binding of the SPLs to the FRUITFULL promoter without a transactivator domain, but rather that the plant-specific transcription factor is in this case not recognized by the endogenous transcriptional machinery and thereby cannot activate gene expression on its own in mammalian cells. Therefore, a transactivator such as VP16 is necessary to interact with various proteins during transcriptional initiation. In addition, our results indicate that there is no binding of both SPLs to Amplicon VII. Reducing the amount of promoter-reporter plasmid, led to an enormous increase in the dynamic range and a reduction in basal activity.

As this system was functional with highly reproducible and robust SEAP values, we took a closer look at the possible binding regions (amplicon VII and amplicon X). Therefore, we built mutated versions of the full-length FRUITFULL promoter as well as the two amplicons by replacing the putative binding motif GTAC (predicted by the group of G. Coupland) with ATAA or TTAA. We co-transfected HEK293T cells with the different versions of the FRUITFULL promoter and SPL9-VP16 or SPL15-VP16 (**Figure 23**).

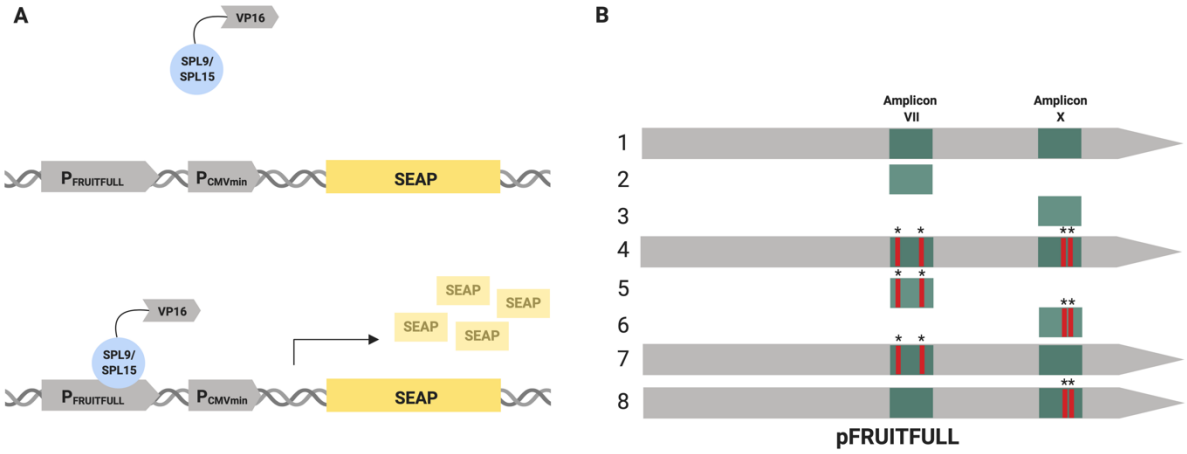

Figure 23: Schematic of a M1H system for the analysis of the TF-binding to a specific region within a promoter. (A) M1H system mode of function. The binding of SPL9/SPL15-VP16 to $P_{FRUITFULL}$ brings the VP16 transactivator in close proximity to the P_{CMVmin} promoter recruiting the transcriptional machinery and thus SEAP is expressed. (B) Different $P_{FRUITFULL}$ versions. 1: full-length, 2: amplicon VII, 3: amplicon X, 4: full-length with 2 mutation sites in each amplicon (marked in red with a star), 5: amplicon VII with 2 mutation sites, 6: amplicon X with 2 mutation sites, 7: full-length with 2 mutation sites in amplicon VII, 8: full-length with 2 mutation sites in amplicon X. This figure was created with BioRender.

As already observed in the previous experiments, both, SPL9-VP16 as well as SPL15-VP16, bind to the wt version and the short version containing P_{FUL} amplicon X. However, when amplicon X is mutated, both SPLs neither bind to the full-length nor the short P_{FUL} amplicon X

version. As both SPLs do not bind to amplicon VII anyway, the mutated version does not make a difference here as expected (**Figure 24**).

A

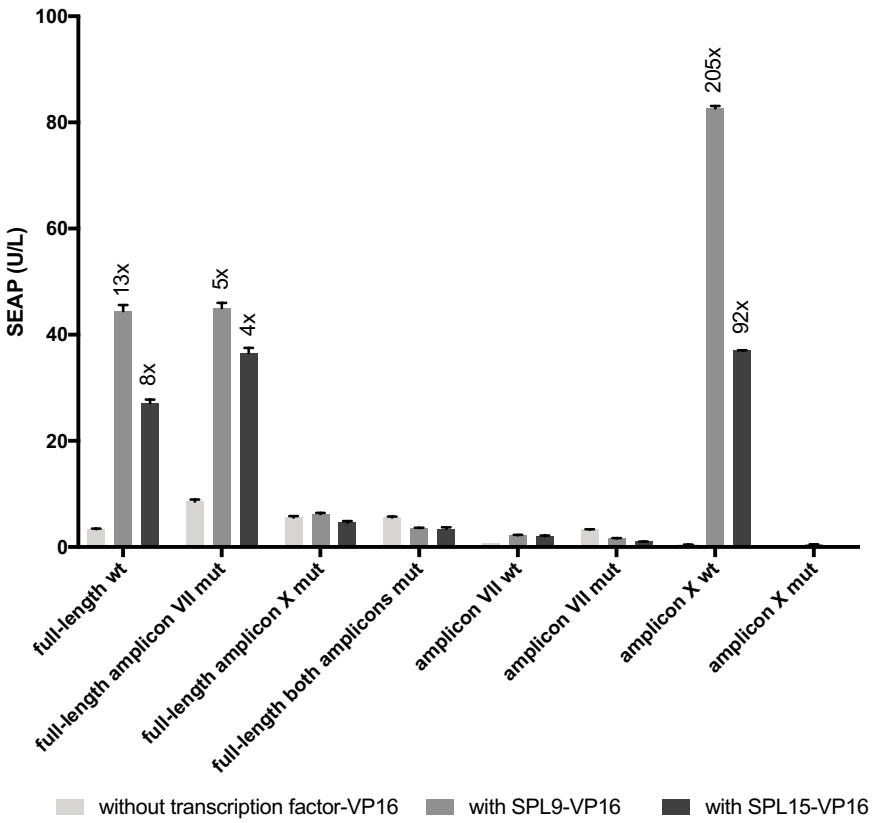

B

	SPL9-VP16	SPL15-VP16
full-length wt	Binding	Binding
full-length Amp VII mut	Binding	Binding
full-length Amp X mut	No binding	No binding
full-length Both amp mut	No binding	No binding
short Amp VII wt	No binding	No binding
short Amp VII mut	No binding	No binding
short Amp X wt	Binding	Binding
short Amp X mut	No binding	No binding

Figure 24: Binding of SPL9/SPL15-VP16 to different $P_{FRUITFULL}$ versions. A) SEAP assay results. HEK293T cells were transfected with the indicated configurations and incubated for 24 h before the quantification of the SEAP reporter gene. The data shown in this graph correspond to one representative experiment of at least three replicated experiments. The error bars represent the SEM for this individual experiment with *n*=4. Abbreviations: wt: wildtype, mut: mutated. (B) Summary table.

In this chapter, the development and implementation of a novel quantitative M1H system for investigating the binding of a plant-specific transcription factor to a promoter region in mammalian cells is described. With this system, we could show that SPL9-VP16 as well as SPL15-VP16 bind to the FRUITFULL promoter without the assistance of any other plant-specific factor. In addition, we determined the exact binding region of these two SPLs to the promoter. Furthermore, the results in this orthogonal mammalian cell-based system indicate that SPL9 and SPL15 are not able to activate the transcriptional machinery on their own, which suggests that they are not recognized by the endogenous transcriptional machinery in HEK293T cells. This newly built system is highly sensitive; even small nucleotide changes in promoter sequences can be detected and prevent the binding of a plant-specific transcription factor to a promoter region. This in turn can be translated into a highly quantitative readout, for instance SEAP. Moreover, the experimental setup for our M1H system is easy to implement; the cloning of the constructs is flexible and modular. Depending on the properties of the transcription factor of choice, it can be fused to a transactivator N- or C-terminally. During the course of this work, the toolbox was expanded with plasmids containing normalization elements (renilla, gaussia and cypridina luciferases) on the same readout plasmid.

3.2.2 Mammalian-one-Hybrid$^+$ (M1H$^+$) assays to analyze the effect of DELLAs as regulators of transcription factors

Next, we expanded our already established and robust, quantitative M1H system with an additional element. For this, we analyzed the effect of DELLA proteins on the binding of type-B ARABIDOPSIS RESPONSE REGULATOR 1 (ARR1) to synthetic *cis*-element sequences containing binding sites for ARR1 (TCS, Müller and Sheen, 2008). ARRs comprise a group of DNA-binding transcription factors mediating cytokinin signaling. Y2H and CHIP analyses revealed that DELLAs act as transcriptional co-activators promoting the binding of ARR1 to the TCS element (Marín-de la Rosa et al., 2015). To show that these questions can be answered in an orthogonal quantitative system like mammalian cells, which display good expression levels of functional plant-specific proteins and several options for quantitative readout systems (Wend et al., 2013; Beyer et al., 2015b), we co-transfected HEK293T cells with three constructs containing i) ARR1 (without and with a VP16 fusion and an NLS) under control of the P_{SV40} promoter ii) RGA or GAI (each without and with a VP16 fusion and an NLS) under control of the P_{SV40} promoter and iii) a TCS element upstream of a CMV minimal promoter with SEAP as a reporter gene.

The TCS element on its own showed almost no basal activity (**Figure 25**), whereas co-transfection with ARR1 increased the SEAP level by almost 200-fold without VP16 and more than 120-fold with VP16. Although both variants show similar SEAP expression levels, the leakiness in case of the ARR1-VP16 experiment is a bit higher (0,23 compared to 0,16 SEAP units without VP16) which explains the differences in SEAP unit enhancement. Nevertheless, the basal activity for both is really low, indicating that no mammalian TF is binding. The SEAP levels are further enhanced when RGA or GAI are added to the system (M1H$^+$, up to more than 300-fold in total) independent of the presence of VP16. These results indicate that RGA and GAI indeed promote ARR1-binding to the TCS element and that HEK293T cells provide an ideal system to observe and analyze co-activation (or de-activation/downregulation) of a plant-specific transcription factor. In this case, the M1H$^+$ system works without a transactivator demonstrating that not all plant-specific transcription factors necessarily require a transactivator to activate gene expression in mammalian cells. In the future, it would be interesting to show the deactivation, i.e. the repression of transcriptional activation through a transcriptional regulator.

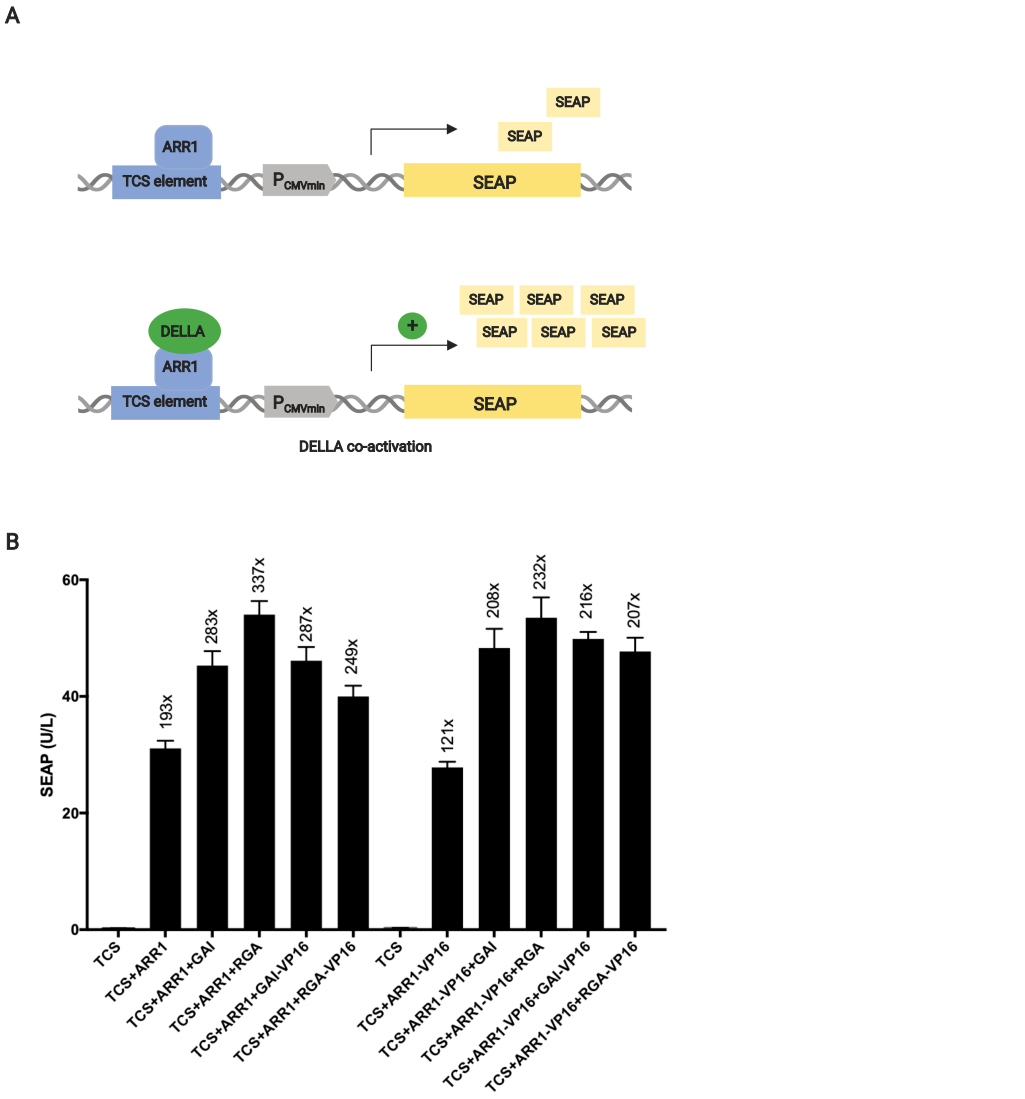

Figure 25: M1H$^+$ system to analyze DELLA co-activation activity. (A) Schematic drawing of the M1H$^+$ experimental setup. ARR1 is cloned under the control of a P_{SV40} promoter and the TCS element, which is the ARR1 DNA-binding element, upstream of a P_{CMVmin} promoter controlling SEAP expression. When ARR1 binds to the TCS element, it induces SEAP expression. Additionally, one DELLA (either RGA or GAI) is co-transfected with ARR1 and the reporter plasmid containing the TCS element to analyze a possible co-activation mediated by the DELLA protein. (B) SEAP assay results for the M1H$^+$ system establishment. HEK293T cell were transfected with the indicated configurations and incubated for 24 h before quantification of the SEAP reporter gene. The data shown in this graph correspond to one representative experiment of three independent technical replicates. The error bars represent the SEM for this individual experiment with *n*=4. Figure (A) was created with BioRender.

3.2.3 Mammalian-two-Hybrid (M2H) system to investigate protein-protein interactions

After having established M1H/M1H$^+$ systems to analyze the binding of a transcription factor to a promoter region, we aimed at introducing a quantitative M2H system in mammalian cells which would enable the investigation of plant protein-protein interactions. This novel synthetic tool is based on the constructs of the red light-inducible split transcription factor system by Müller *et al*. (2013). A bicistronic expression vector under the control of the SV40 promoter comprises: i) in the first cistron, one protein of interest (POI; in this case a DELLA protein) fused C-terminally to a VP16 transactivator domain, and ii) in the second cistron, a second protein of interest (here: PIF) N-terminally fused to a tetracycline repressor (tetR). Both cistrons are separated by a polioviral internal ribosome entry site ($IRES_{PV}$) that induces the translation of the second cistron. A second vector contains 13 repeats of the tetR-specific operator (tetO) fused via a spacer to a minimal human cytomegalovirus immediate early promoter (P_{CMVmin}) that controls SEAP expression (**Figure 26**). The tetR-POI fusion binds to its operator (tetO) and if both proteins of interest interact, VP16 comes in close proximity to the P_{CMV} minimal promoter, recruits the transcriptional machinery and thus activates SEAP gene expression. DELLAs, as the central regulators in GA signaling, have been reported to interact with PIFs and thereby block their ability to bind DNA (Feng et al., 2008; Li et al., 2016; Zheng et al., 2016). As the proposed interaction mechanism is the sequestration of PIFs from promoter regions by DELLA proteins, we determined whether DELLAs and PIFs interact per se without any other factors being involved in our orthogonal mammalian system. Both above described plasmids were co-transfected in HEK293T cells and 48 h post transfection, SEAP units were determined. As illustrated in **Figure 26B**, the reporter plasmid alone shows almost no basal activity, whereas a constitutive tetR-VP16 expression vector (positive control) co-transfected with the reporter plasmid enhances the SEAP expression level to more than 13 SEAP unit/L. Only when GAI is co-transfected with PIF1, we could observe an increase in SEAP expression levels of about 4-fold compared to the reporter level. This indicates an interaction between GAI and PIF1.

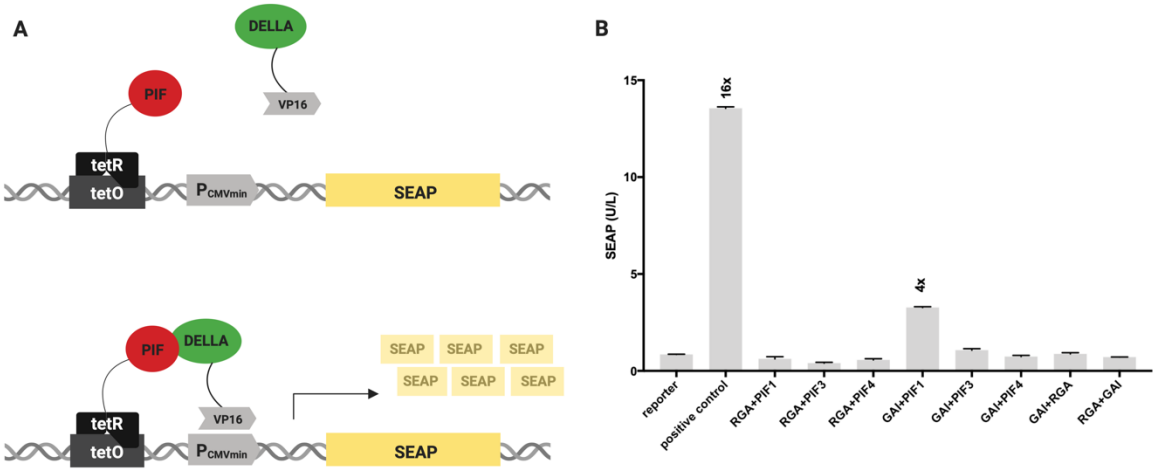

Figure 26: Design and validation of the split transcription factor system for the analysis of protein-protein interactions. (A) Mode of function of the split TF system (M2H). The two building blocks for the M2H system are encoded on a bicistronic expression vector under the control of the P_{SV40}. In the first cistron, the DELLA protein is C-terminally fused to a VP16 transactivator and an NLS. In the second cistron, a tetracycline repressor (TetR) is N-terminally fused to a PIF protein. A polioviral internal ribosome entry site, $IRES_{PV}$, induces the translation of the second cistron. The response vector comprises 13 repeats of the TetR-specific operator tetO. PIF is tethered via TetR to the $tetO_{13}$ operator site and if PIF and DELLA interact, VP16 recruits the transcription initiation complex thereby triggering activation of transcription from P_{CMVmin} (modified from Müller et al., 2013). (B) Validation of the split TF system. HEK293T cells were transfected with the indicated configurations and the response vector. After incubation for 48 h, SEAP activity was quantified. The positive control contains a TetR-VP16 fusion under the control of P_{SV40} with the response plasmid. The data shown in this graph correspond to one representative experiment of three independent technical replicates. The error bars represent the SEM for this individual experiment with *n*=4. Figure (A) was created with BioRender.

Additional to the M1H and M1H$^+$ systems, we could establish a M2H system based on the split transcription factor system by Müller et al. (2013) to investigate protein-protein interactions. This new system allows the observation of a hormone-independent GAI-PIF1 interaction. For the other combinations with PIF3 and PIF4, no increase in SEAP expression and thus no interaction could be determined, although there is evidence that PIF1, 3 and 4 interact with RGA and GAI (Gallego-Bartolome et al., 2010; Li et al., 2016). To exclude false negative results, for instance caused by steric hindrance effects, the opposite fusions directions have to be tested, namely tetR-DELLA and PIF-VP16. As we are working in an orthogonal system here, it might be possible that other components, that facilitate or mediate this interaction, might be missing. Another possible explanation could be that PIF3 and PIF4 interact with the DELLA proteins when bound to the promoter. To investigate this thesis, the M1H+ system could be utilized.

3.2.4 Mammalian-three-Hybrid (M3H) assays for the analysis of gibberellin-induced protein-protein interactions during GA perception

Protein-protein interactions are difficult to analyze in plants due to the complexity of different signaling pathways and the possible influence of other factors present. We built a novel system to investigate the gibberellin-induced interaction between distinct proteins involved in GA perception (M3H) and the order of complex-formation during GA perception (M4H). Gibberellin perception and signaling comprise three key components: i) GA receptors (GID1a, -b and -c), ii) a F-Box protein associated to a SCF E3 ubiquitin-ligase complex (SLY1), and iii) regulators proteins (DELLA proteins: RGA, GAI, RGL1, RGL2 and RGL3). Starting off with RGA/GAI and GID1a/b/c, we aimed at investigating all hormone-independent or -dependent interactions. For this, we utilized the bicistronic expression vector system (Müller et al., 2013) and constructed two different variants where either RGA/GAI are fused to VP16 and tetR is fused to GID1a/b/c, or vice versa to detect and eliminate false negative results (**Figure 27A**). The different constructs were co-transfected with our reporter plasmid in HEK293T cells and 24 h post transfection induced with 10 µM gibberellic acid acetoxymethyl ester (GA_3-AM) dissolved in DMSO or DMSO as a control. GA_3-AM is a synthetic GA analog which is cell permeable and cleaved by cytosolic esterases to release functional GA_3. Previous studies showed the functionality of GA_3-AM in mammalian cells (Miyamoto et al., 2012). Therefore, this was the first GA to be tested in the M3H experiments. 24 h post hormone induction, SEAP was measured in a microplate reader. As illustrated in **Figure 27B**, there is no autoactivation of the system when the reporter plasmid alone is transfected, whereas the SEAP level is enhanced to 25 SEAP U/L in the positive control (constitutive tetR-VP16) in a hormone-independent fashion as expected. The DMSO controls show no increase in SEAP expression for all twelve combinations (**Figure 27B+D**). However, the combinations of DELLA-VP16 and tetR-GID1 (**Figure 27A**) reveal a GA_3-AM-dependent enhancement in SEAP expression with up to 13 SEAP U/L for the strongest combination of GAI and GID1b (**Figure 27B**). On the contrary, the alternative protein-fusion configuration (GID1-VP16 and tetR-DELLA) had a much weaker SEAP production with a maximum of less than 2 SEAP U/L (**Figure 27C**). As depicted in **Figure 27B**, the orientation of DELLA-VP16 and tetR-GID1 shows a more efficient SEAP production and thus no interaction interference. Hereafter all experiments shown were performed with this protein-fusion combination.

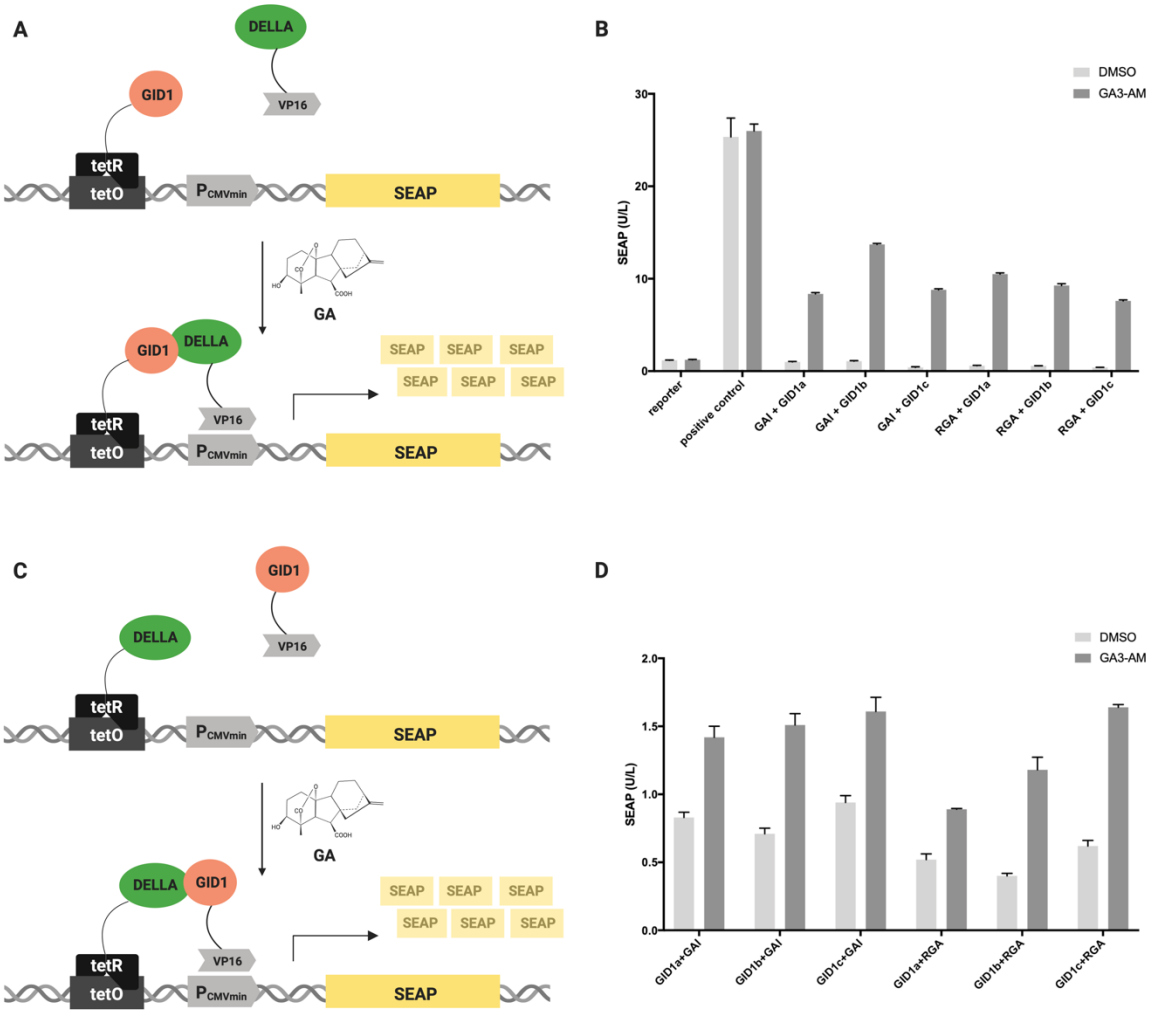

Figure 27: Design and validation of a M3H split transcription factor system. (A) Mode of function of the split TF system. The two building blocks for the split TF system are encoded on a bicistronic expression vector under the control of the P_{SV40}. In the first cistron, the DELLA protein is C-terminally fused to a VP16 transactivator and an NLS. In the second cistron, a tetracycline repressor (TetR) is N-terminally fused to GID1. A polioviral internal ribosome entry site, $IRES_{PV}$, induces the translation of the second cistron. The response vector comprises 13 repeats of the TetR-specific operator tetO. GID1 is tethered via TetR to the $tetO_{13}$ operator site and if GID1 and DELLA interact upon induction with GA_3-AM, VP16 recruits the transcription initiation complex thereby triggering activation of transcription of SEAP expression via P_{CMVmin} (modified from Müller et al., 2013). (B) Validation of the split TF system. HEK293T cells were transfected with the indicated configurations in combination with the response vector. After incubation for 24 h, medium containing either 10 µM GA_3-AM or the same volume of DMSO as a control was added, followed by 24 h incubation before SEAP activity quantification. The positive control contains a TetR-VP16 fusion under the control of P_{SV40} with the response plasmid. (C) Mode of function of the Split TF system. The setup is the same as in (A) except from the protein fusions within the bicistronic expression vector. In this experimental setup, GID1 is C-terminally fused to a VP16 transactivator whereas TetR is N-terminally fused to a DELLA protein. (D) Validation of the split TF system. The experimental setup is the same as in (B). The data shown in these graphs correspond to one representative experiment of three independent technical replicates. The error bars represent the SEM for this individual experiment with *n*=4. Figure (A) and (C) were created with BioRender.

Next, the endogenous, natural gibberellins GA_3 and GA_4 of *A. thaliana* were applied instead of GA_3-AM. Following the same experimental setup, the co-transfected cells were induced with GAs 24 h post transfection and after additional 24 h SEAP was determined. Since GA_3 and GA_4 are dissolved in ethanol, the latter is utilized as a control (instead of DMSO). As it was

unclear before these experiments whether GA_3 and GA_4 could efficiently enter mammalian cells, we used 100 µM instead of 10 µM of the hormones.

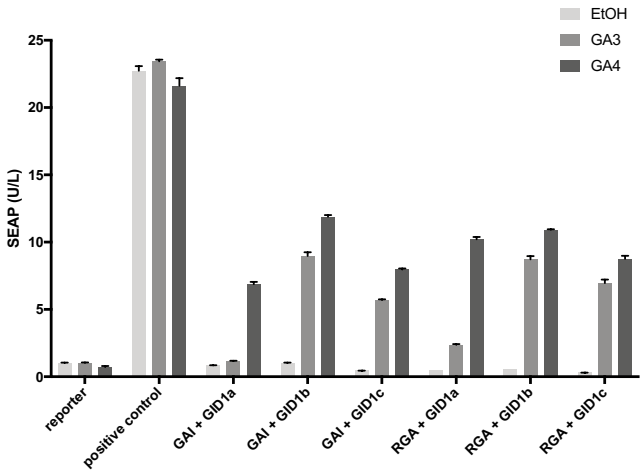

Figure 28: Validation of the M3H split TF system with natural gibberellins. HEK293T cells were transfected with the indicated configurations in combination with the response vector (reporter). After incubation for 24 h, medium containing either 100 µM GA_3, GA_4 or the same amount of EtOH as a control was added with a following incubation step of another 24 h before SEAP activity quantification. The positive control contains a TetR-VP16 fusion under the control of P_{SV40} with the response plasmid. The data shown in this graph correspond to one representative experiment of three independent technical replicates. The error bars represent the SEM for this individual experiment with *n*=4.

When induced with GA_4, the SEAP values were similar to the ones obtained with GA_3-AM, with more than 10 SEAP U/L for the GAI-GID1b combination and slightly lower values for the other combinations (**Figure 28**). The pattern for the combinations GAI and RGA with GID1a with GA_3 seems to differ from the other two GAs. Here, almost no interaction could be observed whereas the other combinations were similar to the other GAs. The fact that GA_3 induces interactions between GAI/RGA and GID1b/c clearly shows that GA_3 enters the cell and is functional, indicating that the GID1a-GA_3 binding itself might be affected. It has been shown that GA_3 displays an inefficient membrane permeability (at physiological pH) because of a negatively charged carboxylic acid group (Miyamoto et al., 2012). Therefore, the group of Miyamoto et al. masked this negatively charged carboxylic acid by using an acetoxymethyl (AM) group to increase cell permeability. It could be possible that only a small amount of GA_3 enters the HEK293T cells which is sufficient for the GID1b/c binding to RGA and GAI due to the high sensitivity of these interactions. However, the GID1a-GAI/RGA interaction seems to be less sensitive indicating that more GA_3 is needed for its induction. Future experiments should include titration curves with higher concentrations of GA_3 (as they were performed here with GA_3-AM, **Figure 29**).

To test if the applied GA_3-AM amount in the previous experiment (**Figure 27**) already saturates the GID1a-GA_3-AM binding, titration curves were performed with increasing concentrations from 100 pM to 10 µM GA_3-AM. As depicted in **Figure 29**, the supplementation of 100 nM GA_3-

AM leads to an increase in SEAP expression indicating that low GA_3-AM concentrations already induce the GID1a-GAI/RGA binding. Further experiments, with GA_3-AM concentrations ranging from 1 µM to 10 µM, demonstrated that the system is already saturated at 3 µM GA_3-AM supplementation (data not shown).

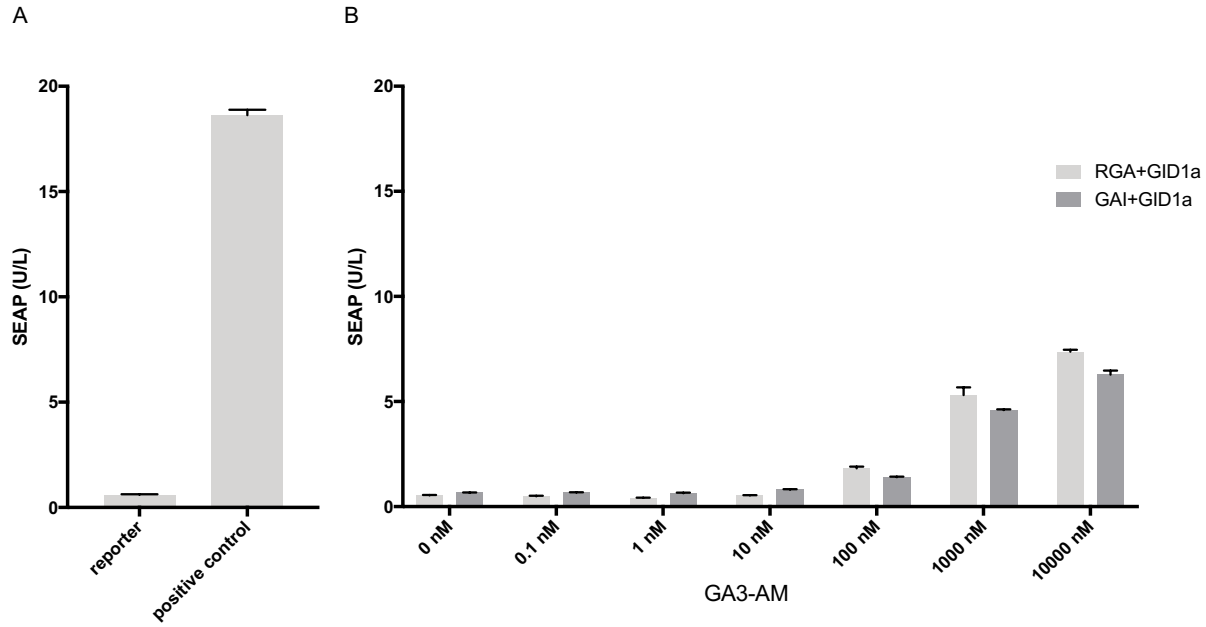

Figure 29: Dose-response curve for the GA_3-AM dependent interaction of RGA/GAI with GID1a. (A) SEAP assay with corresponding controls. HEK293T cells were transfected with the indicated configurations: the response vector alone (reporter) and a positive control containing the response vector and a tetR-VP16 fusion under the control of a P_{SV40} promoter. (B) SEAP assay with the dose-response curves for RGA/GAI and GID1a. HEK293T cells were transfected with RGA+GID1a and GAI+GID1a in combination with the response vector. After incubation for 24 h, medium containing the indicated GA_3-AM concentrations was added with a following incubation step of 24 h before SEAP activity quantification. The data shown in this graph correspond to one representative experiment of three independent technical replicates. The error bars represent the SEM for this individual experiment with *n*=4.

In these first experiments, we could show that DELLAs and GID1s seemed to have a preferred fusion site, at least in this kind of interaction analysis. Nevertheless, both fusion sites are possible, which makes the system flexible for other protein pairs to be tested. In addition, we could show the hormone-dependent interaction between RGA/GAI and the GID1s for all combinations with GA_3-AM and GA_4. This was demonstrated for the first time in a quantitative manner during this work. Furthermore, these experiments revealed the functionality of natural GAs like GA_3 and GA_4 in mammalian cells. In the future, experiments with a decreased hormone concentration could be conducted. In summary, we were able to extend our M2H assays with a third component: the phytohormone gibberellin. Future experiments with other hormones could follow.

The next combinations to test with this newly established system were the putative interactions between RGA/GAI and GID1 with SLY1. For this, we kept the protein-fusions which were already running in this system, namely DELLA-VP16 and tetR-GID1, and complemented them with the corresponding SLY1 fusions (**Figure 30A+B**). The experiments were conducted as described above and SEAP activity was determined. As illustrated in **Figure 30C**, no increase

in SEAP expression could by observed for any combination neither hormone-dependent nor -independent. However, this experiment needs to be repeated with the opposite fusion configurations, namely SLY1-VP16 + tetR-DELLA and GID1-VP16 + tetR-SLY1, to exclude false negative results due to steric hindrance effects.

In summary, this indicates that SLY1 is not interacting with any of the mentioned candidates which leads to the question about the gibberellin complex formation order.

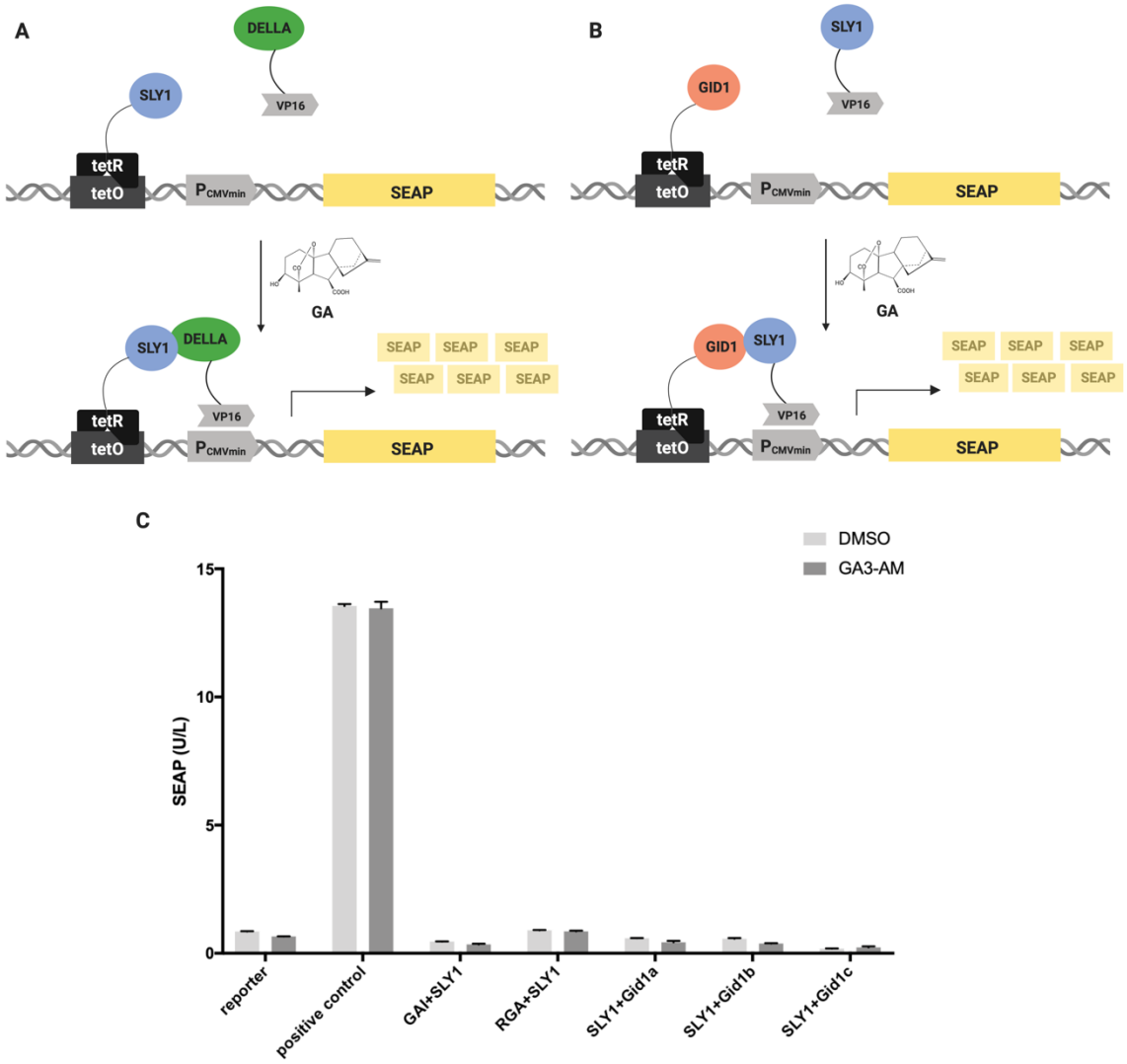

Figure 30: Design and validation of a M3H split transcription factor system. (A) Mode of function of the split TF system. The two building blocks for the split TF system are encoded on a bicistronic expression vector under the control of the P_{SV40}. In the first cistron, the DELLA protein is C-terminally fused to a VP16 transactivator and an NLS. In the second cistron, a tetracycline repressor (TetR) is N-terminally fused to SLY1. A polioviral internal ribosome entry site, $IRES_{PV}$, induces the translation of the second cistron. The response vector comprises 13 repeats of the TetR-specific operator tetO. SLY1 is tethered via TetR to the $tetO_{13}$ operator site and if SLY1 and DELLA interact upon induction with GA_3-AM, VP16 recruits the transcription initiation complex and thereby triggers

activation of P_{CMVmin} and SEAP expression. (B) Mode of function of the split TF system. The setup is the same as in (A) except from the protein fusions within the bicistronic expression vector. In this experimental setup, SLY1 is C-terminally fused to a VP16 transactivator whereas TetR is N-terminally fused to GID1. (C) Validation of the split TF system. HEK293T cells were transfected with the indicated configurations in combination with the response vector. After incubation for 24 h, medium containing either 10 µM GA_3-AM or the same amount of DMSO as a control was added with a following incubation step of another 24 h before SEAP activity quantification. The positive control contains a TetR-VP16 fusion under the control of P_{SV40} with the response plasmid. The data shown in this graph correspond to one representative experiment of three replicated experiments. The error bars represent the SEM for this individual experiment with *n*=4. Figure (A) and (B) were created with BioRender.

3.2.5 Mammalian-four-Hybrid (M4H) system for the investigation of the order of complex-formation during GA perception

After the three main GA perception components (GID1, SLY1 and DELLA) have already been tested for their hormone-dependent or -independent interactions amongst each other with our M3H system, we were now interested in the order of GA perception complex formation. First evidence was provided in the M3H tests which indicated that only RGA/GAI and GID1 interact hormone-dependent, whereas SLY1 neither interacted with RGA/GAI nor with GID1. To investigate this complex-formation process further, we developed a M4H assay. In this assay, we utilized the already tested bicistronic vector encoding SLY1-VP16 and tetR-GID1. An additional plasmid containing RGA/GAI under the control of the SV40 promoter was supplemented to the transfection setup as well as the reporter plasmid (**Figure 31B**). The three plasmids were co-transfected and the samples were induced with GA_3-AM as already explained earlier, SEAP values were determined 48 h post transfection.

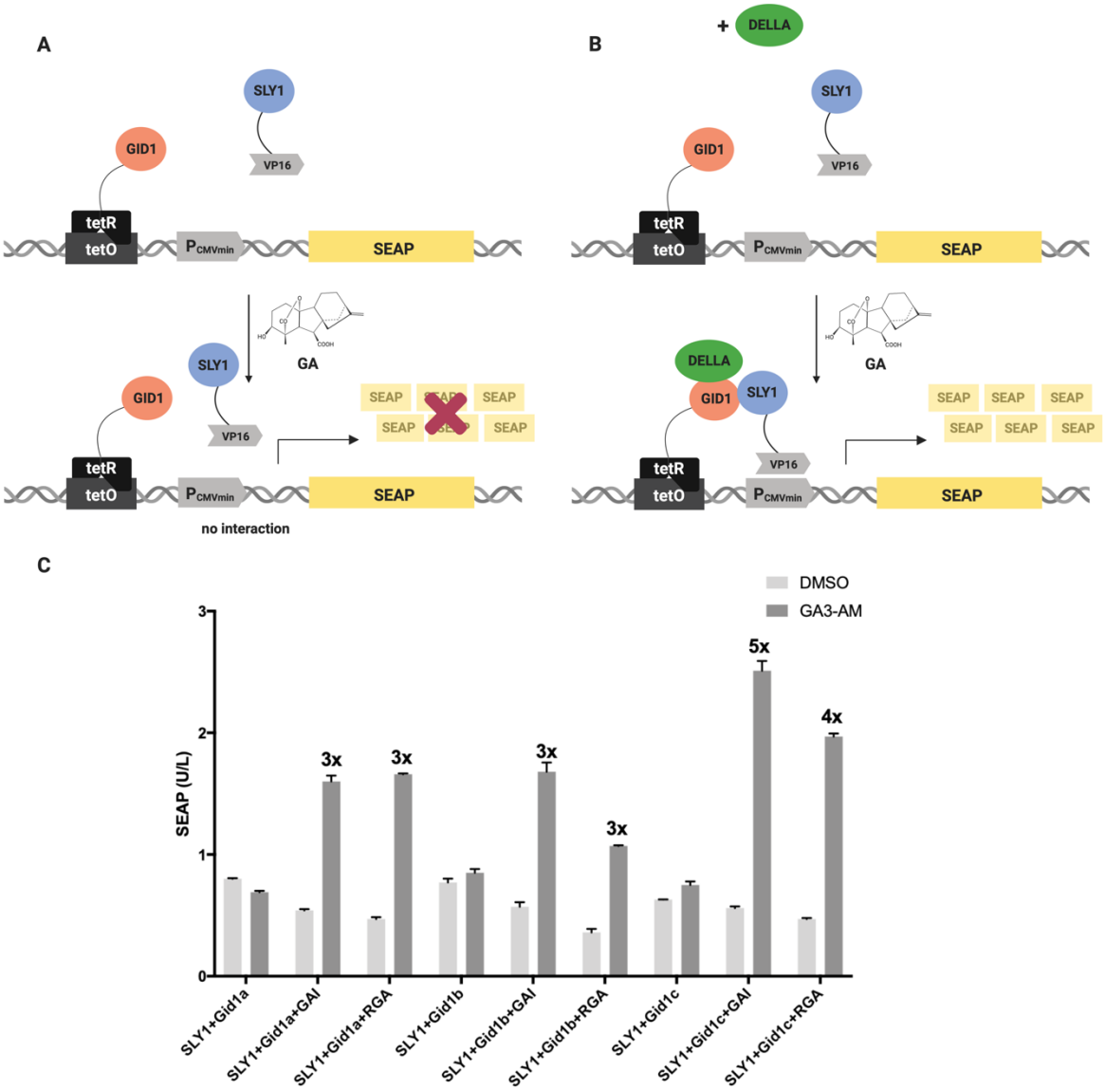

Figure 31: Design and validation of a M4H split transcription factor System. (A) Mode of function of the M3H split TF system. The two building blocks for the split TF system are encoded on a bicistronic expression vector under the control of the P_{SV40}. In the first cistron, SLY1 is C-terminally fused to a VP16 transactivator and an NLS. In the second cistron, a tetracycline repressor (TetR) is N-terminally fused to GID1. A polioviral internal ribosome entry site, $IRES_{PV}$, induces the translation of the second cistron. The response vector comprises 13 repeats of the TetR-specific operator tetO. GID1 is tethered via TetR to the $tetO_{13}$ operator site and if GID1 and SLY1 interact upon induction with GA_3-AM, VP16 recruits the transcription initiation complex and thereby triggers activation of P_{CMVmin} and SEAP expression. (B) Extension of the M3H system in (A) to a M4H system. In addition to the experimental setup in (A) a DELLA-containing plasmid is added to the system. (C) Validation of the M4H system. HEK293T cells were transfected with the indicated configurations in combination with the response vector. After incubation for 24 h, medium containing either 10 µM GA_3-AM or the same amount of DMSO as a control was added with a following incubation step of another 24 h before SEAP activity quantification. The data shown in this graph correspond to one representative experiment of three independent technical replicates. The error bars represent the SEM for this individual experiment with *n*=4. Figure (A) and (B) were created with BioRender.

As already observed in the previous experiments, no hormone-independent and -dependent interactions between SLY1 and GID1a, b and c could be monitored. However, supplementing RGA or GAI exogenously (from a different plasmid) to this split transcription factor system leads to a 3- to 5-fold increase in SEAP expression when GA_3-AM is present (**Figure 31C**). Therefore, RGA or GAI is necessary to form this GA-dependent perception complex with SLY1 and GID1. All experiments taken into account, our M3H and M4H systems reveal the order of GA complex formation. In the presence of GA, it is bound by the receptors GID1a, b and c and as a consequence, DELLA proteins interact with the GA-GID1 complex. Next, the F-Box SLY1, being engaged in a SKP1/CUL1/F-box E3 ubiquitin ligase complex (SCF^{SLY1}*),* associates to this perception complex and GA downstream signaling can proceed. This order of complex formation is supported by earlier results in Y3H systems in yeast (Griffiths et al., 2006).

In conclusion, we have established quantitative synthetic biology approaches to screen and analyze various TFs and their bindings to promoter regions as well as hormone-dependent and -independent protein-protein interactions. We have expanded our toolbox for the investigation of plant signaling components in mammalian cells as an orthogonal system by adding M1H up to M4H systems. These novel systems allow not only the reconstruction of perception complex formation, but also the identification and analysis of the order of this complex formation for the first time in mammalian cells. Our M3H and M4H systems provide a powerful platform to analyze complex formation also for other plant hormones and an expansion to already existing methods in plants. Our systems are robust and display a high dynamic range, signal-to-noise ratio as well as sensitivity. Even nucleotide changes within a promoter region can be detected. In addition, all systems show no or only little leakiness. Taken all established systems in account, we cover a broad spectrum of distinct quantitative readouts and systems with the potential uses for the analysis and reconstruction of single plant signaling pathways being far from exhausted.

4 Conclusion

In conclusion, synthetic biology tools were designed, constructed and applied to address key challenges in the field of phytohormone research:

First, numerous quantitative genetically encoded phytohormone biosensors were constructed towards the analysis of strigolactone, auxin and gibberellin signaling. The biosensors were designed following the principles of a previous auxin sensor in our lab by Wend et al. (2013). For the deeper analysis of strigolactone perception and the role of eight SMXL-regulators, all SMXLs were cloned into the biosensor platform and characterized towards their degradation behavior in response to *rac*-GR24, Kar1 and Kar2. In addition, several strigolactone/karrikin signaling mutant protoplasts were transformed to obtain the first quantitative data about SMAX1 and SMXL2 degradation and their role in strigolactone/karrikin signaling. The combinatorial approach of the production of experimental quantitative data and mathematical modeling revealed novel information about the dynamic behavior of the StrigoQuant sensor incorporating SMXL6 as a sensor module (Samodelov et al., 2016) as well as the D14 receptor. Moreover, the most comprehensive Aux/IAA degradation study in *A. thaliana* protoplasts was conducted by investigating the degradation of all 29 Aux/IAAs in response to IAA. The knowledge of their differential degradation behavior led to the hypothesis that other external stimuli, such as temperature, might affect Aux/IAA stability which could be verified in another screening for some of them. A future challenge will be to unveil the mechanism of temperature-dependent degradation. Furthermore, gibberellin biosensors comprising each one DELLA protein were applied to investigate their specificities and sensitivities towards distinct bioactive and non-bioactive GAs. Because of their high sensitivity and a good dynamic range, the biosensors allowed answering GA-related metabolic questions in protoplasts.

Second, mammalian cells as an orthogonal system were utilized to answer remaining questions that cannot be answered in plant systems due to the complexity and redundancy of plant signaling pathways. For this, different levels of GA signaling were investigated for the establishment of M1H – M4H systems. These systems allow for the analysis on the level of TF binding to a specific DNA-binding region, phytohormone-independent and -dependent analysis of protein-protein interactions as well as even the reconstruction of complex formation.

Finally, distinct methods and tools in protoplasts as well as mammalian cells were introduced to collectively answer open questions regarding phytohormone signaling. Mathematical modeling approaches were combined with quantitative experimental data to obtain new insights on mechanistic aspects.

In addition to the synthetic biology approaches presented here, a comprehensive analysis of synthetic switches in bacteria, mammalian cells and plants are extensively discussed in the following review.

Update on Synthetic Switches and Regulatory Circuits

Synthetic Switches and Regulatory Circuits in Plants[1][OPEN]

Jennifer Andres,[2] Tim Blomeier,[2] and Matias D. Zurbriggen[3,4]

Institute of Synthetic Biology and CEPLAS, University of Düsseldorf, 40225 Duesseldorf, Germany

ORCID ID: 0000-0002-3523-2907 (M.D.Z.).

Synthetic biology is an established but ever-growing interdisciplinary field of research currently revolutionizing biomedicine studies and the biotech industry. The engineering of synthetic circuitry in bacterial, yeast, and animal systems prompted considerable advances for the understanding and manipulation of genetic and metabolic networks; however, their implementation in the plant field lags behind. Here, we review theoretical-experimental approaches to the engineering of synthetic chemical- and light-regulated (optogenetic) switches for the targeted interrogation and control of cellular processes, including existing applications in the plant field. We highlight the strategies for the modular assembly of genetic parts into synthetic circuits of different complexity, ranging from Boolean logic gates and oscillatory devices up to semi- and fully synthetic open- and closed-loop molecular and cellular circuits. Finally, we explore potential applications of these approaches for the engineering of novel functionalities in plants, including understanding complex signaling networks, improving crop productivity, and the production of biopharmaceuticals.

Signaling processes are central to the organization and existence of any form of life. Exogenous and endogenous inputs are sensed and integrated by molecular networks in cells with feedback loops and Boolean logic decision making, resulting in a specific response (output). For this purpose, regulatory circuits are structured as a tightly and finely coordinated network of information with transfer and processing steps and chains, each individually fulfilling a specific task. These processes are in turn organized in time and space: within subcellular compartments (membranes, organelles, cytosol, and nuclei) and between cells and tissues. Signal mediators include proteins, nucleic acids, and small molecules (Lim, 2010). A key characteristic of biological regulatory networks is their modular architecture, in which building blocks are assembled in a combinatorial fashion. The constituent individual components perform a given distinct, particular function within the network, be it signals per se or switches (i.e. components that are able to detect an input signal and transform it into an output cue; Stein and Alexandrov, 2015).

Plants have evolved complex networks to integrate environmental, genetic (via spatial and temporal cues), developmental, and metabolic programs as well as the current physiological status. The output is a response tailored to adjust the cell welfare and function in the context of a multicellular organism (Trewavas, 2005; Sheen, 2010). These systems are constantly active, monitoring the ever-varying conditions and executing outputs following both open- and closed-loop programming principles for optimal responses. Recent advances in molecular biology, genetics, and systems biology-associated technologies have led to the identification of a huge number of signaling components, cascades, and regulatory mechanisms thereof. The field of plant signaling is growing rapidly, as is our knowledge of the complexity of these networks (Jaeger et al., 2013; Lavedrine et al., 2015). Most signaling pathways comprise many components and exhibit redundancy of function, extensive feedback control, and cross-interaction with other networks. The fine-tuning involves different types of posttranslational modifications, as exemplified by the complex mesh integrating light and hormone signaling, the circadian clock, and developmental and growth processes (Pokhilko et al., 2013; Fogelmark and Troein, 2014). In addition, there is a lack of quantitative molecular tools to interrogate and monitor the dynamics of these systems (Liu and Stewart, 2015; Samodelov and Zurbriggen, 2017). This not only hinders a comprehensive understanding of the function, regulation, and effects of signaling circuits but also the targeted manipulation of metabolic and signaling networks and, consequently, the introduction of novel functionalities into plants. In combination with modern analytical technologies, synthetic biology approaches represent the key to overcoming these limitations, and they are currently revolutionizing fundamental bacterial, yeast, and metazoan research as well as the biotechnology and biomedicine industries (Lu et al., 2009; Lienert et al., 2014).

[1]This work was supported by the Excellence Initiatives of the German Federal States Governments (DFG, EXC-1028-CEPLAS), a stipend from the Max-Planck-Gesellschaft (Max Planck Society), the University of Düsseldorf, and the University of Cologne.

[2]These authors contributed equally to the article.

[3]Author for contact: matias.zurbriggen@uni-duesseldorf.de.

[4]Senior author.

J.A., T.B., and M.D.Z. performed research and wrote the article.

[OPEN]Articles can be viewed without a subscription.

www.plantphysiol.org/cgi/doi/10.1104/pp.18.01362

ADVANCES

- Interplay of mathematical modeling and quantitatively characterized synthetic modules enabled the engineering of predictable and more complex synthetic signaling networks in a multiplicity of organisms; however, the implementation of these approaches in plants lags behind.
- Successful engineering of functional, fully synthetic, autoregulated, molecular and cellular devices is revolutionizing biomedical research and industrial applications.
- The first fully synthetic regulatory circuits in plants to be designed, provided the existing experimental limitations are overcome, will represent a breakthrough in the plant research paradigm and will be important for many biotechnological applications fostering a second green revolution.

Synthetic biology is a relatively new discipline bridging engineering with life sciences. It applies basic engineering principles for the modular, combinatorial assembly of biological parts into higher order complex signaling and metabolic structures. Key to the strategy is the implementation of mathematical modeling for the design and quantitative functional characterization of the molecular parts and for guiding the assembly, implementation, and optimization of the individual modules and networks (Ellis et al., 2009; Lim, 2010). Thus, inspired by nature, synthetic biology harnesses the modular architecture of biological systems. However, the goal is to develop novel molecular and cellular systems with desired properties and biological functionalities that are not present in nature. These properties range from gene switches and genetically encoded biosensors to fully synthetic autonomous molecular and cellular circuits and organelles as well as biohybrid smart materials and biopharmaceuticals (Brophy and Voigt, 2014; Lienert et al., 2014; Xie and Fussenegger, 2018). This field has already taken root in microbial systems as well as other higher eukaryotes. However, the generalized implementation of these approaches in the plant field lags behind.

This review is intended to serve as inspiration for plant scientists, raising interest in the field-changing potential of widely implementing synthetic biology principles. We will give an overview on the state of the technology and progress achieved with the application of synthetic biology strategies for studying, manipulating, and de novo engineering of signaling circuitry, with exemplary illustration of bacterial, yeast, and animal systems. The first implementations and future prospects in plant research will be highlighted, and the limitations and necessary technological advances for a straightforward implementation in plants will be discussed. The article is structured in three parts, following a hierarchy of molecular and realization complexity, starting off with molecular switches. Chemical-inducible devices will be introduced. In particular, the implementation of light as a trigger will be highlighted, describing the groundbreaking experimental advances enabled by optogenetics and its applications for the control of cellular processes. The concepts of orthogonality in the design of the molecular parts and the need for hand-in-hand work with theoreticians/mathematical modeling will be discussed. Further aspects include the functional combination of simple synthetic switches into molecular devices implemented in cells to perform decision-making processes, such as oscillators and molecular Boolean logic gates. Finally, we will focus on semi- or fully synthetic molecular signaling networks with open- and closed-loop control configurations and the transition into cellular devices with ad hoc functionalities for applications. For example, these systems will facilitate personalized nutrition, the production of biopharmaceuticals, and the obtainment of higher crop yields in an ecologically sustainable manner.

SYNTHETIC GENETIC SWITCHES

The rational combination of sensing and effector modules allows the wiring of inputs and outputs that are normally not functionally linked in nature, with the goal of performing novel functions. These functions range from the targeted control of a cellular process and the quantitative monitoring of a molecule to the induction of enzymatic activity or posttranslational modifications. The molecular mechanisms behind the signal integration and transfer mostly involve conformational changes. These allosteric modifications are induced by interactions between proteins, nucleic acids, and small molecules (e.g. protein/protein, small molecule/protein, and RNA/DNA; Stein and Alexandrov, 2015). Synthetic switches are engineered in a modular fashion, integrating natural and de novo-designed molecular parts. Unfortunately, switches often do not perform as expected when introduced into living systems. As in engineering, having a complete quantitative functional characterization of the modules and a supporting mathematical model contributes to straightforward and optimal implementation. A series of functional parameters of switches to be evaluated include dynamic range (ratio between maximal and basal activation), leakiness (basal activity in the absence of an inducing signal), kinetics, and reversibility of function. This is also critical when using switches as building blocks for the assembly of higher order circuits (see next section). Finally, the use of orthogonal components helps to maximize the insulation of the system, with the objective of achieving independent function and reducing unwanted effects on the endogenous networks, which are not targets of the synthetic regulation. Next, chemical- and light-inducible switches for the control

of gene expression and other cellular processes will be discussed. Protein and RNA switches used for quantitative monitoring of molecules and processes (sensors) will not be discussed in this review; for a comprehensive description, see Okumoto et al. (2012) and Walia et al. (2018).

Gene Expression Control

Transcriptional Switches

The principle of autoregulation is a key architectural element in genetic or biochemical networks, shared by prokaryotic and eukaryotic cells (Freeman, 2000). Therefore, the synthesis of proteins is essentially influenced by the genetic program and cellular environment and underlies a tight regulation through gene switches. A gene switch can be considered as any natural or synthetically designed module controlling gene expression at the level of DNA, RNA, or protein (post-translational modifications and stability; Xie and Fussenegger, 2018). Key building blocks of natural switches were first described by Jacob and Monod (1961) for the regulation of the lactose (lac) operon in *Escherichia coli*, which is regarded as the classic model for gene expression control. They characterized the promoter as the point of transcriptional initiation and identified controlling elements (repressors and inducers), which, upon binding with highly specific affinity to the upstream-located operator motif, quantitatively enhance or repress mRNA transcription. This binding is dependent on the presence of a metabolite that changes the conformation (allosteric regulation) of the regulator protein (Dickson et al., 1975).

While prokaryotic gene expression circuits mostly utilize autoregulatory inhibition (negative feedback) to guarantee homeostasis, eukaryotic transcriptional regulation comprises more complex combinations of negative and positive regulators engaging in feedback loops and Boolean logic gate computing mechanisms (Savageau, 1974; Bateman, 1998; Thieffry et al., 1998; Becskei and Serrano, 2000; Freeman, 2000). A mechanistic and functional characterization of some of these simple prokaryotic regulatory elements (Beck et al., 1982; Berens et al., 1992) enabled the engineering of artificial, exogenously controlled systems of gene expression in prokaryotic and eukaryotic cells (Gardner et al., 2000; Ajo-Franklin et al., 2007). One of the first inducible gene switches is based on the tetracycline-regulated promoter of *E. coli* that controls the expression of the tetracycline-resistance-mediating tetA gene (Fig. 1A). In brief, a simple C-terminal fusion of the tetracycline repressor (TetR) to a transcriptional activation domain from the herpes simplex virus type 1 virion protein16 (VP16) converted the transcriptional repressor into a tetracycline-controlled transcriptional transactivator (tTA) in eukaryotic cells (Gossen and Bujard, 1992). In the absence of tetracycline, tTA binds

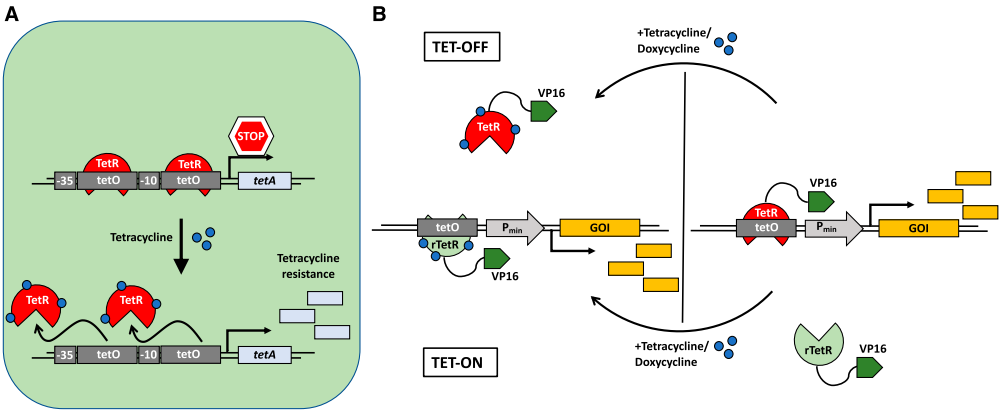

Figure 1. Illustration of the natural bacterial tetracycline resistance mechanism and synthetic tetracycline-based gene expression systems. A, In the absence of tetracycline (tet), the tet repressor (TetR) is bound to its cognate tet operator (tetO) DNA-binding motif, repressing the expression of the tet resistance-mediating tetA gene. Upon increasing cellular levels of tet, tet binding induces a conformational change of TetR, leading to its dissociation from the operator sequence, and expression of tetA ensues. B, The tet-OFF system designed for use in mammalian cells is based on a synthetic switch comprising the natural TetR fused to the activating domain of VP16 of the herpes simplex virus and a synthetic promoter with a series of repeats of the tetO motif placed upstream of a minimal promoter (e.g. human cytomegalovirus minimal promoter). The system is constitutively active and is turned OFF in the presence of the antibiotic. Implementation of a reversed TetR mutant (rTetR) generates a tet-ON system: tet induces the binding of rTetR to the target sequence, which in turn induces gene expression (tet can be replaced by other antibiotics of the tetracycline family like doxycycline). Replacement of VP16 by a transrepressor such as KRAB inverts the effect of the switch (not depicted here). GOI, Gene of interest. (Adapted from Gossen et al., 1995.)

to the cognate tet-operator region on the synthetic promoter construct, activating transcription from an adjacent minimal promoter sequence. Upon addition of tetracycline, tTA is removed from the promoter and gene expression is shut off (Fig. 1B). A reversed TetR was generated by random mutagenesis (Gossen et al., 1995), which, when fused to the VP16 domain, enables tetracycline-induced transcriptional activation (Fig. 1B). Alternatively, fusion of a transrepressor instead of a transactivator to TetR or modification of the synthetic promoter region enables other positive and negative regulation configurations (Kramer et al., 2004a). Following these simple molecular engineering principles, and modifications thereof, a vast set of chemically inducible gene switches were developed for use in yeast and animal cells sensitive to antibiotics, primary and secondary metabolites, and volatiles, among other substances (for review, see Hörner and Weber, 2012).

To achieve tight and predictable control over gene expression, a quantitative characterization and mathematical modeling of the regulator/promoter-switch is needed (for the implementation of mathematical modeling into synthetic circuitry approaches, refer to the detailed works of Ellis et al. [2009] and Lim [2010]). The optimization of key parameters such as strength and kinetics of expression, leakiness, etc., can be performed subsequently by reengineering the switch components. Usual approaches include the redesign of promoter regions: introduction of multiple repeats of binding sites, point mutations to alter affinity, protein engineering, and use of different transactivators/transrepressors (Ajo-Franklin et al., 2007). The incorporation of positive and/or negative feedback loop configurations (e.g. by placing the regulator under control of its own target synthetic promoter) enables a greater dynamic range of the dose-dependent response (Gossen et al., 1995; Becskei et al., 2001). Promoters can be engineered further by combining activation and repression of gene expression in a simultaneous manner, thereby facilitating a deeper insight into gene network regulation by increasing the possible regulation conditions. Studying unregulated, repressed, activated, or simultaneously repressed/activated gene expression helped develop a model for precise prediction of the behavior of genetic networks in vivo (Guido et al., 2006). Other examples include the implementation of several chemical-, hormone-, or CRISPR/Cas-inducible or repressible switches for the control of multiregulated systems, especially for pharmacological application in mammalian cells (Weber et al., 2002; Nielsen and Voigt, 2014). Broad implementation of these gene switches in cell culture and in vivo (mouse, rat, *Drosophila* spp., zebrafish, *Caenorhabditis elegans*) represented a paradigm change in the way metabolic and signaling networks can be studied and redesigned synthetically.

In plant systems, several chemically inducible switches have been developed for a temporal and quantitative regulation of expression (Table 1). For instance, these switches are triggered by IPTG (Wilde et al., 1992), antibiotics such as tetracycline (Gatz et al., 1992; Weinmann et al., 1994; Müller et al., 2014), macrolides and pristinamycin (Frey et al., 2001; Müller et al., 2014), copper (McKenzie et al., 1998), or ethanol (Caddick et al., 1998; Roslan et al., 2001). The most widely employed switch is a steroid-based system that allows precise temporal control over cellular processes in whole plants (Schena et al., 1991). Recently, gene switches comprising a Cas9-based repressor and regulatory modules of hormone signaling pathways (auxin, GA, and jasmonate) have been implemented in Arabidopsis (*Arabidopsis thaliana*; hormone activated Cas9-based repressor [HACRs]; Khakhar et al., 2018). The HACRs are sensitive to both exogenous hormone treatments and varying endogenous hormone levels, leading to degradation of the switch and thereby regulating target gene expression (the single guide RNA-Cas9 complex dictates the specificity). This tool can be applied to regulate hormone signaling or any other target of interest, thus allowing the manipulation of stress tolerance and yield in crop plants.

However, chemical switches have limitations concerning defined spatiotemporal activation of the system due to abundance, administration, and diffusion of the inducer molecules as well as usual toxicity effects. Recently, light-controlled genetically encoded molecular devices have been engineered and implemented in living cells to control cellular processes, giving rise to the nascent field of optogenetics (Box 1). These devices overcome the inherent restrictions of chemically regulated switches. Light-regulated switches comprise bacterial and plant photoreceptors, such as UV-B RESISTANCE8, phototropin1/EL222/CRYPTOCHROME2, CarH, PYHTOCHROME B/A, and the bacterial phytochrome BphP1, among others (for a comprehensive list, see Kolar et al., 2018). Upon absorption of light, they undergo a conformational change leading to homo/hetero-association/dissociation (Kolar and Weber, 2017). This light-dependent protein interaction relays a signal to an output module that then fulfills a cellular function. In the last decade, a multitude of optogenetic gene switches regulated by UV-B, blue, green, red, and far-red/near infrared light have been engineered and implemented for the noninvasive control of gene expression with a precise temporal and spatial resolution in prokaryotic and eukaryotic systems (Zhang and Cui, 2015; Fig. 2).

Contrary to most nonautotrophic organisms, the life cycle of plants requires exposure to sunlight, which might lead to nonintentional activation of the optogenetic systems. Therefore, the simple transfer of optogenetic tools developed in other organisms is challenging. While long-term experiments in dark conditions are harmful, exposure to a specific wavelength of light may interfere with the natural light-sensitive signaling and photosynthetic circuitry of the plant through their photoreceptors or light-sensitive pigments. These natural light-absorbing moieties might in turn interfere with the inducing light and the

Table 1. *Representative synthetic switches and regulatory circuits in plants*

AlcR, Promoter of the ALCR transcription factor; AlcA, alcohol dehydrogenase I from *Aspergillus nidulans*; XVE, chimeric transcription factor based on LexA-VP16-ER; OlexA, DNA-binding domain of the bacterial LexA repressor; pOp, chimeric promoter, comprising lac operators cloned upstream of a minimal cauliflower mosaic virus promoter; LhGR, transcription activator, a fusion between a high-affinity DNA-binding mutant of the lac repressor, lacI His-17, and the transcription-activation domain II of GAL4 and the ligand-binding domain of the rat glucocorticoid receptor; TraR, autoinducer-dependent transcriptional activator from *Agrobacterium tumefaciens*; OOHL, 3-oxooctanyl-L-homoserine lactone; lacO, lac operator; LacI, lac repressor; IPTG, isopropyl β-D-thiogalactopyranoside; ACE1, promoter of the copper-binding regulatory protein; rTetR, reversed tetracycline repressor; TetR, tetracycline repressor; tetO, tetracycline operator; GAL4, Gal-responsive transcription factor GAL4; UAS, upstream activation sequence; PiP, pristinamycin repressor protein; PIR, pristinamycin I-responsive element; E, macrolide repressor protein from *E. coli*; etr8, eight MphR (A) [macrolide 2′-phosphotransferase I]-binding operators; N1, 10 N1-TATA minimal promoter; NEV, three finger protein N1-ER-VP64; HACR, hormone-activated Cas9-based repressor; dCAS9, nuclease-dead Cas9; PIF6, phytochrome-interacting factor6; CarH, light-responsive transcription factor; CarO, CarH-binding site-containing operator; TIR1, TRANSPORT INHIBITOR RESPONSE1; Aux/IAA, auxin/indole-3-acetic acid protein; Trg, transmembrane signaling protein; PhoB, phosphate regulon transcriptional regulatory protein; PhoR, phosphate regulon sensor protein; VP64, four copies of the virion protein16 domain of the herpes simplex virus type 1; ABA, abscisic acid.

Feature	System	Properties	References
Chemically inducible switches for gene expression	AlcR/AlcA	Ethanol inducible	Caddick et al. (1998) Roslan et al. (2001) Roberts et al. (2005)
	XVE/OlexA	β-Estradiol inducible	Zuo et al. (2000) Curtis and Grossniklaus (2003) Böhmdorfer et al. (2010)
	pOp/LhGR	Dexamethasone inducible	Schena et al. (1991) Aoyama and Chua (1997)
	TraR	OOHL inducible (quorum sensing system)	You et al. (2006)
	lac operator/LacI	IPTG inducible	Wilde et al. (1992)
	ACE1-based Cu-inducible promoter	Copper inducible	McKenzie et al. (1998)
	(r)TetR/tetO	Tetracycline inducible (rTet)/ repressible (TetR)	Gatz et al. (1992) Weinmann et al. (1994) Müller et al. (2014)
	GAL4-UAS	Enhancer trap lines	Gardner et al. (2009) Johnson et al. (2005) Laplaze et al. (2005)
	PiP/PIR	Pristinamycin repressible	Frey et al. (2001) Müller et al. (2014)
	E/etr8	Macrolide regulated	Müller et al. (2014)
	10xN1/NEV	4-Hydroxytamoxifen inducible	Beerli et al. (2000)
Cas-based gene expression	HACR	Phytohormone inducible	Khakhar et al. (2018)
	dCAS9	gRNA-mediated gene-specific induction	Piatek et al. (2015) Lowder et al. (2015)
Light-regulated gene expression	Phytochrome B/PIF6	Red light induced/far-red light repressed	Müller et al. (2014) Ochoa-Fernandez et al. (2016)
	CarH/CarO	Green light repressed/dark induced	Chatelle et al. (2018)
Synthetic riboswitch	Synthetic theophylline riboswitch in plastids	Theophylline inducible	Verhounig et al. (2010)
MicroRNA-based gene silencing	Artificial microRNA	Gene-specific silencing	Schwab et al. (2006)
Posttranslational degradation	N-terminal degradation signal (It degron)	Temperature-controlled protein degradation	Faden et al. (2016)
Optogenetic manipulation of endogenous signaling networks	Red light-controlled up- or down-regulation of TIR1 in combination with a ratiometric auxin sensor to monitor the manipulated signaling	Red light-controlled tuning of auxin signaling	Müller et al. (2014)
Synthetic ligand detection and signal relay	TgR/PhoR fusion phosphorylates PhoB-VP64	Synthetic programmable ligand detection system	Antunes et al. (2011)
Synthetic ABA agonist	Cyanabactin: agonist of ABA IIIA receptors	Synthetic manipulation of transpiration and other physiological processes	Park et al. (2015) Vaidya et al. (2017)

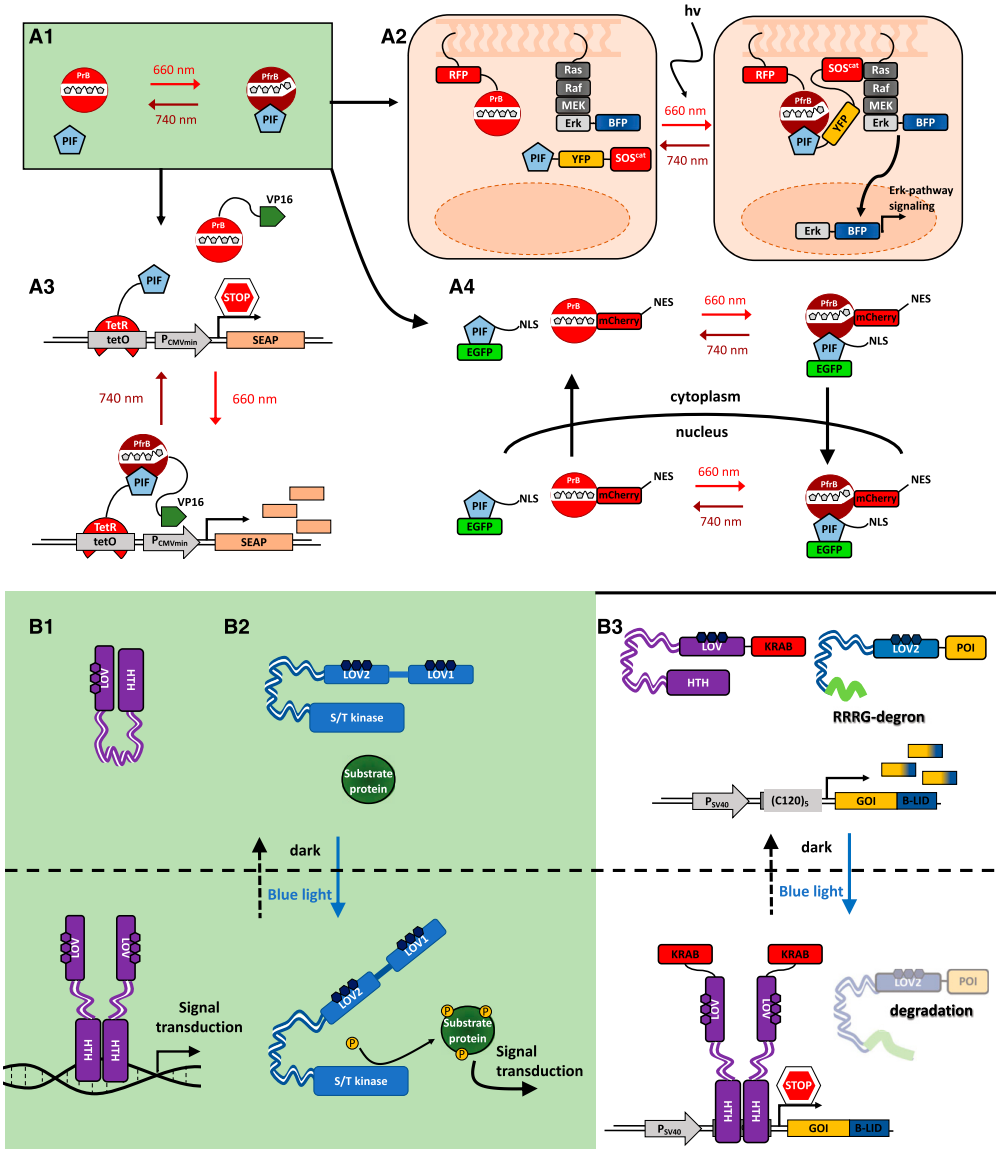

Figure 2. Optogenetic switches. Molecular principles of light-induced signaling and optogenetic tools are illustrated. A, Natural red light-inducible signaling mediated by the plant photoreceptor phytochrome B (phyB) and optogenetic tools developed based on it. A1, The red/far-red light-perceiving photoreceptor phyB remains in its inactive Pr conformation in the dark. Upon absorption of a red light photon, the photoreceptor undergoes a conformational change, converting to its active Pfr conformation. The active form can interact with several transcription factors like the bHLH transcription factors of the PHYTOCHROME INTERACTING FACTOR (PIF) family. This interaction triggers light-signaling responses. In contrast, illumination with far-red light reconverts phyB to its inactive Pr form, abolishing the interaction with PIFs (Rockwell and Lagarias, 2006). Several optogenetic approaches make use of the red light/far-red light switchable interaction of phyB and PIFs. A2, Selective activation of intracellular signaling

high autofluorescence of plants, posing limitations to microscopy analysis. In addition, compared with the genetic engineering of simpler organisms, generating stable transformed plants expressing the synthetic components of the switches is a lengthy process that slows down the implementation and characterization processes.

Despite these technical and experimental constraints, the first optogenetic tools have already been successfully implemented in plants (Table 1). These include a phytochrome-based red light-inducible and a CarH-based green light-regulated expression system (Müller et al., 2014; Ochoa-Fernandez et al., 2016; Chatelle et al., 2018). The former is activated by red light and inactivated by far-red light. Simple supplementation of ambient illumination in greenhouses with low intensities of far-red light keeps the system repressed. Irradiation with red light leads to quantitatively controlled activation of gene expression (Müller et al., 2014; Chatelle et al., 2018). The second strategy comprises the engineering of a green light-inducible bacterial photoreceptor, CarH. Use of green light as a stimulus minimizes the interference with endogenous plant photoreceptors, as this region of the sunlight spectrum normally does not produce physiologically active signaling responses of relevance (Chatelle et al., 2018).

Translational and Posttranslational Switches

While transcriptional gene switches currently play a major role in customized gene expression and are used for a broad range of applications, synthetic RNA-based switches constitute a complementary approach for controlling gene expression on the translational level. The most prominent components of RNA-based tools include RNA interference (RNAi; Fire et al., 1998), microRNAs (Lagos-Quintana, 2001), aptamers, and ribozymes. While RNAi, microRNAs, and ribozymes lead to cleavage or splicing of the target mRNA (Fire et al., 1998; Warashina et al., 2000; Lagos-Quintana, 2001), aptamers bind to specific targets like metal ions, small molecules, DNA, or proteins (Xiao et al., 2008). Aptamers are structured noncoding RNAs, naturally found in riboswitches that interfere with the accessibility of the ribosomes to the mRNA, affecting translational control (Breaker, 2012; Ausländer and Fussenegger, 2017). Using the in vitro selection method SELEX (for systematic evolution of ligands by exponential enrichment; Ellington and Szostak, 1990), many aptamers for new targets have been developed, such as the synthetic tetracycline-binding aptamer (Hanson et al., 2005; Xiao et al., 2008). By integrating protein-binding aptamers, the control of translational regulation via repression or alternative splicing can be achieved (Culler et al., 2010; Endo et al., 2013). In

Figure 2. (*Continued.*)
pathways with light. Red light illumination induces the recruitment of the cytoplasmic fusion protein consisting of a PIF, C-terminally fused to the fluorescent protein YFP and the catalytic domain of the SOS protein (SOS^{cat}), to the membrane-bound, RFP-tagged phyB. When recruited to the membrane, SOS^{cat} is capable of activating the Ras-signaling cascade and inducing nuclear transport of BFP-Erk and subsequent Erk pathway signaling. (Adapted from Toettcher et al., 2013.) A3, Construction of a phyB-PIF-based, red light-inducible split-transcription factor system. A truncated PIF6 was N-terminally fused to the tetracycline repressor (TetR), and the synthetic protein is bound to the tetracycline operator motif tetO of a synthetic reporter construct (as in Fig. 1). In the absence of light or under far-red light illumination (740 nm), there is no expression from the minimal promoter, P_{CMVmin}. Upon illumination with red light, phyB, C-terminally fused to the VP16 transactivation domain, interacts with the PIF. The spatial proximity of the transactivator recruits the transcriptional machinery to the minimal promoter. Only in this condition is the expression of the secreted human alkaline phosphatase (SEAP) reporter gene activated. (Adapted from Müller et al., 2013a.) An adaptation of this system was engineered in Arabidopsis and tobacco (*Nicotiana tabacum*) cells and the moss *Physcomitrella patens* (Müller et al., 2014; Ochoa-Fernandez et al., 2016). A4, Reversible red light-inducible nuclear transport of phyB fusion proteins. phyB was C-terminally fused to the fluorescent protein mCherry and a nuclear export sequence (NES), while PIF3, containing an intrinsic nuclear localization sequence (NLS), was C-terminally fused to enhanced GFP (EGFP). Upon illumination with red light, the nucleocytoplasmic shuttling PIF induces nuclear transport of phyB, while far-red radiation reversed the translocation of the photoreceptor-mediated by the NES. (Adapted from Beyer et al., 2015.) B, Natural blue light-induced signal transduction mediated by the plant photoreceptor phototropin1 and the light-sensitive bacterial transcription factor EL222. A synthetic approach based on blue light-triggered conformational change of EL222 and the LOV2 domain for the dual-controlled optogenetic down-regulation of proteins in animal cells was used. B1, EL222 is a light-sensitive transcription factor from the gram-negative bacterium *Erythrobacter litoralis*. It contains a blue light-sensitive LOV domain and a helix-turn-helix (HTH)-DNA-binding domain. In the dark, the HTH domain is docked to the LOV core. Upon illumination with blue light, the interaction of LOV and the HTH domain is disrupted, enabling homodimerization of the protein via the HTH and subsequent binding to the C120-DNA motif (Nash et al., 2011). B2, Schematic illustration of light-induced signal transduction via the blue light plant photoreceptor phototropin1. In the dark, the kinase domain is bound to the LOV domain, inhibiting its phosphorylation activity. Under blue light, the kinase domain is released, inducing protein phosphorylation and downstream signal transduction. (Adapted from Kimura et al., 2006.) B3, The dual optogenetic system for targeted degradation and repression of expression of a protein of interest (POI) consists of a synthetic reporter module comprising the P_{SV40} promoter, for constitutive expression of a POI fused to the B-LID (Bonger et al., 2014) module, and the $C120_5$-DNA-binding motif of the EL222 protein. EL222 is fused to the trans-repressor KRAB. In the dark, the degron (peptide RRRG) is docked to the LOV domain of the B-LID, and KRAB-EL222 is not able to bind to the C120 motif on the reporter plasmid. In this case, the POI accumulates. Upon illumination with blue light, the degron is exposed, triggering proteasomal degradation of the POI-B-LID fusion protein. Simultaneously, KRAB-EL222 dimerizes binding to the C120 motif, repressing transcription of the POI-B-LID. (Adapted from Baaske et al., 2018.)

BOX 1. Optogenetics

For chemically controlled molecular switches, drawbacks such as difficulties in removing the inducer and diffusion-rate-limited transport and availability, hamper rapid inducibility and reversibility as well as space-resolved activation. By contrast, light as an input offers unprecedented spatiotemporal resolution, tight quantitative control, and minimized invasiveness. The introduction of light-gated ion channels (opsins) into neurons (reviewed in Deisseroth and Hegemann, 2017) initiated optogenetics, a novel discipline focusing on the control of biological systems with light. Development of light-sensitive switches uses photoreceptors as the input-sensing part of the switch. A multiplicity of different optogenetic switches for the minimally invasive control of cellular processes, with precise temporal and spatial resolution, have been engineered by combining bacterial and plant photoreceptors (with absorption spectra spanning from the UV-B up to the far-red regions of the white light spectrum) with output modules (molecular function) (reviewed by Fan and Lin, 2015; Müller et al., 2015; Kolar and Weber, 2017; Salinas et al., 2017). Common applications in mammalian cells include light-controlled gene expression and genome editing using transcriptional inducers or repressors (Müller et al., 2013b; Müller et al., 2013a; Motta-Mena et al., 2014; Kaberniuk et al., 2016), two-hybrid systems for recruitment of TALE- (Konermann et al., 2013) and CRISPR/Cas9-based-tools (Nihongaki et al., 2015; Polstein and Gersbach, 2015), and light-induced nuclear import of transcriptional effectors (Niopek et al., 2014; Beyer et al., 2015; Niopek et al., 2016) (Figure 2). In addition, light-regulated tools for controlling subcellular localization of proteins and even whole organelles (van Bergeijk et al., 2015; Beyer et al., 2015), protein stability (Bonger et al., 2014), kinase activity, and receptor activation, among others, have been applied for precisely controlling sensitive cellular processes. We refer the reader to the webtool OptoBase, designed to guide the user in the choice of a suitable optogenetic switch for a given application (Kolar et al., 2018). Optogenetics has made key contributions of molecular tools and experimental approaches, for molecular and cell biology research, as well as biotechnological applications (Zhang and Cui, 2015). The development of optogenetic systems lags behind in plants, mostly because of the experimental constraints posed by the unavoidable exposure to environmental light. However, optogenetic approaches in plants have been reported, including phytochrome- and CarH-based, red- and green-light-inducible expression systems (Müller et al., 2014; Ochoa-Fernandez et al., 2016; Chatelle et al., 2018). This opens novel perspectives for engineering synthetic, light-triggered circuits in plants.

Box 1 Optogenetics. Citations: Konermann et al., 2013; Müller et al., 2013a, 2013b, 2014, 2015; Bonger et al., 2014; Motta-Mena et al., 2014; Niopek et al., 2014, 2016; Beyer et al., 2015; Fan and Lin, 2015; Nihongaki et al., 2015; Polstein and Gersbach, 2015; van Bergeijk et al., 2015; Zhang and Cui, 2015; Kaberniuk et al., 2016; Ochoa-Fernandez et al., 2016; Deisseroth and Hegemann, 2017; Kolar and Weber, 2017; Salinas et al., 2017; Chatelle et al., 2018; Kolar et al., 2018.

addition, fusion of the aptamer to translational repressors or enhancers permits the up- or down-regulation of the translation rate of the target protein (Pillai et al., 2004; Van Etten et al., 2012; Paek et al., 2015). Compared with transcriptional switches, translational switches can control endogenous genes without any alteration of the genomic sequence. They are relatively small in size and therefore are amenable for use in combination with transcriptional switches when the size and number of cassettes imposes an experimental limitation (Ausländer and Fussenegger, 2017).

In plants, specific RNA-based gene silencing, using artificial antisense mRNAs or microRNAs under the control of tissue-specific or inducible promoters, has been widely used for more than 20 years. However, these approaches usually suffer from off-target effects and provide limited exogenous and quantitative control and reduced efficiency (Schwab et al., 2006). Other examples for the translational control of gene expression in plants are limited to applications in plastids (Verhounig et al., 2010). Recently, Faden et al. (2016) reported a posttranscriptional switch for the in planta down-regulation of protein levels based on a temperature-controlled N-terminal degradation signal. Similar to other techniques already implemented in simpler, unicellular organisms, the transfer of the system to multicellular organisms, like plants, strongly depended on the adaptation to the corresponding physiological conditions. To test the functionality of the system for reversible protein accumulation, trichome formation was manipulated after shifting the plants from a permissive to a restrictive temperature (29°C).

This led to the degradation of the protein of interest, TRANSPARENT TESTA GLABRA1, thus affecting the spatiotemporal development of trichomes (Table 1).

Switches Regulating Cellular Processes

Besides transcriptional and translational switches, a plethora of chemical- and light-regulated systems have been developed for the targeted regulation of a multiplicity of cellular processes ranging from the activation/inactivation of signaling cascades (receptors, kinases, transcription factors, etc.) and membrane trafficking to the controlled movement of organelles from one pole of the cell to the other (for review, see Hörner and Weber, 2012; Kolar and Weber, 2017). Selected examples include the utilization of optogenetic tools for (1) the control of the subcellular localization of proteins (e.g. red light; Beyer et al., 2015; Fig. 2A) and blue light-induced (Niopek et al., 2014, 2016) nuclear import and export of transcriptional effectors; and (2) the light-mediated degradation/depletion of proteins (Bonger et al., 2014; Baaske et al., 2018; Fig. 2B). A comprehensive list of approaches is reviewed elsewhere (Hörner and Weber, 2012; Kolar and Weber, 2017).

SYNTHETIC GENETIC CIRCUITS

Genetic circuits combine a series of synthetic switches into networks that can perceive a signal (exogenous or endogenous, natural or synthetic), process the information, and generate an output, normally triggering gene expression (e.g. induction of a given phenotype or change in cellular morphology) and expression of a reporter to monitor a process or activation of a metabolic pathway (Lim, 2010; Xie and Fussenegger, 2018). Simple circuits perform basic functionalities and integrate few signals. Next, we will discuss toggle switches, synthetic oscillators, and Boolean logic gates, which are built up from simple combinations of a reduced number of modules. Then we will review more complex arrays of switches integrated into cell-cell communication systems, open- and closed-loop circuit control, and synthetic cellular devices and their applicability.

Simple Circuits

Since therapeutic applications are one of the driving forces for the development of functional, robust, and complex genetic circuits, many recent technical breakthroughs have been made in mammalian cell systems. First approaches included the transfer and optimization of basic synthetic circuits, previously engineered in lower organisms. An illustrative example is a simple negative feedback circuit in yeast based on the combination of two tetracycline-inducible modules, controlling the expression of EGFP and the TetR repressor (Nevozhay et al., 2009). This loop enabled a tightly controlled, dose-dependent activation of gene expression in mammalian cells. Expression of both EGFP and TetR is regulated by the rate of influx of the inducer but subsequently restricted by the increasing level of TetR protein (Nevozhay et al., 2013).

Toggle Switches

The first combined synthetic gene switches date back to the early 2000s with the design of bistable transcriptional repression toggle switches in bacteria and mammalian cells (Ajo-Franklin et al., 2007). Here, mutual inhibition of two independent chemical- and temperature-controlled (Gardner et al., 2000) or antibiotic-inducible (Kramer et al., 2004b) promoters, each controlling the expression of the counterpart's repressor, generates two equilibrium states of induction, switchable by the respective transient induction.

Plants also employ natural toggle switches for the control of endogenous processes, such as the CLAVATA pathway for stem cell fate. In line with this, the implementation of synthetic toggle switches in plants could open new perspectives for the development of, for instance, a programmable path of stem cell differentiation (Medford and Prasad, 2016) or trichome development. However, the intrinsic complexity of plant signaling networks restricts the straightforward transferability of already existing synthetic systems into plants. Plants integrate a wide range of biotic and abiotic external cues like light and temperature with genetic programs in an intertwined or redundant manner. This poses experimental and theoretical constraints (resources, time, lack of thorough knowledge of regulatory mechanisms, limited genetic tools, etc.). Therefore, exhaustive design and implementation phases will be needed for engineering all the synthetic circuits discussed in this article.

Oscillators

Autonomous and self-sustained oscillating gene expression patterns, like the circadian clock or the cell cycle, are crucial to sustain pulsatile cellular activities; therefore, there is much interest in understanding their regulation and function (for review, see Schibler and Sassone-Corsi, 2002; Fig. 3A). By designing and implementing synthetic oscillators, key insights on the mechanistic principles of cellular processes can be obtained, and novel functionalities could be engineered, as described below.

After the discovery of the first gene regulation model (Jacob and Monod, 1961), theoreticians started developing mathematical models on genetic oscillatory networks, and ideas for synthetic circuits were proposed. The first prototypical oscillator, termed the Goodwin oscillator, utilizes a single protein that inhibits its own transcription; namely, it can be seen as a closed negative feedback loop (Goodwin, 1963, 1965). Several decades later, the advances in genetics and molecular and cell biology allowed engineers to implement this and other

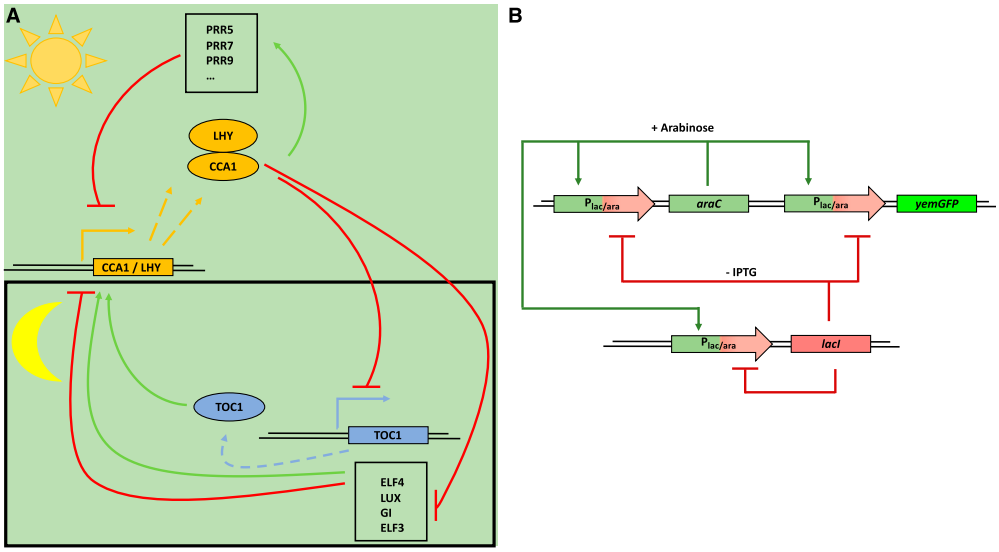

Figure 3. Molecular principle of a natural and synthetic oscillator. A, Simplified molecular model of the circadian clock in Arabidopsis (natural oscillator). The core oscillator feedback loop consists of TOC1, CCA1, and LHY. In this core oscillator, LHY and CCA1 repress the transcription of TOC1; TOC1 in turn is a positive regulator of CCA1 and LHY. In a second loop, LHY and CCA1 are also positive regulators of three TOC1 paralogs (PRR5, PRR7, and PRR9), which in turn are negative regulators of CCA1 and LHY. In a third loop, CCA1 and LHY positively regulate GI, ELF3, ELF4, and LUX; these in turn regulate CCA1 and LHY. The circadian oscillator of Arabidopsis is illustrated here in a simplified form; for clarity, several other components involved were not included. (Adapted from McClung, 2006.) B, Scheme of a synthetic oscillator engineered by Stricker et al. (2008). This synthetic oscillator comprises positive and negative feedback loops. The *araC*, *lacI*, and *yemGFP* (as a readout) genes are all under the control of the hybrid synthetic promoter $P_{lac/ara\text{-}1}$, comprising the activation operator site from the *araBAD* promoter and the repression operator site from the *lacZYA* promoter (Lutz and Bujard, 1997). In the presence of arabinose, the AraC protein activates the hybrid promoter and, thus, the gene expression of *araC*, *lacI*, and *yemGFP*, which results in two feedback loops: a positive feedback loop mediated by the produced AraC and the resulting activation of the hybrid promoter, and a negative feedback loop due to the production of the LacI protein. In the absence of IPTG, LacI negatively regulates the expression of all three genes under the control of the hybrid promoter. Both engineered feedback loops together constitute the synthetic oscillator. (Adapted from Stricker et al., 2008.)

oscillators in living cell systems (Elowitz and Leibler, 2000; Fung et al., 2005; Stricker et al., 2008; Danino et al., 2010; Ryback et al., 2013). The first of these genetic circuits implemented in *E. coli* was a synthetic oscillatory network of transcriptional regulators, known as the repressilator (Elowitz and Leibler, 2000). A repressilator is defined as a subset of genes that can repress their successor in the cycle; thus, it can be seen as an extension of the one-gene Goodwin oscillator (Müller et al., 2006; Purcell et al., 2010). The Elowitz synthetic repressilator consists of a cyclic negative feedback loop composed of three repressor proteins, which are not part of any natural biological clock/oscillator, namely, LacI (*E. coli*), TetR (Tn10 transposon), and cI (λ phage), and their corresponding cognate promoters. However, it suffered from noisy behavior, with only 40% of the *E. coli* cells showing oscillations (Elowitz and Leibler, 2000). Theoretical studies revealed that by implementing a positive feedback loop, the robustness of the oscillations and the tunability of the amplitude and period could be improved (Hasty et al., 2002; Atkinson et al., 2003; Stricker et al., 2008; Purcell et al., 2010; Tomazou et al., 2018). Later, a dual-feedback oscillator developed by Stricker et al. (2008) achieved faster oscillatory periods, 99% oscillating cells, and decoupling from the cell cycle. The period was tuned by either IPTG, arabinose, or temperature (Fig. 3B). In most of these approaches, mathematical model-assisted design was essential for identifying the experimental parameters and molecular components (relative amounts thereof) used to tune the oscillations.

Autonomous, self-sustained, and tunable oscillatory behavior was also achieved in mammalian cells with an amplified negative feedback oscillatory mechanism (Tigges et al., 2009). The oscillator is based on an autoregulated sense-antisense transcription control circuit in the negative feedback loop leading to a delay in the repressive effect (Tigges et al., 2009; Purcell et al.,

2010). An alternative approach applied in mammalian cells involved the combination of both natural and synthetic elements to create oscillatory behavior by manipulating amplitude, damping, and frequency in an independent fashion. For this purpose, the endogenous transcription factor p53, which is activated in response to cellular stress, and its negative regulator Mdm2 were utilized (Toettcher et al., 2010). This simple core negative feedback loop served as an example to define and modulate the dynamics of naturally occurring oscillatory systems in a controlled fashion. Considerable progress has been made recently to link different kinds of genetic circuits to functional synthetic self-regulated networks. This is necessary for integrating synthetic control into endogenous signaling networks, for instance, the Elowitz repressilator coupled to a modified quorum-sensing circuit of *Vibrio fischeri* and *A. tumefaciens* (Fernández-Niño et al., 2017).

Despite almost two decades of in vivo experiments and associated theoretical background on oscillators, there are still no oscillators implemented in plants. This represents a big experimental challenge. As discussed above, a major obstacle for the implementation of synthetic oscillatory networks in multicellular organisms like plants is the existence of a multiplicity of internal or external parameters, regulating metabolic and signaling pathways. A first attempt at this would be the engineering of hybrid oscillators, employing a similar approach to the one introduced by Toettcher et al. (2010). The introduction of synthetic orthogonal modules to achieve tight control over oscillatory parameters of an endogenous pathway minimizing cross talk could contribute to a broader understanding of oscillatory behavior in plant signaling and metabolic networks. In the future, fully synthetic systems could be implemented to bypass endogenous oscillators. A potential application of this would be the decoupling of endogenous metabolic pathways from the circadian clock to allow, for example, a prolonged bioproductive/anabolic daily phase, thereby increasing crop yield.

Boolean Logic Gates

Boolean logic gates utilize Boolean algebra to convert multiple input signals into truth values, meaning a true or false answer (1 or 0). In a simple way, cells use this mechanism for a plethora of decision-making processes (e.g. promoters integrate the information encoded in the combination of positive and negative transcriptional regulators bound at any given point in time, translating it into an output signal [gene expression]; Fig. 4). Following these principles, synthetic genetic circuits have been designed and successfully implemented in prokaryotes (Tamsir et al., 2011; Moon et al., 2012), yeast (Gander et al., 2017), and mammalian cells (Xie et al., 2011; Ausländer et al., 2012; Lebar et al., 2014) controlling various biological functions. They can integrate multiple molecular input signals following a set of algorithms and generate a response only if strictly defined conditions are met (Xie and Fussenegger, 2018). For instance, an OR gate only generates an output when either input signal A or B is present, whereas both input signals have to concur for an AND gate to be true. More complex logic gates could be built in a combinatorial fashion out of these simple ones (Xie and Fussenegger, 2018). Different transcriptional regulators were used to meet these demands, including promoters functioning as input and output (Tamsir et al., 2011; Moon et al., 2012), RNAi (Xie et al., 2011), and TALE repressor- (Gaber et al., 2014) and dCas9-based switches in bacteria (Nielsen and Voigt, 2014), yeast (Gander et al., 2017), and mammalian cells (Gao et al., 2016).

An illustration of such a circuit using chemically controlled transcription factors was depicted in the work of Gao et al. (2016). An efficient gene activation and repression system was designed by combining plant hormone signaling components with Sp-dCas9, which enabled the manipulation of multiple gene targets in an orthogonal mammalian cell setup. To achieve this, ABA and GA phytohormone signaling components that heterodimerize in the presence of the individual hormones (PYRABACTIN RESISTANCE1-LIKE [PYL] with ABA INSENSITIVE [ABI] for ABA and GA INSENSITIVE DWARF1 [GID1] with GIBBERELLIC ACID INSENSITIVE [GAI] for GA) were fused to either a transcriptional activator (VPR) or repressor (KRAB) or to Sp-dCas9. When the corresponding hormones are added, GID1-VPR/-KRAB and GAI-Sp-dCas9 (or PYL1-VPR/-KRAB and ABI-Sp-dCas9, respectively) heterodimerize, thereby activating or repressing gene expression from a target synthetic promoter. These switches perform very well, are robust, and show almost no leakiness. Based on these characteristics, both systems were customized and combined to construct AND, OR, NAND, and NOR Boolean logic gates. A NOT IF gate was successfully built in which expression of a gene was possible only in the presence of one inducer (e.g. ABA) while it was OFF in the presence of the second one (e.g. GA; Gao et al., 2016). This approach therefore utilized phytohormone signaling components to control multiple transcriptional outputs in an orthogonal system, namely, mammalian cells. Despite its potential applicability, to our knowledge, there has not been any synthetic Boolean logic gate implemented in plants yet.

Higher Order Genetic Circuits

The characteristics of the different levels of genetic circuits are summarized in Box 2. More complex synthetic devices connecting multiple layers of signal processing, including detection of the inducer, signal transduction, and precise (nuclear) activation of the defined output, have been implemented in prokaryotic and eukaryotic cell systems. Most of these circuits partially rely on endogenous elements, utilized for a desired purpose, in combination with the integrated synthetic, orthogonal components. Here, we describe

cell-cell communication systems and illustrate differential characteristics and applicability, currently in biomedicine, of open- and closed-loop circuit control configurations and prosthetic synthetic circuits (Box 2).

Cell-Cell Communication Systems

Unicellular and multicellular organisms rely on cell-cell communication mechanisms to regulate crucial life decisions (e.g. growth, development, organ identity, and metabolism/nutrition, among a wide range of processes). Bacteria, for instance, employ quorum sensing to assess the density of cells in their surroundings (Fig. 5A). Depending on the population density, genes responsible for key processes such as biofilm formation are up- or down-regulated (Fuqua et al., 1994; Abisado et al., 2018). Multicellular organisms coordinate processes such as tissue development or immune cell responses employing cell-cell communication networks (Thurley et al., 2018). Different signaling molecules are used for this purpose in unicellular and multicellular organisms, including metabolites, small RNAs, peptides, and proteins. The synthetic reconstruction or de novo engineering of these communication processes can contribute to experimental strategies to both understand these processes and develop biotechnological applications (Prindle et al., 2011). In tissue engineering approaches, tight control and manipulation of cell-cell communication is needed for the establishment of edges between different populations of cells, as achieved by Kolar et al. (2015). Targeted spatiotemporally resolved induction of cell death was engineered by using bacterial quorum sensing-regulated systems (You et al., 2004). Finally,

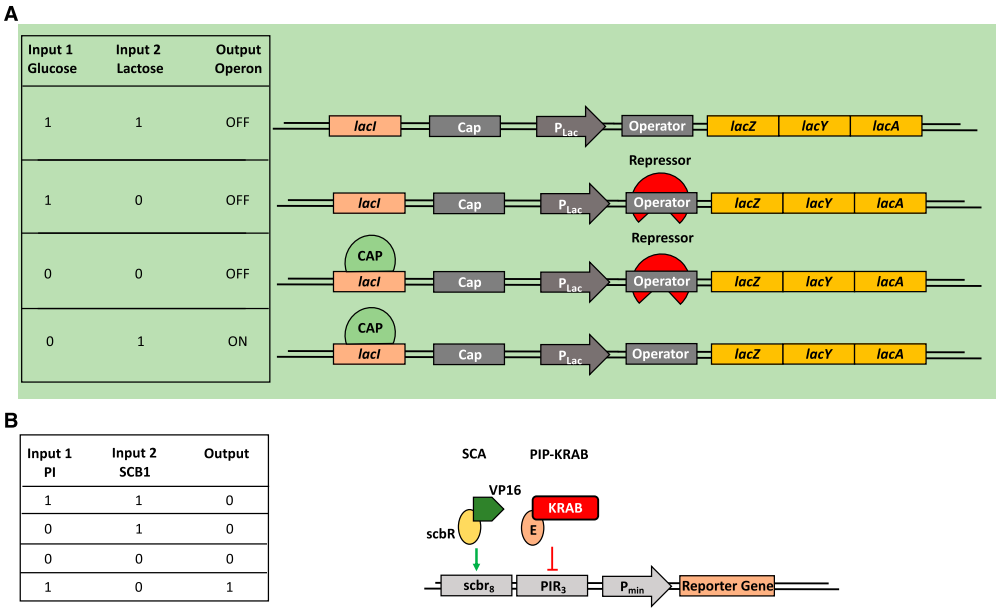

Figure 4. Natural and synthetically built AND NOT (NOT IF) Boolean logic gates. An AND NOT gate generates an output when only one specific single input signal is present, but not when there is no input signal, nor a second input, nor both signals. A, Truth table and scheme of the regulatory region of the Lac operon as an AND NOT (NOT IF) gate. This AND NOT gate only generates an output when lactose is the only single input available. If Glc and lactose are available in the cell, the lac operon is OFF because the catabolite activator protein, CAP, is not bound. The same is true when Glc, but no lactose, is available. In this case, the lac repressor is bound. In the case when there is neither Glc nor lactose, the lac operon is OFF because even though CAP is bound, the lac repressor prevents transcriptional initiation. Only when there is lactose, but no Glc, available is the lac operon ON. In the absence of Glc, CAP can bind, and because of the availability of lactose, the *lac* repressor is not bound. Both actions are necessary for transcriptional initiation of the *lac* operon. (Adapted from Phillips et al., 2009.) B, An example of an AND NOT (NOT IF) gate in synthetic biology. In this synthetic system, the transactivator SCA (transactivator of the streptogramin-responsive gene regulation system) and the transrepressor PIP-KRAB are constitutively expressed along with a reporter plasmid containing a chimeric SCA- and PIP-specific promoter. The absence of SCB1 [racemic 2-(1V-hydroxy-6-methylheptyl)-3-(hydroxymethyl)butanolide] enables the binding of the transactivator SCA to its corresponding promoter region. The presence of the transrepressor pristinamycin (PI) in turn prevents the binding of PIP-KRAB to its promoter. Thus, this engineered AND NOT gate generates an output only in the presence of pristinamycin and the absence of SCB1. (Adapted from Kramer et al., 2004a.)

BOX 2. Synthetic regulatory open- and close-loop circuits

To program novel cellular behavior, synthetic networks can be designed to respond to exogenous or endogenous biological signals in a predictable manner and yield a determined quantity of an output of choice (Kobayashi et al., 2004). Depending on the desired input and the necessity of a negative or positive feedback to fine-tune the response, open or closed genetic cellular loops can be engineered. In an open-loop system, the exogenous or endogenous biological input signal (control) is processed by a synthetic gene regulatory network that produces an output, e.g., a biological response via an effector. In this configuration, the output itself exerts no effect on the input control signal (see illustration). One typical example would be the exogenous activation of a circuit with light, as with optogenetic tools, in which the output has no effect on the input used to control the process (no feedback involved). A closed-loop system in turn implements an additional module, namely, a negative or positive feedback, directly linking the output to the input signal. These circuits are programmed to reach and maintain a target output level by continuously evaluating, comparing, and correcting the actual values, thus leading to autonomous self-regulation with improved stability, robustness, and reliability (Briat et al., 2016).

When functionally integrated into the endogenous cellular circuitry, synthetic open- and closed-loop systems offer a wide range of customized biomedical applications. Examples include designs for detecting and responding to disease-related signals or biopharmaceutical screening devices. These "prosthetic networks" are able to correct malfunctions or rectify limitations of the endogenous cellular machinery, while, compared to traditional medication, reducing the susceptibility to side effects or interference with endogenous mechanisms. Encapsulation and implantation of the system- containing " desiner cells" allows these devices to be used in vivo (reviewed by Heng et al., 2015).

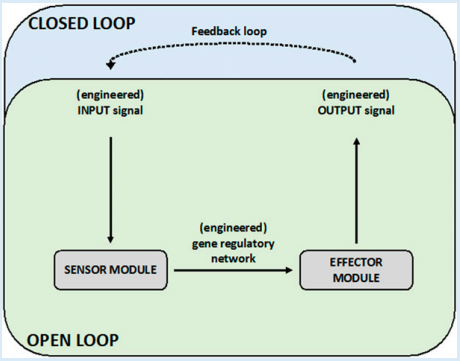

Box 2 Synthetic regulatory open- and closed-loop circuits. Citations: Kobayashi et al., 2004; Heng et al., 2015; Briat et al., 2016.

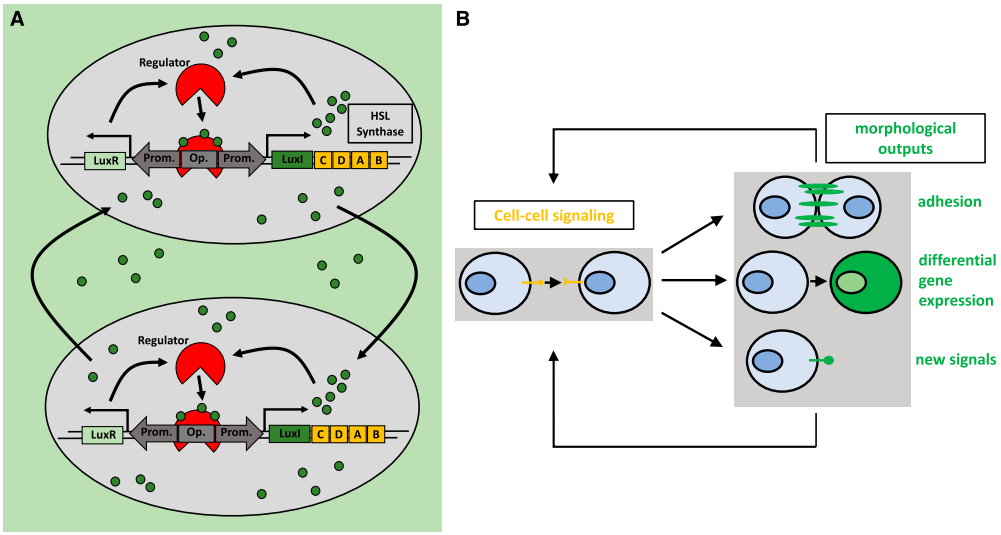

Figure 5. Cell-cell communication in bacteria and synthetic cell-cell communication networks. A, Simplified illustration of the natural homoserine lactone (HSL) quorum-sensing network in *V. fischeri*. Quorum sensing describes the ability of bacteria to assess the cell density of a population by sensing chemical signals that are produced by surrounding cells (Davis et al., 2015). HSLs, in the case of *V. fischeri* AHL, bind to the LuxR protein. LuxR then binds to its cognate operator, inducing the transcription of LuxI, which catalyzes the synthesis of AHL. AHL is able to diffuse out of the cell, accumulating in the external milieu and entering surrounding cells, thus activating the circuit in those cells. B, Engineered cell-cell communication networks in mammalian cells. Engineered cell-cell signaling via two synNotch ligand-receptor pairs was used to manipulate cell adhesion, differentiation, and the production of new cell-cell signals (Toda et al., 2018). Upon binding of the ligand to the synNotch receptor, an orthogonal transcription factor is cleaved from the cytoplasmic tail of the receptor, migrates to the nucleus, and then drives gene expression of the output proteins. These genes include fluorescent proteins as cellular markers for differentiation, several cadherins as morphological outputs, and two synNotch ligand-receptor pairs as input signals. In this way, the outputs are propagated to the next generation. (Adapted from Toda et al., 2018.)

cell adhesion through cell-cell communication was achieved by linking the synthetic notch receptor system to the expression of specific cadherin molecules and new synthetic Notch (synNotch) ligands (Toda et al., 2018; Fig. 5B). Importantly, the synNotch receptor mechanism is also utilized in potentially therapeutic engineered T-cells, which can detect given combinations of antigens (for details, see Fig. 6) instead of only one antigen (Roybal et al., 2016). These engineered combinatorial T-cells represent a breakthrough in the treatment of cancer.

In plants, cell-cell communication also plays an important role. Key regulators such as phytohormones not only control almost every aspect of plant life, like coordinating responses between tissues and organs, but also mediate interactions with symbiotic microorganisms. An example is the phytohormone strigolactone, which can act both as an endogenous phytohormone and as an exogenous signal molecule in the rhizosphere (for review, see Morffy et al., 2016). As an exogenous signal, it recruits arbuscular mycorrhizal fungi to the root to provide the plant with nutrients (i.e. phosphate) under nutrient-limiting conditions (Akiyama et al., 2005). However, strigolactone also mediates the recognition of host roots by parasitic weeds, leading to severe yield losses (Parker, 2009). Inspired by these natural mechanisms, semi- or fully synthetic networks could be engineered to exploit novel useful symbiotic interactions under abiotic and biotic stress or to develop orthogonal signaling networks among organs. Therefore, the manipulation on command of the information flow can be used in strategies to improve crop productivity. It can also be used to abolish or reprogram detrimental or beneficial interactions between microorganisms and plants.

Open- Versus Closed-Loop Circuit Control, and Prosthetic Network Devices Two exemplary realizations of semi-hybrid open-loop control strategies are optogenetic and radio wave-inducible devices for the in vivo regulation of blood Glc levels in mice. Both devices have been developed by integrating a synthetic input module with the native Ca^{2+}-inducible NFAT-signaling pathway, activating the expression of genes involved in several developmental processes and immune responses (Crabtree and Olson, 2002; Crabtree and

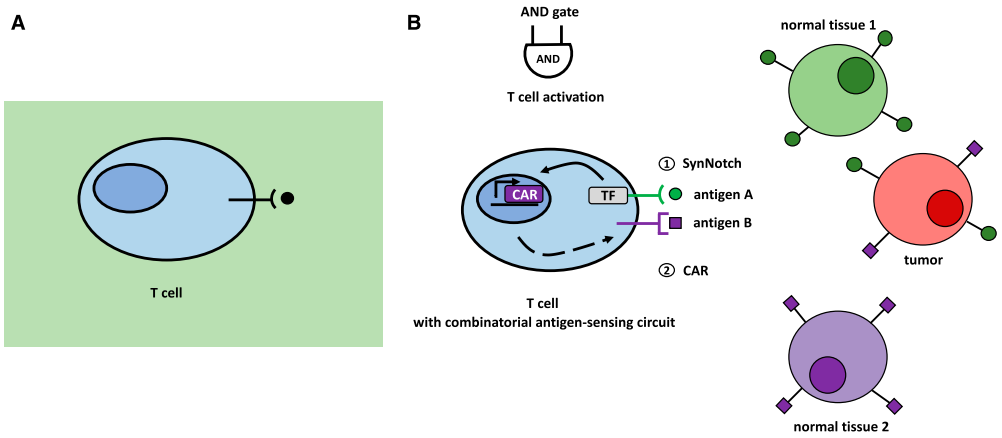

Figure 6. Natural and engineered combinatorial T-cells. A, Natural T-cell with its T-cell receptor, targeting only single antigens. This single-antigen recognition without any further control machinery can lead to off-target tissue damage. B, An engineered synthetic T-cell with new types of receptors specific for detecting given combinations of antigens. Upon binding of antigen A to the synNotch receptor, an orthogonal transcription factor is cleaved from the cytoplasmic tail of the receptor, which in turn activates CAR transcription. If a second antigen, antigen B, is recognized by the newly synthesized CAR receptor, the T-cell is activated. (Adapted from Roybal et al., 2016; Roybal and Lim, 2017.)

Schreiber, 2009). The optogenetic approach uses blue light to activate melanopsin and triggers a signaling cascade to ultimately induce a Ca^{2+} influx (Ye et al., 2011). The second circuit utilizes an engineered temperature-sensitive Ca^{2+} channel. This channel is bound by antibodies coated with ferrous oxide nanoparticles, which are heated with radio waves to trigger channel opening, leading to subsequent Ca^{2+} influx (Stanley et al., 2012).

Smole et al. (2017) reported an exemplary case of a fully synthetic network that can sense an inflammatory signal in mice and produce a response to suppress this signal (Fig. 7). They engineered a synthetic device consisting of a sensor module that, upon activation by inflammation signals, triggers the expression of a transcriptional activator, GAL4-VP16. The fusion protein not only acts as an inducer of expression of anti-inflammatory proteins by the output module but also triggers the positive feedback loop of an amplifying module, leading to enhanced levels of GAL4-VP16. A fourth module constitutively expresses GAL4 lacking the transactivation domain, competing with the GAL4-VP16 for restricting the level of activation of the system, therefore acting as a thresholder device. Due to its autonomous activation by inflammatory signals, the activation of the circuit is independent of external induction. Furthermore, the system includes signal enhancement, while leakage is minimized by the thresholding module. Nevertheless, it still needs external inhibition for resetting the system to the OFF state due to the self-activating positive feedback characteristics and therefore is not strictly a closed-loop system. Ye et al. (2017) accomplished the construction of a closed-loop, prosthetic network for the self-adjusting regulation of the insulin level in vivo, consisting of an implant of encapsulated engineered HEK cells (Fig. 8). Here, perception of insulin by the cell via its native insulin receptor leads to phosphorylation of the insulin receptor substrate 1 protein, triggering a signaling cascade that induces nuclear transport of a MAPK. In the nucleus, the MAPK phosphorylates the ELK1 domain of the synthetic fusion protein TetR-ELK1, initiating the transcriptional activity of a target gene, otherwise tightly disrupted in the absence of insulin or external supplementation of doxycycline. Programming the circuit for the production of adiponectin, a therapeutic protein involved in regulating insulin homeostasis, turns the network into a closed, self-regulating loop, increasing insulin sensitivity in different tissues. The increased sensitivity subsequently leads to reduced insulin production by pancreatic β-cells. Fulfilling a function that is missing in the cellular genetic network, synthetic regulatory circuits in mammalian systems can overcome the constraints of endogenous cellular processes. This illustrates the potential of synthetic biology for developing functional therapeutic devices and tailor-made medicine. Such complexity has not been reached yet in synthetic circuitry in plants; however, the first synthetic networks have already started to be implemented in plants, as described below.

First Attempts at Genetic Circuits in Plants Future development of complex circuitry with predictable and controllable features in plants for biotechnological applications (e.g. production of biopharmaceuticals and

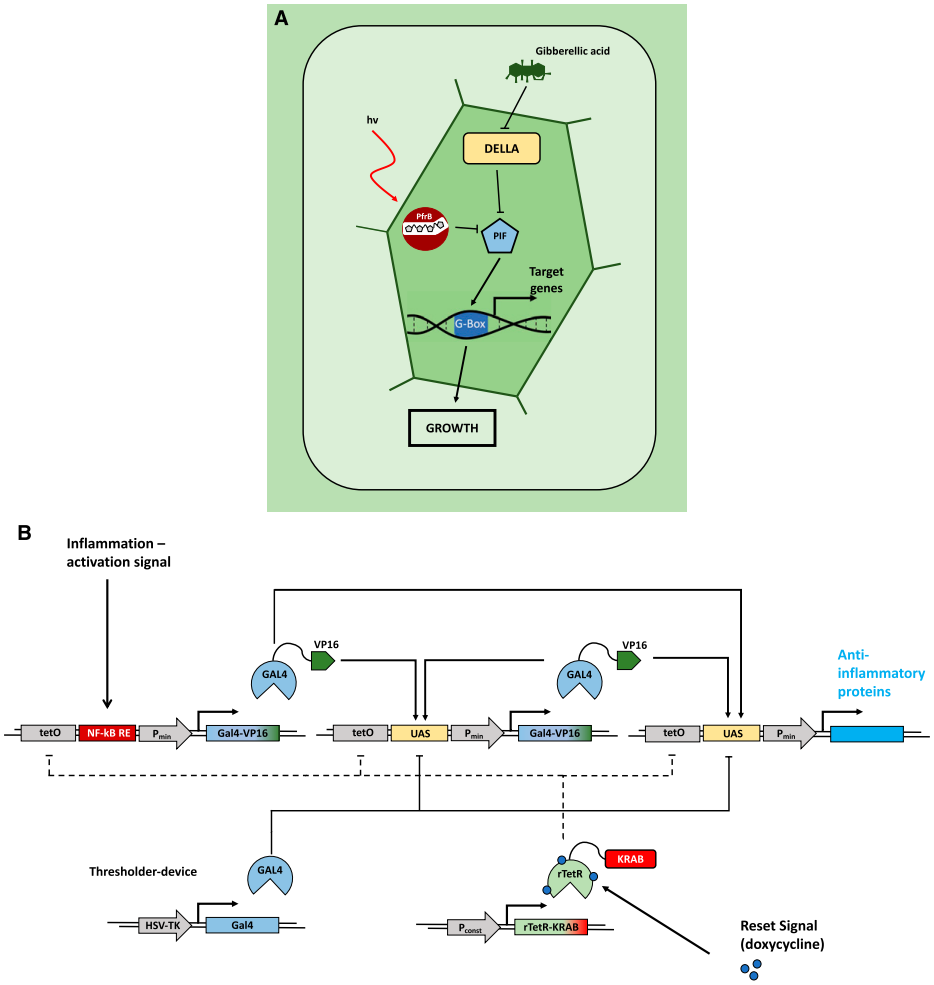

Figure 7. Natural and engineered open-loop regulatory circuits. A, GA_3-induced degradation of DELLA proteins suppresses the repression of PHYTOCHROME INTERACING FACTORs (PIFs). The PIFs subsequently bind to G-box cis regulatory elements in the promotors of response genes, promoting growth responses. In parallel, transcription of PIFs is inhibited by the red light-induced active conformer of phytochrome B, modulating the growth promotion in response to the light conditions. (Adapted from Havko et al., 2016.) B, Schematic overview of a synthetic device for detection of inflammation signals in mammalian systems. Detection of inflammatory signals through the NF-kB-responsive element of the sensor module leads to expression of the transcriptional regulator GAL4 fused to the VP16 transactivation domain (GAL4-VP16). GAL4-VP16 subsequently binds to the UAS motif in the amplifier and effector modules, increasing the abundance of GAL4-VP16 through a self-activating positive feedback loop from the amplifier module. This triggers production of anti-inflammatory proteins via the effector module. Additionally, the system is equipped with a thresholder device, constitutively expressing GAL4 lacking the transactivation domain. GAL4 competes for binding the UAS motifs with the activating GAL4-VP16, thereby restricting the initiation of the expression of the therapeutic output. A fifth module constitutively expresses the doxycycline-inducible reversed tetracycline repressor protein (rTetR) fused to the inhibitory KRAB domain. Exogenous application of doxycycline inhibits the activation of the sensor, amplifier, and effector modules by binding to their upstream tetO motifs, thus deactivating the system. (Adapted from Smole et al., 2017.)

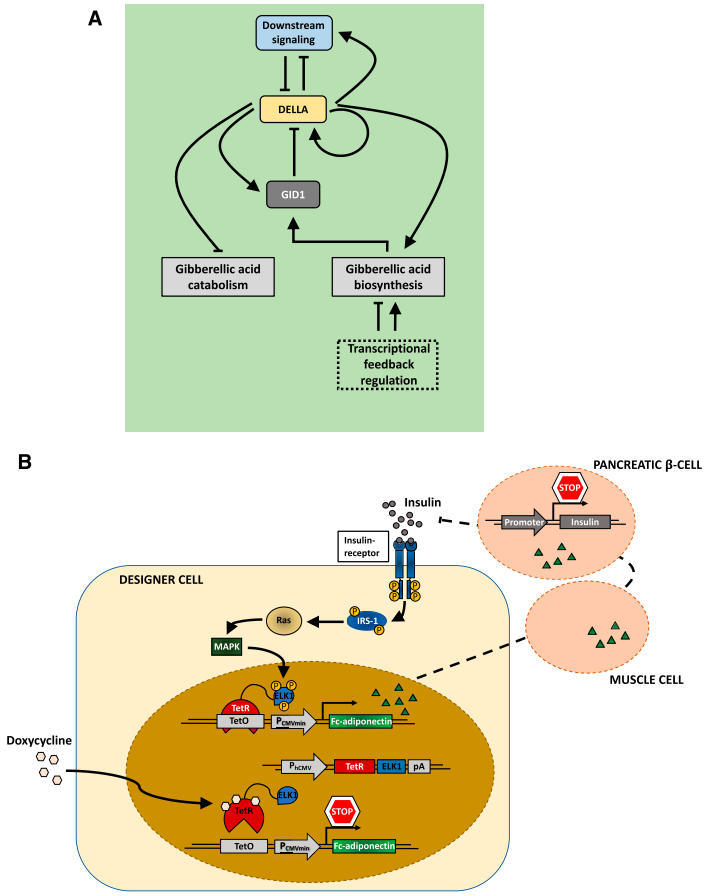

Figure 8. Natural and engineered closed-loop regulatory circuits. A, Simplified model of the homeostatic regulation of GA_3 metabolism and signaling in Arabidopsis. In the absence of the phytohormone GA, the regulator DELLA proteins accumulate. Through transcriptional control of GA metabolism and catabolism, DELLAs boost the level of GA and subsequently of the GA receptor GID1 proteins. Accumulation of the GID1 proteins and of GA eventually leads to GID1-mediated DELLA degradation. These feedback loops ensure GA homeostasis. (Adapted from Hedden and Thomas, 2012.) B, Schematic overview of a synthetic autoregulatory gene circuit for adjusting insulin resistance in mammalian systems. Upon binding of insulin to the insulin receptor of the designer cell, the intracellular β-subunit of the receptor is autophosphorylated. This leads to further phosphorylation of Tyr residues of the insulin receptor substrate 1 (IRS-1), among other proteins, triggering their interaction with several signaling components. Induced by this interaction, the GTPase Ras and the MAPK are activated, triggering nuclear import of the MAPK. In the nucleus, the MAPK phosphorylates the ELK1 domain of the synthetic regulator protein, consisting of the tet repressor (TetR) and the regulated activation domain of the transcription factor ELK1, expressed under the control of the constitutive human cytomegalovirus immediate early promoter (P_{hCMV}). The hybrid transcription factor binds to the tet operator motif (tetO) in a synthetic effector device; however, the activation domain remains inactive. It gets activated and initiates the expression of the therapeutic Fc-adiponectin protein only upon MAPK-induced phosphorylation of the ELK1 domain. Subsequent secretion of Fc-adiponectin increases the sensitivity for insulin in other tissues (e.g. muscle cells), leading to a decreased insulin production of pancreatic β-cells. (Adapted from Ye et al., 2017.)

other fine chemicals and engineering of stress-tolerant traits and enhanced nutritional content) requires one key prerequisite: namely, to have functionally well-characterized synthetic modules and switches. However, the quantitative characterization of genetic parts in plants is a time-consuming process, and the library of available parts to be used in modular assemblies is still rather limited. Moreover, the complexity of plants as multicellular organisms still remains experimentally challenging for constructing and implementing synthetic genetic circuits with a predictable outcome and robustness. A first step toward a consistent functional and quantitative categorization of molecular switches in plants was reported by Schaumberg et al. (2016); Table 1). The authors built a simple genetic circuit in plant protoplasts, comprising two genetic transcriptional switches and a dual-luciferase output. Addition of an inducer (dexamethasone or 4-hydroxytamoxifen) activates expression of a repressor protein and a firefly luciferase, which are both under the control of the same inducible promoter but on different plasmid constructs. In this case, firefly luciferase acts as a proxy for the amount of repressor. The repressor protein, on the other hand, represses Renilla luciferase expression from a second plasmid. In this way, it is possible to obtain quantitative data on the levels of a repressor protein and correlate it with its repressing activity over a target promoter (Schaumberg et al., 2016). This approach could be expanded easily to characterize, in a standardized fashion, transcriptional regulators, promoter sequences, and higher order circuitry arising from combinations of simple modules. As a note, in a recent example following the principle of bypassing endogenous pathways (in this case, a metabolic one), South et al. (2019) engineered an alternate, synthetic glycolate metabolic route. This pathway is more efficient than the endogenous photorespiratory route, increasing photosynthetic efficiency considerably (~40%), thereby leading to increased biomass production of tobacco plants. This example represents a milestone, fostering future similar strategies for other metabolic and signaling networks.

Optogenetically regulated systems have been implemented in plant cells (e.g. protoplasts) for the targeted control of signaling pathways. In a first approach, auxin regulatory networks were manipulated using a red light-inducible gene switch that allowed the quantitative control of the expression of the receptor of auxin, the F-box protein TIR1 (up-regulation and down-regulation upon expression of an antisense microRNA; Müller et al., 2014; Samodelov and Zurbriggen, 2017; Table 1). The effects of precisely tuning the sensitivity of the regulatory network to the hormone was monitored with a genetically encoded biosensor designed ad hoc (Wend et al., 2013). This open-loop system enabled inducible quantitative control and monitoring of a signaling network for the study of complex regulatory principles. This is performed in a simple experimental platform without the need for generating mutants (Müller et al., 2014).

Another example of an open-loop system in plants is a fully synthetic signal transduction system that could potentially be used for the programmable detection of ligands (Antunes et al., 2011). In this approach, bacterial signal transduction components were adapted to eukaryotic target sequences and consequently transferred into transgenic plants. The engineered chimeric His kinase included a bacterial receptor, Tgr, fused to the His kinase PhoR. Upon binding a redesigned periplasmic binding protein in complex with the ligand of interest, this chimeric receptor phosphorylates its cognate chimeric response regulator PhoB-VP64. The response regulator in turn activates the expression of a reporter gene. Drought, in the context of climate changes, is one of the biggest challenges to food security. One promising approach to improve plant water usage is to manipulate the ABA signaling pathway, which plays a major role in drought tolerance (Helander et al., 2016). Recent advances have been made in manipulating different aspects of ABA signaling (e.g. receptor engineering and developing an ABA agonist; Park et al., 2015; Vaidya et al., 2017; Table 1). Cyanabactin is a potent, selective agonist for one distinct ABA receptor family, namely, the subfamily of IIIA receptors. These targeted approaches help bypass pleiotropic or unwanted side effects, resulting in more specific, controllable manipulation of a given signaling network. The promising case of cyanabactin could be a model for further directed design of synthetic substances and synthetic cognate receptors.

DISCUSSION AND PERSPECTIVES

In the almost 20 years since the foundational publications of synthetic devices, synthetic biology has evolved into a mature discipline that already revolutionizes fundamental research, most noticeably biomedicine, as well as the biotechnology industry. A broad range of synthetic molecular tools, regulatory and metabolic circuitry, and even synthetic organelles and genomes have been engineered and successfully applied in bacterial, yeast, and animal systems (Brophy and Voigt, 2014). As described in this article, several synthetic biosensors and switches for the control of gene expression (including a couple of optogenetic modules), genome editing, and protein stability have already been implemented in plants (for review, see Liu et al., 2013; Braguy and Zurbriggen, 2016; Walia et al., 2018). The first approaches toward combinations of switches in plant cell systems are arising, including (1) the use of an optogenetic gene switch to control hormone signaling, coupled to a genetically encoded biosensor, as a proxy of the activity of the signaling pathway (Müller et al., 2014); and (2) a semi- and a fully synthetic transduction pathway, sensing a plant hormone or a foreign metabolite, respectively, by transducing the signal into a phenotypic response (sentinel

OUTSTANDING QUESTIONS

- What technical and theoretical approaches are needed for implementing more complex genetic circuitry in plants? How can the current slow, error-prone synthetic circuitry engineering be improved for a more efficient and predictable assembly of circuits?
- Is it possible to engineer self-regulated, 'smart' pathways that have a novel function in plants with minimized interference over endogenous regulatory networks, thus avoiding negative effects on traits?
- How can the social acceptance of genetically modified plants be improved, in particular in developed countries, to contribute to solving the global question on how to feed the ever-growing world population in an ecologically sustainable manner?

approach; Antunes et al., 2006, 2009). However, engineering and implementation of more complex circuitry is not yet a reality in plant research. Plants are multicellular organisms with complex metabolism and highly regulated and intertwined signaling networks, integrating different environmental cues, like light and temperature, with the genetic program and metabolic status. Experimental constraints and slow generation times often make it cumbersome to implement and evaluate genetic circuits in the whole plant. Altogether, it is still challenging to build synthetic circuits with a predictable output and function.

In order to transition the plant synthetic biology field from a slow and error-prone engineering phase into a more automated, rational, and reliable discipline, a series of approaches have to be implemented. In this way, the development and introduction of advanced circuitry could be achieved, as is already the case for other organisms. In the first place, biosynthetic platforms for the rational design, construction, and quantitative characterization of a bigger number of variants of genetic parts need to be established. Toward this goal, adequate vectors and high-throughput DNA assembly methods are already in place (Patron, 2014; Vazquez-Vilar et al., 2018). However, experimental approaches to quantitatively and functionally describe synthetic modules, as well as hand-in-hand work with mathematical modelers to improve predictability and reliability, still lag behind. Finally, based on the experiences in yeast and animal cells, generalized incorporation of orthogonal components (sensing modules, signaling molecules, and output elements) in the designs will contribute to optimal functionality, including high control specificity, robustness of the networks, and a reduced cross-modulation of the endogenous pathways.

Given the creative and successful applications reported in other organisms, it is easy to imagine that engineering of synthetic circuits in plants will help solve many problems in the near future (see Outstanding Questions). One future goal is to achieve a quantitative increase in crop yield, a much-needed second Green Revolution, to satisfy the demands of the ever-growing world population (Wollenweber et al., 2005). Another goal is to improve plant stress tolerance to environmental hardships by manipulating phytohormone signaling pathways or introducing orthogonal networks, targeting key plant stress responses. First steps toward this were recently reported based on engineering the receptor for the phytohormone ABA and developing chemical agonists thereof to control the responses to drought (Park et al., 2015; Vaidya et al., 2017). A next step would be to design hybrid circuitry to overcome limitations and bypass endogenous regulation of plant signaling networks to improve the efficiency of existing cascades. Self-regulating, smart pathways that bypass endogenous regulation may be easier to design using fully synthetic circuits. These can be engineered to achieve a high target specificity and are orthogonal to the organism, reducing off-target effects. A further application of such smart plants could be the incorporation of synthetic circuitry to integrate information on environmental cues and the genetic program with long-distance synthetic signal transduction. For example, flowering time could be regulated upon computation of the nutrient availability (roots) and perception of environmental stress, thereby optimizing seed production. An alternative approach to increase productivity would be to decouple growth and development from regulatory elements, such as the circadian clock or other genetic programs, thereby achieving longer biosynthetic periods. It is evident that the possible applications of these approaches are endless and would completely reshape plant science. A long-term vision encompasses the implementation of synthetic cellular circuits, such as closed-loop prosthetic networks, which are capable of generating new functionalities, including immune system-like properties or optimized nutrient assimilation and production of high-value compounds. By virtue of the fast development and achievements in other higher eukaryotic systems, we will witness a paradigm change in experimental plant fundamental research and the development of green biotechnological applications in the near future.

ACKNOWLEDGMENTS

We thank Leonie-Alexa Koch for fruitful discussions and comments on the article as well as reviewer 1 for the thorough review and the valuable comments and suggestions that contributed to improve the quality of the article. We apologize to our colleagues whose work could not be cited due to space constraints.

Received November 2, 2018; accepted January 18, 2019; published January 28, 2019.

LITERATURE CITED

Abisado RG, Benomar S, Klaus JR, Dandekar AA, Chandler JR (2018) Bacterial quorum sensing and microbial community interactions. MBio **9:** e02331-17

Ajo-Franklin CM, Drubin DA, Eskin JA, Gee EPS, Landgraf D, Phillips I, Silver PA (2007) Rational design of memory in eukaryotic cells. Genes Dev **21:** 2271–2276

Akiyama K, Matsuzaki K, Hayashi H (2005) Plant sesquiterpenes induce hyphal branching in arbuscular mycorrhizal fungi. Nature **435:** 824–827

Antunes MS, Ha SB, Tewari-Singh N, Morey KJ, Trofka AM, Kugrens P, Deyholos M, Medford JI (2006) A synthetic de-greening gene circuit provides a reporting system that is remotely detectable and has a re-set capacity. Plant Biotechnol J **4:** 605–622

Antunes MS, Morey KJ, Tewari-Singh N, Bowen TA, Smith JJ, Webb CT, Hellinga HW, Medford JI (2009) Engineering key components in a synthetic eukaryotic signal transduction pathway. Mol Syst Biol **5:** 270

Antunes MS, Morey KJ, Smith JJ, Albrecht KD, Bowen TA, Zdunek JK, Troupe JF, Cuneo MJ, Webb CT, Hellinga HW, et al (2011) Programmable ligand detection system in plants through a synthetic signal transduction pathway. PLoS ONE **6:** e16292

Aoyama T, Chua NH (1997) A glucocorticoid-mediated transcriptional induction system in transgenic plants. Plant J **11:** 605–612

Atkinson MR, Savageau MA, Myers JT, Ninfa AJ (2003) Development of genetic circuitry exhibiting toggle switch or oscillatory behavior in Escherichia coli. Cell **113:** 597–607

Ausländer S, Fussenegger M (2017) Synthetic RNA-based switches for mammalian gene expression control. Curr Opin Biotechnol **48:** 54–60

Ausländer S, Ausländer D, Müller M, Wieland M, Fussenegger M (2012) Programmable single-cell mammalian biocomputers. Nature **487:** 123–127

Baaske J, Gonschorek P, Engesser R, Dominguez-Monedero A, Raute K, Fischbach P, Müller K, Cachat E, Schamel WWA, Minguet S, et al (2018) Dual-controlled optogenetic system for the rapid down-regulation of protein levels in mammalian cells. Sci Rep **8:** 15024

Bateman E (1998) Autoregulation of eukaryotic transcription factors. Prog Nucleic Acid Res Mol Biol **60:** 133–168

Beck CF, Mutzel R, Barbé J, Müller W (1982) A multifunctional gene (tetR) controls Tn10-encoded tetracycline resistance. J Bacteriol **150:** 633–642

Becskei A, Serrano L (2000) Engineering stability in gene networks by autoregulation. Nature **405:** 590–593

Becskei A, Séraphin B, Serrano L (2001) Positive feedback in eukaryotic gene networks: Cell differentiation by graded to binary response conversion. EMBO J **20:** 2528–2535

Beerli RR, Schopfer U, Dreier B, Barbas CF III (2000) Chemically regulated zinc finger transcription factors. J Biol Chem **275:** 32617–32627

Berens C, Altschmied L, Hillen W (1992) The role of the N terminus in Tet repressor for tet operator binding determined by a mutational analysis. J Biol Chem **267:** 1945–1952

Beyer HM, Juillot S, Herbst K, Samodelov SL, Müller K, Schamel WW, Römer W, Schäfer E, Nagy F, Strähle U, et al (2015) Red light-regulated reversible nuclear localization of proteins in mammalian cells and zebrafish. ACS Synth Biol **4:** 951–958

Böhmdorfer G, Tramontano A, Luxa K, Bachmair A (2010) A synthetic biology approach allows inducible retrotransposition in whole plants. Syst Synth Biol **4:** 133–138

Bonger KM, Rakhit R, Payumo AY, Chen JK, Wandless TJ (2014) General method for regulating protein stability with light. ACS Chem Biol **9:** 111–115

Braguy J, Zurbriggen MD (2016) Synthetic strategies for plant signalling studies: Molecular toolbox and orthogonal platforms. Plant J **87:** 118–138

Breaker RR (2012) Riboswitches and the RNA world. Cold Spring Harb Perspect Biol **4:** a003566

Briat C, Zechner C, Khammash M (2016) Design of a synthetic integral feedback circuit: Dynamic analysis and DNA implementation. ACS Synth Biol **5:** 1108–1116

Brophy JAN, Voigt CA (2014) Principles of genetic circuit design. Nat Methods **11:** 508–520

Caddick MX, Greenland AJ, Jepson I, Krause KP, Qu N, Riddell KV, Salter MG, Schuch W, Sonnewald U, Tomsett AB (1998) An ethanol inducible gene switch for plants used to manipulate carbon metabolism. Nat Biotechnol **16:** 177–180

Chatelle C, Ochoa-Fernandez R, Engesser R, Schneider N, Beyer HM, Jones AR, Timmer J, Zurbriggen MD, Weber W (2018) A green-light-responsive system for the control of transgene expression in mammalian and plant cells. ACS Synth Biol **7:** 1349–1358

Crabtree GR, Olson EN (2002) NFAT signaling: Choreographing the social lives of cells. Cell (Suppl) **109:** S67–S79

Crabtree GR, Schreiber SL (2009) SnapShot: Ca^{2+}-calcineurin-NFAT signaling. Cell **138:** 210.e1

Culler SJ, Hoff KG, Smolke CD (2010) Reprogramming cellular behavior with RNA controllers responsive to endogenous proteins. Science **330:** 1251–1255

Curtis MD, Grossniklaus U (2003) A Gateway cloning vector set for high-throughput functional analysis of genes in planta. Plant Physiol **133:** 462–469

Danino T, Mondragón-Palomino O, Tsimring L, Hasty J (2010) A synchronized quorum of genetic clocks. Nature **463:** 326–330

Davis RM, Muller RY, Haynes KA (2015) Can the natural diversity of quorum-sensing advance synthetic biology? Front Bioeng Biotechnol **3:** 30

Deisseroth K, Hegemann P (2017) The form and function of channelrhodopsin. Science **357:** eaan5544

Dickson RC, Abelson J, Barnes WM, Reznikoff WS (1975) Genetic regulation: The Lac control region. Science **187:** 27–35

Ellington AD, Szostak JW (1990) In vitro selection of RNA molecules that bind specific ligands. Nature **346:** 818–822

Ellis T, Wang X, Collins JJ (2009) Diversity-based, model-guided construction of synthetic gene networks with predicted functions. Nat Biotechnol **27:** 465–471

Elowitz MB, Leibler S (2000) A synthetic oscillatory network of transcriptional regulators. Nature **403:** 335–338

Endo K, Stapleton JA, Hayashi K, Saito H, Inoue T (2013) Quantitative and simultaneous translational control of distinct mammalian mRNAs. Nucleic Acids Res **41:** e135

Faden F, Ramezani T, Mielke S, Almudi I, Nairz K, Froehlich MS, Höckendorff J, Brandt W, Hoehenwarter W, Dohmen RJ, et al (2016) Phenotypes on demand via switchable target protein degradation in multicellular organisms. Nat Commun **7:** 12202

Fan LZ, Lin MZ (2015) Optical control of biological processes by light-switchable proteins. Wiley Interdiscip Rev Dev Biol **4:** 545–554

Fernández-Niño M, Giraldo D, Gomez-Porras JL, Dreyer I, González Barrios AF, Arevalo-Ferro C (2017) A synthetic multi-cellular network of coupled self-sustained oscillators. PLoS ONE **12:** e0180155

Fire A, Xu S, Montgomery MK, Kostas SA, Driver SE, Mello CC (1998) Potent and specific genetic interference by double-stranded RNA in Caenorhabditis elegans. Nature **391:** 806–811

Fogelmark K, Troein C (2014) Rethinking transcriptional activation in the Arabidopsis circadian clock. PLOS Comput Biol **10:** e1003705

Freeman M (2000) Feedback control of intercellular signalling in development. Nature **408:** 313–319

Frey AD, Rimann M, Bailey JE, Kallio PT, Thompson CJ, Fussenegger M (2001) Novel pristinamycin-responsive expression systems for plant cells. Biotechnol Bioeng **74:** 154–163

Fung E, Wong WW, Suen JK, Bulter T, Lee SG, Liao JC (2005) A synthetic gene-metabolic oscillator. Nature **435:** 118–122

Fuqua WC, Winans SC, Greenberg EP (1994) Quorum sensing in bacteria: The LuxR-LuxI family of cell density-responsive transcriptional regulators. J Bacteriol **176:** 269–275

Gaber R, Lebar T, Majerle A, Šter B, Dobnikar A, Benčina M, Jerala R (2014) Designable DNA-binding domains enable construction of logic circuits in mammalian cells. Nat Chem Biol **10:** 203–208

Gander MW, Vrana JD, Voje WE, Carothers JM, Klavins E (2017) Digital logic circuits in yeast with CRISPR-dCas9 NOR gates. Nat Commun **8:** 15459

Gao Y, Xiong X, Wong S, Charles EJ, Lim WA, Qi LS (2016) Complex transcriptional modulation with orthogonal and inducible dCas9 regulators. Nat Methods **13:** 1043–1049

Gardner MJ, Baker AJ, Assie JM, Poethig RS, Haseloff JP, Webb AAR (2009) GAL4 GFP enhancer trap lines for analysis of stomatal guard cell development and gene expression. J Exp Bot **60:** 213–226

Gardner TS, Cantor CR, Collins JJ (2000) Construction of a genetic toggle switch in Escherichia coli. Nature **403:** 339–342

Gatz C, Frohberg C, Wendenburg R (1992) Stringent repression and homogeneous de-repression by tetracycline of a modified CaMV 35S promoter in intact transgenic tobacco plants. Plant J **2:** 397–404

Goodwin BC (1963) Temporal Organization in Cells: A Dynamic Theory of Cellular Control Processes. Academic Press, London

Goodwin BC (1965) Oscillatory behavior in enzymatic control processes. Adv Enzyme Regul **3:** 425–438

Gossen M, Bujard H (1992) Tight control of gene expression in mammalian cells by tetracycline-responsive promoters. Proc Natl Acad Sci USA **89:** 5547–5551

Gossen M, Freundlieb S, Bender G, Müller G, Hillen W, Bujard H (1995) Transcriptional activation by tetracyclines in mammalian cells. Science **268:** 1766–1769

Guido NJ, Wang X, Adalsteinsson D, McMillen D, Hasty J, Cantor CR, Elston TC, Collins JJ (2006) A bottom-up approach to gene regulation. Nature **439:** 856–860

Hanson S, Bauer G, Fink B, Suess B (2005) Molecular analysis of a synthetic tetracycline-binding riboswitch. RNA **11:** 503–511

Hasty J, Dolnik M, Rottschäfer V, Collins JJ (2002) Synthetic gene network for entraining and amplifying cellular oscillations. Phys Rev Lett **88:** 148101

Havko NE, Major IT, Jewell JB, Attaran E, Browse J, Howe GA (2016) Control of carbon assimilation and partitioning by jasmonate: An accounting of growth-defense tradeoffs. Plants (Basel) **5:** 7

Hedden P, Thomas SG (2012) Gibberellin biosynthesis and its regulation. Biochem J **444:** 11–25

Helander JDM, Vaidya AS, Cutler SR (2016) Chemical manipulation of plant water use. Bioorg Med Chem **24:** 493–500

Heng BC, Aubel D, Fussenegger M (2015) Prosthetic gene networks as an alternative to standard pharmacotherapies for metabolic disorders. Curr Opin Biotechnol **35:** 37–45

Hörner M, Weber W (2012) Molecular switches in animal cells. FEBS Lett **586:** 2084–2096

Jacob F, Monod J (1961) Genetic regulatory mechanisms in the synthesis of proteins. J Mol Biol **3:** 318–356

Jaeger KE, Pullen N, Lamzin S, Morris RJ, Wigge PA (2013) Interlocking feedback loops govern the dynamic behavior of the floral transition in Arabidopsis. Plant Cell **25:** 820–833

Johnson AAT, Hibberd JM, Gay C, Essah PA, Haseloff J, Tester M, Guiderdoni E (2005) Spatial control of transgene expression in rice (Oryza sativa L.) using the GAL4 enhancer trapping system. Plant J **41:** 779–789

Kaberniuk AA, Shemetov AA, Verkhusha VV (2016) A bacterial phytochrome-based optogenetic system controllable with near-infrared light. Nat Methods **13:** 591–597

Khakhar A, Leydon AR, Lemmex AC, Klavins E, Nemhauser JL (2018) Synthetic hormone-responsive transcription factors can monitor and reprogram plant development. eLife **7:** e34702

Kimura M, Kagawa T, Kieber J, Araki T (2006) Phototropin and light-signaling in phototropism. Curr Opin Plant Biol **9:** 503–508

Kobayashi H, Kaern M, Araki M, Chung K, Gardner TS, Cantor CR, Collins JJ (2004) Programmable cells: Interfacing natural and engineered gene networks. Proc Natl Acad Sci USA **101:** 8414–8419

Kolar K, Weber W (2017) Synthetic biological approaches to optogenetically control cell signaling. Curr Opin Biotechnol **47:** 112–119

Kolar K, Wischhusen HM, Müller K, Karlsson M, Weber W, Zurbriggen MD (2015) A synthetic mammalian network to compute population borders based on engineered reciprocal cell-cell communication. BMC Syst Biol **9:** 97

Kolar K, Knobloch C, Stork H, Žnidarič M, Weber W (2018) OptoBase: A web platform for molecular optogenetics. ACS Synth Biol **7:** 1825–1828

Konermann S, Brigham MD, Trevino A, Hsu PD, Heidenreich M, Cong L, Platt RJ, Scott DA, Church GM, Zhang F (2013) Optical control of mammalian endogenous transcription and epigenetic states. Nature **500:** 472–476

Kramer BP, Fischer C, Fussenegger M (2004a) BioLogic gates enable logical transcription control in mammalian cells. Biotechnol Bioeng **87:** 478–484

Kramer BP, Viretta AU, Daoud-El-Baba M, Aubel D, Weber W, Fussenegger M (2004b) An engineered epigenetic transgene switch in mammalian cells. Nat Biotechnol **22:** 867–870

Lagos-Quintana M (2001) Identification of novel genes coding for small expressed RNAs. Science **294:** 853–858

Laplaze L, Parizot B, Baker A, Ricaud L, Martinière A, Auguy F, Franche C, Nussaume L, Bogusz D, Haseloff J (2005) GAL4-GFP enhancer trap lines for genetic manipulation of lateral root development in Arabidopsis thaliana. J Exp Bot **56:** 2433–2442

Lavedrine C, Farcot E, Vernoux T (2015) Modeling plant development: From signals to gene networks. Curr Opin Plant Biol **27:** 148–153

Lebar T, Bezeljak U, Golob A, Jerala M, Kadunc L, Pirš B, Stražar M, Vučko D, Zupančič U, Benčina M, et al (2014) A bistable genetic switch based on designable DNA-binding domains. Nat Commun **5:** 5007

Lienert F, Lohmueller JJ, Garg A, Silver PA (2014) Synthetic biology in mammalian cells: Next generation research tools and therapeutics. Nat Rev Mol Cell Biol **15:** 95–107

Lim WA (2010) Designing customized cell signalling circuits. Nat Rev Mol Cell Biol **11:** 393–403

Liu W, Stewart CN Jr (2015) Plant synthetic biology. Trends Plant Sci **20:** 309–317

Liu W, Yuan JS, Stewart CN Jr (2013) Advanced genetic tools for plant biotechnology. Nat Rev Genet **14:** 781–793

Lowder LG, Zhang D, Baltes NJ, Paul JW III, Tang X, Zheng X, Voytas DF, Hsieh TF, Zhang Y, Qi Y (2015) A CRISPR/Cas9 toolbox for multiplexed plant genome editing and transcriptional regulation. Plant Physiol **169:** 971–985

Lu TK, Khalil AS, Collins JJ (2009) Next-generation synthetic gene networks. Nat Biotechnol **27:** 1139–1150

Lutz R, Bujard H (1997) Independent and tight regulation of transcriptional units in Escherichia coli via the LacR/O, the TetR/O and AraC/I1-I2 regulatory elements. Nucleic Acids Res **25:** 1203–1210

McClung CR (2006) Plant circadian rhythms. Plant Cell **18:** 792–803

McKenzie MJ, Mett V, Stewart Reynolds PH, Jameson PE (1998) Controlled cytokinin production in transgenic tobacco using a copper-inducible promoter. Plant Physiol **116:** 969–977

Medford JI, Prasad A (2016) Towards programmable plant genetic circuits. Plant J **87:** 139–148

Moon TS, Lou C, Tamsir A, Stanton BC, Voigt CA (2012) Genetic programs constructed from layered logic gates in single cells. Nature **491:** 249–253

Morffy N, Faure L, Nelson DC (2016) Smoke and hormone mirrors: Action and evolution of karrikin and strigolactone signaling. Trends Genet **32:** 176–188

Motta-Mena LB, Reade A, Mallory MJ, Glantz S, Weiner OD, Lynch KW, Gardner KH (2014) An optogenetic gene expression system with rapid activation and deactivation kinetics. Nat Chem Biol **10:** 196–202

Müller K, Engesser R, Metzger S, Schulz S, Kämpf MM, Busacker M, Steinberg T, Tomakidi P, Ehrbar M, Nagy F, et al (2013a) A red/far-red light-responsive bi-stable toggle switch to control gene expression in mammalian cells. Nucleic Acids Res **41:** e77

Müller K, Engesser R, Schulz S, Steinberg T, Tomakidi P, Weber CC, Ulm R, Timmer J, Zurbriggen MD, Weber W (2013b) Multi-chromatic control of mammalian gene expression and signaling. Nucleic Acids Res **41:** e124

Müller K, Siegel D, Rodriguez Jahnke F, Gerrer K, Wend S, Decker EL, Reski R, Weber W, Zurbriggen MD (2014) A red light-controlled synthetic gene expression switch for plant systems. Mol Biosyst **10:** 1679–1688

Müller K, Naumann S, Weber W, Zurbriggen MD (2015) Optogenetics for gene expression in mammalian cells. Biol Chem **396:** 145–152

Müller S, Hofbauer J, Endler L, Flamm C, Widder S, Schuster P (2006) A generalized model of the repressilator. J Math Biol **53:** 905–937

Nash AI, McNulty R, Shillito ME, Swartz TE, Bogomolni RA, Luecke H, Gardner KH (2011) Structural basis of photosensitivity in a bacterial light-oxygen-voltage/helix-turn-helix (LOV-HTH) DNA-binding protein. Proc Natl Acad Sci USA **108:** 9449–9454

Nevozhay D, Adams RM, Murphy KF, Josic K, Balázsi G (2009) Negative autoregulation linearizes the dose-response and suppresses the heterogeneity of gene expression. Proc Natl Acad Sci USA **106:** 5123–5128

Nevozhay D, Zal T, Balázsi G (2013) Transferring a synthetic gene circuit from yeast to mammalian cells. Nat Commun **4:** 1451

Nielsen AAK, Voigt CA (2014) Multi-input CRISPR/Cas genetic circuits that interface host regulatory networks. Mol Syst Biol **10:** 763

Nihongaki Y, Yamamoto S, Kawano F, Suzuki H, Sato M (2015) CRISPR-Cas9-based photoactivatable transcription system. Chem Biol **22:** 169–174

Niopek D, Benzinger D, Roensch J, Draebing T, Wehler P, Eils R, Di Ventura B (2014) Engineering light-inducible nuclear localization signals for precise spatiotemporal control of protein dynamics in living cells. Nat Commun **5:** 4404

Niopek D, Wehler P, Roensch J, Eils R, Di Ventura B (2016) Optogenetic control of nuclear protein export. Nat Commun **7:** 10624

Ochoa-Fernandez R, Samodelov SL, Brandl SM, Wehinger E, Müller K, Weber W, Zurbriggen MD (2016) Optogenetics in plants: Red/far-red light control of gene expression. Methods Mol Biol **1408:** 125–139

Okumoto S, Jones A, Frommer WB (2012) Quantitative imaging with fluorescent biosensors. Annu Rev Plant Biol **63:** 663–706

Paek KY, Hong KY, Ryu I, Park SM, Keum SJ, Kwon OS, Jang SK (2015) Translation initiation mediated by RNA looping. Proc Natl Acad Sci USA **112:** 1041–1046

Park SY, Peterson FC, Mosquna A, Yao J, Volkman BF, Cutler SR (2015) Agrochemical control of plant water use using engineered abscisic acid receptors. Nature **520:** 545–548

Parker C (2009) Observations on the current status of *Orobanche* and *Striga* problems worldwide. Pest Manag Sci **65:** 453–459

Patron NJ (2014) DNA assembly for plant biology: Techniques and tools. Curr Opin Plant Biol **19:** 14–19

Phillips R, Kondev J, Theriot J (2009) Physical Biology of the Cell. Garland Science, New York

Piatek A, Ali Z, Baazim H, Li L, Abulfaraj A, Al-Shareef S, Aouida M, Mahfouz MM (2015) RNA-guided transcriptional regulation *in planta* via synthetic dCas9-based transcription factors. Plant Biotechnol J **13:** 578–589

Pillai RS, Artus CG, Filipowicz W (2004) Tethering of human Ago proteins to mRNA mimics the miRNA-mediated repression of protein synthesis. RNA **10:** 1518–1525

Pokhilko A, Mas P, Millar AJ (2013) Modelling the widespread effects of TOC1 signalling on the plant circadian clock and its outputs. BMC Syst Biol **7:** 23

Polstein LR, Gersbach CA (2015) A light-inducible CRISPR-Cas9 system for control of endogenous gene activation. Nat Chem Biol **11:** 198–200

Prindle A, Samayoa P, Razinkov I, Danino T, Tsimring LS, Hasty J (2011) A sensing array of radically coupled genetic 'biopixels.' Nature **481:** 39–44

Purcell O, Savery NJ, Grierson CS, di Bernardo M (2010) A comparative analysis of synthetic genetic oscillators. J R Soc Interface **7:** 1503–1524

Roberts GR, Garoosi GA, Koroleva O, Ito M, Laufs P, Leader DJ, Caddick MX, Doonan JH, Tomsett AB (2005) The alc-GR system: A modified alc gene switch designed for use in plant tissue culture. Plant Physiol **138:** 1259–1267

Rockwell NC, Lagarias JC (2006) The structure of phytochrome: A picture is worth a thousand spectra. Plant Cell **18:** 4–14

Roslan HA, Salter MG, Wood CD, White MRH, Croft KP, Robson F, Coupland G, Doonan J, Laufs P, Tomsett AB, et al (2001) Characterization of the ethanol-inducible alc gene-expression system in Arabidopsis thaliana. Plant J **28:** 225–235

Roybal KT, Lim WA (2017) Synthetic immunology: Hacking immune cells to expand their therapeutic capabilities. Annu Rev Immunol **35:** 229–253

Roybal KT, Williams JZ, Morsut L, Rupp LJ, Kolinko I, Choe JH, Walker WJ, McNally KA, Lim WA (2016) Engineering T cells with customized therapeutic response programs using synthetic notch receptors. Cell **167:** 419–432.e16

Ryback BM, Odoni DI, van Heck RGA, van Nuland Y, Hesselman MC, Martins Dos Santos VAP, van Passel MWJ, Hugenholtz F (2013) Design and analysis of a tunable synchronized oscillator. J Biol Eng **7:** 26

Salinas F, Rojas V, Delgado V, Agosin E, Larrondo LF (2017) Optogenetic switches for light-controlled gene expression in yeast. Appl Microbiol Biotechnol **101:** 2629–2640

Samodelov SL, Zurbriggen MD (2017) Quantitatively understanding plant signaling: Novel theoretical-experimental approaches. Trends Plant Sci **22:** 685–704

Savageau MA (1974) Comparison of classical and autogenous systems of regulation in inducible operons. Nature **252:** 546–549

Schaumberg KA, Antunes MS, Kassaw TK, Xu W, Zalewski CS, Medford JI, Prasad A (2016) Quantitative characterization of genetic parts and circuits for plant synthetic biology. Nat Methods **13:** 94–100

Schena M, Lloyd AM, Davis RW (1991) A steroid-inducible gene expression system for plant cells. Proc Natl Acad Sci USA **88:** 10421–10425

Schibler U, Sassone-Corsi P (2002) A web of circadian pacemakers. Cell **111:** 919–922

Schwab R, Ossowski S, Riester M, Warthmann N, Weigel D (2006) Highly specific gene silencing by artificial microRNAs in Arabidopsis. Plant Cell **18:** 1121–1133

Sheen J (2010) Discover and connect cellular signaling. Plant Physiol **154:** 562–566

Smole A, Lainšček D, Bezeljak U, Horvat S, Jerala R (2017) A synthetic mammalian therapeutic gene circuit for sensing and suppressing inflammation. Mol Ther **25:** 102–119

South PF, Cavanagh AP, Liu HW, Ort DR (2019) Synthetic glycolate metabolism pathways stimulate crop growth and productivity in the field. Science **363:** eaat9077

Stanley SA, Gagner JE, Damanpour S, Yoshida M, Dordick JS, Friedman JM (2012) Radio-wave heating of iron oxide nanoparticles can regulate plasma glucose in mice. Science **336:** 604–608

Stein V, Alexandrov K (2015) Synthetic protein switches: Design principles and applications. Trends Biotechnol **33:** 101–110

Stricker J, Cookson S, Bennett MR, Mather WH, Tsimring LS, Hasty J (2008) A fast, robust and tunable synthetic gene oscillator. Nature **456:** 516–519

Tamsir A, Tabor JJ, Voigt CA (2011) Robust multicellular computing using genetically encoded NOR gates and chemical 'wires.' Nature **469:** 212–215

Thieffry D, Huerta AM, Pérez-Rueda E, Collado-Vides J (1998) From specific gene regulation to genomic networks: A global analysis of transcriptional regulation in Escherichia coli. BioEssays **20:** 433–440

Thurley K, Wu LF, Altschuler SJ (2018) Modeling cell-to-cell communication networks using response-time distributions. Cell Syst **6:** 355–367.e5

Tigges M, Marquez-Lago TT, Stelling J, Fussenegger M (2009) A tunable synthetic mammalian oscillator. Nature **457:** 309–312

Toda S, Blauch LR, Tang SKY, Morsut L, Lim WA (2018) Programming self-organizing multicellular structures with synthetic cell-cell signaling. Science **361:** 156–162

Toettcher JE, Mock C, Batchelor E, Loewer A, Lahav G (2010) A synthetic-natural hybrid oscillator in human cells. Proc Natl Acad Sci USA **107:** 17047–17052

Toettcher JE, Weiner OD, Lim WA (2013) Using optogenetics to interrogate the dynamic control of signal transmission by the Ras/Erk module. Cell **155:** 1422–1434

Tomazou M, Barahona M, Polizzi KM, Stan GB (2018) Computational redesign of synthetic genetic oscillators for independent amplitude and frequency modulation. Cell Syst **6:** 508–520.e5

Trewavas A (2005) Green plants as intelligent organisms. Trends Plant Sci **10:** 413–419

Vaidya AS, Peterson FC, Yarmolinsky D, Merilo E, Verstraeten I, Park SY, Elzinga D, Kaundal A, Helander J, Lozano-Juste J, et al (2017) A rationally designed agonist defines subfamily IIIA abscisic acid receptors as critical targets for manipulating transpiration. ACS Chem Biol **12:** 2842–2848

van Bergeijk P, Adrian M, Hoogenraad CC, Kapitein LC (2015) Optogenetic control of organelle transport and positioning. Nature **518:** 111–114

Van Etten J, Schagat TL, Hrit J, Weidmann CA, Brumbaugh J, Coon JJ, Goldstrohm AC (2012) Human Pumilio proteins recruit multiple deadenylases to efficiently repress messenger RNAs. J Biol Chem **287:** 36370–36383

Vazquez-Vilar M, Orzaez D, Patron N (2018) DNA assembly standards: Setting the low-level programming code for plant biotechnology. Plant Sci **273:** 33–41

Verhounig A, Karcher D, Bock R (2010) Inducible gene expression from the plastid genome by a synthetic riboswitch. Proc Natl Acad Sci USA **107:** 6204–6209

Walia A, Waadt R, Jones AM (2018) Genetically encoded biosensors in plants: Pathways to discovery. Annu Rev Plant Biol **69:** 497–524

Warashina M, Takagi Y, Stec WJ, Taira K (2000) Differences among mechanisms of ribozyme-catalyzed reactions. Curr Opin Biotechnol **11:** 354–362

Weber W, Fux C, Daoud-el Baba M, Keller B, Weber CC, Kramer BP, Heinzen C, Aubel D, Bailey JE, Fussenegger M (2002) Macrolide-based transgene control in mammalian cells and mice. Nat Biotechnol **20:** 901–907

Weinmann P, Gossen M, Hillen W, Bujard H, Gatz C (1994) A chimeric transactivator allows tetracycline-responsive gene expression in whole plants. Plant J **5:** 559–569

Wend S, Dal Bosco C, Kämpf MM, Ren F, Palme K, Weber W, Dovzhenko A, Zurbriggen MD (2013) A quantitative ratiometric sensor for time-resolved analysis of auxin dynamics. Sci Rep **3:** 2052

Wilde RJ, Shufflebottom D, Cooke S, Jasinska I, Merryweather A, Beri R, Brammar WJ, Bevan M, Schuch W (1992) Control of gene expression in tobacco cells using a bacterial operator-repressor system. EMBO J **11:** 1251–1259

Wollenweber B, Porter JR, Lübberstedt T (2005) Need for multidisciplinary research towards a second green revolution. Curr Opin Plant Biol **8:** 337–341

Xiao H, Edwards TE, Ferré-D'Amaré AR (2008) Structural basis for specific, high-affinity tetracycline binding by an in vitro evolved aptamer and artificial riboswitch. Chem Biol **15:** 1125–1137

Xie M, Fussenegger M (2018) Designing cell function: Assembly of synthetic gene circuits for cell biology applications. Nat Rev Mol Cell Biol **19:** 507–525

Xie Z, Wroblewska L, Prochazka L, Weiss R, Benenson Y (2011) Multi-input RNAi-based logic circuit for identification of specific cancer cells. Science **333:** 1307–1311

Ye H, Baba MD, Peng R, Fussenegger M (2011) A synthetic optogentic transcription device enhances blood-glucose homeostasis in mice. Science **332:** 1565–1569

Ye H, Xie M, Xue S, Charpin-El Hamri G, Yin J, Zulewski H, Fussenegger M (2017) Self-adjusting synthetic gene circuit for correcting insulin resistance. Nat Biomed Eng **1:** 0005

You L, Cox RS III, Weiss R, Arnold FH (2004) Programmed population control by cell-cell communication and regulated killing. Nature **428:** 868–871

You YS, Marella H, Zentella R, Zhou Y, Ulmasov T, Ho THD, Quatrano RS (2006) Use of bacterial quorum-sensing components to regulate gene expression in plants. Plant Physiol **140:** 1205–1212

Zhang K, Cui B (2015) Optogenetic control of intracellular signaling pathways. Trends Biotechnol **33:** 92–100

Zuo J, Niu QW, Chua NH (2000) Technical advance: An estrogen receptor-based transactivator XVE mediates highly inducible gene expression in transgenic plants. Plant J **24:** 265–273

5 Material and Methods

5.1 Plant hormone biosensor studies in protoplasts

Specific methods as well as the general protocols for protoplast isolation, transformation and hormone induction are described in the Andres et al. protocol (**Appendix 7.3**).

5.1.2 Plasmid Generation/Construction

Plasmids and Oligos designed and constructed in this work are described in **Table 1** and **Table 2**.

5.1.3 Plant material

Before seeding the *Arabidopsis thaliana* col-0 wt *seeds* on SCA plates, the seeds were surface-sterilized with 5% (w/v) calcium hypochlorite and 0.02% (v/v) Triton X-100 in 80% (v/v) ethanol solution. Then, 200 – 300 seeds were seeded on filter paper strips (approx. 200 – 300 seeds per strip) with two strips per each 12 cm^2 plate (Greiner Bio-One). The plates contained each 50 ml of SCA (seedling culture *Arabidosis*) growth medium [0.32% (w/v) Gamborg B5 basal salt powder with vitamins (bioWORLD), 4 mM $MGSO_4$•$7H_2O$, 43.8 mM sucrose, 0.1% (v/v) Gamborg B5 Vitamin Mix (bioWORLD), and 0.8% (w/v) phytoagar in H_2O (pH 5.8)]. The seedlings for protoplast isolation were grown for 2 weeks in a Sanyo/Panasonic MLR-352-PE growth chamber at 22°C with 16h light per day.

5.1.4 Protoplast isolation and transformation

A. thaliana protoplast isolation and transformation are performed as described in the protocol Andres et al. (**Appendix 7.3**).

5.1.5 Hormone induction/treatment and luminescence analysis

The phytohormones *rac*-GR24, GA_1, GA_3, GA_4, GA_7, GA_9, GA_{20}, IAA as well as Karrikin1 and Karrikin2 were obtained from OlChemIm Ltd. GA_3-AM was purchased from Santa Cruz Biotechnology. Stock solution of either 10 mM or 50 mM were prepared in Acetone (*rac*-GR24), Ethanol (GA_1, GA_3, GA_4, GA_7, GA_9, GA_{20} and IAA) or dimethyl sulfoxide (Karrikin1, Karrikin2 and GA_3-AM). In addition, a 40 mM stock solution of the proteasomal inhibitor MG132 was solved in dimethyl sulfoxide. For proteasomal inhibitor experiments, MG132 was added 2 h prior to hormone induction at the final concentrations indicated.

The hormone induction and the luminescence analysis were performed as described in Andres et al. (**Appendix 7.3**).

5.1.6 Temperature treatment and luminescence analysis

The transformation replicates were pooled 20 h post transformation and transferred in 4 different 24-well plates (Sarstedt) with 3 technical replicates per plate. Each plate was placed in a LED box [illuminated with red light (660 nM, 10 µMol m^{-2} s^{-1}), far-red light (740 nM, 10 µMol m^{-2} s^{-1}) and blue light (460 nM, 10 µMol m^{-2} s^{-1})] with a different temperature condition: either 6 h at 22 °C, 5 h at 22 °C and 1 h at 28 °C, 3 h at 22 °C and 3 h at 28 °C, or 6 h at 28

°C. After the treatment, luminescence analyses were performed. 80 µl of each replicate were transferred into two separate white 96-well assay plates to measure renilla and firefly luciferase simultaneously in two plate readers. Before the measurement, 20 µl of firefly substrate [0.47 mM D-luciferin (Biosynth AG), 20 mM tricine, 2.67 mM $MgSO_4 \cdot 7H_2O$, 0.1 mM $EDTA \cdot 2H_2O$, 33.3 mM dithiothreitol, 0.52 mM adenosine 5′-triphosphate, 0.27 mM acetyl–coenzyme A, 5 mM NaOH, 0.26 mM $MgCO_3 \cdot 5H_2O$, in H_2O] or coelenterazine (472 mM coelenterazine stock solution in methanol, diluted directly before use 1:15 in phosphate-buffered saline) were added to the samples. Firefly luminescence was determined in a Berthold Technologies Centro XS^3 LB 960 Microplate luminometer and renilla luminescence in a Berthold technologies $Tristar^2S$ LB942 Multimode Plate Reader.

5.1.7 Light Boxes

LED boxes were constructed and used as described in Müller et al. (2014).

5.1.8 Statistical Analysis

Ordinary one-way ANOVAs and multiple comparisons for statistical significance were performed with GraphPad Prism 7 for Mac Os X version 10.13.1.

5.2 Reconstruction of plant signaling pathways in mammalian cells

5.2.1 Plasmid generation

Plasmids and Oligos designed and constructed in this work are described in **Table 1** and **Table 2**.

5.2.2 Cell culture

Human embryonic kidney cells (HEK293T; DSMZ, Braunschweig, Germany) were cultivated in Dulbecco´s modified Eagle´s medium (DMEM, PAN Biotech, cat. no. P04-03550) supplemented with 10% (v/v) tetracycline-free fetal bovine serum (FBS; PAN Biotech; cat. no. P30-3602; batch no. P080317TC) and 1.4% (v/v) penicillin/streptomycin (PAN Biotech; cat. no. P06-07100).

5.2.3 PEI Transfection

50,000 HEK293T cells/well were seeded in 500 µl DMEM cell culture medium 24h prior to transfection in 24 well plates (Corning). 0.75 µg DNA per well were diluted in 50 µL OptiMEM (Invitrogen, Thermo Fisher Scientific) and mixed with a PEI/OptiMEM mix [2.5 µL PEI solution (1 mg/ml, Polysciences Europe GmbH cat. no. 23966-1) in 50 µL OptiMEM] (Baaske et al., 2018). After 15 min incubation at RT, 100 µl of the transfection mixes were added to each well in a dropwise manner. The medium was exchanged 4 h post transfection.

5.2.4 Hormone Induction (gibberellin reconstruction)

Culture Medium was exchanged 24 h post transfection with medium containing either 10 µM GA_3-AM, 100 µM GA_3, 100 µM GA_4 (for stock preparation see chapter 5.1.5) or the same

amount of DMSO and ethanol as a control. After 24 h of hormone induction, samples were taken for SEAP reporter assays.

5.2.5 SEAP reporter assay

After 24 h of hormone induction, 200 µl supernatant of each sample were taken for an heat-inactivation step of the endogenous phosphatases at 65 °C for 1 h. Afterwards, 80 µl of the heat-inactivated samples were transferred to a transparent 96 well assay plate and supplemented with 100 µl SEAP buffer (20 mM L-homoarginine, 1 mM $MgCl_2$ 21 % (v/v) diethanolamine). Before the measurement, 20 µl of 120 nM para-Nitrophenylphosphate (pNPP, Sigma-Aldrich) were added and the absorbance was measured at 405 nM for 1 h in a Berthold technologies Tristar^{2}S LB942 Multimode Plate Reader.

The determination of the SEAP activity [U/L] was performed by calculating the slope of the obtained curves [OD/min] in combination with the Lambert-Beer´s-law which results in the following formula:

$$\frac{U}{L} = \frac{E}{\varepsilon \times d} \cdot 10^6 \cdot \frac{200}{80}$$

E = increase in optical density/para-nitrophenolate per minute; ε = 18,600 $M^{-1}cm^{-1}$; d= length of the light path [cm], 0.6 cm; $\frac{200}{80}$ = amount of SEAP-containing supernatant / dilution factor of the sample.

5.2.6 Software

Geneious 10.2.2 for cloning

GraphPad Prism 7.0a for graphs and statistical analysis

BioRender for graphical design

5.3 Plasmids

Table 1: Generation and description of plasmids used in this work. All plasmids are constructed with AQUA or Gibson assembly cloning (Gibson et al., 2009; Beyer et al., 2015a).

Plasmid	Description	Reference
CtrlQuant	**P_{35S}-Renilla-2A-GAGAGAGAGAGAGA-Firefly-myc-pA** Vector for the expression of a ratiometric luminescent biosensor used as a control, where the SM is replaced with a repeated GA sequence.	Samodelov et al., 2016
StrigoQuant	**P_{35S}-Renilla-2A-SMXL6-Firefly-myc-pA** Vector for the expression of a ratiometric luminescent biosensor with SMXL6 as a sensor module.	Samodelov et al., 2016
pGEN016	**P_{35S}-mEGFP-Tnos** Vector encoding mEGFP under the control of P_{35S}.	Received from M. Rodriguez-Franco (University of Freiburg)
pKM018	**P_{SV40}-PhyB(1-650)-L-VP16-NLS-pA** Vector for expression of PhyB fused to VP16 with NLS under control of P_{SV40}.	Müller et al., 2013
pKM195	**(pifO)4-pCMVmin-SEAP-pA** Vector for the expression of SEAP under control of a pif operator-CMVmin promoter.	K. Müller (unpublished)
pMK147	**$P_{EF1\alpha}$-Renilla-2A-Aux/IAA-Firefly-myc** Vector for mammalian expression of Renilla luciferase and auxin sensor module fused to firefly luciferase-myc.	Wend et al., 2013
pMZ124	**P_{35S}-Renilla-2A-OsJAZ5-Firefly-myc** Vector for plant expression of Renilla luciferase and a rice jasmonate sensor module fused to firefly luciferase with myc tag.	S. Wend (unpublished)
pMZ333	**P_{SV40}-PhyB(1-908)-L-mCherry-pA** PhyB expression plasmid encoding the first 908 amino acids of PhyB, a short linker and mCherry.	Beyer et al., 2015
pRSET	**PT7-driven bacterial expression vector**	Novagen
pSAM200	**P_{SV40}–TetR–VP16–pA** Constitutive TetR–VP16 expression vector.	Fussenegger et al., 1997
pTB210	**P_{SV40}- ARR1ΔDDK-eGFP-pA** Mammalian vector for expression of ARR1ΔDDK fused to eGFP control of P_{SV40}.	T.Blomeier (unpublished)
pPF001	**P_{SV40}-PhyB(1-650)-VP16-tetR-PIF6(1-100)-TA** Bicistronic Vector encoding PhyB(1-650)-VP16 and tetR-PIF6(1-100) under control of P_{SV40}.	P. Fischbach (unpublished)
pPF002	**tetO-P_{CMVmin}-SEAP-BGHTA; P_{SV40}-Renilla-SV40TA** Vector for the expression of SEAP under control of a tet operator-CMV-min promoter with a renilla luciferase under control of P_{SV40} as a normalization element.	P. Fischbach (unpublished)
pPF034	**tetO-P_{CMVmin}-SEAP-BGHTA; P_{SV40}-Gaussia-SV40TA** Vector for the expression of SEAP under control of a tet operator-CMV-min promoter with a gaussia luciferase under control of P_{SV40} as a normalization element.	Golonka et al., 2019
pPF100	**P_{35S}-Renilla-2A-IAA10-Firefly-myc-pA** Ratiometric auxin sensor plasmid with *A. thaliana* IAA10 (AT1G04100) as a SM for use in plant cells. IAA10 was amplified from clone DKLAT1G04100 (ABRC)	this work (with P.Fischbach)

	with the oligos oPF202/oPF203 including AQUA overhangs and cloned into pMZ124 backbone which was amplified with oPF074/oPF075.	
pPF101	**P_{35S}-Renilla-2A-IAA11-Firefly-myc-pA** Ratiometric auxin sensor plasmid with *A. thaliana* IAA11 (AT4G28640) as a SM for use in plant cells. IAA11 was amplified from clone DKLAT4G28640 (ABRC) with the oligos oPF205/oPF206 including AQUA overhangs and cloned into pMZ124 backbone which was amplified with oPF074/oPF075.	this work (with P.Fischbach)
pPF102	**P_{35S}-Renilla-2A-IAA29-Firefly-myc-pA** Ratiometric auxin sensor plasmid with *A. thaliana* IAA29 (AT4G32280) as a SM for use in plant cells. IAA29 was amplified from clone U12501 (ABRC) with the oligos oPF208/oPF209 including AQUA overhangs and cloned into pMZ124 backbone which was amplified with oPF074/oPF075.	this work (with P.Fischbach)
pPF103	**P_{35S}-Renilla-2A-IAA33-Firefly-myc-pA** Ratiometric auxin sensor plasmid with *A. thaliana* IAA33 (AT5G57420) as a SM for use in plant cells. IAA33 was amplified from clone C105341 (ABRC) with the oligos oPF211/oPF212 including AQUA overhangs and cloned into pMZ124 backbone which was amplified with oPF074/oPF075.	this work (with P.Fischbach)
pPF104	**P_{35S}-Renilla-2A-IAA32-Firefly-myc-pA** Ratiometric auxin sensor plasmid with *A. thaliana* IAA32 (AT2G01200) as a SM for use in plant cells. IAA32 was amplified from clone DKLAT2G01200 (ABRC) with the oligos oPF200/oPF213 including AQUA overhangs and cloned into pMZ124 backbone which was amplified with oPF074/oPF075.	this work (with P.Fischbach)
pPF105	**P_{35S}-Renilla-2A-IAA34-Firefly-myc-pA** Ratiometric auxin sensor plasmid with *A. thaliana* IAA34 (AT1G15050) as a SM for use in plant cells. IAA34 was amplified from clone DKLAT1G15050 (ABRC) with the oligos oPF217/oPF218 including AQUA overhangs and cloned into pMZ124 backbone which was amplified with oPF074/oPF075.	this work (with P.Fischbach)
pPF106	**P_{35S}-Renilla-2A-IAA12-Firefly-myc-pA** Ratiometric auxin sensor plasmid with *A. thaliana* IAA12 (AT1G04550) as a SM for use in plant cells. IAA12 was amplified from clone DKLAT1G04550 (ABRC) with the oligos oPF220/oPF221 including AQUA overhangs and cloned into pMZ124 backbone which was amplified with oPF074/oPF075.	this work (with P.Fischbach)
pPF107	**P_{35S}-Renilla-2A-IAA13-Firefly-myc-pA** Ratiometric auxin sensor plasmid with *A. thaliana* IAA13 (AT2G33310) as a SM for use in plant cells. IAA13 was amplified from clone DKLAT2G33310 (ABRC) with the oligos oPF223/oPF224 including AQUA overhangs and cloned into pMZ124 backbone which was amplified with oPF074/oPF075.	this work (with P.Fischbach)
pPF108	**P_{35S}-Renilla-2A-IAA5-Firefly-myc-pA** Ratiometric auxin sensor plasmid with *A. thaliana* IAA5 (AT1G15580) as a SM for use in plant cells. IAA5 was amplified from clone DKLAT1G15580 (ABRC) with the oligos oPF226/oPF227 including AQUA overhangs and cloned into pMZ124 backbone which was amplified with oPF074/oPF075.	this work (with P.Fischbach)
pPF109	**P_{35S}-Renilla-2A-IAA6-Firefly-myc-pA** Ratiometric auxin sensor plasmid with *A. thaliana* IAA6 (AT1G52830) as a SM for use in plant cells. IAA6 was amplified from clone DKLAT1G52830 (ABRC) with the oligos oPF229/oPF230 including AQUA overhangs and cloned into pMZ124 backbone which was amplified with oPF074/oPF075.	this work (with P.Fischbach)
pPF110	**P_{35S}-Renilla-2A-IAA19-Firefly-myc-pA** Ratiometric auxin sensor plasmid with *A. thaliana* IAA19 (AT3G15540) as a SM for use in plant cells. IAA19 was amplified from clone DKLAT3G15540 (ABRC) with the oligos oPF232/oPF233 including AQUA overhangs and cloned into pMZ124 backbone which was amplified with oPF074/oPF075.	this work (with P.Fischbach)

pPF111	**P_{35S}-Renilla-2A-IAA15-Firefly-myc-pA** Ratiometric auxin sensor plasmid with *A. thaliana* IAA15 (AT1G80390) as a SM for use in plant cells. IAA15 was amplified from clone DKLAT1G80390 (ABRC) with the oligos oPF235/oPF236 including AQUA overhangs and cloned into pMZ124 backbone which was amplified with oPF074/oPF075.	this work (with P.Fischbach)
pPF112	**P_{35S}-Renilla-2A-IAA27-Firefly-myc-pA** Ratiometric auxin sensor plasmid with *A. thaliana* IAA27 (AT4G29080) as a SM for use in plant cells. IAA27 was amplified from clone DKLAT4G29080 (ABRC) with the oligos oPF238/oPF239 including AQUA overhangs and cloned into pMZ124 backbone which was amplified with oPF074/oPF075.	this work (with P.Fischbach)
pPF113	**P_{35S}-Renilla-2A-IAA1-Firefly-myc-pA** Ratiometric auxin sensor plasmid with *A. thaliana* IAA1 (AT4G14560) as a SM for use in plant cells. IAA1 was amplified from clone DKLAT4G14560 (ABRC) with the oligos oPF241/oPF242 including AQUA overhangs and cloned into pMZ124 backbone which was amplified with oPF074/oPF075.	this work (with P.Fischbach)
pPF114	**P_{35S}-Renilla-2A-IAA2-Firefly-myc-pA** Ratiometric auxin sensor plasmid with *A. thaliana* IAA2 (AT3G23030) as a SM for use in plant cells. IAA2 was amplified from clone DKLAT3G23030 (ABRC) with the oligos oPF244/oPF245 including AQUA overhangs and cloned into pMZ124 backbone which was amplified with oPF074/oPF075.	this work (with P.Fischbach)
pPF115	**P_{35S}-Renilla-2A-IAA3-Firefly-myc-pA** Ratiometric auxin sensor plasmid with *A. thaliana* IAA3 (AT1G04240) as a SM for use in plant cells. IAA3 was amplified from clone DKLAT1G04240 (ABRC) with the oligos oPF247/oPF248 including AQUA overhangs and cloned into pMZ124 backbone which was amplified with oPF074/oPF075.	this work (with P.Fischbach)
pPF116	**P_{35S}-Renilla-2A-IAA4-Firefly-myc-pA** Ratiometric auxin sensor plasmid with *A. thaliana* IAA4 (AT5G43700) as a SM for use in plant cells. IAA4 was amplified from clone DKLAT5G43700A (ABRC) with the oligos oPF250/oPF251 including AQUA overhangs and cloned into pMZ124 backbone which was amplified with oPF074/oPF075.	this work (with P.Fischbach)
pPF117	**P_{35S}-Renilla-2A-IAA16-Firefly-myc-pA** Ratiometric auxin sensor plasmid with *A. thaliana* IAA16 (AT3G04730) as a SM for use in plant cells. IAA16 was amplified from clone DKLAT3G04730 (ABRC) with the oligos oPF253/oPF254 including AQUA overhangs and cloned into pMZ124 backbone which was amplified with oPF074/oPF075.	this work (with P.Fischbach)
pPF118	**P_{35S}-Renilla-2A-IAA17-Firefly-myc-pA** Ratiometric auxin sensor plasmid with *A. thaliana* IAA17 (AT1G04250) as a SM for use in plant cells. IAA17 was amplified from clone pda03372 (the *Arabidopsis* full-length cDNA clone was developed by the plant genome project of RIKEN Genomic Sciences Center) with the oligos oPF256/oPF257 including AQUA overhangs and cloned into pMZ124 backbone which was amplified with oPF074/oPF075.	this work (with P.Fischbach)
pPF119	**P_{35S}-Renilla-2A-IAA7-Firefly-myc-pA** Ratiometric auxin sensor plasmid with *A. thaliana* IAA7 (AT3G23050) as a SM for use in plant cells. IAA7 was amplified from clone DKLAT3G23050 (ABRC) with the oligos oPF259/oPF260 including AQUA overhangs and cloned into pMZ124 backbone which was amplified with oPF074/oPF075.	this work (with P.Fischbach)
pPF120	**P_{35S}-Renilla-2A-IAA14-Firefly-myc-pA** Ratiometric auxin sensor plasmid with *A. thaliana* IAA14 (AT4G14550) as a SM for use in plant cells. IAA14 was amplified from clone DKLAT4G14550 (ABRC) with the oligos oPF262/oPF263 including AQUA overhangs and cloned into pMZ124 backbone which was amplified with oPF074/oPF075.	this work (with P.Fischbach)

pPF121	**P_{35S}-Renilla-2A-IAA8-Firefly-myc-pA** Ratiometric auxin sensor plasmid with *A. thaliana* IAA8 (AT2G22670) as a SM for use in plant cells. IAA8 was amplified from clone DKLAT2G22670 (ABRC) with the oligos oPF265/oPF266 including AQUA overhangs and cloned into pMZ124 backbone which was amplified with oPF074/oPF075.	this work (with P.Fischbach)
pPF122	**P_{35S}-Renilla-2A-IAA9-Firefly-myc-pA** Ratiometric auxin sensor plasmid with *A. thaliana* IAA9 (AT5G65670) as a SM for use in plant cells. IAA9 was amplified from clone DKLAT5G65670 (ABRC) with the oligos oPF268/oPF269 including AQUA overhangs and cloned into pMZ124 backbone which was amplified with oPF074/oPF075.	this work (with P.Fischbach)
pPF123	**P_{35S}-Renilla-2A-IAA28-Firefly-myc-pA** Ratiometric auxin sensor plasmid with *A. thaliana* IAA28 (AT5G25890) as a SM for use in plant cells. IAA28 was amplified from clone DKLAT5G25890.1 (ABRC) with the oligos oPF271/oPF272 including AQUA overhangs and cloned into pMZ124 backbone which was amplified with oPF074/oPF075.	this work (with P.Fischbach)
pPF124	**P_{35S}-Renilla-2A-IAA18-Firefly-myc-pA** Ratiometric auxin sensor plasmid with *A. thaliana* IAA18 (AT1G51950) as a SM for use in plant cells. IAA18 was amplified from clone DKLAT1G51950 (ABRC) with the oligos oPF274/oPF275 including AQUA overhangs and cloned into pMZ124 backbone which was amplified with oPF074/oPF075.	this work (with P.Fischbach)
pPF125	**P_{35S}-Renilla-2A-IAA26-Firefly-myc-pA** Ratiometric auxin sensor plasmid with *A. thaliana* IAA26 (AT3G16500) as a SM for use in plant cells. IAA26 was amplified from clone PYAT3G16500 (ABRC) with the oligos oPF277/oPF278 including AQUA overhangs and cloned into pMZ124 backbone which was amplified with oPF074/oPF075.	this work (with P.Fischbach)
pPF126	**P_{35S}-Renilla-2A-IAA31-Firefly-myc-pA** Ratiometric auxin sensor plasmid with *A. thaliana* IAA31 (AT3G17600) as a SM for use in plant cells. IAA31 was amplified from clone DKLAT3G17600 (ABRC) with the oligos oPF280/oPF281 including AQUA overhangs and cloned into pMZ124 backbone which was amplified with oPF074/oPF075.	this work (with P.Fischbach)
pPF127	**P_{35S}-Renilla-2A-IAA20-Firefly-myc-pA** Ratiometric auxin sensor plasmid with *A. thaliana* IAA20 (AT2G46990) as a SM for use in plant cells. IAA20 was amplified from clone DKLAT2G46990 (ABRC) with the oligos oPF283/oPF284 including AQUA overhangs and cloned into pMZ124 backbone which was amplified with oPF074/oPF075.	this work (with P.Fischbach)
pPF128	**P_{35S}-Renilla-2A-IAA30-Firefly-myc-pA** Ratiometric auxin sensor plasmid with *A. thaliana* IAA30 (AT3G62100) as a SM for use in plant cells. IAA30 was amplified from clone DKLAT3G62100 (ABRC) with the oligos oPF286/oPF287 including AQUA overhangs and cloned into pMZ124 backbone which was amplified with oPF074/oPF075.	this work (with P.Fischbach)
pSLS404	**P_{35S}-Renilla-2A-GAI-Firefly-myc-pA** Ratiometric gibberellin sensor plasmid with *A. thaliana* GAI DELLA as SM for use in plant cells. GAI was amplified from clone U14047 (ABRC) with oligos oSLS401/oSLS402 including Gibson overhangs, Ren-2A was PCR-amplified from pMK147 with oSLS009/oSLS407 including Gibson overhangs. REN-2A and the GAI-amplicon were combined via fusion PCR and cloned into NotI/NheI digested CtrlQuant by Gibson cloning.	provided by L. Schmunk/S. Samodelov in our lab Andres *et al*. manuscript
pSLS405	**P_{35S}-Renilla-2A-RGA-Firefly-myc-pA** Ratiometric gibberellin sensor plasmid with the *A. thaliana* RGA DELLA as SM for use in plant cells. RGA was amplified from clone U13937 (ABRC) with oligos oSLS403/oSLS404 including Gibson overhangs. REN-2A and the RGA-amplicon were combined via fusion PCR and cloned into NotI/NheI digested CtrlQuant by Gibson-cloning.	provided by L. Schmunk/S. Samodelov in our lab Andres *et al*. manuscript

pSLS406	**P_{35S}-Renilla-2A-RGL1-Firefly-myc-pA** Ratiometric gibberellin sensor plasmid with *A. thaliana* RGL1 DELLA as SM for use in plant cells. RGL1 (AY096506) was amplified from clone U18422 (ABRC) with oligos oSLS405/oSLS406 including Gibson overhangs. REN-2A and the RGL1-amplicon were combined via fusion PCR and cloned into NotI/NheI digested CtrlQuant by Gibson-cloning.	provided by L. Schmunk/S. Samodelov in our lab Andres *et al*. manuscript
pSLS411	**P_{SV40}-GID1a-pA** Expression vector encoding the gibberellin receptor GID1a under control of P_{SV40}.	provided by L. Schmunk/S. Samodelov
pSLS412	**P_{SV40}-GID1b-pA** Expression vector encoding the gibberellin receptor GID1b under control of P_{SV40}.	provided by L. Schmunk/S. Samodelov
pSLS413	**P_{SV40}-GID1c-pA** Expression vector encoding the gibberellin receptor GID1c under control of P_{SV40}.	provided by L. Schmunk/S. Samodelov
pSLS414	**P_{SV40}-SLY1-pA** Expression vector encoding SLY1 under control of P_{SV40}.	provided by L. Schmunk/S. Samodelov
pSLS417	**P_{35S}-Renilla-2A-RGL2-Firefly-myc-pA** Ratiometric gibberellin sensor plasmid with *A. thaliana* RGL2 DELLA as SM for use in plant cells. RGL2 (NM_111216) was amplified from RGL2 in S/D-TOPO vector (Invitrogen) received from S. Prat (Centro Nacional de Biotecnología, Madrid) with oSLS422/oSLS423, Ren-2A was PCR amplified with oSLS009/oSLS407 and Gibson-cloned into NotI/NheI digested CtrlQuant.	provided by L. Schmunk/S. Samodelov in our lab Andres *et al*. manuscript
pSLS418	**P_{35S}-Renilla-2A-RGL3-Firefly-myc-pA** Ratiometric gibberellin sensor plasmid with *A. thaliana* RGL3 DELLA as SM for use in plant cells. RGL3 (NM_121755) was amplified from RGL3 in S/D-TOPO vector (Invitrogen) received from S. Prat (Centro Nacional de Biotecnología, Madrid) with oSLS424/oSLS425, Ren-2A was PCR amplified with oSLS009/oSLS407 and Gibson-cloned into NotI/NheI digested CtrlQuant.	provided by L. Schmunk/S. Samodelov in our lab Andres *et al*. manuscript
pSLS443	**P_{SV40}-ARR1ΔDDK-NLS-HA-pA** Mammalian Vector encoding ARR1ΔDDK under control of P_{SV40}.	provided by L. Schmunk/S. Samodelov
pSLS444	**P_{SV40}-ARF19-NLS-HA-pA** Mammalian Vector encoding ARF19 under control of P_{SV40}.	provided by L. Schmunk/S. Samodelov
pSLS470	**P_{35S}-Renilla-2A-RGAΔ17-Firefly-myc-pA** Ratiometric gibberellin sensor plasmid with *A. thaliana* RGAΔ17 DELLA as SM for use in plant cells. RGAΔ17 was amplified from RGAΔ17-containing plasmid received from the group of M. Blazquez with oligos oSLS403/oSLS404 including Gibson overhangs. REN-2A and the RGAΔ17-amplicon were combined via fusion PCR and cloned into NotI/NheI digested CtrlQuant by Gibson-cloning.	provided by L. Schmunk/S. Samodelov in our lab Andres *et al*. manuscript
pSLS479	**P_{35S}-GA2ox-1-Tnos** Vector encoding GA2Ox1 under the control of P_{35S} for the use in plant cells. GA2ox-1 was amplified from ABRC clone (stock number: C105372) using oligos oSLS310/oSLS311. pGEN016 was digested (AgeI/NotI) and the backbone was assembled with the PCR-fragment by GIBSON cloning.	Provided by R. Ochoa-Fernandez/ Andres *et al*. manuscript
pSLS480	**P_{35S}-GA2ox-2-Tnos** Vector encoding GA2Ox2 under the control of P_{35S} for the use in plant cells. GA2ox-2 was amplified from ABRC clone (stock number: U20502) using oligos oSLS312/oSLS313. pGEN016 was digested (AgeI/NotI) and the backbone was assembled with the PCR-fragment by GIBSON cloning.	Provided by R. Ochoa-Fernandez/ Andres *et al*. manuscript
pSLS481	**P_{35S}-GA2ox-8-Tnos** Vector encoding GA2Ox8 under the control of P_{35S} for the use in plant cells. GA2ox-8 was amplified from ABRC clone (stock number: DQ653213) using oligos oSLS314/oSLS315. pGEN016 was digested (AgeI/NotI) and the backbone was assembled with the PCR-fragment by GIBSON cloning.	Provided by R. Ochoa-Fernandez/ Andres *et al*. manuscript

pJA001	**P_{SV40}-SPL9-NLS-pA**	this work
	Mammalian Expression vector for *A. thaliana* SPL9. SPL9 was amplified from pDONR201:SPL9 (provided by G. Coupland) with the oligos oJA001 and oJA002 with AQUA cloning overhangs. pMZ333 was linearized with NotI and XbaI. The fragments were assembled via AQUA cloning.	
pJA003	**P_{SV40}-SPL15-NLS-pA**	this work
	Mammalian Expression vector for *A. thaliana* SPL15. SPL15 was amplified from pDONR201:SPL15 (provided by G. Coupland) with the oligos oJA005 and oJA006 with AQUA cloning overhangs. pMZ333 was linearized with NotI and XbaI. The fragments were assembled via AQUA cloning	
pJA012	**(pifO)4-pCMVmin-SEAP-pA; P_{SV40}-Firefly-SV40TA**	this work
	Vector for the expression of SEAP under control of a pif operator-CMVmin promoter with Firefly as a normalization element under control of P_{SV40} BGHpA was amplified from pPF002 with oPF007 and oPF008, P_{SV40} was amplified from pMZ333 with oPF009 and oJA034. Firefly was amplified from CtrlQUANT with oJA033 and oJA028. pKM195 was linearized with NotI and HindIII. All fragments were assembled by AQUA cloning.	
pJA032	**P_{SV40}-SPL9-VP16-NLS-HAtag-pA**	this work
	Mammalian Expression vector for *A. thaliana* SPL9-VP16. SPL9 was amplified from pJA001 with the oligos oJA058 and oJA059 and VP16 was amplified from pKM018 with oJA060 and oSLS466 with AQUA cloning overhangs. pMZ333 was linearized with NotI and XbaI. The fragments were assembled via AQUA cloning.	
pJA035	**P_{SV40}-Kozak-SPL9-VP16-NLS-HAtag-pA**	this work
	Mammalian Expression vector for *A. thaliana* SPL9-VP16. SPL9 was amplified from pJA001 with the oligos oJA001 and oJA059 and VP16 was amplified from pKM018 with oJA060 and oSLS466 with AQUA cloning overhangs. pMZ333 was linearized with NotI and XbaI. The fragments were assembled via AQUA cloning.	
pJA044	**P_{SV40}-Kozak-SPL15-VP16-NLS-HAtag-pA**	this work
	Mammalian expression vector for *A. thaliana* SPL15-VP16. SPL15 was amplified from pJA003 with the oligos oJA005 and oJA062. pJA032 was amplified with oJA063 and oSLS442. The fragments were assembled via AQUA cloning.	
pJA045	**(pifO)4-pCMVmin-SEAP-pA; P_{SV40}-Gaussia-SV40TA**	this work
	Vector for the expression of SEAP under control of a pif operator-CMVmin promoter with Gaussia as a normalization element under control of P_{SV40}. Gaussia was amplified from pPF034 with oJA082 and oJA083. pJA012 was linearized with AscI and NotI. All fragments were assembled by AQUA cloning.	
pJA052	**pFUL_AmpliconVII_mutated-P_{CMVmin}-SEAP-BGHpA-P_{SV40}-GLuc-SV40pA**	this work
	A. thaliana pFUL-AmpliconVII-mutated was PCR amplified from pFUL-mutated template (provided by G. Coupland) with the oligos oJA096/oJA097. pJA045 was linearized by NheI and EcoRV. The fragments were assembled by AQUA cloning.	
pJA053	**pFUL_AmpliconX_mutated-P_{CMVmin}-SEAP-BGHpA-P_{SV40}-GLuc-SV40pA**	this work
	A. thaliana pFUL-AmpliconX-mutated was PCR amplified from pFUL-mutated template (provided by G. Coupland) with the oligos oJA098/oJA099. pJA045 was linearized by NheI and EcoRV. The fragments were assembled by AQUA cloning.	
pJA057	**pFUL_AmpliconX_wt-P_{CMVmin}-SEAP-BGHpA-P_{SV40}-GLuc-SV40pA**	this work
	A. thaliana pFUL-AmpliconX-wt was PCR amplified from pFUL-wt template (provided by G. Coupland) with the oligos oJA007/oJA008. pJA045 was linearized by NheI and EcoRV. The fragments were assembled by AQUA cloning.	
pJA058	**pFUL_full length-P_{CMVmin}-SEAP-BGHpA-P_{SV40}-GLuc-SV40pA**	this work
	A. thaliana pFUL-full length was PCR amplified from pFUL-wt template (provided by G. Coupland) with the oligos oJA052/oJA053. pJA045 was linearized by NheI and EcoRV. The fragments were assembled by AQUA cloning.	

pJA071	**pFUL_AmpliconVII_wt-P_{CMVmin}-SEAP-BGHpA-P_{SV40}-GLuc-SV40pA** *A. thaliana* pFUL-AmpliconVII-wt was PCR amplified from pFUL-wt template (provided by G. Coupland) with the oligos oJA096/oJA097. pJA045 was linearized by NheI and EcoRV. The fragments were assembled by AQUA cloning.	this work
pJA098	**P_{SV40}-RGA-mCherry-pA** Mammalian expression vector for *Cardamine hirsuta* RGA-mCherry. RGA was amplified from RGA-containing plasmid (provided by the group of M.Tsiantis) and amplified with the oligos oJA218/oJA219. pMZ333 was linearized with NotI and XbaI. The fragments were assembled by AQUA cloning.	this work
pJA106	**P_{35S}-Renilla-2A-SMAX1-Firefly-myc-pA** Ratiometric strigolactone sensor plasmid with *A. thaliana* SMAX1 as SM for use in plant cells. SMAX1 was amplified from a synthesis (IDT) with the oligos oJA109/oJA154 including AQUA overhangs and cloned into pMZ124 backbone which was amplified with oPF074/oPF075.	this work
pJA107	**P_{35S}-Renilla-2A-SMXL7-Firefly-myc-pA** Ratiometric strigolactone sensor plasmid with *A. thaliana* SMXL7 as SM for use in plant cells. SMXL7 was amplified from pdx06209 (the Arabidopsis full-length cDNA clone was developed by the plant genome project of RIKEN Genomic Sciences Center) with the oligos oJA114/oJA156 including AQUA overhangs and cloned into pMZ124 backbone which was amplified with oPF074/oPF075.	this work
pJA108	**P_{35S}-Renilla-2A-SMXL8-Firefly-myc-pA** Ratiometric strigolactone sensor plasmid with *A. thaliana* SMXL8 as SM for use in plant cells. SMXL8 was amplified from pdx45595 (the Arabidopsis full-length cDNA clone was developed by the plant genome project of RIKEN Genomic Sciences Center) with the oligos oJA118/oJA158 including AQUA overhangs and cloned into pMZ124 backbone which was amplified with oPF074/oPF075.	this work
pJA114	**P_{SV40}-SMXL6-mCherry-pA** Mammalian expression vector for *A. thaliana* SMXL6-mCherry. SMXL6 was amplified from pHB1105 with the oligos oJA226 and oJA227. pJA098 was amplified with oJA278 and oJA228. The fragments were assembled by AQUA cloning.	this work
pJA115	**P_{SV40}-SMXL7-mCherry-pA** Mammalian expression vector for *A. thaliana* SMXL7-mCherry. SMXL7 was amplified from pJA107 with the oligos oJA230 and oJA231. pJA098 was amplified with oJA278 and oJA232. The fragments were assembled by AQUA cloning.	this work
pJA116	**P_{SV40}-SMXL8-mCherry-pA** Mammalian expression vector for *A. thaliana* SMXL8-mCherry. SMXL8 was amplified from pJA108 with the oligos oJA233 and oJA234. pJA098 was amplified with oJA278 and oJA235. The fragments were assembled by AQUA cloning.	this work
pJA117	**P_{35S}-Renilla-2A-D14-Firefly-myc-pA** Ratiometric strigolactone sensor plasmid with *A. thaliana* D14 for use in plant cells. D14 was amplified from pda05576 (the Arabidopsis full-length cDNA clone was developed by the plant genome project of RIKEN Genomic Sciences Center) with the oligos oJA237/oJA238 including AQUA overhangs and cloned into pMZ124 backbone which was amplified with oPF074/oPF075.	this work
pJA118	**P_{SV40}-D14-mEGFP-pA** Mammalian expression vector for *A. thaliana* D14-mEGFP. D14 was amplified from pJA117 with the oligos oJA239 and oJA240. pTB210 was amplified with oJA278 and oJA241. The fragments were assembled by AQUA cloning.	this work
pJA119	**P_{35S}-Renilla-2A-SMXL5-Firefly-myc-pA** Ratiometric strigolactone sensor plasmid with *A. thaliana* SMXL5 as SM for use in plant cells. SMXL5 was amplified from pdz37424 (the *Arabidopsis* full-length cDNA clone was developed by the plant genome project of RIKEN Genomic Sciences Center) with the oligos oJA245/oJA246 including AQUA overhangs and cloned into pMZ124 backbone which was amplified with oPF074/oPF075.	this work

pJA134 **P_{35S}-Renilla-2A-SMXL2-Firefly-myc-pA** this work

Ratiometric strigolactone sensor plasmid with *A. thaliana* SMXL2 as SM for use in plant cells. SMXL2 was amplified from SMXL2 template (provided by A. Hiltbrunner) with the oligos oJA285/oJA286 including AQUA overhangs and cloned into pMZ124 backbone which was amplified with oPF074/oPF075.

pJA135 **P_{35S}-Renilla-2A-SMXL3-Firefly-myc-pA** this work

Ratiometric strigolactone sensor plasmid with *A. thaliana* SMXL3 as SM for use in plant cells. SMXL3 was amplified from clone S65279 (ABRC) with the oligos oJA287/oJA288 including AQUA overhangs and cloned into pMZ124 backbone which was amplified with oPF074/oPF075.

pJA136 **P_{35S}-Renilla-2A-SMXL4-Firefly-myc-pA** this work

Ratiometric strigolactone sensor plasmid with *A. thaliana* SMXL4 as SM for use in plant cells. SMXL4 was amplified from CD253079 (ABRC) with the oligos oJA289/oJA290 including AQUA overhangs and cloned into pMZ124 backbone which was amplified with oPF074/oPF075.

pJA140 **P_{35S}-Renilla-2A-RGA(1-61)-Firefly-myc-pA** this work

Ratiometric gibberellin sensor plasmid with *A. thaliana* RGA (first 61 amino acids) for use in plant cells. RGA (1-61) was amplified from pSLS405 with the oligos oJA304/oJA305 including AQUA overhangs and cloned into pMZ124 backbone which was amplified with oPF074/oPF075.

pJA141 **P_{35S}-Renilla-2A-RGA(1-110)-Firefly-myc-pA** this work

Ratiometric gibberellin sensor plasmid with *A. thaliana* RGA (first 110 amino acids) as a SM for use in plant cells. RGA (1-110) was amplified from pSLS405 with the oligos oJA304/oJA308 including AQUA overhangs and cloned into pMZ124 backbone which was amplified with oPF074/oPF075.

pJA148 **P_{35S}-Renilla-2A-RGA(1-200)-Firefly-myc-pA** this work

Ratiometric gibberellin sensor plasmid with *A. thaliana* RGA (first 200 amino acids) as a SM for use in plant cells. RGA (1-200) was amplified from pSLS405 with the oligos oJA304/oJA323 including AQUA overhangs and cloned into pMZ124 backbone which was amplified with oPF074/oPF075.

pJA152 **P_{35S}-NPF3-NOSterm** this work

Expression vector for *A. thaliana* NPF3 for the use in plant cells. NPF3 was amplified from clone U21885 (ABRC) with the oligos oJA332/oJA333. pGEN016 was amplified with oJA105/oJA106. The fragments were assembled by AQUA cloning.

pJA155 **pFUL_full length_mGTAC_AmpliconX-P_{CMVmin}-SEAP-BGHpA-P_{SV40}-GLuc-SV40pA** this work

A. thaliana pFUL-full length-mGTAC-AmpliconX was PCR amplified from pFUL template (provided by G. Coupland) with the oligos oJA052/oJA053. pJA045 was linearized by NheI and EcoRV. The fragments were assembled by AQUA cloning.

pJA157 **pFUL_full length_mGTAC_AmpliconVII-P_{CMVmin}-SEAP-BGHpA-P_{SV40}-GLuc-SV40pA** this work

A. thaliana pFUL-full length-mGTAC-AmpliconVII was PCR amplified from pFUL template (provided by G. Coupland) with the oligos oJA052/oJA053. pJA045 was linearized by NheI and EcoRV. The fragments were assembled by AQUA cloning.

pJA163 **P_{35S}-Renilla-2A-RGA(1-349)-Firefly-myc-pA** this work

Ratiometric gibberellin sensor plasmid with *A. thaliana* RGA (first 349 amino acids) as a SM for use in plant cells. RGA (1-349) was amplified from pSLS405 with the oligos oJA304/oJA368 including AQUA overhangs and cloned into pMZ124 backbone which was amplified with oPF074/oPF075.

pJA164 **P_{35S}-Renilla-2A-Kai2-Firefly-myc-pA** this work

	Ratiometric strigolactone/karrikin receptor sensor plasmid with *A. thaliana* Kai2 for use in plant cells. Kai2 was amplified from AY056190 (the *Arabidopsis* full-length cDNA clone was developed by the plant genome project of RIKEN Genomic Sciences Center) with the oligos oJA369/oJA370 including AQUA overhangs and cloned into pMZ124 backbone which was amplified with oPF074/oPF075.	
pJA165	**pFUL_full length_mGTAC_both Amplicons-P_{CMVmin}-SEAP-BGHpA-P_{SV40}-GLuc-SV40pA**	this work
	A. thaliana pFUL-full length-mGTAC-both Amplicons was PCR amplified from pFUL_mutated template (provided by G. Coupland) with the oligos oJA052/oJA053. pJA045 was linearized by NheI and EcoRV. The fragments were assembled by AQUA cloning.	
pJATB001	**P_{SV40}-GAI-VP16-IRES-TetR-PIF6(1-100)-pA**	this work
	Bicistronic vector encoding GAI-VP16 and TetR–PIF6(1–100) under control of P_{SV40}. GAI was PCR amplified from pSLS404 with oJATB001/oJATB002. pPF001 was linearized with SpeI/EcoRV. The fragments were assembled by AQUA cloning.	
pJATB002	**P_{SV40}-RGA-VP16-IRES-TetR-PIF6(1-100)-pA**	this work
	Bicistronic vector encoding RGA-VP16 and TetR–PIF6(1–100) under control of P_{SV40}. RGA was PCR amplified from pSLS405 with oJATB003/oJATB004. pPF001 was linearized with SpeI/EcoRV. The fragments were assembled by AQUA cloning.	
pJATB003	**P_{SV40}-GAI-VP16-IRES-TetR-Gid1a-pA**	this work
	Bicistronic vector encoding GAI-VP16 and TetR–Gid1a under control of P_{SV40}. Gid1a was PCR amplified from pSLS411 with oJATB005/oJATB006. pJATB001 was linearized with BsrGI/AscI. The fragments were assembled by AQUA cloning.	
pJATB004	**P_{SV40}-GAI-VP16-IRES-TetR-Gid1b-pA**	this work
	Bicistronic vector encoding GAI-VP16 and TetR–Gid1b under control of P_{SV40}. Gid1b was PCR amplified from pSLS412 with oJATB007/oJATB008. pJATB001 was linearized with BsrGI/AscI. The fragments were assembled by AQUA cloning.	
pJATB005	**P_{SV40}-GAI-VP16-IRES-TetR-Gid1c-pA**	this work
	Bicistronic vector encoding GAI-VP16 and TetR–Gid1c under control of P_{SV40}. Gid1c was PCR amplified from pSLS413 with oJATB009/oJATB010. pJATB001 was linearized with BsrGI/AscI. The fragments were assembled by AQUA cloning.	
pJATB006	**P_{SV40}-RGA-VP16-IRES-TetR-Gid1a-pA**	this work
	Bicistronic vector encoding RGA-VP16 and TetR–Gid1a under control of P_{SV40}. Gid1a was PCR amplified from pSLS411 with oJATB005/oJATB006. pJATB002 was linearized with BsrGI/AscI. The fragments were assembled by AQUA cloning.	
pJATB007	**P_{SV40}-RGA-VP16-IRES-TetR-Gid1b-pA**	this work
	Bicistronic vector encoding RGA-VP16 and TetR–Gid1b under control of P_{SV40}. Gid1b was PCR amplified from pSLS412 with oJATB007/oJATB008. pJATB002 was linearized with BsrGI/AscI. The fragments were assembled by AQUA cloning.	
pJATB008	**P_{SV40}-RGA-VP16-IRES-TetR-Gid1c-pA**	this work
	Bicistronic vector encoding RGA-VP16 and TetR–Gid1c under control of P_{SV40}. Gid1c was PCR amplified from pSLS413 with oJATB009/oJATB010. pJATB002 was linearized with BsrGI/AscI. The fragments were assembled by AQUA cloning.	
pJATB009	**P_{SV40}-GAI-VP16-IRES-TetR-ARF19-pA**	this work
	Bicistronic vector encoding GAI-VP16 and TetR–ARF19 under control of P_{SV40}. ARF19 was PCR amplified from pSLS444 with oJATB011/oJATB012. pJATB001 was linearized with BsrGI/AscI. The fragments were assembled by AQUA cloning.	
pJATB010	**P_{SV40}-GAI-VP16-IRES-TetR-ARR1ΔDKK -pA**	this work
	Bicistronic vector encoding GAI-VP16 and TetR–ARR1 under control of P_{SV40}.	

	ARR1ΔDKK was PCR amplified from pSLS443 with oJATB015/oJATB014. pJATB001 was linearized with BsrGI/AscI. The fragments were assembled by AQUA cloning.	
pJATB011	**P_{SV40}-RGA-VP16-IRES-TetR-ARF19-pA**	this work
	Bicistronic vector encoding RGA-VP16 and TetR–ARF19 under control of P_{SV40}. ARF19 was PCR amplified from pSLS444 with oJATB011/oJATB012. pJATB002 was linearized with BsrGI/AscI. The fragments were assembled by AQUA cloning.	
pJATB012	**P_{SV40}-RGA-VP16-IRES-TetR-ARR1ΔDKK-pA**	this work
	Bicistronic vector encoding RGA-VP16 and TetR–ARR1 under control of P_{SV40}. ARR1ΔDKK was PCR amplified from pSLS443 with oJATB015/oJATB014. pJATB002 was linearized with BsrGI/AscI. The fragments were assembled by AQUA cloning.	
pJATB013	**P_{SV40}-GAI-VP16-IRES-TetR-SPL9-pA**	this work
	Bicistronic vector encoding GAI-VP16 and TetR–SPL9 under control of P_{SV40}. SPL9 was PCR amplified from pJA001 with oJATB018/oJATB019. pJATB001 was linearized with BsrGI/AscI. The fragments were assembled by AQUA cloning.	
pJATB014	**P_{SV40}-GAI-VP16-IRES-TetR-SPL15-pA**	this work
	Bicistronic vector encoding GAI-VP16 and TetR–SPL15 under control of P_{SV40}. SPL15 was PCR amplified from pJA003 with oJATB020/oJATB021. pJATB001 was linearized with BsrGI/AscI. The fragments were assembled by AQUA cloning.	
pJATB015	**P_{SV40}-RGA-VP16-IRES-TetR-SPL9-pA**	this work
	Bicistronic vector encoding RGA-VP16 and TetR–SPL9 under control of P_{SV40}. SPL9 was PCR amplified from pJA001 with oJATB018/oJATB019. pJATB002 was linearized with BsrGI/AscI. The fragments were assembled by AQUA cloning.	
pJATB016	**P_{SV40}-RGA-VP16-IRES-TetR-SPL15-pA**	this work
	Bicistronic vector encoding RGA-VP16 and TetR–SPL15 under control of P_{SV40}. SPL15 was PCR amplified from pJA003 with oJATB020/oJATB021. pJATB002 was linearized with BsrGI/AscI. The fragments were assembled by AQUA cloning.	
pJATB017	**P_{SV40}-RGA-VP16-IRES-TetR-PIF1-pA**	this work
	Bicistronic vector encoding RGA-VP16 and TetR–PIF1 under control of P_{SV40}. PIF1 was PCR amplified from pHB090 with oJATB023/oJATB024. pJATB002 was linearized with BsrGI/AscI. The fragments were assembled by AQUA cloning.	
pJATB018	**P_{SV40}-RGA-VP16-IRES-TetR-PIF3-pA**	this work
	Bicistronic vector encoding RGA-VP16 and TetR–PIF3 under control of P_{SV40}. PIF3 was PCR amplified from pMZ725 with oJATB025/oJATB026. pJATB002 was linearized with BsrGI/AscI. The fragments were assembled by AQUA cloning.	
pJATB019	**P_{SV40}-RGA-VP16-IRES-TetR-PIF4-pA**	this work
	Bicistronic vector encoding RGA-VP16 and TetR–PIF4 under control of P_{SV40}. PIF4 was PCR amplified from pHB091 with oJATB027/oJATB028. pJATB002 was linearized with BsrGI/AscI. The fragments were assembled by AQUA cloning.	
pJATB020	**P_{SV40}-GAI-VP16-IRES-TetR-PIF1-pA**	this work
	Bicistronic vector encoding GAI-VP16 and TetR–PIF1 under control of P_{SV40}. PIF1 was PCR amplified from pHB090 with oJATB023/oJATB024. pJATB001 was linearized with BsrGI/AscI. The fragments were assembled by AQUA cloning.	
pJATB021	**P_{SV40}-GAI-VP16-IRES-TetR-PIF3-pA**	this work
	Bicistronic vector encoding GAI-VP16 and TetR–PIF3 under control of P_{SV40}. PIF3 was PCR amplified from pMZ725 with oJATB025/oJATB026. pJATB001 was linearized with BsrGI/AscI. The fragments were assembled by AQUA cloning.	
pJATB022	**P_{SV40}-GAI-VP16-IRES-TetR-PIF4-pA**	this work
	Bicistronic vector encoding GAI-VP16 and TetR–PIF4 under control of P_{SV40}. PIF4 was PCR amplified from pHB091 with oJATB025/oJATB026. pJATB001 was linearized with BsrGI/AscI. The fragments were assembled by AQUA cloning.	

pJATB023	**P_{SV40}-GAI-VP16-IRES-TetR-SLY1-pA**	this work
	Bicistronic vector encoding GAI-VP16 and TetR–SLY1 under control of P_{SV40}. SLY1 was PCR amplified from pSLS414 with oJATB029/oJATB030. pJATB001 was linearized with BsrGI/AscI. The fragments were assembled by AQUA cloning.	
pJATB024	**P_{SV40}-RGA-VP16-IRES-TetR-SLY1-pA**	this work
	Bicistronic vector encoding RGA-VP16 and TetR–SLY1 under control of P_{SV40}. SLY1 was PCR amplified from pSLS414 with oJATB029/oJATB030. pJATB002 was linearized with BsrGI/AscI. The fragments were assembled by AQUA cloning.	
pJATB025	**P_{SV40}-SLY1-VP16-IRES-TetR-Gid1a-pA**	this work
	Bicistronic vector encoding SLY1-VP16 and TetR–Gid1a under control of P_{SV40}. SLY1 was PCR amplified from pSLS414 with oJATB031/oJATB032. pJATB003 was linearized with SpeI/EcoRV. The fragments were assembled by AQUA cloning.	
pJATB026	**P_{SV40}-SLY1-VP16-IRES-TetR-Gid1b-pA**	this work
	Bicistronic vector encoding SLY1-VP16 and TetR–Gid1b under control of P_{SV40}. SLY1 was PCR amplified from pSLS414 with oJATB031/oJATB032. pJATB004 was linearized with SpeI/EcoRV. The fragments were assembled by AQUA cloning.	
pJATB027	**P_{SV40}-SLY1-VP16-IRES-TetR-Gid1c-pA**	this work
	Bicistronic vector encoding SLY1-VP16 and TetR–Gid1c under control of P_{SV40}. SLY1 was PCR amplified from pSLS414 with oJATB031/oJATB032. pJATB005 was linearized with SpeI/EcoRV. The fragments were assembled by AQUA cloning.	
pJATB028	**P_{SV40}-GAI-VP16-IRES-TetR-RGA-pA**	this work
	Bicistronic vector encoding GAI-VP16 and TetR–RGA under control of P_{SV40}. RGA was PCR amplified from pSLS405 with oJATB033/oJATB034. pJATB001 was linearized with BsrGI/AscI. The fragments were assembled by AQUA cloning.	
pJATB029	**P_{SV40}-RGA-VP16-IRES-TetR-GAI-pA**	this work
	Bicistronic vector encoding RGA-VP16 and TetR–GAI under control of P_{SV40}. GAI was PCR amplified from pSLS404 with oJATB035/oJATB036. pJATB002 was linearized with BsrGI/AscI. The fragments were assembled by AQUA cloning.	
pJATB030	**P_{SV40}-Gid1a-VP16-IRES-TetR-GAI-pA**	this work
	Bicistronic vector encoding Gid1a-VP16 and TetR–GAI under control of P_{SV40}. Gid1a was PCR amplified from pSLS411 with oJATB037/oJATB038. pJATB029 was linearized with SpeI/EcoRV. The fragments were assembled by AQUA cloning.	
pJATB031	**P_{SV40}-Gid1b-VP16-IRES-TetR-GAI-pA**	this work
	Bicistronic vector encoding Gid1b-VP16 and TetR–GAI under control of P_{SV40}. Gid1b was PCR amplified from pSLS412 with oJATB039/oJATB040. pJATB029 was linearized with SpeI/EcoRV. The fragments were assembled by AQUA cloning.	
pJATB032	**P_{SV40}-Gid1c-VP16-IRES-TetR-GAI-pA**	this work
	Bicistronic vector encoding Gid1c-VP16 and TetR–GAI under control of P_{SV40}. Gid1c was PCR amplified from pSLSL413 with oJATB041/oJATB042. pJATB029 was linearized with SpeI/EcoRV. The fragments were assembled by AQUA cloning.	
pJATB033	**P_{SV40}-Gid1a-VP16-IRES-TetR-RGA-pA**	this work
	Bicistronic vector encoding Gid1a-VP16 and TetR–RGA under control of P_{SV40}. Gid1a was PCR amplified from pSLS411 with oJATB037/oJATB038. pJATB028 was linearized with SpeI/EcoRV. The fragments were assembled by AQUA cloning.	
pJATB034	**P_{SV40}-Gid1b-VP16-IRES-TetR-RGA-pA**	this work
	Bicistronic vector encoding Gid1b-VP16 and TetR–RGA under control of P_{SV40}.	

	Gid1b was PCR amplified from pSLS412 with oJATB039/oJATB040. pJATB028 was linearized with SpeI/EcoRV. The fragments were assembled by AQUA cloning.	
pJATB035	**P_{SV40}-Gid1c-VP16-IRES-TetR-RGA-pA** Bicistronic vector encoding Gid1c-VP16 and TetR–RGA under control of P_{SV40}. Gid1c was PCR amplified from pSLS413 with oJATB041/oJATB042. pJATB028 was linearized with SpeI/EcoRV. The fragments were assembled by AQUA cloning.	this work
pJATB036	**P_{SV40}-RGAΔ17-VP16-IRES-TetR-Gid1a-pA** Bicistronic vector encoding RGAΔ17-VP16 and TetR–Gid1a under control of P_{SV40}. RGAΔ17 was PCR amplified from pSLS470 with oJATB003/oJATB004. pJATB003 was linearized with SpeI/EcoRV. The fragments were assembled by AQUA cloning.	this work
pJATB037	**P_{SV40}-RGAΔ17-VP16-IRES-TetR-Gid1b-pA** Bicistronic vector encoding RGAΔ17-VP16 and TetR–Gid1b under control of P_{SV40}. RGAΔ17 was PCR amplified from pSLS470 with oJATB003/oJATB004. pJATB004 was linearized with SpeI/EcoRV. The fragments were assembled by AQUA cloning.	this work
pJATB038	**P_{SV40}-RGAΔ17-VP16-IRES-TetR-Gid1c-pA** Bicistronic vector encoding RGAΔ17-VP16 and TetR–Gid1c under control of P_{SV40}. RGAΔ17 was PCR amplified from pSLS470 with oJATB003/oJATB004. pJATB005 was linearized with SpeI/EcoRV. The fragments were assembled by AQUA cloning.	this work

The plasmids pPF100 - pPF128 were designed by P. Fischbach and S. Romero and cloned by P. Fischbach.

The plasmids pJATB001 – pJATB038 were designed and cloned together with T. Blomeier.

5.4 Oligonucleotides

Table 2: Oligonucleotides used in this work.

oligo	Sequence (5´->3´)	description
oJA001	TCTTTTATTTCAGGTCCCGGATCGAATTGCCCACCATGGAGATGGGTTCCAACTCG	Fw SPL9
oJA002	CTGGATCGAAGCTTGGGCTGCAGGTCGACTCTACACCTTCCTCTTCTTCTTTGGGAGAGACCAGTTGGTATGGTG	Rev SPL9
oJA005	TCTTTTATTTCAGGTCCCGGATCGAATTGCCCACCATGGAGTTGTTAATGTGTTCGG	Fw SPL15
oJA006	CTGGATCGAAGCTTGGGCTGCAGGTCGACTCTACACCTTCCTCTTCTTCTTTGGAAGAGACCAATTGAAATGTTGA	Rev SPL15
oJA007	CGAAAAGTGCCACCTGACGTCGTCGACGATGATATCAGTCGTTATAGTGTTACTGTAGA	Fw FUL Amplicon X
oJA008	AACGAGCTCTGCTTATATAGGGCTAGCTCGTGTGCTTGTAACTCGTTCGT	Rev FUL Amplicon X
oJA028	CGATTGATCAGGCGCGCCCGGGCCGGCCGCCACGGCGATCTTTCCGCCCTTCT	Rev FF
oJA033	GGTCCCGGATCGGAATTGCGGCCGCCCACCATGGAAGACGCCAAAAACATAAAGAAAGGC	FW FF
oJA034	ATGTTTTTGGCGTCTTCCATGGTGGGCGGCCGCAATTCCGATCCGGGACCTGAAATAAAA	Rev SV40
oJA052	CCGAAAAGTGCCACCTGACGTCGTCGACGATGATATCACTGACTTACTGTGATCTAAATGTT	Fw FUL full length
oJA053	AACGAGCTCTGCTTATATAGGGCTAGCTCGTCGCGACATATCTCTCTCTCTTCAAAATCTCA	Rev FUL full length
oJA058	TTTTATTTCAGGTCCCGGATCGAATTGCGGGCGGCCGCATGGAGATGGGTTCCAACT	Fw SPL9
oJA059	ACTACCAGCACTACCAGCACTATCGAATTCACCGGTGAGAGACCAGTTGGTATGGT	Rev SPL9
oJA060	TCTTCTTCTCACCATACCAACTGGTCTCTCACCGGTGAATTCGATAGTGCTGGTAGTGCTGGTAG	Fw VP16
oJA062	CTACCAGCACTACCAGCACTATCGAATTCACCGGTAAGAGACCAATTGAAATGTTGAGG	Rev SPL15
oJA063	TCCTCTCCTCAACATTTCAATTGGTCTCTTACCGGTGAATTCGATAGTGCTGGTAGTGCTGGTAGT	Fw VP16
oJA082	TTTATTTCAGGTCCCGGATCGGAATTGCGCGGCCGCCCACCATGGGAGTCAAAGT	Fw Gaussia
oJA083	TGTTTTAAGTTTAAACATCGATTGATCAGGCGCGCCTTAGTCACCACCGGCC	Rev Gaussia
oJA096	CGAAAAGTGCCACCTGACGTCGTCGACGATGATATCACAACTCGACATAAGGAATCAC	Fw FUL Amplicon VII
oJA097	AACGAGCTCTGCTTATATAGGGCTAGCTCGTCGCGAATTGATAACTGATAGTCTGATACCAAAC	Rev FUL Amplicon VII
oJA098	CGAAAAGTGCCACCTGACGTCGTCGACGATGATATCAGTCGTTATAGTGTTACTGTAGAAAGTA	Fw FUL Amplicon X
oJA099	AACGAGCTCTGCTTATATAGGGCTAGCTCGTCGCGATTTGTGCCTCCCTTTAGCT	Rev FUL Amplicon X
oJA105	AAGGCCAAGAAGGGCGGAAAGATCGCCGTGTAACTGATCTCGAGGCGAATTTCCCCGA	Fw pGEN016
oJA106	TTGTTCTGGATCATAAACTTTCGAAGTCATGGTGGCGACCGGTAGCG	Rev pGEN016
oJA109	GCCGGCGACGTGGAATCAAATCCTGGACCCATGAGAGCTGGTTTAAGTACGAT	Fw SMAX1
oJA114	GCCTTTCTTTATGTTTTTGGCGTCTTCCATTACTGCCAAAGTAATAGTTGTCG	Fw SMXL7
oJA118	GCCGGCGACGTGGAATCAAATCCTGGACCCATGCCAACGGCGGTGA	Fw SMXL8
oJA154	CGCCGGGCCTTTCTTTATGTTTTTGGCGTCTTCCATGCTAGCTACTGCCAAAGTAATAGTTGTCG	Rev SMAX1
oJA156	CGCCGGGCCTTTCTTTATGTTTTTGGCGTCTTCCATGCTAGCGATCACTTCGACTCTCGC	Rev SMXL7
oJA158	CGCCGGGCCTTTCTTTATGTTTTTGGCGTCTTCCATGCTAGCCTGAGATTTTACAAAGAACAAGTCCATTTG	Rev SMXL8
oJA226	TGTCTTTTATTTCAGGTCCCGGATCGAATTGCGCGGCCGCATGCCGACGCCGGT	Fw SMXL6
oJA227	TTATCCTCCTCGCCCTTGCTCACCATTGCTGACCATATCACATCCACCTTCGCC	Rev SMXL6
oJA230	TGTCTTTTATTTCAGGTCCCGGATCGAATTGCGCGGCCGCATGCCGACACCAGTAACCAC	Fwd SMXL7
oJA231	TTATCCTCCTCGCCCTTGCTCACCATTGCTGAGATCACTTCGACTCTCGCCG	Rev SMXL7
oJA232	TACAACAGTTTCCGGCGAGAGTCGAAGTGATCTCAGCAATGGTGAGCAAGGG	Fw mCherry
oJA233	TGTCTTTTATTTCAGGTCCCGGATCGAATTGCGCGGCCGCATGCCAACGGCGGTG	Fw SMXL8
oJA234	TTATCCTCCTCGCCCTTGCTCACCATTGCTGACTGAGATTTTACAAAGAACAAGTCCATTTGATC	Rev SMXL8
oJA237	TGGCCGGCGACGTGGAATCAAATCCTGGACCCATGAGTCAACACAACATCTTAGAAG	Fw D14
oJA238	GGCCTTTCTTTATGTTTTTGGCGTCTTCCATGCTAGCCCGAGGAAGAGCTCG	Rev D14
oJA239	TGTCTTTTATTTCAGGTCCCGGATCGAATTGCGCGGCCGCATGAGTCAACACAACATCTTAGAAGC	Fw D14
oJA240	AACAGCTCCTCGCCCTTGCTCACCATGCTGCCCCGAGGAAGAGCTCGC	Rev D14
oJA241	TTGCTCAGTTTCTCCGGCGAGCTCTTCCTCGGGGCAGCATGGTGAGCAAGGGCG	Fw mEGFP
oJA245	TGGCCGGCGACGTGGAATCAAATCCTGGACCCATGCGAACAGGTGGTTATAC	Fw SMXL5
oJA246	GGGCCTTTCTTTATGTTTTTGGCGTCTTCCATGCTAGCCTCGAACTTGGAAACTTGGA	Rev SMXL5
oJA278	GCAATTCGATCCGGGACCT	Rev pMZ333
oJA285	TGGCCGGCGACGTGGAATCAAATCCTGGACCCATGAGAGCAGATTTGATTACTATACAGCAAAC	Fw SMXL2
oJA286	GGGCCTTTCTTTATGTTTTTGGCGTCTTCCATGCTAGCAACGACCACCGTCCTGATAC	Rev SMXL2
oJA287	TGGCCGGCGACGTGGAATCAAATCCTGGACCCATGAGAGCTGGAGGCTGCA	Fw SMXL3

oJA288	GGGCCTTTCTTTATGTTTTTGGCGTCTTCCATGCTAGCTGTTGATGAACACTTGAAATGAAACCGTG	Rev SMXL3
oJA289	TGGCCGGCGACGTGGAATCAAATCCTGGACCCATGCGTACAGGGGCTTATACC	Fw SMXL4
oJA290	GGGCCTTTCTTTATGTTTTTGGCGTCTTCCATGCTAGCATCAACAAAGGAAACATGGATTCTG	Rev SMXL4
oJA304	TGGCCGGCGACGTGGAATCAAATCCTGGACCCGCGCGCATGAAGAGAGATCA	Fw RGA short
oJA305	GGGCCTTTCTTTATGTTTTTGGCGTCTTCCATTCCGCCATCTCCGATGACC	Rev RGA short
oJA308	GGGCCTTTCTTTATGTTTTTGGCGTCTTCCATAGGAGGATTAAGCTCAGAGAGCAT	Rev RGA short 2 domains
oJA323	GGGCCTTTCTTTATGTTTTTGGCGTCTTCCATCGTCGTTGTCGTGGTGGTT	Rev RGA short 3
oJA368	GCCTTTCTTTATGTTTTTGGCGTCTTCCATACCTCCTTCTCGAAGCGC	Rev RGA short 4
oJA369	TGGCCGGCGACGTGGAATCAAATCCTGGACCCATGGGTGTGGTAGAAGAAGC	Fw Kai2
oJA370	GGGCCTTTCTTTATGTTTTTGGCGTCTTCCATCATAGCAATGTCATTACGAATGTG	Rev Kai2
oJATB001	GTCTTTTATTTCAGGTCCCGGATCGGAATTGACTAGTCCACCATGAAGAGAGATCAT	Fw GAI
oJATB002	CTACCAGCACTACCAGCACTATCGAATTCGATATCATTGGTGGAGAGTTTCCAAG	Rev GAI
oJATB003	GTCTTTTATTTCAGGTCCCGGATCGGAATTGACTAGTCCACCATGAAGAGAGATCATCACCAATTCC	Fw RGA
oJATB004	CTACCAGCACTACCAGCACTATCGAATTCGATATCGTACGCCGCCGTCGA	Rev RGA
oJATB005	AGGCGGTGGAAGTGGTGGCGGAGGTAGCGATTGTACAATGGCTGCGAGCGAT	Fw GID1a
oJATB006	TATCTTATCATGTCTGGATCGAAGCTTTTAGGCGCGCCTTAACATTCCGCGTTTACAAACG	Rev GID1a
oJATB007	AGGCGGTGGAAGTGGTGGCGGAGGTAGCGATTGTACAATGGCTGGTGGTAACGA	Fw GID1b
oJATB008	TATCTTATCATGTCTGGATCGAAGCTTTTAGGCGCGCCCTAAGGAGTAAGAAGCACAGGA	Rev GID1b
oJATB009	GAGGCGGTGGAAGTGGTGGCGGAGGTAGCGATTGTACAATGGCTGGAAGTGAAGAAG	Fw GID1c
oJATB010	TATCTTATCATGTCTGGATCGAAGCTTTTAGGCGCGCCTCATTGGCATTCTGCGTTTA	Rev GID1c
oJATB011	AGGCGGTGGAAGTGGTGGCGGAGGTAGCGATTGTACAATGAAAGCTCCATCAAATGGAT	Fw ARF19
oJATB012	TATCTTATCATGTCTGGATCGAAGCTTTTAGGCGCGCCCTATCTGTTGAAAGAAGCTGCA	Rev ARF19
oJATB014	TATCTTATCATGTCTGGATCGAAGCTTTTAGGCGCGCCTCAAACCGGAATGTTATCGATGGA	Rev ARR1ΔDKK
oJATB015	GAGGCGGTGGAAGTGGTGGCGGAGGTAGCGATTGTACAATGTCACGGAAGAGGAAAGACG	Fw ARR1ΔDKK
oJATB018	AGGCGGTGGAAGTGGTGGCGGAGGTAGCGATTGTACAATGGAGATGGGTTCCAACTC	Fw SPL9
oJATB019	TATCTTATCATGTCTGGATCGAAGCTTTTAGGCGCGCCTCAGAGAGACCAGTTGGTATG	Rev SPL9
oJATB020	AGGCGGTGGAAGTGGTGGCGGAGGTAGCGATTGTACAATGGAGTTGTTAATGTGTTCGG	Fw SPL15
oJATB021	TATCTTATCATGTCTGGATCGAAGCTTTTAGGCGCGCCTCAAAGAGACCAATTGAAATGTTGA	Rev SPL15
oJATB023	GGCGGTGGAAGTGGTGGCGGAGGTAGCGATTGTACAATGCATCATTTTGTCCCTG	Fw PIF1
oJATB024	TATCTTATCATGTCTGGATCGAAGCTTTTAGGCGCGCCTTAACCTGTTGTGTGGTTTC	Rev PIF1
oJATB025	GGCGGTGGAAGTGGTGGCGGAGGTAGCGATTGTACAATGCCTCTGTTTGAGCTTTT	Fw PIF3
oJATB026	TATCTTATCATGTCTGGATCGAAGCTTTTAGGCGCGCCCTACGACGATCCACAAAACTGAT	Rev PIF3
oJATB027	GGCGGTGGAAGTGGTGGCGGAGGTAGCGATTGTACAATGGAACACCAAGGTTGG	Fw PIF4
oJATB028	TATCTTATCATGTCTGGATCGAAGCTTTTAGGCGCGCCCTAGTGGTCCAAACGAGAAC	Rev PIF4
oJATB029	GGCGGTGGAAGTGGTGGCGGAGGTAGCGATTGTACAATGAAGCGCAGTACTACC	Fw SLY1
oJATB030	TATCTTATCATGTCTGGATCGAAGCTTTTAGGCGCGCCTTATTTGGATTCTGGAAGAGGTC	Rev SLY1
oJATB031	TCTTTTATTTCAGGTCCCGGATCGGAATTGACTAGTCCACCATGAAGCGCAGT	Fw SLY1
oJATB032	ACTACCAGCACTACCAGCACTATCGAATTCGATATCTTTGGATTCTGGAAGAGGTCTCTTA	Rev SLY1
oJATB033	GGCGGTGGAAGTGGTGGCGGAGGTAGCGATTGTACAATGAAGAGAGATCATCACCAATTCCAAGGT	Fw RGA
oJATB034	TATCTTATCATGTCTGGATCGAAGCTTTTAGGCGCGCCCTAGTACGCCGCCGTCGA	Rev RGA
oJATB035	GGCGGTGGAAGTGGTGGCGGAGGTAGCGATTGTACAATGAAGAGAGATCATCATCATCATC	Fw GAI
oJATB036	TATCTTATCATGTCTGGATCGAAGCTTTTAGGCGCGCCCTAATTGGTGGAGAGTTTCCAAG	Rev GAI
oJATB037	ACTACCAGCACTACCAGCACTATCGAATTCGATATCACATTCCGCGTTTACAAACGC	Fw GID1a
oJATB038	CTTTTATTTCAGGTCCCGGATCGGAATTGACTAGTCCACCATGGCTGCGAGCGAT	Rev GID1a
oJATB039	ACTACCAGCACTACCAGCACTATCGAATTCGATATCAGGAGTAAGAAGCACAGGACTTG	Fw GID1b
oJATB040	CTTTTATTTCAGGTCCCGGATCGGAATTGACTAGTCCACCATGGCTGGTGG	Rev GID1b
oJATB041	CTTTTATTTCAGGTCCCGGATCGGAATTGACTAGTCCACCATGGCTGGAAG	Fw GID1c
oJATB042	ACTACCAGCACTACCAGCACTATCGAATTCGATATCTTGGCATTCTGCGTTTACAAATG	Rev GID1c
oPF007	ACCTACAGCCCAGTGGCCTCGAGCTGCAGAAAGCTTCTTAAGCGACTGTGCCTTCTAGTTGCCAGC	Fw BGH TA
oPF008	GACACACATTCCACAGCCATAGAGCCCACCGCATCCC	Rev BGH TA
oPF009	GCGGTGGGCTCTATGGCTGTGGAATGTGTGTCAGTTAGGGTG	Fw SV40
oPF074	ATGGAAGACGCCAAAAACATAAAGAAAGGCC	Fw pMZ124 BB
oPF075	GGGTCCAGGATTTGATTCCACGTCG	Rev pMZ124 BB
oPF202	AACTGGCCGGCGACGTGGAATCAAATCCTGGACCCATGAATGGTTTGCAAGAAGTTTGTTCGTCAAGTG	Fw IAA10
oPF203	GCCTTTCTTTATGTTTTTGGCGTCTTCCATGCTAGACTTACCTACTCCAGCTCCAATTGATG	Rev IAA10
oPF205	AACTGGCCGGCGACGTGGAATCAAATCCTGGACCCATGGAAGGCGGTTCCGCTAGTGG	Fw IAA11
oPF206	CCTTTCTTTATGTTTTTGGCGTCTTCCATGCTAGATAATATCATCTGAGCTTTACCAGTAGCCTC	Rev IAA11

oPF208	ACTGGCCGGCGACGTGGAATCAAATCCTGGACCCATGGAGTTGGATCTTGGTCTATCTCTTTCAC	Fw IAA29
oPF209	GCCTTTCTTTATGTTTTTGGCGTCTTCCATGCTAGAAAACAAACATCTTGTATATGCACACGGTCG	Rev IAA29
oPF211	AACTGGCCGGCGACGTGGAATCAAATCCTGGACCCATGAATAGTTTCGAGCCACAAAGCCAAGAC	Fw IAA33
oPF212	ATGTTTTTGGCGTCTTCCATGCTAGACTCGTTTCTTTTAACTTGTCTTGTGTTTCCCTTG	Rev IAA33
oPF214	AACTGGCCGGCGACGTGGAATCAAATCCTGGACCCATGGACCCAAACACACCTGCAGAC	Fw IAA32
oPF215	CTTTCTTTATGTTTTTGGCGTCTTCCATGCTAGAAAAGGGAAGAAGAGCATCGTTTCTTC	Rev IAA32
oPF217	AACTGGCCGGCGACGTGGAATCAAATCCTGGACCCATGTATTGCAGCGATCCTCCCCATC	Fw IAA34
oPF218	TCTTTATGTTTTTGGCGTCTTCCATGCTAGAAAAGGGAAGTACAGCATCGTTTCTTCTTG	Rev IAA34
oPF220	AACTGGCCGGCGACGTGGAATCAAATCCTGGACCCATGCGTGGTGTGTCAGAATTGGAGG	Fw IAA12
oPF221	TCTTTATGTTTTTGGCGTCTTCCATGCTAGAAACAGGGTTGTTTCTTTGTCTATCCTTC	Rev IAA12
oPF223	CCGGCGACGTGGAATCAAATCCTGGACCCATGATTACTGAACTTGAGATGGGGAAAGGTG	Fw IAA13
oPF224	GGGCCTTTCTTTATGTTTTTGGCGTCTTCCATGCTAGAAACCGGCTGCTTTCGCTGTCTC	Rev IAA13
oPF226	ACTGGCCGGCGACGTGGAATCAAATCCTGGACCCATGGCGAATGAGAGTAATAATCTTGGACTC	Fw IAA5
oPF227	TTTCTTTATGTTTTTGGCGTCTTCCATGCTAGATCCTCTGTTACATGATCTCTTCATAATCC	Rev IAA5
oPF229	ACTGGCCGGCGACGTGGAATCAAATCCTGGACCCATGGCAAAGGAAGGTCTAGCACTCGAG	Fw IAA6
oPF230	TTTCTTTATGTTTTTGGCGTCTTCCATGCTAGAATCTTGCTGGAGACCAAAACCAGTTGC	Rev IAA6
oPF232	AACTGGCCGGCGACGTGGAATCAAATCCTGGACCCATGGAGAAGGAAGGACTCGGGCTTG	Fw IAA19
oPF233	GCCTTTCTTTATGTTTTTGGCGTCTTCCATGCTAGACTCGTCTACTCCTCTAGGCTGC	Rev IAA19
oPF235	ACTGGCCGGCGACGTGGAATCAAATCCTGGACCCATGTCACCGGAGGAATACGTTAGGG	Fw IAA15
oPF236	TCTTTATGTTTTTGGCGTCTTCCATGCTAGATAATCCAATAGCATCTCCGGTTTTCATTAAC	Rev IAA15
oPF238	TGGCCGGCGACGTGGAATCAAATCCTGGACCCATGTCTGTATCTGTAGCAGCAGAGCATG	Fw IAA27
oPF239	CCTTTCTTTATGTTTTTGGCGTCTTCCATGCTAGAGTTCCTGCTTCTGCACTTCTCCATC	Rev IAA27
oPF241	TGGCCGGCGACGTGGAATCAAATCCTGGACCCATGGAAGTCACCAATGGGCTTAACCTTAAG	Fw IAA1
oPF242	CCTTTCTTTATGTTTTTGGCGTCTTCCATGCTAGATAAGGCAGTAGGAGCTTCGGATCC	Rev IAA1
oPF244	ACTGGCCGGCGACGTGGAATCAAATCCTGGACCCATGGCGTACGAGAAAGTCAACGAGC	Fw IAA2
oPF245	CCTTTCTTTATGTTTTTGGCGTCTTCCATGCTAGATAAGGAAGAGTCTAGAGCAGGAGCG	Rev IAA2
oPF247	ACTGGCCGGCGACGTGGAATCAAATCCTGGACCCATGGATGAGTTTGTTAACCTCAAGGAAACAG	Fw IAA3
oPF248	TTTCTTTATGTTTTTGGCGTCTTCCATGCTAGATACACCACAGCCTAAACCTTTGGCTTC	Rev IAA3
oPF250	ACTGGCCGGCGACGTGGAATCAAATCCTGGACCCATGGAAAAAGTTGATGTTTATGATGAGCTTG	Fw IAA4
oPF251	TTCTTTATGTTTTTGGCGTCTTCCATGCTAGAAAGACCACCACAACCTAAACCTTTAACTTC	Rev IAA4
oPF253	AACTGGCCGGCGACGTGGAATCAAATCCTGGACCCATGATTAATTTTGAGGCCACGGAGCTGAG	Fw IAA16
oPF254	TTTCTTTATGTTTTTGGCGTCTTCCATGCTAGAACTTCTGTTCTTGCACTTTTCTAATGCCC	Rev IAA16
oPF256	AACTGGCCGGCGACGTGGAATCAAATCCTGGACCCATGATGGGCAGTGTCGAGCTGAATC	Fw IAA17
oPF257	TTTCTTTATGTTTTTGGCGTCTTCCATGCTAGAAGCTCTGCTCTTGCACTTCTCCATC	Rev IAA17
oPF259	TGGCCGGCGACGTGGAATCAAATCCTGGACCCATGATCGGCCAACTTATGAACCTCAAGG	Fw IAA7
oPF260	TCTTTATGTTTTTGGCGTCTTCCATGCTAGAAGATCTGTTCTTGCAGTACTTCTCCATTG	Rev IAA7
oPF262	TGGCCGGCGACGTGGAATCAAATCCTGGACCCATGAACCTTAAGGAGACGGAGCTTTGTC	Fw IAA14
oPF263	TTCTTTATGTTTTTGGCGTCTTCCATGCTAGATGATCTGTTCTTGAACTTCTCCATTGCTC	Rev IAA14
oPF265	TGGCCGGCGACGTGGAATCAAATCCTGGACCCATGTCTTATCGATTGCTAAGTGTGGATAAGG	Fw IAA8
oPF266	TCTTTATGTTTTTGGCGTCTTCCATGCTAGAAACCCGCTCTTTGTTCTTCGATTTCTCC	Rev IAA8
oPF268	TGGCCGGCGACGTGGAATCAAATCCTGGACCCATGTCCCCGGAAGAGGAGCTACAG	Fw IAA9
oPF269	TCTTTATGTTTTTGGCGTCTTCCATGCTAGAAGCTCTCATCTTCGATTTCTCCATTGCTC	Rev IAA9
oPF271	ACTGGCCGGCGACGTGGAATCAAATCCTGGACCCATGGAAGAAGAAAAGAGATTGGAGCTAAGG	Fw IAA28
oPF272	CCTTTCTTTATGTTTTTGGCGTCTTCCATGCTAGATTCCTTGCCATGTTTTCTAGGTGAGAGTG	Rev IAA28
oPF274	TGGCCGGCGACGTGGAATCAAATCCTGGACCCATGGAGGGTTATTCAAGAAACGGTGAAATC	Fw IAA18
oPF275	TTTCTTTATGTTTTTGGCGTCTTCCATGCTAGATCTTCTCATTTTCTCTTGCTTACCATTTCC	Rev IAA18
oPF277	ACTGGCCGGCGACGTGGAATCAAATCCTGGACCCATGGAAGGTTGTCCAAGAAACAGAGAAATCG	Fw IAA26
oPF278	TTCTTTATGTTTTTGGCGTCTTCCATGCTAGAGTGCATCATCTTCTCTTGCTTACTGCATC	Rev IAA26
oPF280	TGGCCGGCGACGTGGAATCAAATCCTGGACCCATGGAGGTCTCTAACTCTTGTTCTTCATTTTC	Fw IAA31
oPF281	TTTCTTTATGTTTTTGGCGTCTTCCATGCTAGAATACCTCTCCGGTCTCGTGATCTTTAG	Rev IAA31
oPF283	ACTGGCCGGCGACGTGGAATCAAATCCTGGACCCATGGGAAGAGGGAGAAGTTCATCGTC	Fw IAA20
oPF284	TTTCTTTATGTTTTTGGCGTCTTCCATGCTAGAGTAGTGGTAATTAGCTCTTGAAATCTTCAGTC	Rev IAA20
oPF286	ACTGGCCGGCGACGTGGAATCAAATCCTGGACCCATGGGAAGAGGGAGAAGCTCATCG	Fw IAA30

oPF287	TCTTTATGTTTTTGGCGTCTTCCATGCTAGAGTAGTGATAAGCTCTTGAGATCTTTAGTCTTCTC	Rev IAA30
oSLS401	AATCCTGGACCCGCGCGCATGAAGAGAGATCATCATCATCATCATCATCAAGATAAG	Fw GAI
oSLS402	GGCGTCTTCCATGCTAGCATTGGTGGAGAGTTTCCAAGCCGAG	Rev GAI
oSLS009	GAGAGAACACGGGGACTCTAGCGCTACCGGTTGGCTAGGTAAGCTTGGTACCACCATGACTTCGAAAGTTTATGATCCAGAAC	Fw REN-2A
oSLS403	AATCCTGGACCCGCGCGCATGAAGAGAGATCATCACCAATTCCAAGGTC	Fw RGA
oSLS404	GGCGTCTTCCATGCTAGCGTACGCCGCCGTCGAGAGTTTC	Rev RGA
oSLS405	AATCCTGGACCCGCGCGCATGAAGAGAGAGCACAACCACCGTGAATC	Fw RGL1
oSLS406	GGCGTCTTCCATGCTAGCTTCCACACGATTGATTCGCCACGCAG	Rev RGL1
oSLS407	GCGCGCGGGTCCAGGATTTGATTCCACGTCG	Rev REN-2A
oSLS422	CGACGTGGAATCAAATCCTGGACCCGCGCGCATGAAGAGAGGATACGGAGAAACATGGG	Fw RGL2
oSLS423	CTTTATGTTTTTGGCGTCTTCCATGCTAGCGGCGAGTTTCCACGCCGAGG	Rev RGL2
oSLS424	CGACGTGGAATCAAATCCTGGACCCGCGCGCATGAAACGAAGCCATCAAGAAACGTCTGTAG	Fw RGL3
oSLS425	CTTTATGTTTTTGGCGTCTTCCATGCTAGCCCGCCGCAACTCCGCCG	Rev RGL3
oSLS310	TGGAGAGAACACGGGGACTCTAGCGCTACCGGTTGGCTAGGTAAGCTTGGTACCACCATGGCGGTATTGTCTAAACCGGTAGC	Fw GA2Ox1
oSLS311	AATTCGGCCGCTGCCGCAGCGGCAGCGGCCGCTTAATTTAGGAGATTTTTTATAGTCTTCCTT TCGAATTGTTG	Rev GA2Ox1
oSLS312	TGGAGAGAACACGGGGACTCTAGCGCTACCGGTTGGCTAGGTAAGCTTGGTACCACCATGGTGGTTTTGCCACAGCCAGTC	Fw GA2Ox2
oSLS313	AATTCGGCCGCTGCCGCAGCGGCAGCGGCCGCTTATACAAGGGTTTTATGATTGAGAAGAGGTTGTTTC	Rev GA2Ox2
oSLS314	TGGAGAGAACACGGGGACTCTAGCGCTACCGGTTGGCTAGGTAAGCTTGGTACCACCATGGATCCACCATTCAACGAAATATACAATAACC	Fw GA2Ox8
oSLS315	AATTCGGCCGCTGCCGCAGCGGCAGCGGCCGCTTATCCGTAGACGTGATTAAGGAACCTAG G	Rev GA2Ox8
oSLS442	CCGCAATTCGATCCGGGACCTG	
oSLS466	AGCGTAATCTGGAACATCGTATGGGTACACCTTCCGCTTTTTCTTGGGCC	

6 References

Abe S, Sado A, Tanaka K, Kisugi T, Asami K, Ota S, Kim H Il, Yoneyama K, Xie X, Ohnishi T, et al (2014) Carlactone is converted to carlactonoic acid by MAX1 in Arabidopsis and its methyl ester can directly interact with AtD14 in vitro. Proc Natl Acad Sci U S A **111**: 18084–9

Akiyama K, Matsuzaki K, Hayashi H (2005) Plant sesquiterpenes induce hyphal branching in arbuscular mycorrhizal fungi. Nature **435**: 824–827

Al-Babili S, Bouwmeester HJ (2015) Strigolactones, a Novel Carotenoid-Derived Plant Hormone. Annu Rev Plant Biol **66**: 161–186

Alabadí D, Gallego-Bartolomé J, Orlando L, García-Cárcel L, Rubio V, Martínez C, Frigerio M, Iglesias-Pedraz JM, Espinosa A, Deng XW, et al (2007) Gibberellins modulate light signaling pathways to prevent Arabidopsis seedling de-etiolation in darkness. Plant J **53**: 324–335

Andres J, Blomeier T, Zurbriggen MD (2019) Synthetic Switches and Regulatory Circuits in Plants. Plant Physiol **179**: 862–884

Ariizumi T, Lawrence PK, Steber CM (2011) The role of two f-box proteins, SLEEPY1 and SNEEZY, in Arabidopsis gibberellin signaling. Plant Physiol **155**: 765–75

Arite T, Umehara M, Ishikawa S, Hanada A, Maekawa M, Yamaguchi S, Kyozuka J (2009) d14, a Strigolactone-Insensitive Mutant of Rice, Shows an Accelerated Outgrowth of Tillers. Plant Cell Physiol **50**: 1416–1424

Baaske J, Gonschorek P, Engesser R, Dominguez-Monedero A, Raute K, Fischbach P, Müller K, Cachat E, Schamel WWA, Minguet S, et al (2018) Dual-controlled optogenetic system for the rapid down-regulation of protein levels in mammalian cells. Sci Rep **8**: 15024

Bernier G, Périlleux C (2005) A physiological overview of the genetics of flowering time control. Plant Biotechnol J **3**: 3–16

Besserer A, Bécard G, Jauneau A, Roux C, Séjalon-Delmas N (2008) GR24, a synthetic analog of strigolactones, stimulates the mitosis and growth of the arbuscular mycorrhizal fungus Gigaspora rosea by boosting its energy metabolism. Plant Physiol **148**: 402–13

Beyer HM, Gonschorek P, Samodelov SL, Meier M, Weber W, Zurbriggen MD (2015a) AQUA Cloning: A Versatile and Simple Enzyme-Free Cloning Approach. PLoS One **10**: e0137652

Beyer HM, Juillot S, Herbst K, Samodelov SL, Müller K, Schamel WW, Römer W, Schäfer E, Nagy F, Strähle U, et al (2015b) Red Light-Regulated Reversible Nuclear Localization of Proteins in Mammalian Cells and Zebrafish. ACS Synth Biol **4**: 951–958

Blilou I, Xu J, Wildwater M, Willemsen V, Paponov I, Friml J, Heidstra R, Aida M, Palme K, Scheres B (2005) The PIN auxin efflux facilitator network controls growth and patterning in Arabidopsis roots. Nature **433**: 39–44

Brunoud G, Wells DM, Oliva M, Larrieu A, Mirabet V, Burrow AH, Beeckman T, Kepinski S, Traas J, Bennett MJ, et al (2012) A novel sensor to map auxin response and distribution at high spatio-temporal resolution. Nature **482**: 103–106

Bythell-Douglas R, Rothfels CJ, Stevenson DWD, Graham SW, Wong GK-S, Nelson DC, Bennett T (2017) Evolution of strigolactone receptors by gradual neo-functionalization of KAI2 paralogues. BMC Biol **15**: 52

Calderón Villalobos LIA, Lee S, De Oliveira C, Ivetac A, Brandt W, Armitage L, Sheard LB, Tan

X, Parry G, Mao H, et al (2012) A combinatorial TIR1/AFB–Aux/IAA co-receptor system for differential sensing of auxin. Nat Chem Biol **8**: 477–485

Chevalier F, Nieminen K, Sánchez-Ferrero JC, Rodríguez ML, Chagoyen M, Hardtke CS, Cubas P (2014) Strigolactone promotes degradation of DWARF14, an α/β hydrolase essential for strigolactone signaling in Arabidopsis. Plant Cell **26**: 1134–50

Darwin C, Darwin F (1880) The power of movement in plants. Power Mov Plants. doi: 10.1017/CBO9780511693670

Davière J-M, Achard P (2013) Gibberellin signaling in plants. Development **140**: 1147–51

Depuydt S, Hardtke CS (2011) Hormone signalling crosstalk in plant growth regulation. Curr Biol **21**: R365-73

Dill A, Jung HS, Sun TP (2001) The DELLA motif is essential for gibberellin-induced degradation of RGA. Proc Natl Acad Sci U S A **98**: 14162–7

Dill A, Thomas SG, Hu J, Steber CM, Sun T-P (2004) The Arabidopsis F-box protein SLEEPY1 targets gibberellin signaling repressors for gibberellin-induced degradation. Plant Cell **16**: 1392–405

Dolgikh A V., Kirienko AN, Tikhonovich IA, Foo E, Dolgikh EA (2019) The DELLA Proteins Influence the Expression of Cytokinin Biosynthesis and Response Genes During Nodulation. Front Plant Sci **10**: 432

Ellis T, Wang X, Collins JJ (2009) DIVERSITY-BASED, MODEL-GUIDED CONSTRUCTION OF SYNTHETIC GENE NETWORKS WITH PREDICTED FUNCTIONS. Nat Biotechnol **27**: 465

Fankhauser C, Christie JM (2015) Plant Phototropic Growth. Curr Biol **25**: R384–R389

Farrow SC, Facchini PJ (2014) Functional diversity of 2-oxoglutarate/Fe(II)-dependent dioxygenases in plant metabolism. Front Plant Sci **5**: 524

Feng S, Martinez C, Gusmaroli G, Wang Y, Zhou J, Wang F, Chen L, Yu L, Iglesias-Pedraz JM, Kircher S, et al (2008) Coordinated regulation of Arabidopsis thaliana development by light and gibberellins. Nature **451**: 475–479

Fussenegger M, Moser S, Mazur X, Bailey JE (1997) Autoregulated Multicistronic Expression Vectors Provide One-Step Cloning of Regulated Product Gene Expression in Mammalian Cells. Biotechnol Prog **13**: 733–740

Gallego-Bartolome J, Minguet EG, Marin JA, Prat S, Blazquez MA, Alabadi D (2010) Transcriptional Diversification and Functional Conservation between DELLA Proteins in Arabidopsis. Mol Biol Evol **27**: 1247–1256

Gazzarrini S, Tsai AY-L (2015) Hormone cross-talk during seed germination. Essays Biochem **58**: 151–64

Gibson DG, Young L, Chuang R-Y, Venter JC, Hutchison CA, Smith HO (2009) Enzymatic assembly of DNA molecules up to several hundred kilobases. Nat Methods **6**: 343–345

Golonka D, Fischbach P, Jena SG, Kleeberg JRW, Essen L-O, Toettcher JE, Zurbriggen MD, Möglich A (2019) Deconstructing and repurposing the light-regulated interplay between Arabidopsis phytochromes and interacting factors. Commun Biol **2**: 448

Griffiths J, Murase K, Rieu I, Zentella R, Zhang Z-L, Powers SJ, Gong F, Phillips AL, Hedden P, Sun T, et al (2006) Genetic Characterization and Functional Analysis of the GID1 Gibberellin

Receptors in Arabidopsis. Plant Cell **18**: 3399–3414

Grunewald W, Friml J (2010) The march of the PINs: developmental plasticity by dynamic polar targeting in plant cells. EMBO J **29**: 2700–2714

Guilfoyle TJ (2015) The PB1 Domain in Auxin Response Factor and Aux/IAA Proteins: A Versatile Protein Interaction Module in the Auxin Response. Plant Cell **27**: 33–43

Guo Y, Zheng Z, La Clair JJ, Chory J, Noel JP (2013) Smoke-derived karrikin perception by the α/β-hydrolase KAI2 from Arabidopsis. Proc Natl Acad Sci U S A **110**: 8284–9

Ha C Van, Leyva-González MA, Osakabe Y, Tran UT, Nishiyama R, Watanabe Y, Tanaka M, Seki M, Yamaguchi S, Dong N Van, et al (2014) Positive regulatory role of strigolactone in plant responses to drought and salt stress. Proc Natl Acad Sci **111**: 851–856

Havens KA, Guseman JM, Jang SS, Pierre-Jerome E, Bolten N, Klavins E, Nemhauser JL (2012) A synthetic approach reveals extensive tunability of auxin signaling. Plant Physiol **160**: 135–42

Hedden P (2003) The genes of the Green Revolution. Trends Genet **19**: 5–9

Hedden P, Thomas SG (2012) Gibberellin biosynthesis and its regulation. Biochem J **444**: 11–25

Hou X, Lee LYC, Xia K, Yan Y, Yu H (2010) DELLAs Modulate Jasmonate Signaling via Competitive Binding to JAZs. Dev Cell **19**: 884–894

Hu Q, He Y, Wang L, Liu S, Meng X, Liu G, Jing Y, Chen M, Song X, Jiang L, et al (2017) DWARF14, A Receptor Covalently Linked with the Active Form of Strigolactones, Undergoes Strigolactone-Dependent Degradation in Rice. Front Plant Sci **8**: 1935

Hyun Y, Richter R, Vincent C, Martinez-Gallegos R, Porri A, Coupland Correspondence G (2016) Multi-layered Regulation of SPL15 and Cooperation with SOC1 Integrate Endogenous Flowering Pathways at the Arabidopsis Shoot Meristem. Dev Cell **37**: 254–266

Jiang L, Liu X, Xiong G, Liu H, Chen F, Wang L, Meng X, Liu G, Yu H, Yuan Y, et al (2013) DWARF 53 acts as a repressor of strigolactone signalling in rice. Nature **504**: 401–405

Jun JH, Fiume E, Fletcher JC (2008) The CLE family of plant polypeptide signaling molecules. Cell Mol Life Sci **65**: 743–755

Kevany BM, Tieman DM, Taylor MG, Cin VD, Klee HJ (2007) Ethylene receptor degradation controls the timing of ripening in tomato fruit. Plant J **51**: 458–467

Khakhar A, Leydon AR, Lemmex AC, Klavins E, Nemhauser JL Synthetic hormone-responsive transcription factors can monitor and re-program plant development. doi: 10.7554/eLife.34702.001

Kong L, Cheng J, Zhu Y, Ding Y, Meng J, Chen Z, Xie Q, Guo Y, Li J, Yang S, et al (2015) Degradation of the ABA co-receptor ABI1 by PUB12/13 U-box E3 ligases. Nat Commun **6**: 8630

Koornneef A, Pieterse CMJ (2008) Cross Talk in Defense Signaling. Plant Physiol **146**: 839–844

Korasick DA, Enders TA, Strader LC (2013) Auxin biosynthesis and storage forms. J Exp Bot **64**: 2541–2555

Larrieu A, Champion A, Legrand J, Lavenus J, Mast D, Brunoud G, Oh J, Guyomarc'h S, Pizot M, Farmer EE, et al (2015) A fluorescent hormone biosensor reveals the dynamics of jasmonate signalling in plants. Nat Commun **6**: 6043

Legris M, Nieto C, Sellaro R, Prat S, Casal JJ (2017) Perception and signalling of light and temperature cues in plants. Plant J **90**: 683–697

Li S-B, Xie Z-Z, Hu C-G, Zhang J-Z (2016) A Review of Auxin Response Factors (ARFs) in Plants. Front Plant Sci **7**: 47

Liang Y, Ward S, Li P, Bennett T, Leyser O (2016) SMAX1-LIKE7 Signals from the Nucleus to Regulate Shoot Development in Arabidopsis via Partially EAR Motif-Independent Mechanisms. Plant Cell **28**: 1581–601

Lim WA (2010) Designing customized cell signalling circuits. Nat Rev Mol Cell Biol **11**: 393–403

de Lucas M, Davière J-M, Rodríguez-Falcón M, Pontin M, Iglesias-Pedraz JM, Lorrain S, Fankhauser C, Blázquez MA, Titarenko E, Prat S (2008) A molecular framework for light and gibberellin control of cell elongation. Nature **451**: 480–484

Luo J, Zhou J-J, Zhang J-Z (2018) Aux/IAA Gene Family in Plants: Molecular Structure, Regulation, and Function. Int J Mol Sci. doi: 10.3390/ijms19010259

Di Mambro R, De Ruvo M, Pacifici E, Salvi E, Sozzani R, Benfey PN, Busch W, Novak O, Ljung K, Di Paola L, et al (2017) Auxin minimum triggers the developmental switch from cell division to cell differentiation in the Arabidopsis root. Proc Natl Acad Sci U S A **114**: E7641–E7649

Marín-de la Rosa N, Pfeiffer A, Hill K, Locascio A, Bhalerao RP, Miskolczi P, Grønlund AL, Wanchoo-Kohli A, Thomas SG, Bennett MJ, et al (2015) Genome Wide Binding Site Analysis Reveals Transcriptional Coactivation of Cytokinin-Responsive Genes by DELLA Proteins. PLOS Genet **11**: e1005337

Matiolli CC, Melotto M (2018) A Comprehensive *Arabidopsis* Yeast Two-Hybrid Library for Protein-Protein Interaction Studies: A Resource to the Plant Research Community. Mol Plant-Microbe Interact **31**: 899–902

Mehla J, Caufield JH, Sakhawalkar N, Uetz P (2017) A Comparison of Two-Hybrid Approaches for Detecting Protein-Protein Interactions. Methods Enzymol **586**: 333–358

Meng Y, Shuai H, Luo X, Chen F, Zhou W, Yang W, Shu K (2016) Karrikins: Regulators Involved in Phytohormone Signaling Networks during Seed Germination and Seedling Development. Front Plant Sci **7**: 2021

Miyamoto T, DeRose R, Suarez A, Ueno T, Chen M, Sun T, Wolfgang MJ, Mukherjee C, Meyers DJ, Inoue T (2012) Rapid and orthogonal logic gating with a gibberellin-induced dimerization system. Nat Chem Biol **8**: 465–470

Müller B, Sheen J (2008) Cytokinin and auxin interaction in root stem-cell specification during early embryogenesis. Nature **453**: 1094–1097

Müller K, Engesser R, Metzger S, Schulz S, Kämpf MM, Busacker M, Steinberg T, Tomakidi P, Ehrbar M, Nagy F, et al (2013) A red/far-red light-responsive bi-stable toggle switch to control gene expression in mammalian cells. Nucleic Acids Res **41**: e77–e77

Müller K, Zurbriggen MD, Weber W (2014) Control of gene expression using a red- and far-red light–responsive bi-stable toggle switch. Nat Protoc **9**: 622–632

Murase K, Hirano Y, Sun T, Hakoshima T (2008) Gibberellin-induced DELLA recognition by the gibberellin receptor GID1. Nature **456**: 459–463

Nakajima M, Shimada A, Takashi Y, Kim Y-C, Park S-H, Ueguchi-Tanaka M, Suzuki H, Katoh E, Iuchi S, Kobayashi M, et al (2006) Identification and characterization of Arabidopsis gibberellin receptors. Plant J **46**: 880–889

Nelson DC, Scaffidi A, Dun EA, Waters MT, Flematti GR, Dixon KW, Beveridge CA, Ghisalberti EL, Smith SM (2011) F-box protein MAX2 has dual roles in karrikin and strigolactone signaling in Arabidopsis thaliana. Proc Natl Acad Sci U S A **108**: 8897–902

Nguyen L-T, Schmidt HA, von Haeseler A, Minh BQ (2015) IQ-TREE: A Fast and Effective Stochastic Algorithm for Estimating Maximum-Likelihood Phylogenies. Mol Biol Evol **32**: 268–274

Notredame C, Higgins DG, Heringa J (2000) T-coffee: a novel method for fast and accurate multiple sequence alignment. J Mol Biol **302**: 205–217

Ochoa-Fernandez R, Samodelov SL, Brandl SM, Wehinger E, Müller K, Weber W, Zurbriggen MD (2016) Optogenetics in Plants: Red/Far-Red Light Control of Gene Expression. Methods Mol. Biol. pp 125–139

Oh E, Zhu J-Y, Bai M-Y, Arenhart RA, Sun Y, Wang Z-Y (2014) Cell elongation is regulated through a central circuit of interacting transcription factors in the Arabidopsis hypocotyl. Elife. doi: 10.7554/eLife.03031

Okamoto M, Hanada A, Kamiya Y, Yamaguchi S, Nambara E (2009) Measurement of Abscisic Acid and Gibberellins by Gas Chromatography/Mass Spectrometry. Humana Press, Totowa, NJ, pp 53–60

Otegui MS (2018) Vacuolar degradation of chloroplast components: autophagy and beyond. J Exp Bot **69**: 741–750

Overvoorde P, Fukaki H, Beeckman T (2010) Auxin control of root development. Cold Spring Harb Perspect Biol **2**: a001537

Parker C (2009) Observations on the current status of *Orobanche* and *Striga* problems worldwide. Pest Manag Sci **65**: 453–459

Parry G, Calderon-Villalobos LI, Prigge M, Peret B, Dharmasiri S, Itoh H, Lechner E, Gray WM, Bennett M, Estelle M (2009) Complex regulation of the TIR1/AFB family of auxin receptors. Proc Natl Acad Sci U S A **106**: 22540–5

Peng J, Carol P, Richards DE, King KE, Cowling RJ, Murphy GP, Harberd NP (1997) The Arabidopsis GAI gene defines a signaling pathway that negatively regulates gibberellin responses. Genes Dev **11**: 3194–205

Ramos JA, Zenser N, Leyser O, Callis J (2001) Rapid degradation of auxin/indoleacetic acid proteins requires conserved amino acids of domain II and is proteasome dependent. Plant Cell **13**: 2349–60

Rieu I, Eriksson S, Powers SJ, Gong F, Griffiths J, Woolley L, Benlloch R, Nilsson O, Thomas SG, Hedden P, et al (2008) Genetic analysis reveals that C19-GA 2-oxidation is a major gibberellin inactivation pathway in Arabidopsis. Plant Cell **20**: 2420–36

Rizza A, Walia A, Lanquar V, Frommer WB, Jones AM (2017) In vivo gibberellin gradients visualized in rapidly elongating tissues. Nat Plants **3**: 803–813

Salehin M, Bagchi R, Estelle M (2015) SCFTIR1/AFB-based auxin perception: mechanism and role in plant growth and development. Plant Cell **27**: 9–19

Samodelov SL, Beyer HM, Guo X, Augustin M, Jia K-P, Baz L, Ebenhöh O, Beyer P, Weber W, Al-Babili S, et al (2016) StrigoQuant: A genetically encoded biosensor for quantifying strigolactone activity and specificity. Sci Adv **2**: e1601266

Samodelov SL, Zurbriggen MD (2017) Quantitatively Understanding Plant Signaling: Novel Theoretical–Experimental Approaches. Trends Plant Sci **22**: 685–704

Sang D, Chen D, Liu G, Liang Y, Huang L, Meng X, Chu J, Sun X, Dong G, Yuan Y, et al (2014) Strigolactones regulate rice tiller angle by attenuating shoot gravitropism through inhibiting auxin biosynthesis. Proc Natl Acad Sci U S A **111**: 11199–204

Santner A, Calderon-Villalobos LIA, Estelle M (2009) Plant hormones are versatile chemical regulators of plant growth. Nat Chem Biol **5**: 301–307

Santner A, Estelle M (2009) Recent advances and emerging trends in plant hormone signalling. Nature **459**: 1071–1078

Scheuring D, Künzl F, Viotti C, Yan MSW, Jiang L, Schellmann S, Robinson DG, Pimpl P (2012) Ubiquitin initiates sorting of Golgi and plasma membrane proteins into the vacuolar degradation pathway. BMC Plant Biol **12**: 164

Schomburg FM, Bizzell CM, Lee DJ, Zeevaart JAD, Amasino RM (2003) Overexpression of a novel class of gibberellin 2-oxidases decreases gibberellin levels and creates dwarf plants. Plant Cell **15**: 151–63

Sheen J (2010) Discover and connect cellular signaling. Plant Physiol **154**: 562–6

Shimada A, Ueguchi-Tanaka M, Nakatsu T, Nakajima M, Naoe Y, Ohmiya H, Kato H, Matsuoka M (2008) Structural basis for gibberellin recognition by its receptor GID1. Nature **456**: 520–523

Shimizu-Mitao Y, Kakimoto T (2014) Auxin Sensitivities of All Arabidopsis Aux/IAAs for Degradation in the Presence of Every TIR1/AFB. Plant Cell Physiol **55**: 1450–1459

Silverstone AL, Ciampaglio CN, Sun T (1998) The Arabidopsis RGA gene encodes a transcriptional regulator repressing the gibberellin signal transduction pathway. Plant Cell **10**: 155–69

Song J, Liu Q, Hu B, Wu W (2017) Photoreceptor PhyB Involved in Arabidopsis Temperature Perception and Heat-Tolerance Formation. Int J Mol Sci. doi: 10.3390/IJMS18061194

Soundappan I, Bennett T, Morffy N, Liang Y, Stanga JP, Abbas A, Leyser O, Nelson DC (2015) SMAX1-LIKE/D53 Family Members Enable Distinct MAX2-Dependent Responses to Strigolactones and Karrikins in Arabidopsis. Plant Cell **27**: 3143–59

Stanga JP, Morffy N, Nelson DC (2016) Functional redundancy in the control of seedling growth by the karrikin signaling pathway. Planta **243**: 1397–1406

Stirnberg P, Furner IJ, Ottoline Leyser HM (2007) MAX2 participates in an SCF complex which acts locally at the node to suppress shoot branching. Plant J **50**: 80–94

Su S-H, Gibbs NM, Jancewicz AL, Masson PH (2017) Current Biology Review Molecular Mechanisms of Root Gravitropism. Curr Biol **27**: R964–R972

Sun T (2011) The Molecular Mechanism and Evolution of the GA–GID1–DELLA Signaling Module in Plants. Curr Biol **21**: R338–R345

Suzuki H, Park S-H, Okubo K, Kitamura J, Ueguchi-Tanaka M, Iuchi S, Katoh E, Kobayashi M, Yamaguchi I, Matsuoka M, et al (2009) Differential expression and affinities of Arabidopsis gibberellin receptors can explain variation in phenotypes of multiple knock-out mutants. Plant J **60**: 48–55

Swarup R, Friml J, Marchant A, Ljung K, Sandberg G, Palme K, Bennett M (2001) Localization of the auxin permease AUX1 suggests two functionally distinct hormone transport pathways

operate in the Arabidopsis root apex. Genes Dev **15**: 2648–53

Swarup R, Kargul J, Marchant A, Zadik D, Rahman A, Mills R, Yemm A, May S, Williams L, Millner P, et al (2004) Structure-function analysis of the presumptive Arabidopsis auxin permease AUX1. Plant Cell **16**: 3069–83

Szemenyei H, Hannon M, Long JA (2008) TOPLESS mediates auxin-dependent transcriptional repression during Arabidopsis embryogenesis. Science **319**: 1384–6

Thomas SG, Phillips AL, Hedden P (1999) Molecular cloning and functional expression of gibberellin 2- oxidases, multifunctional enzymes involved in gibberellin deactivation. Proc Natl Acad Sci U S A **96**: 4698–703

Ueda H, Kusaba M (2015) Strigolactone Regulates Leaf Senescence in Concert with Ethylene in Arabidopsis. Plant Physiol **169**: 138–47

Ueguchi-Tanaka M, Ashikari M, Nakajima M, Itoh H, Katoh E, Kobayashi M, Chow T, Hsing YC, Kitano H, Yamaguchi I, et al (2005) GIBBERELLIN INSENSITIVE DWARF1 encodes a soluble receptor for gibberellin. Nature **437**: 693–698

Umehara M, Hanada A, Yoshida S, Akiyama K, Arite T, Takeda-Kamiya N, Magome H, Kamiya Y, Shirasu K, Yoneyama K, et al (2008) Inhibition of shoot branching by new terpenoid plant hormones. Nature **455**: 195–200

Urbanová T, Tarkowská D, Novák O, Hedden P, Strnad M (2013) Analysis of gibberellins as free acids by ultra performance liquid chromatography–tandem mass spectrometry. Talanta **112**: 85–94

Vanstraelen M, Benková E (2012) Hormonal Interactions in the Regulation of Plant Development. Annu Rev Cell Dev Biol **28**: 463–487

Végh A, Incze N, Fábián A, Huo H, Bradford KJ, Balázs E, Soós V (2017) Comprehensive Analysis of DWARF14-LIKE2 (DLK2) Reveals Its Functional Divergence from Strigolactone-Related Paralogs. Front Plant Sci **8**: 1641

Velasquez SM, Barbez E, Kleine-Vehn J, Estevez JM (2016) Auxin and Cellular Elongation. Plant Physiol **170**: 1206–15

Verma V, Ravindran P, Kumar PP (2016) Plant hormone-mediated regulation of stress responses. BMC Plant Biol **16**: 86

Vierstra RD (2009) The ubiquitin–26S proteasome system at the nexus of plant biology. Nat Rev Mol Cell Biol **10**: 385–397

Walia A, Waadt R, Jones AM (2018) Genetically Encoded Biosensors in Plants: Pathways to Discovery. Annu Rev Plant Biol. doi: 10.1146/annurev-arplant-042817-040104

Wallner E-S, López-Salmerón V, Belevich I, Poschet G, Jung I, Grünwald K, Sevilem I, Jokitalo E, Hell R, Helariutta Y, et al (2017) Strigolactone- and Karrikin-Independent SMXL Proteins Are Central Regulators of Phloem Formation. Curr Biol **27**: 1241–1247

Wang J-W, Czech B, Weigel D (2009) miR156-Regulated SPL Transcription Factors Define an Endogenous Flowering Pathway in Arabidopsis thaliana. Cell **138**: 738–749

Wang L, Wang B, Jiang L, Liu X, Li X, Lu Z, Meng X, Wang Y, Smith SM, Li J (2015) Strigolactone Signaling in Arabidopsis Regulates Shoot Development by Targeting D53-Like SMXL Repressor Proteins for Ubiquitination and Degradation. Plant Cell **27**: 3128–42

Waters MT, Gutjahr C, Bennett T, Nelson DC (2017) Strigolactone Signaling and Evolution. Annu Rev Plant Biol **68**: 291–322

Waters MT, Nelson DC, Scaffidi A, Flematti GR, Sun YK, Dixon KW, Smith SM (2012) Specialisation within the DWARF14 protein family confers distinct responses to karrikins and strigolactones in Arabidopsis. Development **139**: 1285–1295

Waters MT, Scaffidi A, Flematti G, Smith SM (2015) Substrate-Induced Degradation of the α/β-Fold Hydrolase KARRIKIN INSENSITIVE2 Requires a Functional Catalytic Triad but Is Independent of MAX2. doi: 10.1016/j.molp.2014.12.020

Waters MT, Scaffidi A, Flematti GR, Smith SM (2013) The origins and mechanisms of karrikin signalling. Curr Opin Plant Biol **16**: 667–673

Waters MT, Scaffidi A, Sun YK, Flematti GR, Smith SM (2014) The karrikin response system of Arabidopsis. Plant J **79**: 623–631

Weber W, Fussenegger M (2010) Synthetic gene networks in mammalian cells. Curr Opin Biotechnol **21**: 690–696

Wells DM, Laplaze L, Bennett MJ, Vernoux T (2013) Biosensors for phytohormone quantification: challenges, solutions, and opportunities. Trends Plant Sci **18**: 244–249

Wend S, Bosco CD, Kämpf MM, Ren F, Palme K, Weber W, Dovzhenko A, Zurbriggen MD (2013) A quantitative ratiometric sensor for time-resolved analysis of auxin dynamics. Sci Rep **3**: 2052

Went, FW (1926) On growth-accelerating substances in the coleoptile of Avena sativa.

Winkler M, Niemeyer M, Hellmuth A, Janitza P, Christ G, Samodelov SL, Wilde V, Majovsky P, Trujillo M, Zurbriggen MD, et al (2017) Variation in auxin sensing guides AUX/IAA transcriptional repressor ubiquitylation and destruction. Nat Commun **8**: 15706

Wu G, Wang X, Li X, Kamiya Y, Otegui MS, Chory J (2011) Methylation of a Phosphatase Specifies Dephosphorylation and Degradation of Activated Brassinosteroid Receptors. Sci Signal **4**: ra29–ra29

Wu W, Liu Y, Wang Y, Li H, Liu J, Tan J, He J, Bai J, Ma H (2017) Evolution Analysis of the Aux/IAA Gene Family in Plants Shows Dual Origins and Variable Nuclear Localization Signals. Int J Mol Sci. doi: 10.3390/ijms18102107

Yamada Y, Furusawa S, Nagasaka S, Shimomura K, Yamaguchi S, Umehara M (2014) Strigolactone signaling regulates rice leaf senescence in response to a phosphate deficiency. Planta **240**: 399–408

Yamaguchi S (2008) Gibberellin Metabolism and its Regulation. Annu Rev Plant Biol **59**: 225–251

Yoneyama K, Mori N, Sato T, Yoda A, Xie X, Okamoto M, Iwanaga M, Ohnishi T, Nishiwaki H, Asami T, et al (2018) Conversion of carlactone to carlactonoic acid is a conserved function of MAX 1 homologs in strigolactone biosynthesis. New Phytol **218**: 1522–1533

Zhao Y (2010) Auxin Biosynthesis and Its Role in Plant Development. Annu Rev Plant Biol **61**: 49–64

Zheng Y, Gao Z, Zhu Z (2016) DELLA-PIF Modules: Old Dogs Learn New Tricks. Trends Plant Sci **21**: 813–815

Zhou F, Lin Q, Zhu L, Ren Y, Zhou K, Shabek N, Wu F, Mao H, Dong W, Gan L, et al (2013) D14-SCF(D3)-dependent degradation of D53 regulates strigolactone signalling. Nature **504**: 406–10

7 APPENDIX: ORIGINAL PUBLICATIONS/MANUSCRIPTS, PROTOCOLS AND REVIEWS

Original publications and manuscripts

Jennifer Andres, Lisa Schmunk, Tim Blomeier, Sophia Samodelov, Rocio Ochoa-Fernandez, David Alabadi, Miguel A. Blazquez, Matias D. Zurbriggen. Quantitative ratiometric biosensors for the analysis of gibberellin signaling dynamics and metabolism. Manuscript in preparation.

Contribution: Design, performance, and analysis of all experiments. Preparation of all figures and writing of the manuscript.

Jennifer Andres*, Nima Saadat*, Oliver Ebenhöh, Matias D. Zurbriggen. StrigoQuant dynamic analyses reveal new insights on strigolactone signaling. Manuscript in preparation.
*equal contribution

Contribution: Design, performance, and analysis of experiments. Preparation of the figures and writing of the manuscript related to the experimental part.

Protocol

Jennifer Andres and Matias D. Zurbriggen. Quantitative ratiometric biosensors for the analysis of auxin dynamics. Accepted in Methods in Molecular Biology – Plant Synthetic Biology – Springer (2020).

Contribution: Design, performance, and analysis of all experiments. Preparation of all figures and writing of the manuscript.

Review

Jennifer Andres*, Tim Blomeier* and Matias D. Zurbriggen. Synthetic Switches and Regulatory Circuits in Plants. Plant Physiology **179**: 862–884. 2019.
doi: https://doi.org/10.1104/pp.18.01362
*equal contribution

Contribution: Research and writing of the manuscript.

7.1 Quantitative ratiometric biosensors for the analysis of gibberellin signaling dynamics and metabolism

Quantitative ratiometric biosensors for the analysis of gibberellin signaling dynamics and metabolism

Jennifer Andres[1], Lisa Schmunk[2], Tim Blomeier[1], Sophia Samodelov[3], Rocio Ochoa-Fernandez[1], David Alabadi[4], Miguel A. Blazquez[4], Matias D. Zurbriggen[1*]

[1]Institute of Synthetic Biology, University of Düsseldorf and CEPLAS, Düsseldorf, Germany
[2]Cardiovascular Strategic Research Initiative, University of Cambridge
[3]Department of Clinical Pharmacology and Toxicology, University Hospital Zurich, Zurich, Switzerland
[4]Instituto de Biología Molecular y Celular de Plantas (IBMCP), CSIC-Universidad Politécnica de Valencia, Campus UPV CPI 8E, Valencia, Spain

[*]Corresponding author: Email: matias.zurbriggen@uni-duesseldorf.de

Abstract

Gibberellins (GA) are major regulators of developmental and growth processes in plants. We developed here genetically-encoded biosensors to study GA perception and signaling, transporter and metabolic analysis in *Arabidopsis thaliana* protoplasts with a high quantitative and temporal resolution. These degradation-based biosensors display a high sensitivity and specificity towards different bioactive and non-bioactive GAs. Due to their wide applicability and high dynamic ranges, these GA biosensors can be used as proxies to analyze GA-related processes in plant cells.

Keywords: synthetic biology tools, quantitative biosensor, gibberellin signaling and metabolism, protoplasts

Introduction

The phytohormone Gibberellin (GA) plays a major role in a plethora of developmental and growth processes such as seed germination, vegetative growth and flowering[1]. In plants, there is a great number of non-bioactive GAs being intermediates or catabolites, and transported and then converted into only a few bioactive GAs[2]. The biosynthesis of the bioactive GAs GA_1, GA_3, GA_4 and GA_7 is a complex, multi-stepped process with different enzymes, including various GA-oxidases, being involved[3,4](Fig. 1A). Bioactive GAs are perceived, and a signal relay activated leading finally to changes in gene expression. Three key components are involved in GA perception and signaling: i) GA receptors (GA INSENSITIVE DWARF1 (GID) with three family members in *Arabidopsis Thaliana* (GID1a, b and c))[5,6], ii) SLY1 (F-Box protein belonging to a SCF E3 ubiquitin-ligase complex)[7] and iii) five DELLAs which belong to the GRAS-family of transcriptional regulators in plants and negatively regulate GA responses (GA-INSENSITIVE,GAI; REPRESSOR-of-ga1-3, RGA; RGA-like1, RGL1; RGL2 and RGL3 in *A. thaliana*)[1,8–10]. The binding of GAs to the receptor leads to the formation of a co-receptor complex between GA-GID1, DELLA and SLY. This leads to ubiquitylation and proteolysis of the DELLA proteins thereby triggering GA downstream signaling responses[11,12] (Fig. 1B).

To date, GA levels are typically analyzed with mass spectrometry which requires the disruption of the tissue and prevents dynamic analysis[13,14]. Putative GA transporter activities are mainly studied in *Xenopus* oocytes or the yeast *Saccharomyces cerevisiae* which have the limitations of being non-plant systems[15]. First sensors *in planta* have been developed, e.g. a Förster Resonance Energy Transfer (FRET) biosensor[16] or hormone activated Cas9-based repressors (HACR)[17] to monitor *in vivo* bioactive GA distribution. However, it remains still challenging to quantify time-resolved bioactive and non-bioactive GA dynamics and metabolic processes as well as transporter activities *in vivo* at physiological-relevant levels.

Using the above described degradation-based signaling mechanism, we built DELLA-based biosensors which can provide quantifications of hormone levels at high temporal resolution. In addition, the biosensors allow dynamic analyses in a plant system. Following the same modular design, we implemented in *Arabidopsis* protoplasts genetically-encoded biosensors engineered from each of the five different DELLAs. These newly developed biosensors incorporate either GAI, RGA, RGL1, RGL2 and RGL3 fused to a firefly luciferase connected via a 2A peptide to a renilla luciferase which functions as a normalization element (Fig. 1C). We could show quantitatively that the five DELLAs display large variability in GA specificity and sensitivity towards the bioactive GAs 1,3,4 and 7, but also towards the known precursors GA_9 and GA_{20}. Kinetic analysis performed with the most sensitive GA biosensor (RGA) provided deeper insights into gibberellin sensing dynamics. In addition, we demonstrate the applicability of this highly sensitive system (up to low pM-range) to answer questions on GA

metabolism, such as the involvement of certain GA-oxidases in the GA biosynthesis process, as well as the potential use as a quantitative screening platform in protoplasts.

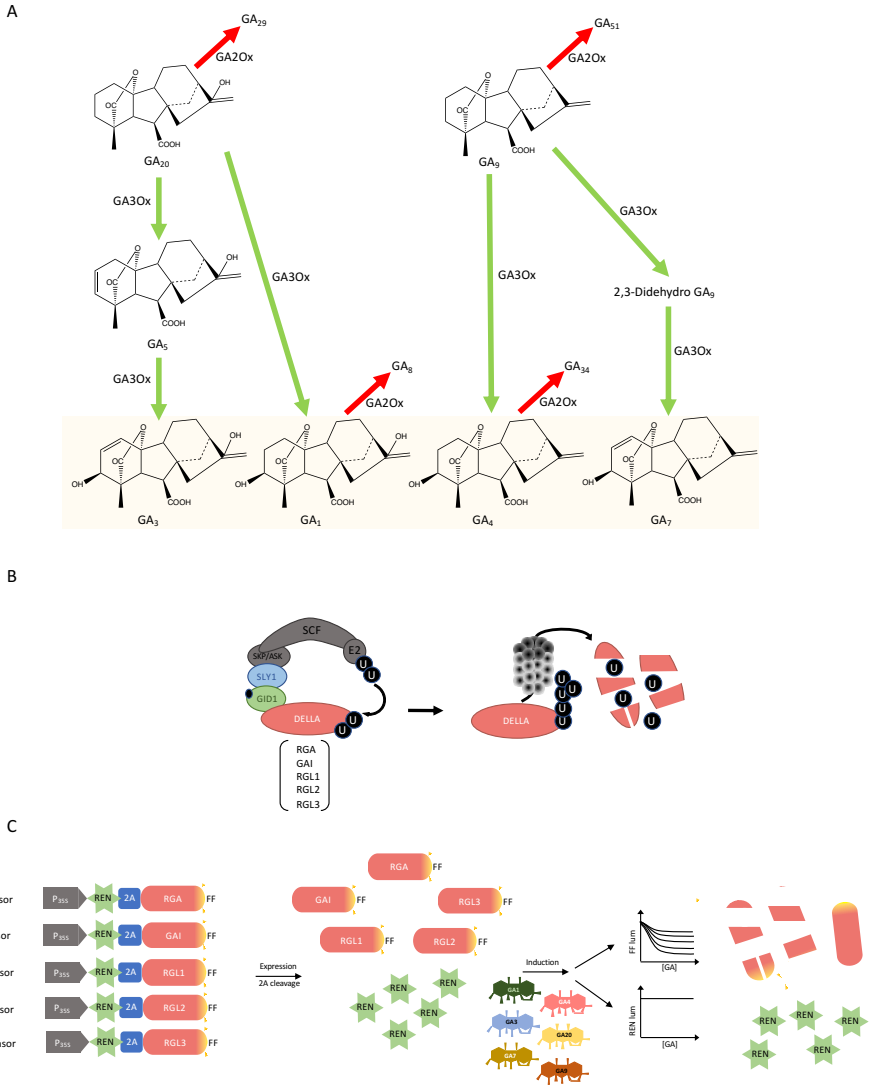

Figure 1: Gibberellin (GA) perception mechanism, GA biosensor design and the biosynthesis and deactivation of bioactive GAs in *Arabidopsis thaliana*. (A) The bioactive GAs 1, 3, 4 and 7 are synthesized from their precursors, GA_{20} or GA_9, in a single-step or multi-step conversions mediated by GA3Oxidases. GA2oxidases catalyze the deactivation of GA_1 and GA_4. (B) Schematic overview of the GA perception mechanism in *A. thaliana*. Upon binding of GAs to the coreceptor GID1, DELLAs associate to the SLY1 and SKP1/CUL1/F-box E2 ubiquitin ligase complex (SCF^{SLY1}) and become polyubiquitinated (U) and thereby targeted for degradation by the 26S proteasome. (C) The five GA biosensor constructs contain each one DELLA as a sensor module (SM) fused to a firefly luciferase (FF). A 2A peptide connects a renilla luciferase (REN) as a normalization element with the DELLA-FF fusion which leads to stoichiometric co-expression. As a consequence of GA induction, DELLA-FF becomes ubiquitinated and consequently degraded, whereas REN levels remain constant, which leads to a decrease in FF/REN ratio.

Results

Design of five genetically encoded distinct GA quantitative biosensors

We designed five degradation-based ratiometric GA biosensors using the intrinsic perception machinery for GAs (Fig 1B and C) and following the molecular engineering principles described previously[18,19]. For this, we employed the full-length cDNA of the five different DELLAs in *A. thaliana* as sensor modules (SM) and fused them to the firefly (FF) luciferase to monitor their degradation. A renilla (REN) luciferase was utilized as a normalization element and connected via a 2A peptide to the SM-FF fusion which enables their stoichiometric co-expression and leads to a decrease in FF luminescence relative to REN luminescence (Fig. 1C). In addition, we used the CtrlQuant sensor construct as a control where the sensor module was replaced by a short repetitive sequence GAGAGAGAGAGAGA that should not be degraded in the presence of the hormone[19].

Sensitivity and Specificity analysis of the different DELLA-based biosensors towards bioactive GAs in Arabidopsis protoplasts

To analyze the specificity and sensitivity of the DELLAs towards the bioactive gibberellins GA_1, GA_3, GA_4 and GA_7, the GA biosensors were expressed in *A. thaliana* wildtype protoplasts. A RGA biosensor with a 17 aminoacid deletion in the DELLA sequence which should not react to GA induction was included as a control[20]. After 5h incubation with increasing concentrations of GAs (from 10 pM to 10 µM), the firefly and renilla luciferase activities were determined, and the FF/REN ratios analyzed.

All DELLAs showed a decrease in FF/REN ratio with increasing concentrations of GA_3, GA_4 und GA_7 meaning that all of them are sensitive towards these GAs. The CtrlQuant sensor and the RGA biosensor version with the 17 amino acids deletion in the DELLA sequence show no degradation (Fig. 2, Fig S1+S3). Nevertheless, there are large differences in sensitivity among the different DELLAs; from 40% degradation of the RGL3 biosensor to almost 70% degradation of the RGA biosensor when incubated with 1 – 10 µM GA_4 for 5h. Additional experiments with the proteasomal inhibitor MG132 showed the dependency on the 26S proteasome (Fig. S2). The various DELLA-based gibberellin biosensors, show high sensitivity and differential behavior towards distinct gibberellins and the sensing at lower hormone concentrations (up to pM range). As a comparison, already existing sensor systems in *Xenopus* oocytes or the yeast *Saccharomyces cerevisiae* have a working range in the µM concentrations[15,16]. All DELLAs (except RGL3) show significant reductions at a low pM range of GA_4 and GA_7, meaning that the biosensors show the highest sensitivity and specificity towards the bioactive GAs GA_4 and GA_7. Induction with GA_1 and GA_3 leads to minor degradation rates (mostly nM range). In particular, the RGA sensor shows the highest sensitivity towards the different GAs with

significant reductions starting at 10 pM for GA_4 or GA_7, and over 50% degradation at low nM concentrations (GA_4). Therefore, this sensor was selected for further studies.

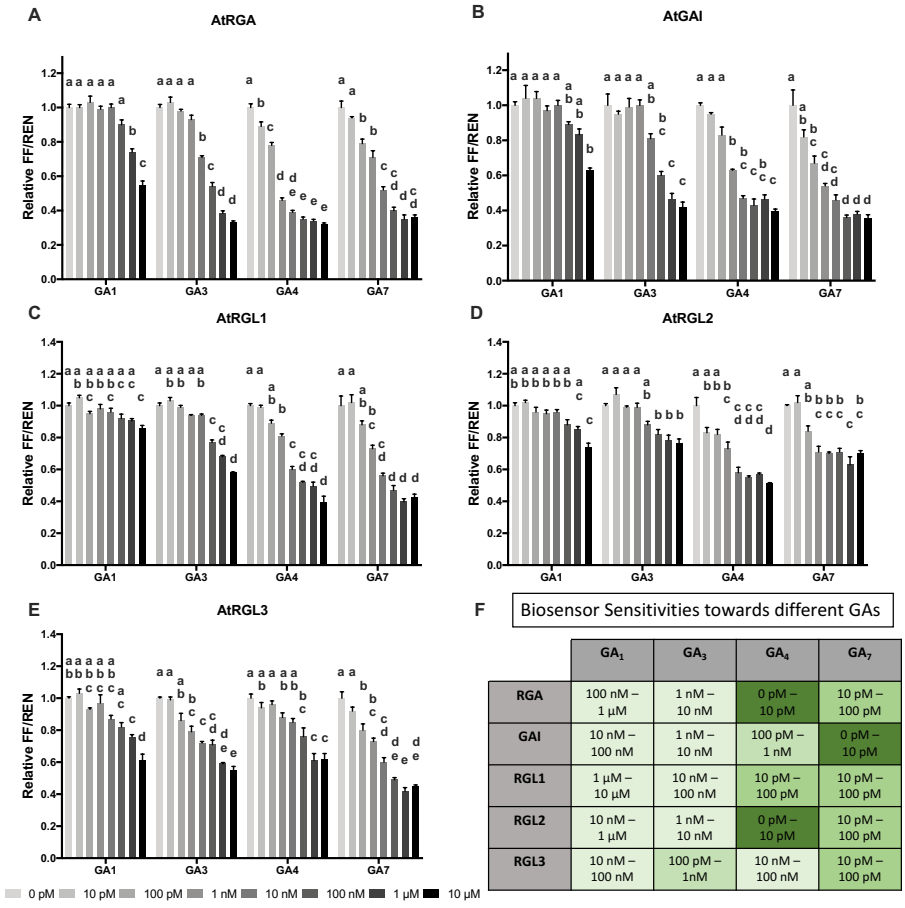

F Biosensor Sensitivities towards different GAs

	GA_1	GA_3	GA_4	GA_7
RGA	100 nM – 1 µM	1 nM – 10 nM	0 pM – 10 pM	10 pM – 100 pM
GAI	10 nM – 100 nM	1 nM – 10 nM	100 pM – 1 nM	0 pM – 10 pM
RGL1	1 µM – 10 µM	10 nM – 100 nM	10 pM – 100 pM	10 pM – 100 pM
RGL2	10 nM – 1 µM	1 nM – 10 nM	0 pM – 10 pM	10 pM – 100 pM
RGL3	10 nM – 100 nM	100 pM – 1nM	10 nM – 100 nM	10 pM – 100 pM

Figure 2: Sensitivity and specificity of RGA-, GAI-, RGL1-, RGL2- and RGL3-based biosensors towards the bioactive gibberellins GA_1, GA_3, GA_4 and GA_7. *A. thaliana* wildtype protoplasts were transformed with the different sensor constructs containing either **A)** RGA, **B)** GAI, **C)** RGL1, **D)** RGL2 or **E)** RGL3 as a sensor module (SM). 20h after transformation, the protoplasts were supplemented with serial dilutions ranging from 10 pM to 10 µM of either GA_1, GA_3, GA_4 or GA_7 for 5h. Afterwards, the luciferase activity was determined. The error bars represent the SEM ($n = 6$). The statistical significance between the different GA concentrations is indicated in lower case letters, where "a" significantly differs from "b", "b" from "c" and so on. One-way analysis of variance (ANOVA) were performed with $p < 0.05$ (for RGL1,2 and 3 with GA_1) or $p < 0.01$. **F)** Table summarizing the biosensor sensitivities towards the different bioactive gibberellins (dark green: sensitivity lower than 10 pM, green: sensitivity between 10 pM and 100 pM, lime-green: sensitivity between 100 pM and 1 nM, lime-green shade: sensitivity higher than 1 nM).

Analysis of the Sensitivity and Specificity of the GA biosensors towards non-bioactive GAs

In the next step, we tested two different known GA precursors, namely GA_{20} and GA_9, precursors of GA_1 and GA_4, respectively[21] (Fig. 1A) to determine if these molecules are converted into bioactive GAs and thereby sensed by the biosensors. *Arabidopsis* wildtype protoplasts were transformed with the DELLA biosensors and then incubated with increasing concentrations of the two GA precursors. The FF and REN luciferase activities were determined after 5h of incubation and afterwards the FF/REN ratios were analyzed.

All five DELLAs showed a decrease in the FF/REN ratio when incubated with GA_9, although large differences in sensitivity were observed. The RGA biosensor shows again the highest sensitivity towards GA_9 with significant reduction at low nM-range and 50 % degradation at high GA_9 concentrations (more than 100 nM), whereas RGL2 shows the lowest sensitivity with 30 % degradation at high GA_9 concentrations (10 µM). The incubation with the GA_1 precursor GA_{20} results in almost no degradation of the DELLAs. Only RGA, GAI and RGL3 show a significant decrease in the FF/REN ratio at high GA_{20} concentrations (1 – 10 µM), whereas RGL1 and RGL2 show no degradation at all.

These results imply that either the precursors are converted into their bioactive products during the GA incubation time and/or that the precursors themselves are sensed.

The different specificities of the DELLA proteins and the high sensitivity of the system, makes it a powerful screening platform for bioactive GAs and their precursors. Furthermore, these sensors can be used as proxies to screen natural, but also putative synthetic GA-analogs.

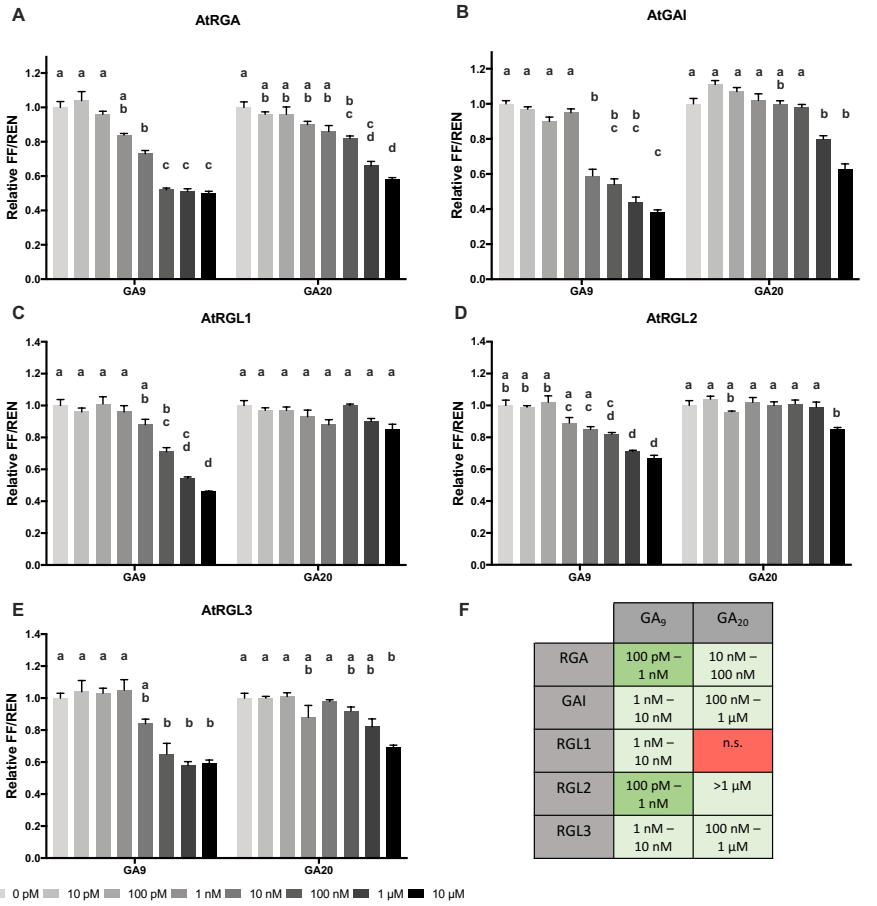

F

	GA_9	GA_{20}
RGA	100 pM – 1 nM	10 nM – 100 nM
GAI	1 nM – 10 nM	100 nM – 1 µM
RGL1	1 nM – 10 nM	n.s.
RGL2	100 pM – 1 nM	>1 µM
RGL3	1 nM – 10 nM	100 nM – 1 µM

Figure 3: Sensitivity and specificity of RGA, GAI, RGL1, RGL2 and RGL3 towards two known precursors of bioactive GAs, GA_9 and GA_{20}. *A. thaliana* wildtype protoplasts were transformed with the different sensor constructs comprising either **A)** RGA, **B)** GAI, **C)** RGL1, **D)** RGL2 or **E)** RGL3 as a sensor module (SM). 20h after transformation, the protoplasts were supplemented with serial dilutions from 10 pM to 10 µM of either GA_9 and GA_{20} for 5h. Afterwards, the luciferase activity was determined. The error bars represent the SEM (n = 6). The statistical significance between the different GA concentrations is indicated in lower case letters, where "a" significantly differs from "b", "b" from "c" and so on. One-way analysis of variance (ANOVA) were performed with $p < 0.05$ (for GAI with GA_{20} and RGL2 with GA_9) or $p < 0.01$. **F)** Table summarizing the biosensor sensitivities towards the different bioactive gibberellins (green: sensitivity between 10 pM and 100 pM, lime-green: sensitivity between 100 pM and 1 nM, lime-green shade: sensitivity higher than 1 nM; red: not significant).

Kinetic characterization of the RGA biosensor

To further characterize the most sensitive GA biosensor, namely the RGA-based module, kinetic analyses were performed. For this, *Arabidopsis* wt protoplasts were transformed with the RGA biosensor and after 20 h, incubated with increasing concentrations of GA_4 (from 100 pM to 1 µM). The luciferase activity was then determined after 30, 60, 120, 240 and 480 min of incubation with the hormone (Fig. 4). After 30 min, a 20 % degradation at high GA_4 concentration (µM-range) is observed. Significant degradation of the RGA-FF fusion at low GA_4 concentrations (pM-range) started after 240 min. Finally, after 480 min, a significant decrease (20 %) in the FF/REN ratio at low GA_4 concentrations (pM-range) occurs. Additionally, the maximum RGA-FF degradation is reached (about 60%) starting at low nM GA_4 concentrations. The kinetic characterization of the system showed that the RGA biosensor does not only have a high sensitivity and specificity towards GA_4, but also a fast response.

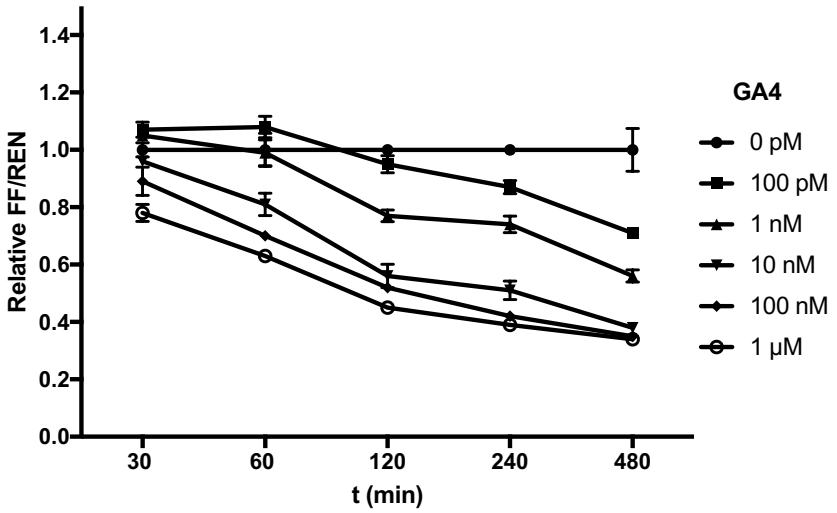

Figure 4: RGA biosensor kinetic analysis. *A. thaliana* wildtype protoplasts were transformed with the RGA biosensor construct. 20h after transformation, the protoplasts were supplemented with serial dilutions from 100 pM to 1 µM of GA_4 for 30 min, 60 min, 120 min, 240 min and 480 min before luciferase activity determination. The error bars represent the SEM for n = 6 replicates.

Study of GA oxidases-dependent gibberellin metabolism

GA2oxidases are a major inactivation pathway for GA signalling in *Arabidopsis*[22]. The GA2oxidases 1,2,3,4 and 6 have been shown to act specifically against C19-GAs including GA_1 and GA_4 [22,23] (Fig. 1A) by catalyzing the 2-β-hydroxylation of GA_4 to GA_{34} and GA_1 to GA_8. GA2Ox7 and 8 on the other hand, catalyze the 2-β-hydroxylation of C20 GAs such as the common precursor GA_{12}[24].

We applied the biosensor to study the specificity and activity of three different GA2oxidases. *Arabidopsis* protoplasts were transformed with the RGA sensor and either GA2ox1, GA2ox2 or GA2ox8 and incubated 20 h post transformation with increasing GA_1 and GA_4 concentrations from 1 nM to 10 µM. In addition, the RGA sensor was co-transformed with a control plasmid. As depicted in Figure 5, the FF/REN ratio at low concentrations remains similar between the control and GA2ox1 and GA2Ox2. Only when incubated with 10 µM GA_1, the dynamic range is sufficient to show a significant difference between the degradation of RGA without and with GA2ox1 or GA2ox2 (Fig. 5) meaning that there is less degradation in the presence of either GA2Ox1 or 2. This indicates that these two oxidases are indeed acting on GA_1 and catabolize it to non-bioactive GAs.

The good dynamic range and high sensitivity of the RGA sensor towards GA_4 allows to analyze the effect of GA2Oxidases on RGA-FF also at lower concentrations. By adding either GA2Ox1 or GA2Ox2, we observed less degradation compared to the control. Especially, GA2Ox2 has a huge effect on GA_4, while GA2Ox1 has a moderate effect (Fig. 5). When incubated with GA2Ox8, we observed repeatedly no effect on GA_4. We could show in this protoplast system that GA2OX1 and GA2Ox2 inactivate bioactive C19-GAs like GA_1 and GA_4 and convert them the non-bioactive catabolites which are no longer able to induce the degradation of RGA. GA2Ox8, which should act on C20 GAs only, does not have a direct effect on GA_4. In general, this GA biosensor can be utilized to address GA biosynthesis and metabolism questions in a quantitative manner. Its high sensitivity allows to distinguish between the effects of different GA2Oxidases on GAs.

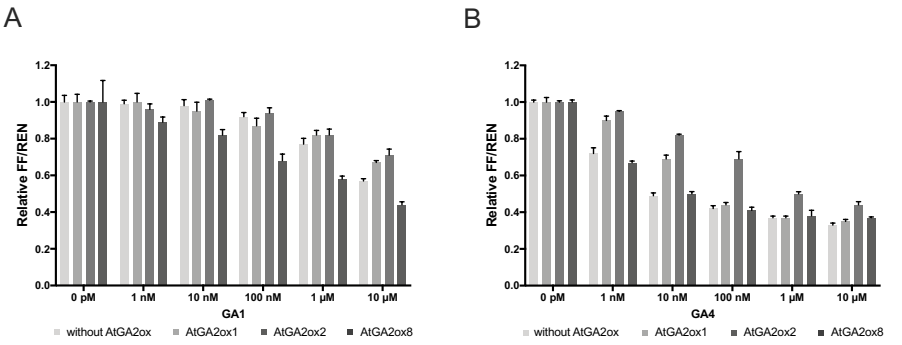

Figure 5: RGA biosensor as a tool to study the activity and specificity of GA oxidases in plant cells. *A. thaliana* wildtype protoplasts were transformed with the RGA biosensor construct and an additional GA2 oxidase (either GA2ox1, GA2ox2, GA2ox8 or a control). 20h after transformation, the protoplasts were supplemented with serial dilutions from 1 nM to 10 µM of GA_1 or GA_4 for 4h. Afterwards, luciferase activity was measured. The error bars represent the SEM (n = 6).

GA transporter activity studies in plant cells

One important topic in gibberellin research is its transport throughout the plant. The knowledge of GA perception and signaling is broadening, however there is still little known about its transport. In general, two systems are extensively used to analyze transporter activities and substrates: *Xenopus* oocytes and the yeast *Saccharomyces cerevisiae*[15]. We set here to test whether the GA-biosensors developed are applicable to study and detect transporter activity in protoplasts. The recently reported GA transporter NPF3 belongs to the large NRT1/PTR FAMILY (NPF) and it has already been shown to transport GA_3 and GA_4 (among other substrates) in yeast and oocytes[25–27], but not in a plant system yet. With the GA biosensors in protoplasts, the transporter specificity towards distinct GAs, but also the direction of the GA transport could be further analyzed. We co-transformed the protoplasts with either NPF3 or a control without transporter activity and our RGA biosensor and incubated with increasing concentrations of GA_3 and GA_4 for 2 and 4 h (Fig. 6 and Fig. S4). Afterwards, the luciferase activity was determined. Our results suggested that indeed GA_3 is transported by NPF3 into the protoplasts (Fig. 6) which is visible at low and high GA_3 concentrations. At high pM/low nM concentrations, there is over 40 % more decrease in RGA-FF/REN ratio in the presence of the NPF3 transporter. For GA_4, no significant transporter activity could be observed in this system (Fig. 6).

Our GA biosensor in protoplasts provides a platform to not only screen for transporter activities, but also gives insight into the specificity towards different GAs and the direction of transport. Therefore, it constitutes an alternative to already existing screening platforms like oocytes and yeast-two-hybrid systems, because as a plant system it comes closer to the physiological conditions in plants. In addition, the sensitivity of the system allows for transporter (direction) analysis even at low hormone concentrations.

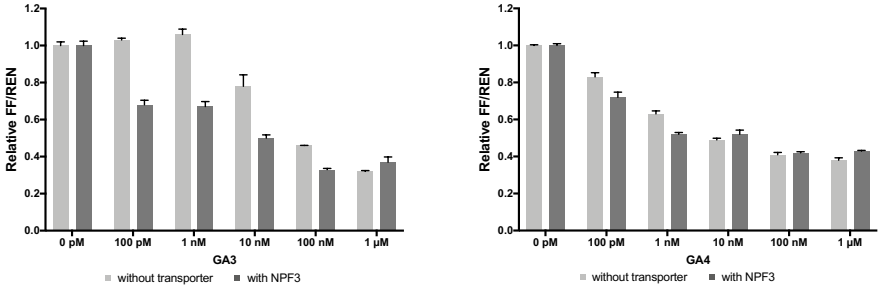

238

239 **Figure 6: RGA biosensor as a tool to study GA transporter in a plant system.** *A. thaliana* wildtype protoplasts
240 were transformed with the RGA biosensor construct and the NPF3 GA transporter or a control. 20h after
241 transformation, the protoplasts were supplemented with serial dilutions from 100 pM to 1 µM of GA_3 or GA_4 for 2h.
242 Afterwards, luciferase activity was measured. The error bars represent the SEM (n = 6).

Discussion

The quantitative *in vivo* monitoring and the dynamic analysis of intracellular GA levels is still challenging. To overcome these limitations we built five genetically-encoded GA biosensors based on the intrinsic GA-induced DELLA proteasomal-mediated degradation mechanism (Fig. 1B). These five biosensors comprise either RGA, GAI, RGL1, RGL2 or RGL3 as sensor modules fused to a firefly luciferase. As a normalization element, a renilla luciferase is connected via a 2A peptide to the DELLA-FF fusion (Fig. 1C). This construct composition allows the highly sensitive analysis of intracellular changes upon exogenous application of GAs within plant cells. These GA biosensors can be utilized as molecular proxies to investigate i) the sensitivity and specificity towards different GAs and precursors, ii) metabolic processes, and iii) hormone transporter activities. For the characterization of the system, we selected proof of principle applications. The high sensitivity towards the bioactive GAs GA_3, GA_4 and GA_7 up to a low pM range, make the biosensors suitable for screenings towards not only endogenous GAs, but also synthetic GA analogues and their precursors. The fact that even known GA precursors like GA_9 and GA_{20} induce a DELLA-FF degradation, implies that either these precursors are also sensed or that they are metabolized into their bioactive products, namely GA_4 and GA_1.

In addition, this biosensor system allows the analysis of GA-related metabolic processes. By co-expression of the highly sensitive RGA biosensor with GA oxidases, we could observe their selectivity towards different GAs. We showed that GA2-oxidase 1 and 2 act on GA_1 and GA_4, whereas GA2-oxidase 8 had no significant effect. This underlines the effect of the GA2-oxidases 1 and 2 on C19-GAs, like for example GA_1 and GA_4, that was already demonstrated earlier via phenotypical *Arabidopsis* mutant analysis, GC/MS or expression analysis via RT-PCR[22–24]. However, all of the above-mentioned methods are either non/semi-quantitative or demand the disruption of the plant tissue. The here presented GA biosensors represent a new biosynthetic tool for the investigation of GA-related metabolic processes in a quantitative manner with a high spatio-temporal resolution in a protoplast system. Future areas of application could include the analysis of additional enzymes associated with GA biosynthesis or even large scale metabolite and enzyme screenings.

In an additional proof of principle experiment, we investigated GA transporter activities. For this, the recently reported NPF3 transporter of the NRT1/PTR FAMILY (NPF) [25,26] was selected and using this experimental approach we could indeed show NPF3 activity as a GA_3-importer (Fig. 6). For GA_4, no significant effect was observed, although a transporter activity has also been proposed for GA_4 in other systems [25,27].

Whereas the conventional methods for analyzing GA contents need the disruption of tissues or demand complex and expensive preparation procedures, the protoplast system in combination with the sensors introduced here is relatively cheap and technically simple. In

combination with other methods, such as genetic analyses, our new system depicts a useful completion for investigating GA signaling and metabolic analyses. Future perspectives could be the expansion of this principle to the implementation of engineered fluorescence sensors in plants and luminescence sensors in an orthogonal system like mammalian cells[18]. Furthermore, GA signaling components could be analyzed in mutant protoplasts as it was already done for strigolactone signaling[19].

Material and Methods

Plasmid Construction

The expression vectors and cloning strategies are described in table S1.

Plant Material, Protoplast Isolation and Transformation

The seeding of the *Arabidopsis thaliana* seeds as well as the protoplast isolation were performed as previously described (Samodelov *et al*., 2016).

For the protoplast transformation, 30 µg of Sensor construct were adjusted to a volume of 20 µl with MMM Medium [MES, mannitol, and magnesium; 15 mM $MgCl_2$, 5 mM MES, 0.465 M mannitol (pH 5.8)]. For the GA-oxidase or transporter studies, 15 µg of the GAoxidase, the transporter or a control plasmid were added to the sensor construct and then adjusted with MMM Medium to a volume of 20 µl.

500,000 protoplasts in 100 µl MMM solution were carefully mixed with the DNA and incubated for 5 min. Afterwards, 120 µl of polyethylene glycol (PEG) solution (2.5 mL 0.8 M mannitol, 1 mL 1 M $CaCl_2$, 4 g PEG4000 from Sigma-Aldrich, and 3 mL H_2O, prepared fresh for each experiment) were added in a dropwise manner. Finally, 120 µl MMM were supplemented, overlaid to a final volume of 1.8 mL per reaction with PCA (protoplast culture *Arabidopsis*, 0.32% (w/v) Gamborg B5 basal salt powder with vitamins from bioWORLD, 2 mM $MgSO_4 \cdot 7H_2O$, 3.4 mM $CaCl_2 \cdot 2H_2O$, 5 mM MES, 0.342 mM L-glutamine, 58.4 mM sucrose, 550 mosmol with glucose, 4.2 µM Ca-pantothenate, 2% (v/v) biotin from a biotin solution of 0.02% (w/v) in H_2O, 0.1% (v/v) Gamborg B5 Vitamin Mix (pH 5.8), and 1:2000 ampicillin (stock solution: 1mg/mL)). In this manner, multiple transformations were performed together and pooled before hormone induction.

Treatment with GA and luminescence analysis

The inducer substrates GA_1, GA_3, GA_4, GA_7, GA_9 and GA_{20} were obtained from OlChemim Ltd and prepared as a 10 mM stock solution in ethanol. The proteasomal inhibitor MG132 (Sigma-Aldrich) was prepared as a 40 mM stock solution in dimethyl sulfoxide and added directly to the protoplasts 2 h before induction with GA at the final concentrations indicated.

The general treatment with GAs and the luminescence analysis were performed as described in Samodelov *et al*., 2016 for strigolactone. Briefly, 20 – 24 h after transformation, the transformation replicates were pooled together and for each concentration of the inducer substrate and for each measuring time point, 960 µl protoplast solution were pipetted into a 2 mL deep-well storage plate (Corning). Serial dilutions of the inducer substrate GA_1, GA_3, GA_4, GA_7, GA_9 or GA_{20} were prepared in PCA at a 11-fold concentration of the desired final experimental concentration and 96 µl were mixed with 960 µl protoplast solution. The durance of the following GA incubation step depended on the type of analysis: 5 h for

selectivity/specificity analysis towards different GAs, 4 h for transporter and GA2oxidase analysis and 30 min, 1 h, 2 h, 4 h and 8 h for kinetic analysis of the RGA sensor.

For the luminescence determination, 80 µl of the induced protoplasts were pipetted into two separate white 96-well assay plates in order that firefly and renilla luminescence could be determined simultaneously in two plate readers. Before the measurement, 20 µl of firefly substrate [0.47 mM D-luciferin (Biosynth AG), 20 mM tricine, 2.67 mM $MgSO_4 \cdot 7H_2O$, 0.1 mM $EDTA \cdot 2H_2O$, 33.3 mM dithiothreitol, 0.52 mM adenosine 5′-triphosphate, 0.27 mM acetyl–coenzyme A, 5 mM NaOH, 0.26 mM $MgCO_3 \cdot 5H_2O$, in H_2O] or coelenterazine (472 mM coelenterazine stock solution in methanol, diluted directly before use 1:15 in phosphate-buffered saline) were added to the samples. Firefly luminescence was determined in a Berthold Technologies Centro XS^3 LB960 Microplate luminometer whereas renilla luminescence was determined in a Berthold technologies $Tristar^2S$ LB942 Multimode Plate Reader.

Statistical Analysis

Ordinary one-way ANOVAS and multiple comparisons for statistical significance were performed with GraphPad Prism 7 for Mac Os X version 10.13.1.

Acknowledgements

We thank Reinhild Wurm, Michaela Gerads and Jessica Müller for valuable technical assistance; Leonie-Alexa Koch and Patrick Fischbach for helpful comments on the manuscript. M. Rodriguez-Franco for providing the plasmid pGEN016. This work was supported by the German Research Foundation (DFG) under Germany´s Excellence Strategy (CEPLAS - EXC-2048/1 – Projekt ID 390686111 to MDZ), and the University of Düsseldorf, Germany.

References

1. Davière, J.-M. & Achard, P. Gibberellin signaling in plants. *Development* **140**, 1147–51 (2013).
2. Yamaguchi, S. Gibberellin Metabolism and its Regulation. *Annu. Rev. Plant Biol.* **59**, 225–251 (2008).
3. Hedden, P. & Phillips, A. L. Gibberellin metabolism: new insights revealed by the genes. *Trends Plant Sci.* **5**, 523–530 (2000).
4. Yamaguchi, S. & Kamiya, Y. Gibberellin Biosynthesis: Its Regulation by Endogenous and Environmental Signals. *Plant Cell Physiol.* **41**, 251–257 (2000).
5. Ueguchi-Tanaka, M. *et al.* GIBBERELLIN INSENSITIVE DWARF1 encodes a soluble receptor for gibberellin. *Nature* **437**, 693–698 (2005).
6. Nakajima, M. *et al.* Identification and characterization of Arabidopsis gibberellin receptors. *Plant J.* **46**, 880–889 (2006).
7. McGinnis, K. M. *et al.* The Arabidopsis SLEEPY1 gene encodes a putative F-box subunit of an SCF E3 ubiquitin ligase. *Plant Cell* **15**, 1120–30 (2003).
8. Achard, P. & Genschik, P. Releasing the brakes of plant growth: how GAs shutdown DELLA proteins. *J. Exp. Bot.* **60**, 1085–1092 (2009).
9. Silverstone, A. L. *et al.* Repressing a repressor: gibberellin-induced rapid reduction of the RGA protein in Arabidopsis. *Plant Cell* **13**, 1555–66 (2001).
10. Peng, J. *et al.* The Arabidopsis GAI gene defines a signaling pathway that negatively regulates gibberellin responses. *Genes Dev.* **11**, 3194–205 (1997).
11. Ariizumi, T., Murase, K., Sun, T.-P. & Steber, C. M. Proteolysis-independent downregulation of DELLA repression in Arabidopsis by the gibberellin receptor GIBBERELLIN INSENSITIVE DWARF1. *Plant Cell* **20**, 2447–59 (2008).
12. Murase, K., Hirano, Y., Sun, T. & Hakoshima, T. Gibberellin-induced DELLA recognition by the gibberellin receptor GID1. *Nature* **456**, 459–463 (2008).
13. Okamoto, M., Hanada, A., Kamiya, Y., Yamaguchi, S. & Nambara, E. Measurement of Abscisic Acid and Gibberellins by Gas Chromatography/Mass Spectrometry. in 53–60 (Humana Press, Totowa, NJ, 2009). doi:10.1007/978-1-59745-477-3_5
14. Urbanová, T., Tarkowská, D., Novák, O., Hedden, P. & Strnad, M. Analysis of gibberellins as free acids by ultra performance liquid chromatography–tandem mass spectrometry. *Talanta* **112**, 85–94 (2013).
15. Corratgé-Faillie, C. & Lacombe, B. Substrate (un)specificity of Arabidopsis NRT1/PTR FAMILY (NPF) proteins. *J. Exp. Bot.* **68**, 3107–3113 (2017).
16. Rizza, A., Walia, A., Lanquar, V., Frommer, W. B. & Jones, A. M. In vivo gibberellin gradients visualized in rapidly elongating tissues. *Nat. Plants* **3**, 803–813 (2017).
17. Khakhar, A., Leydon, A. R., Lemmex, A. C., Klavins, E. & Nemhauser, J. L. Synthetic hormone-responsive transcription factors can monitor and re-program plant development. doi:10.7554/eLife.34702.001
18. Wend, S. *et al.* A quantitative ratiometric sensor for time-resolved analysis of auxin dynamics. *Sci. Rep.* **3**, 2052 (2013).
19. Samodelov, S. L. *et al.* StrigoQuant: A genetically encoded biosensor for quantifying strigolactone activity and specificity. *Sci. Adv.* **2**, e1601266 (2016).
20. Dill, A., Jung, H. S. & Sun, T. P. The DELLA motif is essential for gibberellin-induced degradation of RGA. *Proc. Natl. Acad. Sci. U. S. A.* **98**, 14162–7 (2001).
21. Hedden, P. & Thomas, S. G. Gibberellin biosynthesis and its regulation. *Biochem. J.* **444**, 11–25 (2012).
22. Rieu, I. *et al.* Genetic analysis reveals that C19-GA 2-oxidation is a major gibberellin inactivation pathway in Arabidopsis. *Plant Cell* **20**, 2420–36 (2008).
23. Thomas, S. G., Phillips, A. L. & Hedden, P. Molecular cloning and functional expression of gibberellin 2- oxidases, multifunctional enzymes involved in gibberellin deactivation. *Proc. Natl. Acad. Sci. U. S. A.* **96**, 4698–703 (1999).
24. Schomburg, F. M., Bizzell, C. M., Lee, D. J., Zeevaart, J. A. D. & Amasino, R. M. Overexpression of a novel class of gibberellin 2-oxidases decreases gibberellin levels and creates dwarf plants. *Plant Cell* **15**, 151–63 (2003).
25. Tal, I. *et al.* The Arabidopsis NPF3 protein is a GA transporter. *Nat. Commun.* **7**, 11486 (2016).
26. Chiba, Y. *et al.* Identification of Arabidopsis thaliana NRT1/PTR FAMILY (NPF) proteins capable of transporting plant hormones. *J. Plant Res.* **128**, 679–686 (2015).
27. David, L. C. *et al.* N availability modulates the role of NPF3.1, a gibberellin transporter, in GA-mediated phenotypes in Arabidopsis. *Planta* **244**, 1315–1328 (2016).

Supplementary Information

Quantitative ratiometric biosensors for the analysis of gibberellin signaling dynamics and metabolism

Jennifer Andres[1], Lisa Schmunk[2], Tim Blomeier[1], Sophia Samodelov[3], Rocio Ochoa-Fernandez[1], David Alabadi[4], Miguel A. Blazquez[4], Matias D. Zurbriggen[1]*

[1]Institute of Synthetic Biology, University of Düsseldorf and CEPLAS, Düsseldorf, Germany

[2]Cardiovascular Strategic Research Initiative, University of Cambridge

[3]Department of Clinical Pharmacology and Toxicology, University Hospital Zurich, Zurich, Switzerland

[4]Instituto de Biología Molecular y Celular de Plantas (IBMCP), CSIC-Universidad Politécnica de Valencia, Campus UPV CPI 8E, Valencia, Spain

*Corresponding author: Email: matias.zurbriggen@uni-duesseldorf.de

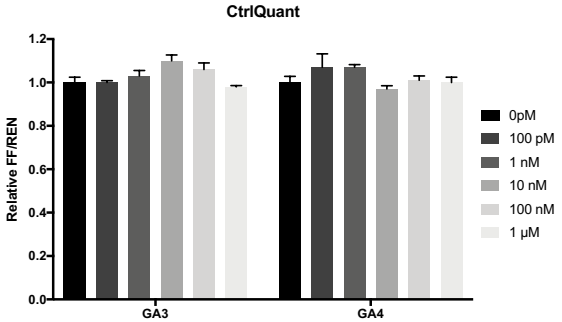

Figure S1: CtrlQuant activity upon induction with GA_3 and GA_4. *Arabidopsis Thaliana* wildtype protoplasts were transformed with the CtrlQuant sensor. 20h after transformation, the protoplasts were supplemented with serial dilutions from 100 pM to 1 µM of either GA_3 or GA_4 for 5h. Afterwards, the luciferase activity was determined and the averaged FF/REN ratios were normalized to the sample without GA addition. The error bars represent the standard error of the mean (SEM) for *n*=6.

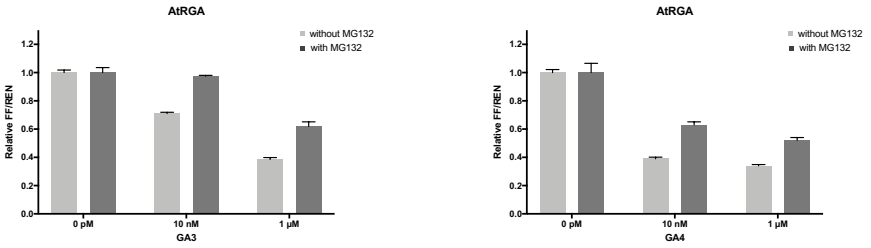

Figure S2: GA-dependent RGA degradation is mediated by the 26S proteasome. *Arabidopsis Thaliana* wildtype protoplasts were transformed with AtRGA sensor construct and treated with 40 µM proteasomal inhibitor MG132 20h after transformation and 2h prior to GA induction. Luciferase activity was determined after 4h. The results are FF/REN ratios normalized to the sample without GA addition. The error bars represent the standard error of the mean (SEM; *n*=6).

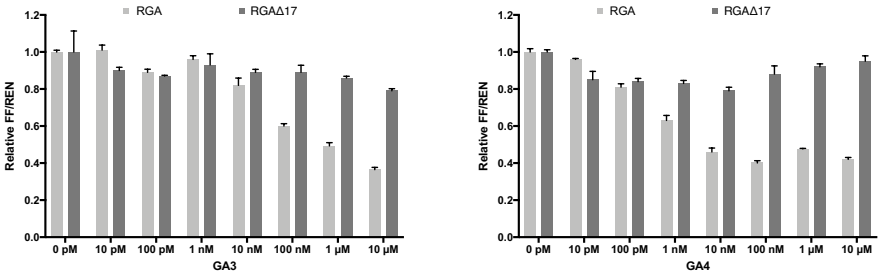

Figure S3: GA-dependent RGA degradation is mediated by the DELLA domain. *Arabidopsis Thaliana* wildtype protoplasts were transformed with either the RGA or the RGAΔ17 sensor construct which has a 17 aminoacid deletion within the DELLA domain. 20h after transformation, the protoplasts were supplemented with serial dilutions from 10 pM to 10 µM of either GA_3 or GA_4 for 5h. Afterwards, the luciferase activity was determined and the averaged FF/REN ratios were normalized to the sample without GA addition. The error bars represent the standard error of the mean (SEM) for *n*=6.

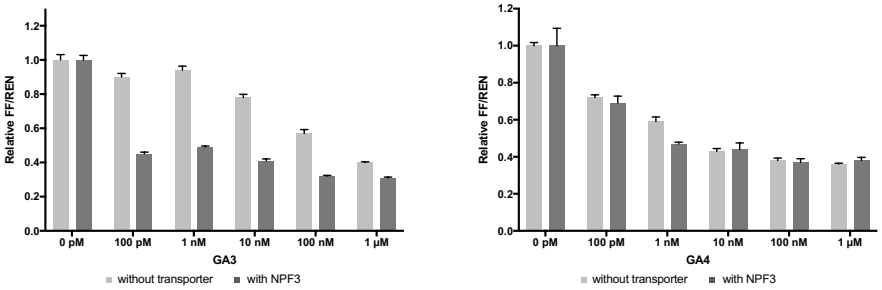

Figure S4: RGA biosensor as a tool to study GA transporter in a plant system. *Arabidopsis Thaliana* wildtype protoplasts were transformed with the RGA biosensor construct and the NPF3 GA transporter or a control. 20h after transformation, the protoplasts were supplemented with serial dilutions from 100 pM to 1 µM of GA_3 or GA_4 for 4h. Afterwards, luciferase activity was measured. The error bars represent the SEM for *n* = 6 replicates.

48 **Table S1: Expression vectors used in this study.**

Plasmid	Description	Reference or Source
pJA152	P_{35S}-NPF3-Tnos Vector encoding AtNPF3 under the control of P_{35S} for the use in plant cells. NPF3 was amplified from the clone U21885 (ABRC) with the oligos oJA332/oJA333 including AQUA overhangs, pGEN016 was amplified with oJA268/oJA271. The fragments were assembled via AQUA cloning. [1]	This work
pSLS404	P_{35S}-Renilla-2A-GAI-Firefly-myc-pA Ratiometric gibberellin sensor plasmid with *Arabidopsis* GAI DELLA as SM for use in plant cells. GAI was amplified from clone U14047 (ABRC) with oligos oSLS401/oSLS402 including Gibson overhangs, Ren-2A was PCR amplified from pMK147 with oSLS009/oSLS407 including Gibson overhangs. REN-2A and the GAI-amplicon were combined via fusion PCR and cloned into NotI/NheI digested CtrlQuant by Gibson cloning.	This work
pSLS405	P_{35S}-Renilla-2A-RGA-Firefly-myc-pA Ratiometric gibberellin sensor plasmid with *Arabidopsis* RGA DELLA as SM for use in plant cells. RGA was amplified from clone U13937 (ABRC) with oligos oSLS403/oSLS404 including Gibson overhangs. REN-2A and the RGA-amplicon were combined via fusion PCR and cloned into NotI/NheI digested CtrlQuant by Gibson-cloning.	This work
pSLS406	P_{35S}-Renilla-2A-RGL1-Firefly-myc-pA Ratiometric gibberellin sensor plasmid with *Arabidopsis* RGL1 DELLA as SM for use in plant cells. RGL1 (AY096506) was amplified from clone U18422 (ABRC) with oligos oSLS405/oSLS406 including Gibson overhangs. REN-2A and the RGL1-amplicon were combined via fusion PCR and cloned into NotI/NheI digested CtrlQuant by Gibson-cloning.	This work
pSLS417	P_{35S}-Renilla-2A-RGL2-Firefly-myc-pA Ratiometric gibberellin sensor plasmid with *Arabidopsis* RGL2 DELLA as SM for use in plant cells. RGL2 (NM_111216) was amplified from RGL2 in S/D-TOPO vector (Invitrogen) received from S. Prat (Centro Nacional de Biotecnología, Madrid) with oSLS422/oSLS423, Ren-2A was PCR amplified with oSLS009/oSLS407 and Gibson-cloned into NotI/NheI digested CtrlQuant.	This work
pSLS418	P_{35S}-Renilla-2A-RGL3-Firefly-myc-pA Ratiometric gibberellin sensor plasmid with *Arabidopsis* RGL3 DELLA as SM for use in plant cells. RGL3 (NM_121755) was amplified from RGL3 in S/D-TOPO vector (Invitrogen) received from S. Prat (Centro Nacional de Biotecnología, Madrid) with oSLS424/oSLS425, Ren-2A was PCR amplified with oSLS009/oSLS407 and Gibson-cloned into NotI/NheI digested CtrlQuant.	This work
pSLS470	P_{35S}-Renilla-2A-RGAΔ17-Firefly-myc-pA Ratiometric gibberellin sensor plasmid with *Arabidopsis* RGAΔ17 DELLA as SM for use in plant cells. RGAΔ17 was amplified from RGAΔ17-containing plasmid received from the group of M. Blazquez with Oligos oSLS403/oSLS404 including Gibson overhangs. REN-2A and the RGAΔ17-amplicon were combined via fusion PCR and cloned into NotI/NheI digested CtrlQuant by Gibson-cloning.	This work
pSLS479	P_{35S}-GA2ox-1-Tnos Vector encoding GA2Ox1 under the control of P_{35S} for the use in plant cells.	This work

	GA2ox-1 was amplified from ABRC clone (stock number: C105372) using oligos oSLS310/oSLS311. pGEN016 was digested (AgeI/NotI) and the backbone was assembled with the PCR-fragment by GIBSON cloning.	
pSLS480	P_{35S}-GA2ox-2-Tnos Vector encoding GA2Ox2 under the control of P_{35S} for the use in plant cells. GA2ox-2 was amplified from ABRC clone (stock number: U20502) using oligos oSLS312/oSLS313. pGEN016 was digested (AgeI/NotI) and the backbone was assembled with the PCR-fragment by GIBSON cloning.	This work
pSLS481	P_{35S}-GA2ox-8-Tnos Vector encoding GA2Ox8 under the control of P_{35S} for the use in plant cells. GA2ox-8 was amplified from ABRC clone (stock number: DQ653213) using oligos oSLS314/oSLS315. pGEN016 was digested (AgeI/NotI) and the backbone was assembled with the PCR-fragment by GIBSON cloning.	This work
pGEN016	P_{35S}-mEGFP-Tnos Vector encoding mEGFP under the control of P_{35S}	Received from M. Rodriguez-Franco (University of Freiburg)
pSW209 (CtrlQuant)	P_{35S}-Renilla-2A-Firefly-myc-pA Vector encoding firefly luciferase and renilla luciferase separated by a 2A-peptide under control of P_{35S}.	2
pMK147	$P_{EF1\alpha}$-Renilla-2A-Aux/IAA-Firefly-myc Vector for mammalian expression of Renilla luciferase and auxin sensor module fused to firefly luciferase-myc.	2

49

Table S 2: Oligonucleotides used in this study.

Oligo	Sequence 5´->3´
oJA332	ACACGGGGACTCTAGCGCTACCGGTCGCCACCATGGAGGAGCAAAGCAAG
oJA333	AACGATCGGGGAAATTCGCCTCGAGATCAGTTATTCATCAACTAAACTCCTATTTGAC
oJA268	GGTGGCGACCGGTAGC
oJA271	TAACTGATCTCGAGGCGAATTTCCCC
oSLS401	AATCCTGGACCCGCGCGCATGAAGAGAGATCATCATCATCATCATCATCAAGATAAG
oSLS402	GGCGTCTTCCATGCTAGCATTGGTGGAGAGTTTCCAAGCCGAG
oSLS009	GAGAGAACACGGGGACTCTAGCGCTACCGGTTGGCTAGGTAAGCTTGGTACCACCATGACTT CGAAAGTTTATGATCCAGAAC
oSLS403	AATCCTGGACCCGCGCGCATGAAGAGAGATCATCACCAATTCCAAGGTC
oSLS404	GGCGTCTTCCATGCTAGCGTACGCCGCCGTCGAGAGTTTC
oSLS405	AATCCTGGACCCGCGCGCATGAAGAGAGAGCACAACCACCGTGAATC
oSLS406	GGCGTCTTCCATGCTAGCTTCCACACGATTGATTCGCCACGCAG
oSLS407	GCGCGCGGGTCCAGGATTTGATTCCACGTCG
oSLS422	CGACGTGGAATCAAATCCTGGACCCGCGCGCATGAAGAGAGGATACGGAGAAACATGGG
oSLS423	CTTTATGTTTTTGGCGTCTTCCATGCTAGCGGCGAGTTTCCACGCCGAGG
oSLS424	CGACGTGGAATCAAATCCTGGACCCGCGCGCATGAAACGAAGCCATCAAGAAACGTCTGTAG
oSLS425	CTTTATGTTTTTGGCGTCTTCCATGCTAGCCCGCCGCAACTCCGCCG
oSLS310	TGGAGAGAACACGGGGACTCTAGCGCTACCGGTTGGCTAGGTAAGCTTGGTACCACCATGG CGGTATTGTCTAAACCGGTAGC
oSLS311	AATTCGGCCGCTGCCGCAGCGGCAGCGGCCGCTTAATTTAGGAGATTTTTTATAGTCTTCCTT TCGAATTGTTG
oSLS312	TGGAGAGAACACGGGGACTCTAGCGCTACCGGTTGGCTAGGTAAGCTTGGTACCACCATGG TGGTTTTGCCACAGCCAGTC
oSLS313	AATTCGGCCGCTGCCGCAGCGGCAGCGGCCGCTTATACAAGGGTTTTATGATTGAGAAGAG GTTGTTTC
oSLS314	TGGAGAGAACACGGGGACTCTAGCGCTACCGGTTGGCTAGGTAAGCTTGGTACCACCATGG ATCCACCATTCAACGAAATATACAATAACC
oSLS315	AATTCGGCCGCTGCCGCAGCGGCAGCGGCCGCTTATCCGTAGACGTGATTAAGGAACCTAG G

1. Beyer, H. M. *et al.* AQUA Cloning: A Versatile and Simple Enzyme-Free Cloning Approach. *PLoS One* **10**, e0137652 (2015).
2. Wend, S. *et al.* A quantitative ratiometric sensor for time-resolved analysis of auxin dynamics. *Sci. Rep.* **3**, 2052 (2013).

7.2 StrigoQuant dynamic analyses reveal new insights on strigolactone signaling

1 StrigoQuant dynamic analyses reveal new insights on strigolactone
2 signaling

3 Jennifer Andres[1*], Nima Saadat[2*], Oliver Ebenhöh[2#], Matias D. Zurbriggen[1#]

4 [1] Institute of Synthetic Biology, University of Düsseldorf and CEPLAS, Düsseldorf, Germany

5 [2] Institute of Quantitative and Theoretical Biology, University of Düsseldorf and CEPLAS,
6 Düsseldorf, Germany

7 [*] contributed equally to this work

8 [#] Corresponding author: Email: Matias.Zurbriggen@uni-duesseldorf.de, Oliver.Ebenhöh@uni-
9 duesseldorf.de

10

11 **ABSTRACT**

INTRODUCTION

Strigolactones (SLs) are carotenoid-derived lactones that affect diverse processes in plants regarding growth and development by acting as endogenous phytohormones as well as exogenous signals in the rhizosphere. Within the plant they fulfil various tasks concerning developmental aspects such as leaf shape (elongation and serration) and senescence, shoot gravitropism, stem secondary thickening and internode elongation, root architecture and drought/stress tolerance [1–7]. Furthermore, they regulate shoot branching [8,9] and mediate plant adaptations to nutrient availability [10,11]. They promote symbiosis with arbuscular mycorrhizal fungi which provides the plants with minerals [12,13]. Nevertheless, SLs also convey the recognition of host roots by parasitic weeds of the genera *Striga* or *Orobanchae*. This causes severe crop yield losses in Africa and Asia [14] resulting in a rapidly growing interest in the strigolactone research. Due to these distinct and important biological functions, understanding the SL signaling mechanisms has become an important research area in plant sciences. However, the investigation and analysis of these processes in plants by quantifying the hormone at high spatial and temporal resolution with biochemical methods such as GC-MS and not disrupting the tissues, still remains a challenge [15] and prevents *in vivo* dynamic assays [16].

The degradation-based SL perception and early signaling mechanism is similar for various phytohormones including auxin, gibberellin and jasmonate and has been used for the development of genetically encoded biosensors [16–19]. From genetic screens of SL-insensitive mutants, three key components have been shown to be required for SL response in Arabidopsis: the α/β fold hydrolase D14 , MAX2 (F-Box protein, constituent of a SCF E3 ubiquitin-ligase complex) and D53-like SMXLs (8 family members in *Arabidopsis thaliana*) which are regulators of the strigolactone response [20–22]. The binding of SLs to D14 leads to the formation of a co-receptor complex with MAX2 and the regulators of the strigolactone response, the D53-like SMXL family, which in turn leads to the ubiquitylation and proteolysis of the latter thereby triggering SL signaling (Fig. 1A) [23–25]. However, there still remain open questions concerning SL signaling kinetics, regulation and the behavior of D14 in this perception machinery. In recent studies we developed the first genetically encoded quantitative biosensor for SLs to quantify the hormone at high spatial and temporal resolution using the degradation-based signaling mechanism [26] (Fig. 1B). The StrigoQuant sensor incorporates SMXL6 as a sensor module fused to a firefly luciferase connected via a 2A peptide to a renilla luciferase as a normalization element (Fig 1B). Due to this modular construction, other SL signaling components can be incorporated and tested easily with this sensor system. The StrigoQuant sensor has a wide applicability *in vivo* in the Arabidopsis

protoplast system being the first SL sensor which is able to translate SL concentrations into a direct readout in a quantitative manner with a high resolution. It allows the functional study of other SL sensing complex components including MAX2 and D14. Moreover, it enables a better understanding of the specificity/selectivity for the different natural SLs [26].

In order to obtain insights into mechanistic, regulatory aspects, we resorted to the StrigoQuant sensor to obtain a quantitative description of the kinetics. We first performed studies on the kinetics of the hormone-dependent degradation of SMXL6. The obtained quantitative kinetic data on SMXL6 degradation was then integrated into an ad-hoc developed theoretical computational modelling which enables a better quantitative description of the process. The modelled data led to the prediction that D14 might also undergo degradation triggered by *rac*-GR24. Subsequently a quantitative sensor was engineered based on D14 and a similar degradation analysis in the presence of *rac*-GR24 was performed hereby demonstrating that D14 is degraded in a hormone dose-dependent manner.

In summary, we implemented a quantitative biosensor as a proxy of sensitivity and kinetic parameters of the SL perception complex and used this data to calibrate a mathematical model describing the process. The generated data allowed to infer that the receptor might also undergo hormone-dependent degradation. We further tested and confirmed this hypothesis experimentally upon development of a D14-based quantitative biosensor. These results illustrate the potential general utility of implementing an approach integrating quantitative experimental data with theoretical analyses for the unravelling of molecular mechanistic and regulatory principles of plant signaling pathways.

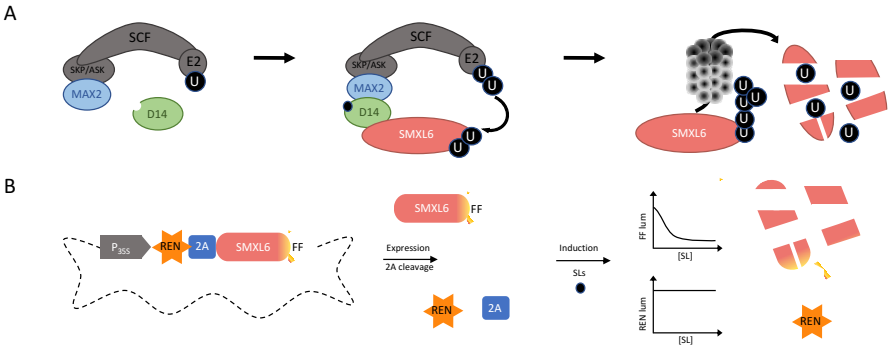

Figure 1: Strigolactone perception mechanism and StrigoQuant sensor design. (A) Schematic overview of the SL perception machinery. Upon binding of SLs to the coreceptor D14, SMXL6 associates to the MAX2 and SKP1/CUL1/F-box E2 ubiquitin ligase complex (SCF^{MAX2}) and becomes polyubiquitinated (U) and thereby targeted for degradation by the 26S proteasome. (B) The StrigoQuant construct, as described in Samodelov et al. 2016, contains a renilla luciferase (REN) connected via a 2A peptide to the sensormodule SMXL6 fused to a firefly

luciferase (FF) under the control of a constitutive 35S promoter. The 2A peptide leads to stoichiometric coexpression of REN as the normalization element and the SMXL6-FF sensormodule. As a consequence of SL induction, SMXL6-FF becomes ubiquitinated and consequently degraded, whereas REN expression remains the same, which leads to a decrease in FF/REN ratio (modified from Samodelov et al.).

69

4

RESULTS

To study and understand strigolactone sensing, we performed sensor kinetics in *Arabidopsis thaliana* protoplasts with the previously developed StrigoQuant biosensor. This degradation-based and ratiometric luminescent biosensor has a wide dynamic range and a high selectivity/sensitivity (pM range) towards the synthetic strigol-like SL analog racemic GR24 (*rac*-GR24) [27].The StrigoQuant construct expresses a renilla luciferase (REN) as a normalization element connected via a self-processing 2A peptide to a strigolactone-dependent degradation sequence as a sensor module (SM), i.e. SMXL6, fused to a firefly luciferase (FF) (Fig. 1B). The sensor construct is under the control of a constitutive 35S promoter. The 2A peptide in this synthetic construct allows cotranslational cleavage resulting in stoichiometric co-expression of the sensor elements from a single transcript. Upon induction with *rac*-GR24 and other SLs, the SMXL6-FF fusion becomes ubiquitinated in a targeted manner and degraded by the 26S proteasome, whereas REN expression remains constant. This leads to a decrease in FF/REN ratio. For the StrigoQuant biosensor establishment, the sensitivity and specificity towards different strigol- and orobanchol-like SLs and also protoplasts isolated from different mutants were tested. However, the hormone induction was always performed for only 2 h [26].

With the functionality of the StrigoQuant sensor already being established, we carried out kinetic measurements with subsequent hormone induction at the indicated *rac*-GR24 concentrations (Fig. 2B/ Suppl. Fig. 1) 20 h after protoplast transformation, for 15 min, 30 min, 1,5 h, 3 h, 6 h and 9 h. 15 min after hormone induction, SMXL6-FF is already degraded up to 50% at high *rac*-GR24 concentration (1 µM) illustrating the high sensitivity of this sensor construct. Over the course of the 9h measurements, significant reduction at concentrations as low as 100 pM could be detected.

To further characterize the degradation mechanism and kinetics of the response, we developed a mathematical model based on ordinary differential equations (ODE) describing the time evolution of the levels of SMXL6 upon incubation with the hormone.

DESCRIPTION OF THE MODEL (Ebenhöh lab)

Modelling approach

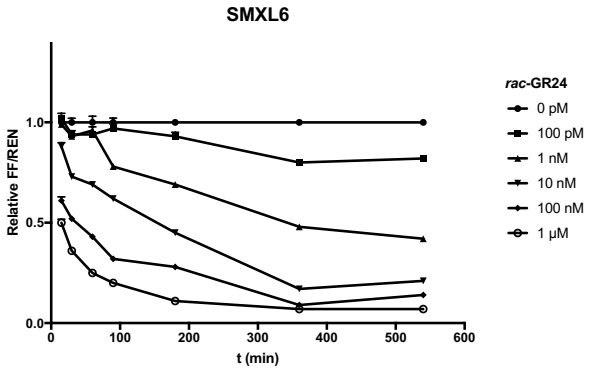

Figure 2: Strigolactone perception model scheme and dose- and time- dependent strigolactone dynamics

The quantitative data on the time course of the degradation described above was used to fit/calibrate the dose response simulations of the model. Using these data, all optimization attempts successfully fitted the SMXL6-FF kinetics, but also resulted in an unrealistic accumulation of the D14 receptor in the same simulations. This led to the hypothesis that the structure of the system only allows good fits of SMXL6-FF data if D14 overaccumulates. We therefore repeated the fitting procedure with the additional constraint that the abundance of D14 is restricted to biologically feasible abundances during optimization. Specifically, we limited the relative abundances to values between 0 and 1 (see Supplement). This results in sub optimal fits of SMXL6-FF. The initial fast degradation cannot be fitted simultaneously with the following slower phase of SMXL6 degradation. The observation that restricting D14 concentrations to biologically realistic levels leads to a poorer fit indicates that the degradation kinetics of SMXL6-FF is strongly dependent on D14 abundance. The experimental and theoretical dynamics displayed in Fig. 2 hint at the existence of two SMXL6 degradation phases: i) at high SL concentrations, where the first phase is very fast, and ii) a second slower one.

These findings suggest that the model lacks structural information and our understanding of the system is yet incomplete. The connection between D14 and the specific SMXL6-FF kinetics further suggest that the missing information is related to the dynamic behavior of D14. One possibility to explain the different time-scales of SMXL6 degradation is a dynamic change in D14 abundance shortly after the stimulus. Indeed, recent results by Hu et al. suggest a SL dependent degradation of D14. Incorporating this reaction to the mathematical model introduces another time-dependent process and therefore a second time-scale in the SL

dependent degradation of SMXL6. Optimizing the modified model to the SMXL6 data results in a good fit for the degradation kinetics, as well as biologically realistic levels of D14 abundance. The theoretical predicted time courses lead to the hypothesis that D14 also exhibits a SL dose dependent degradation.

To test this hypothesis, we engineered a degradation-based ratiometric luminescent D14-receptor biosensor. This construct follows the same modular composition as the StrigoQuant sensor incorporating the D14 receptor in place of the SMXL6 as a sensor module and allows to follow D14 *rac*-GR24-dependent degradation (Fig. 3A). In order to analyze the behaviour and degradation mechanism of D14, we performed kinetics with the same setup as for the StrigoQuant construct with induction of *rac*-GR24 at the indicated hormone concentrations and the same time points as before (Fig. 3B).

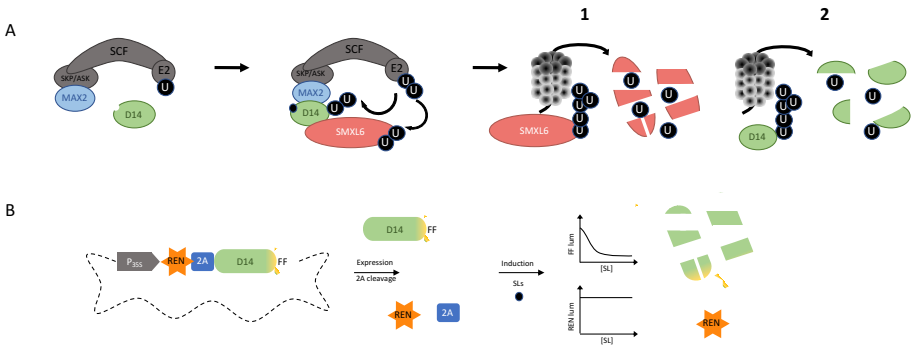

Figure 3: **Strigolactone perception mechanism and D14-receptor sensor design.** (A) Scheme of the SL perception machinery in *A. thaliana*. Upon binding of SLs to the receptor D14, SMXL6 is recruited to the perception machinery complex with MAX2 and SKP1/CUL1/F-box E3 ubiquitin ligase complex (SCF^{MAX2}). As a result, SMXL6 becomes polyubiquitinated (U) and thereby targeted for degradation by the 26S proteasome (1). In a negative feedback loop, D14 becomes also polyubiquitinated and thus degraded by the 26S proteasome, but with slower kinetics. (B) D14-receptor biosensor design. The D14-receptor biosensor expresses a renilla luciferase (REN) connected via a 2A peptide to D14 (as a sensor module) fused to a firefly (FF) luciferase, under the control of a P_{35S} promoter. The 2A peptide leads to the stoichiometric co-expression of REN (as a normalization element) and the D14-FF fusion. In the presence of SLs, D14-FF becomes polyubiquitinated and degraded by the 26S proteasome, whereas REN expression remains constant leading to a decrease in FF/REN ratio.

These measurements showed that D14 is indeed degraded up to almost 30 % after 9 h of *rac*-GR24 induction. However, this degradation process has slower kinetics, starting around 3 h after hormone induction, and a reduced dynamic range (Fig. 4). Furthermore, this degradation is dependent on the 26S proteasome as the treatment with the proteasomal inhibitor MG132 prevented sensor decay (Fig. Suppl. 3). The D14-receptor sensor was also introduced in protoplasts isolated from the *max2* mutant showing the MAX2 dependency of the D14

degradation process (Fig. Suppl. 4). These results indicate that D14 undergoes proteasome-dependent degradation triggered by *rac*-GR24 and mediated by the F-box protein MAX2. This data was used to reparametrize the model, which can now describe not only the SMXL6 but also D14 dynamics. The observation of a hormone dependent degradation of D14 confirms the model derived hypothesis and points towards a regulatory mechanism in the signaling system in which a negative feedback loop would desensitize the system.

Modelling approach

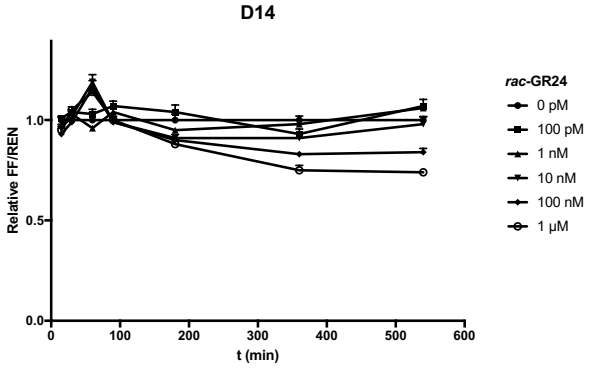

Figure 4: Dose-dependent D14 dynamics (data and simulation).

DISCUSSION

As the interest in strigolactone due to massive yield losses in Asia and Africa caused by the parasitic genera *Striga* and *Orobanchae* is growing, it is important to gain better understanding of the perception and signaling mechanism. If Strigolactone is present, it binds to the receptor D14 which leads to the formation of a coreceptor complex with the F-Box protein MAX2 and the D53-like SMXLs. As a consequence of this complex formation, D53-like SMXLS are ubiquitinated and thereby targeted for degradation by the 26S proteasome [23,24]. With most parts of the strigolactone perception machinery already studied, there still remain open questions concerning a SL signaling kinetic and the role of D14. One important tool for strigolactone analysis besides immunoblots and Y2H is the StrigoQuant biosensor in plant protoplasts [27]. With the functionality of the StrigoQuant biosensor already established [27], we performed kinetic measurements in *Arabidopsis thaliana* protoplasts to gain a broader insight into strigolactone signaling. Thus, SMXL6-FF degradation was measured from 15 min to 9 h after *rac*-GR24 induction. We detected already 50 % degradation at high *rac*-GR24 concentrations (1 µM) after 15 min. Over the course of the measurement, significant reduction at low *rac*-GR24 concentrations (up to 100 pM) could be measured. These data support the ones observed for degraded OsD53/D53-like SMXL protein levels when treated with *rac*-GR24 [24,25]. To further understand strigolactone signaling as well as the involved perception machinery components, we developed a mathematical model. This model suggested the necessity of an additional time scale by adding another component´s turnover in this perception machinery. Because the degradation of other receptors like the potent Karrikin receptor KARRIKIN INSENSITIVE 2 (KAI2) [28]was already known and first groups observed degradation in protein levels for D14 [29–31], we built a luminescence biosensor following the same principle as StrigoQuant with D14 as a sensor module and performed the same measurement in order to get quantitative data about the D14 degradation process to test the hypothesis. As already shown for the D14 protein levels in *Arabidopsis* [29,31] and rice [30], the D14-FF level decreased, starting 3 h after rac-GR24 induction and reaching almost 30 % after 9 h at high concentrations. While SMXL6-FF degradation could be detected even 15 min after *rac*-GR24 induction, D14-FF degradation starts after 3 h with a lower degradation rate. This indicates that the degradation of the receptor D14 might serve as a fine-tuning mechanism of the strigolactone signaling response and can thus be seen as a negative feedback regulation following SMXL6 degradation [30]. Degradation of phytohormone receptors has also been shown for other phytohormones like abscisic acid or jasmonic acid [32,33] indicating that similar feedback mechanisms evolved in different phytohormone pathways. Negative and positive feedback mechanisms play a major role in plants and can be found in the integration of environmental signals, e.g. for hormone signaling or light regulated processes [34]. Plants utilize

185 these feedback mechanisms to either fine-tune signaling processes or return to the basal state
186 which is of great significance for phytohormone signaling. Phytohormones collectively regulate
187 diverse processes in plants from seed germination to flowering [35]. Because of this immense
188 importance of phytohormones, it is crucial for the plant to be able to have regulatory feedback
189 mechanisms. Thus, D14 as a receptor which is able to be degraded and thereby fine-tune the
190 strigolactone signaling response is indispensable.

191 In addition, AtD14 as well as OsD14, which share functional similarity, both hydrolizing SLs to
192 the active form and undergo a conformational change themselves after SL binding allowing
193 other signaling components like the F-Box or regulators to interact [31]. As already suggested in
194 Hu et al. (2017) for rice Chevalier et al. (2014) for *Arabidopsis thaliana*, we could directly show
195 the degradation of D14 through the 26S proteasome (Supplement Figure 3) and the MAX2
196 dependency of this degradation process with our biosensor system (Supplement Figure 4)
197 indicating that D14 is indeed degraded as a consequence of SL perception.

198 In this work, we report a strong interaction of experimental analysis and mathematical
199 modelling to achieve a better insight into strigolactone signaling. In this interdisciplinary
200 cooperation, mathematical modelling could help to describe the kinetic of experimental data
201 and unveil the degradation of a hormone receptor in a plant system which could in turn be
202 confirmed in an experimental approach.

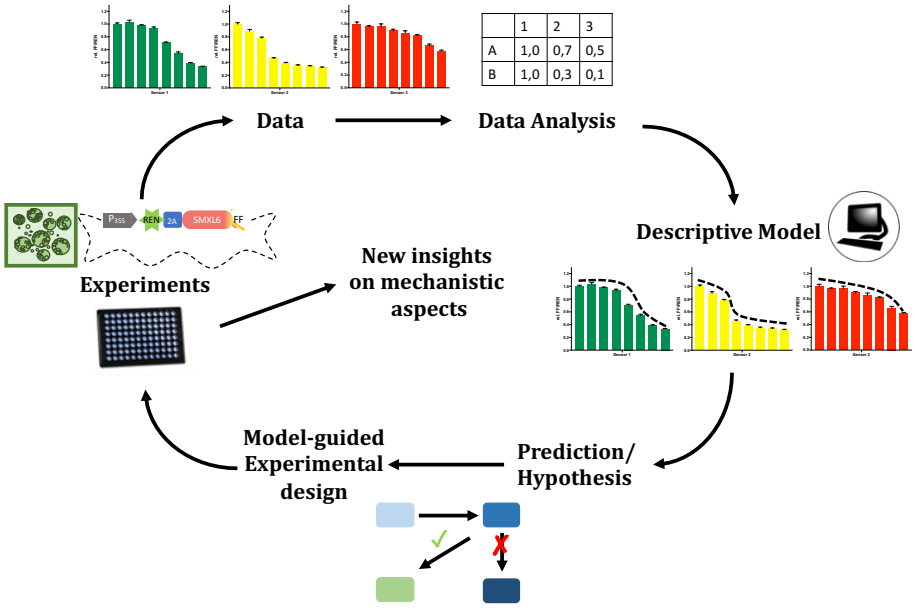

	1	2	3
A	1,0	0,7	0,5
B	1,0	0,3	0,1

203

Figure 5: Experimental Workflow of an exemplary interdisciplinary research project. An already established quantitative biosensor (StrigoQuant) was implemented to gain kinetic data and these data where utilized to generate a mathematical model. From this descriptive model, a new prediction/hypothesis arose, namely that the D14 receptor might also be degraded. This in turn led to a new model-guided experimental design and further biosensor experiments which gave us new insights on mechanistic aspects of the strigolactone perception kinetic.

204

205 # MATERIAL AND METHODS

206 ## Methods experimental part

207 ### Plasmid construction

208 The StrigoQuant and CtrlQuant sensors were engineered as described in Samodelov *et al*.
209 (2016). The D14-Receptor-Sensor was constructed as follows; the cDNA from D14
210 (At3g03990) was PCR (polymerase chain reaction) – amplified with the oligonucleotides
211 oJA237 and oJA238 from pda05576 (the Arabidopsis full-length cDNA clone was developed
212 by the plant genome project of RIKEN Genomic Sciences Center), the StrigoQuant backbone
213 was PCR-amplified with the oligonucleotides oPF074 and oPF075 (table S1 and S2). The two
214 fragments were assembled via AQUA cloning [36].

215

216 ### Plant material, Protoplast isolation and Transformation

217 The seeding of the *Arabidopsis thaliana* seeds as well as the protoplast isolation were
218 performed as previously described [26].

219 Briefly, for the protoplast transformations, 20 µg of StrigoQuant or ControlQuant and 10 µg of
220 D14-Receptor sensor were adjusted to a volume of 20 µl with MMM Medium [MES, mannitol,
221 and magnesium; 15 mM $MgCl_2$, 5 mM MES, 0.465 M mannitol (pH 5.8)]. 500,000 protoplasts
222 in 100 µl MMM solution were carefully mixed with the DNA and incubated for 5 min.
223 Subsequently, 120 µl polyethylene glycol (PEG) solution (2.5 mL 0.8 M mannitol, 1 mL 1 M
224 $CaCl_2$, 4 g PEG4000 from Sigma-Aldrich, and 3 mL H_2O, prepared fresh for each experiment)
225 were supplemented in a dropwise manner and incubated for 8 min. Finally, 120 µl MMM were
226 added, overlaid to a final volume of 1.8 mL per reaction with PCA (protoplast culture
227 *Arabidopsis*, 0.32% (w/v) Gamborg B5 basal salt powder with vitamins from bioWORLD, 2
228 mM $MgSO_4 \cdot 7H_2O$, 3.4 mM $CaCl_2 \cdot 2H_2O$, 5 mM MES, 0.342 mM L-glutamine, 58.4 mM sucrose,
229 550 mosmol with glucose, 4.2 µM Ca-pantothenate, 2% (v/v) biotin from a biotin solution of
230 0.02% (w/v) in H_2O, 0.1% (v/v) Gamborg B5 Vitamin Mix (pH 5.8), and 1:2000 ampicillin (stock
231 solution: 1mg/mL)). In this way, multiple transformations were performed together and pooled
232 before hormone induction.

233

Treatment with SLs and luminescence analysis

The inducer substrate *rac*-GR24 was obtained from OlChemim Ltd and prepared as a 10 mM stock solution in methanol. The proteasomal inhibitor MG132 (Sigma-Aldrich) was prepared as a 40 mM stock solution in dimethyl sulfoxide and added directly to the protoplasts 2 h before induction with *rac*-GR24 at the final concentrations indicated.

The general treatment with SLs and the luminescence analysis were performed as described in Samodelov *et al.*, 2016. Briefly, 20 – 24 h after transformation, the transformation replicates were pooled together and for each concentration of the inducer substrate and for each measuring time point, 960 µl protoplast solution were pipetted into a 2 mL deep-well storage plate (Corning). Serial dilutions of the inducer substrate *rac*-GR24 were prepared in PCA at a 11-fold concentration of the desired final experimental concentration and 96 µl were mixed with 960 µl protoplast solution with a following incubation step of either 15 min, 30 min, 1 h, 1.5 h, 3 h, 6 h or 9 h.

For the luminescence determination, 80 µl of the induced protoplasts were pipetted into two separate white 96-well assay plates in order that firefly and renilla luminescence could be measured simultaneously in two plate readers. Before the measurement, 20 µl of coelenterazine (472 mM coelenterazine stock solution in methanol, diluted directly before use 1:15 in phosphate-buffered saline) or firefly substrate [0.47 mM D-luciferin (Biosynth AG), 20 mM tricine, 2.67 mM $MgSO_4 \cdot 7H_2O$, 0.1 mM $EDTA \cdot 2H_2O$, 33.3 mM dithiothreitol, 0.52 mM adenosine 5′-triphosphate, 0.27 mM acetyl–coenzyme A, 5 mM NaOH, 0.26 mM $MgCO_3 \cdot 5H_2O$, in H_2O] were supplemented to the samples. Renilla luminescence was determined in a Berthold technologies Tristar^{2}S LB942 Multimode Plate Reader whereas firefly luminescence was determined in a Berthold Technologies Centro XS^3 LB960 Microplate luminometer.

Methods modelling part

SUPPLEMENTARY DATA

Supplementary Data are available: Supplementary Table 1, Supplementary Table 2, Supplementary Figure 1, Supplementary Figure 2, Supplementary Figure 3 and Supplementary Figure 4.

ACKNOWLEDGEMENTS

We thank Reinhild Wurm, Michaela Gerads and Jessica Müller for technical assistance as well as Tim Blomeier for comments and aid on figure 1.

FUNDING

This research was supported by funding from deutsche Forschungsgemeinschaft (DFG, German Research Foundation) under Germany´s Excellence Strategy – EXC 2048/1 – Project ID 390686111 and the King Abdullah University of Science and Technology (KAUST).

COMPETING FINANCIAL INTEREST: The authors declare that they have no competing financial interest.

AUTHOR CONTRIBUTION:

JA designed and performed the experiments, analyzed the data and wrote the manuscript. NS performed the mathematical modelling and wrote the manuscript. OE performed the mathematical modelling and wrote the manuscript. MDZ designed and performed the experiments, analyzed the data and wrote the manuscript.

284 **REFERENCES**

285 1. Al-Babili, S. & Bouwmeester, H. J. Strigolactones, a Novel Carotenoid-Derived Plant Hormone.
286 *Annu. Rev. Plant Biol.* **66**, 161–186 (2015).

287 2. Sang, D. *et al.* Strigolactones regulate rice tiller angle by attenuating shoot gravitropism
288 through inhibiting auxin biosynthesis. *Proc. Natl. Acad. Sci. U. S. A.* **111**, 11199–204 (2014).

289 3. Yamada, Y. *et al.* Strigolactone signaling regulates rice leaf senescence in response to a
290 phosphate deficiency. *Planta* **240**, 399–408 (2014).

291 4. Ueda, H. & Kusaba, M. Strigolactone Regulates Leaf Senescence in Concert with Ethylene in
292 Arabidopsis. *Plant Physiol.* **169**, 138–47 (2015).

293 5. Bu, Q. *et al.* Regulation of Drought Tolerance by the F-Box Protein MAX2 in Arabidopsis. *Plant*
294 *Physiol.* **164**, 424–439 (2014).

295 6. Ha, C. Van *et al.* Positive regulatory role of strigolactone in plant responses to drought and salt
296 stress. *Proc. Natl. Acad. Sci.* **111**, 851–856 (2014).

297 7. Waters, M. T., Gutjahr, C., Bennett, T. & Nelson, D. C. Strigolactone Signaling and Evolution.
298 *Annu. Rev. Plant Biol.* **68**, 291–322 (2017).

299 8. Gomez-Roldan, V. *et al.* Strigolactone inhibition of shoot branching. *Nature* **455**, 189–194
300 (2008).

301 9. Umehara, M. *et al.* Inhibition of shoot branching by new terpenoid plant hormones. *Nature* **455**,
302 195–200 (2008).

303 10. Mayzlish-Gati, E. *et al.* Strigolactones Are Involved in Root Response to Low Phosphate
304 Conditions in Arabidopsis. *Plant Physiol.* **160**, 1329–1341 (2012).

305 11. Sun, H. *et al.* Strigolactones are involved in phosphate- and nitrate-deficiency-induced root
306 development and auxin transport in rice. *J. Exp. Bot.* **65**, 6735–6746 (2014).

307 12. Besserer, A., Bécard, G., Jauneau, A., Roux, C. & Séjalon-Delmas, N. GR24, a synthetic
308 analog of strigolactones, stimulates the mitosis and growth of the arbuscular mycorrhizal
309 fungus Gigaspora rosea by boosting its energy metabolism. *Plant Physiol.* **148**, 402–13
310 (2008).

311 13. Akiyama, K., Matsuzaki, K. & Hayashi, H. Plant sesquiterpenes induce hyphal branching in
312 arbuscular mycorrhizal fungi. *Nature* **435**, 824–827 (2005).

313 14. Parker, C. Observations on the current status of *Orobanche* and *Striga* problems worldwide.
314 *Pest Manag. Sci.* **65**, 453–459 (2009).

15. Xie, X. *et al.* Confirming Stereochemical Structures of Strigolactones Produced by Rice and Tobacco. *Mol. Plant* **6**, 153–163 (2013).

16. Wend, S. *et al.* A quantitative ratiometric sensor for time-resolved analysis of auxin dynamics. *Sci. Rep.* **3**, 2052 (2013).

17. Brunoud, G. *et al.* A novel sensor to map auxin response and distribution at high spatio-temporal resolution. *Nature* **482**, 103–106 (2012).

18. Rizza, A., Walia, A., Lanquar, V., Frommer, W. B. & Jones, A. M. In vivo gibberellin gradients visualized in rapidly elongating tissues. *Nat. Plants* **3**, 803–813 (2017).

19. Larrieu, A. *et al.* A fluorescent hormone biosensor reveals the dynamics of jasmonate signalling in plants. *Nat. Commun.* **6**, 6043 (2015).

20. Arite, T. *et al.* d14, a Strigolactone-Insensitive Mutant of Rice, Shows an Accelerated Outgrowth of Tillers. *Plant Cell Physiol.* **50**, 1416–1424 (2009).

21. Nelson, D. C. *et al.* F-box protein MAX2 has dual roles in karrikin and strigolactone signaling in Arabidopsis thaliana. *Proc. Natl. Acad. Sci. U. S. A.* **108**, 8897–902 (2011).

22. Soundappan, I. *et al.* SMAX1-LIKE/D53 Family Members Enable Distinct MAX2-Dependent Responses to Strigolactones and Karrikins in Arabidopsis. *Plant Cell* **27**, 3143–59 (2015).

23. Jiang, L. *et al.* DWARF 53 acts as a repressor of strigolactone signalling in rice. *Nature* **504**, 401–405 (2013).

24. Zhou, F. *et al.* D14-SCF(D3)-dependent degradation of D53 regulates strigolactone signalling. *Nature* **504**, 406–10 (2013).

25. Wang, L. *et al.* Strigolactone Signaling in Arabidopsis Regulates Shoot Development by Targeting D53-Like SMXL Repressor Proteins for Ubiquitination and Degradation. *Plant Cell* **27**, 3128–42 (2015).

26. Samodelov, S. L. *et al.* StrigoQuant: A genetically encoded biosensor for quantifying strigolactone activity and specificity. *Sci. Adv.* **2**, e1601266 (2016).

27. Samodelov, S. L. *et al.* StrigoQuant: A genetically encoded biosensor for quantifying strigolactone activity and specificity. *Sci. Adv.* **2**, e1601266–e1601266 (2016).

28. Waters, M. T., Scaffidi, A., Flematti, G. & Smith, S. M. Substrate-Induced Degradation of the α/β-Fold Hydrolase KARRIKIN INSENSITIVE2 Requires a Functional Catalytic Triad but Is Independent of MAX2. *Mol. Plant* **8**, 814–817 (2015).

29. Chevalier, F. *et al.* Strigolactone promotes degradation of DWARF14, an α/β hydrolase essential for strigolactone signaling in Arabidopsis. *Plant Cell* **26**, 1134–50 (2014).

30. Hu, Q. *et al.* DWARF14, A Receptor Covalently Linked with the Active Form of Strigolactones, Undergoes Strigolactone-Dependent Degradation in Rice. *Front. Plant Sci.* **8**, 1935 (2017).

31. Yao, R. *et al.* DWARF14 is a non-canonical hormone receptor for strigolactone. *Nature* **536**, 469–473 (2016).

32. Yan, J. *et al.* The Arabidopsis F-Box Protein CORONATINE INSENSITIVE1 Is Stabilized by SCFCOI1 and Degraded via the 26S Proteasome Pathway. *Plant Cell* **25**, 486–498 (2013).

33. Kong, L. *et al.* Degradation of the ABA co-receptor ABI1 by PUB12/13 U-box E3 ligases. *Nat. Commun.* **6**, 8630 (2015).

34. Legris, M., Nieto, C., Sellaro, R., Prat, S. & Casal, J. J. Perception and signalling of light and temperature cues in plants. *Plant J.* **90**, 683–697 (2017).

35. Santner, A., Calderon-Villalobos, L. I. A. & Estelle, M. Plant hormones are versatile chemical regulators of plant growth. *Nat. Chem. Biol.* **5**, 301–307 (2009).

36. Beyer, H. M. *et al.* AQUA Cloning: A Versatile and Simple Enzyme-Free Cloning Approach. *PLoS One* **10**, e0137652 (2015).

StrigoQuant dynamic analyses reveal new insights on strigolactone signaling

Jennifer Andres[1*], Nima Saadat[2*], Oliver Ebenhöh[2], Matias D. Zurbriggen[1#]

[1] Institute of Synthetic Biology, University of Düsseldorf and CEPLAS, Düsseldorf, Germany

[2] Institute of Quantitative and Theoretical Biology, University of Düsseldorf and CEPLAS, Düsseldorf, Germany

[*] contributed equally to this work

[#] Corresponding author: Email: Matias.Zurbriggen@uni-duesseldorf.de, Oliver.Ebenhöh@uni-duesseldorf.de

SUPPLEMENTARY INFORMATION

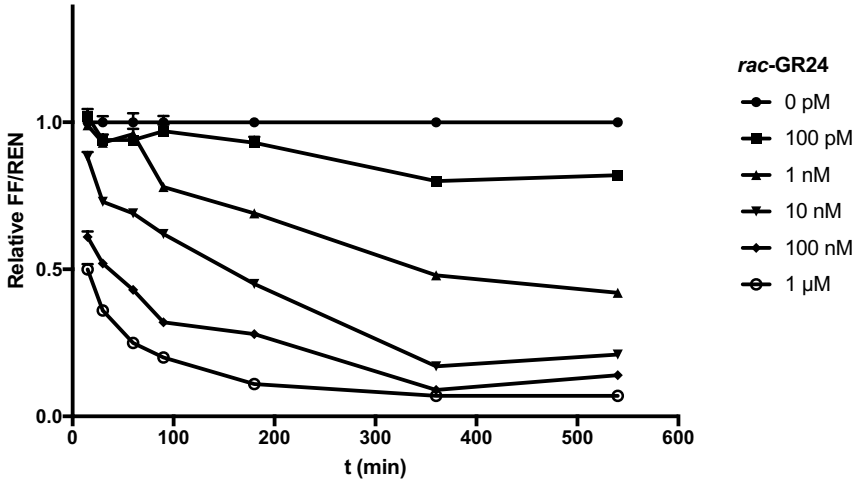

Fig. S1: StrigoQuant kinetics upon induction with *rac*-GR24. *Arabidopsis thaliana* protoplasts were transformed with the StrigoQuant Sensor construct and induced with *rac*-GR24 20 h after transformation. Luciferase activity was determined 15 min, 30 min, 60 min, 90 min, 180 min, 360 min and 540 min after hormone induction. The results are FF/REN ratios normalized to the sample without *rac*-GR24 addition. The error bars represent the standard error of the mean (SEM; *n*=6).

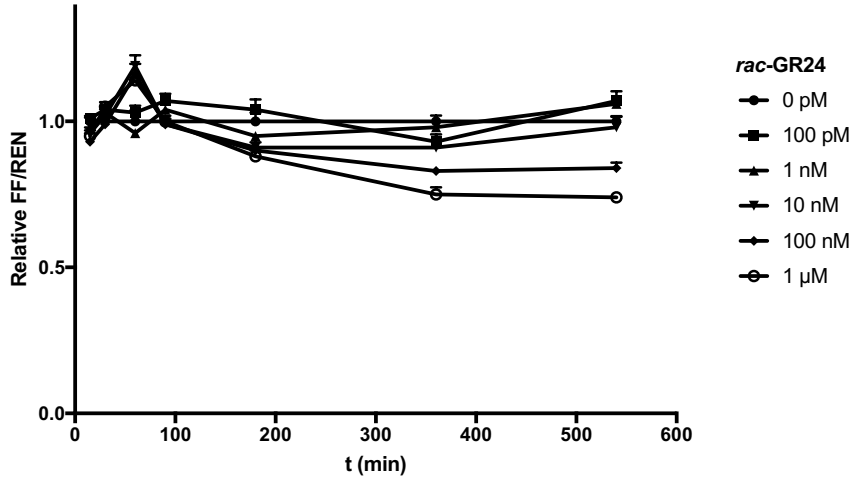

Fig. S2: D14-receptor kinetics upon induction with *rac*-GR24. *Arabidopsis thaliana* protoplasts were transformed with the D14-receptor construct and induced with *rac*-GR24 20 h after transformation. Luciferase activity was determined 15 min, 30 min, 60 min, 90 min, 180 min, 360 min and 540 min after hormone induction. The results are FF/REN ratios normalized to the sample without *rac*-GR24 addition. The error bars represent the standard error of the mean (SEM; *n*=6).

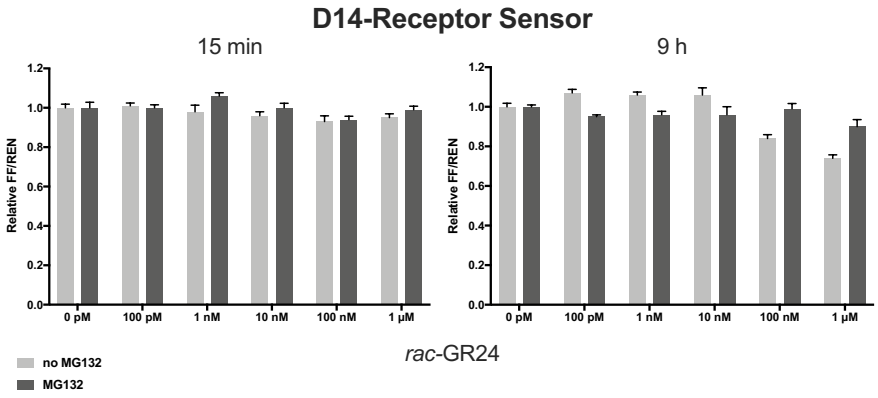

Fig. S3: SL-dependent degradation of the D14-Receptor sensor component is mediated by the 26S proteasome. *Arabidopsis thaliana* wildtype protoplasts were transformed with the D-14 receptor sensor construct and treated with 40 µM proteasomal inhibitor MG132 20h after transformation and 2h prior to *rac*-GR24 induction. Luciferase activity was determined after 15 min and 9h. The results are FF/REN ratios normalized to the sample without *rac*-GR24 addition. The error bars represent the standard error of the mean (SEM; *n*=6).

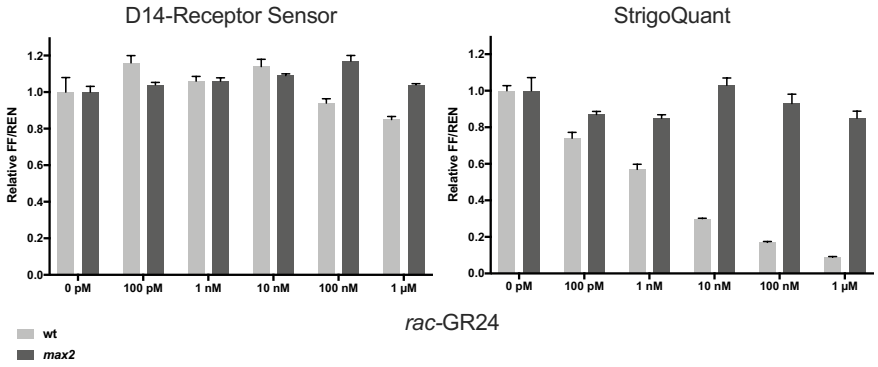

Fig. S4: SL-dependent degradation of the D14-Receptor and the StrigoQuant Sensor components is mediated by the F-Box MAX2. *Arabidopsis thaliana* wildtype and *max2* mutant protoplasts were transformed with either the D14-receptor sensor construct or the StrigoQuant Sensor. 20h after transformation, the samples were induced with *rac*-GR24 and after 9h, the luciferase activity was determined. The results are FF/REN ratios normalized to the sample without *rac*-GR24. The error bars represent the standard error of the mean (SEM; *n*=6).

table S1: Amino acid sequences of the components of the StrigoQuant, CtrlQuant and D14-Receptor Sensors.

Renilla Luciferase	MTSKVYDPEQRKRMITGPQWWARCKQMNVLDSFINYYDSEKHAENAVIFLHGN AASSYLWRHVVPHIEPVARCIIPDLIGMGKSGKSGNGSYRLLDHYKYLTAWFELL NLPKKIIFVGHDWGACLAFHYSYEHQDKIKAIVHAESVVDVIESWDEWPDIEEDIA LIKSEEGEKMVLENNFFVETMPSKIMRKLEPEEFAAYLEPFKEKGEVRRPTLSWP REIPLVKGGKPDVVQIVRNYNAYLRASDDLPKMFIESDPGFFSNAIVEGAKKFPN TEFVKVKGLHFSQEDAPDEMGKYIKSFVERVLKNEQ	
2A peptide	VKQLLNFDLLKLAGDVESNPGP	
Sensor Module	**StrigoQuant**	MPTPVTTARECLTEEAARALDDAVVVARRRSHAQTTSLHAVSA LLAMPSSILREVCVSRAARSVPYSSRLQFRALELCVGVSLDRLP SSKSPATEEDPPVSNSLMAAIKRSQANQRRHPESYHLQQIHAS NNGGGGCQTTVLKVELKYFILSILDDPIVNRVFGEAGFRSSEIKL DVLHPPVTQLSSRFSRGRCPPLFLCNLPNSDPNREFPFSGSSG FDENSRRIGEVLGRKDKKNPLLIGNCANEALKTFTDSINSGKLGF LQMDISGLSLISIEKEISEILADGSKNEEEIRMKVDDLGRTVEQSG SKSGIVLNLGELKVLTSEANAALEILVSKLSDLLKHESKQLSFIGC VSSNETYTKLIDRFPTIEKDWDLHVLPITASTKPSTQGVYPKSSL MGSFVPFGGFFSSTSNFRVPLSSTVNQTLSRCHLCNEKYLQEV AAVLKAGSSLSLADKCSEKLAPWLRAIETKEDKGITGSSKALDD ANTSASQTAALQKKWDNICQSIHHTPAFPKLGFQSVSPQFPVQT EKSVRTPTSYLETPKLLNPPISKPKPMEDLTASVTNRTVSLPLSC VTTDFGLGVIYASKNQESKTTREKPMLVTLNSSLEHTYQKDFKS LREILSRKVAWQTEAVNAISQIICGCKTDSTRRNQASGIWLALLG PDKVGKKKVAMTLSEVFFGGKVNYICVDFGAEHCSLDDKFRGK TVVDYVTGELSRKPHSVVLLENVEKAEFPDQMRLSEAVSTGKIR DLHGRVISMKNVIVVVTSGIAKDNATDHVIKPVKFPEEQVLSARS WKLQIKLGDATKFGVNKRKYELETAQRAVKVQRSYLDLNLPVN ETEFSPDHEAEDRDAWFDEFIEKVDGKVTFKPVDFDELAKNIQE KIGSHFERCFGSETHLELDKEVILQILAASWSSLSSGEEEGRTIV DQWMQTVLARSFAEAKQKYGSNPMLGVKLVASSSGLASGVEL PAKVDVIW
	CtrlQuant	GAGAGAGAGAGAGA
	D14-Receptor	MSQHNILEALNVRVVGTGDRILFLAHGFGTDQSAWHLILPYFTQ NYRVVLYDLVCAGSVNPDYFDFNRYTTLDPYVDDLLNIVDSLGI QNCAYVGHSVSAMIGIIASIRRPELFSKLILIGFSPRFLNDEDYHG GFEEGEIEKVFSAMEANYEAWVHGFAPLAVGADVPAAVREFSR TLFNMRPDISLFVSRTVFNSDLRGVLGLVRVPTCVIQTAKDVSVP ASVAEYLRSHLGGDTTVETLKTEGHLPQLSAPAQLAQFLRRALP R
Firefly Luciferase	MEDAKNIKKGPAPFYPLEDGTAGEQLHKAMKRYALVPGTIAFTDAHIEVDITYAE YFEMSVRLAEAMKRYGLNTNHRIVVCSENSLQFFMPVLGALFIGVAVAPANDIYN ERELLNSMGISQPTVVFVSKKGLQKILNVQKKLPIIQKIIIMDSKTDYQGFQSMYTF VTSHLPPGFNEYDFVPESFDRDKTIALIMNSSGSTGLPKGVALPHRTACVRFSHA RDPIFGNQIIPDTAILSVVPFHHGFGMFTTLGYLICGFRVVLMYRFEEELFLRSLQ DYKIQSALLVPTLFSFFAKSTLIDKYDLSNLHEIASGGAPLSKEVGEAVAKRFHLP GIRQGYGLTETTSAILITPEGDDKPGAVGKVVPFFEAKVVDLDTGKTLGVNQRGE LCVRGPMIMSGYVNNPEATNALIDKDGWLHSGDIAYWDEDEHFFIVDRLKSLIKY KGYQVAPAELESILLQHPNIFDAGVAGLPDDDAGELPAAVVVLEHGKTMTEKEIV DYVASQVTTAKKLRGGVVFVDEVPKGLTGKLDARKIREILIKAKKGGKIAV	

54 **table S2: Oligonucleotides used for the cloning of the sensor constructs.**

Oligonucleotide	Sequence (5´->3´)
oJA237	TGGCCGGCGACGTGGAATCAAATCCTGGACCCATGAGTCAACACAACATCTTAGAAG
oJA238	GGCCTTTCTTTATGTTTTTGGCGTCTTCCATGCTAGCCCGAGGAAGAGCTCG
oPF074	ATGGAAGACGCCAAAAACATAAAGAAAGGCC
oPF075	GGGTCCAGGATTTGATTCCACGTCG

55

7.3 Genetically encoded biosensors for the quantitative analysis of auxin dynamics

Genetically encoded biosensors for the quantitative analysis of auxin dynamics

Jennifer Andres[1] and Matias D. Zurbriggen[1]

[1]Institute of Synthetic Biology and CEPLAS, University of Düsseldorf, Germany

[#]**Corresponding author:** MDZ matias.zurbriggen@uni-duesseldorf.de

Abstract

Plants, as sessile organisms, possess complex and intertwined signaling networks to react and adapt their behavior towards different internal and external stimuli. Due to this high level of complexity, the implementation of quantitative tools *in planta* remains challenging. Synthetic biology as an ever-growing interdisciplinary field applies basic engineering principles in life sciences. A plethora of synthetic switches, circuits and even higher order networks has been implemented in different organisms, such as bacteria and mammalian cells, and facilitates the study of signaling and metabolic pathways. However, the application of such tools in plants lags behind and thus only a few tools have been engineered towards the quantitative investigation of plant signaling. Here, we present a protocol for the quantitative analysis of auxin signaling in *Arabidopsis thaliana* protoplasts. We implemented genetically encoded, ratiometric, degradation-based luminescent biosensors and applied them for studying auxin perception dynamics. For this, we utilized three different Aux/IAAs as sensor modules and analyzed their degradation behavior in response to auxin. Our experimental approach requires simple hardware and experimental reagents and can thus be implemented in every plant-related or cell culture laboratory. The system allows for the analysis of auxin perception and signaling aspects on various levels, and can be easily expanded to other hormones, as for example strigolactones. In addition, the modular sensor design enables the implementation of sensor modules in a straight-forward and time-saving approach.

Key Words: synthetic biology tools, quantitative biosensor, auxin, protoplasts

1 Introduction

Due to a high interconnectivity and redundancy of signaling components, especially the implementation of synthetic biology tools, as they are already designed and implemented in bacteria, yeast and mammalian cells, lags behind *in planta* (Jensen and Keasling, 2014; Samodelov and Zurbriggen, 2017; Liu et al., 2018; Xie and Fussenegger, 2018). For instance, the quantitative analysis of hormone dynamics and signaling *in vivo* is particularly difficult. Methods commonly utilized, such as mass spectrometry, require the plant tissue disruption and thereby prevent dynamic analyses to quantify phytohormone levels (Okamoto et al., 2009; Urbanová et al., 2013). These experimental limitations are overcome with biosensors which can produce quantifiable readouts. First biosensors for the quantification of phytohormone levels *in vivo* have been developed such as Förster Resonance Energy Transfer (FRET) biosensors, DII-Venus auxin sensor or hormone-activated Cas9-based repressors (HACR) *in planta* (Brunoud et al., 2012; Jones et al., 2014; Rizza et al., 2017; Khakhar et al., 2018). To quantitatively monitor phytohormone signaling networks as well as signaling perception and mechanisms and their dynamics at physiologically relevant concentrations (up to fM level), luminescent biosensors have recently been developed as molecular proxies for different phytohormones (Wend et al., 2013; Samodelov et al., 2016).

Here, we present a protocol for the quantitative analysis of *in vivo* phytohormone dynamics in plant cells. We show its applicability in a proof of principle application for the investigation of the sensitivity of three auxin regulators (Aux/IAAs) with distinct auxin degrons towards auxin. In addition, the system is cost-effective, easily customizable and can be scaled up in a mid- to high-throughput set up.

Molecular biosensor design

To quantitatively monitor phytohormone dynamics, genetically encoded biosensors for the use in plant cells have recently been developed (Wend et al., 2013; Samodelov et al., 2016). These ratiometric, luminescent and degradation-based biosensors allow for *in vivo* phytohormone analysis with several applications in protoplasts. The biosensors are based on the similar natural mechanisms used by plants to perceive the phytohormones auxin, jasmonate, strigolactone and gibberellin. Namely, those hormones are detected through either directly by an F-Box receptor protein or via an additional co-receptor. Recognition of the hormone leads to the formation of a perception complex between the F-Box being part of an SCF complex [Skp (Arabidopsis SKP1-related (ASK1))-1-Cullin-F-box (SCF) E3 ubiquitin ligase complex], the optional co-receptor and a specific regulator protein. As a consequence, the regulator proteins are polyubiquitinated by the SCF-complex and thereby targeted for degradation by the 26S proteasome (Santner et al., 2009) (Figure 1A). In the case of auxin, the components of the signaling network are i) TIR1/AFB F-box proteins (TRANSPORT INHIBITOR

RESISTANT1/AUXIN SIGNALING F-BOX) engaged in a SCF protein complex ii) Aux/IAA (AUXIN/INDOLE ACETIC ACID) transcriptional regulators and iii) ARF (AUXIN RESPONSE FACTOR) transcription factors (Salehin et al., 2015) (Figure 1B).The phytohormone regulator proteins (AUX/IAAs) physically interact with transcriptional factors (ARFs) and factors of the signaling response, oftentimes exerting a negative effect on their activity. Upon their hormone-induced degradation the target gene expression is de-regulated. The biosensors harness this degradation-based signaling mechanism and incorporate the AUX/IAA regulator proteins (or sequences/domains thereof) as sensor modules. A renilla luciferase is utilized as a normalization element connected via a 2A peptide to the sensor module fused to a firefly luciferase. The 2A peptide allows for the stoichiometric co-expression of the renilla luciferase and the sensor module firefly fusion by autocatalytic cleavage of the nascent polypeptide chain during translation. In this work, we show the applicability of this biosensor system for the comparative investigation of three auxin regulator proteins, Aux/IAA17, 31 and 34, with differential auxin degron versions being responsible for the binding to the F-Box TIR1 and their degradation in response to auxin treatment. For this, the three Aux/IAAs were cloned as sensor modules in the biosensor platforms and *Arabidopsis thaliana* protoplasts were transformed with them (Figure 1C).

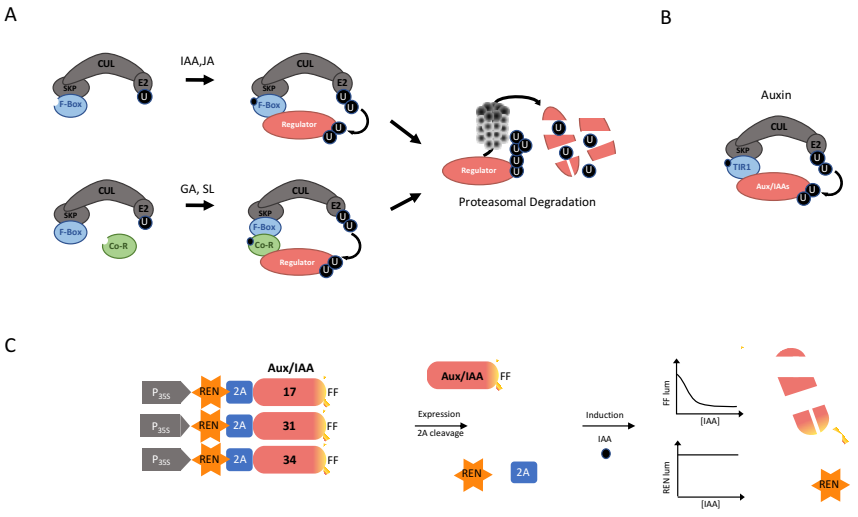

Figure 1: Phytohormone perception mechanism and biosensor design. (A) Phytohormone perception mechanism for auxin, jasmonate, gibberellin and strigolactone. Auxins and jasmonates are perceived by an F-Box protein which engages in an SCF complex comprising SKP/ASK (rice/Arabidopsis), Cullin (CUL), and an E3 ubiquitin ligase [an E2 ubiquitin-conjugating enzyme loaded with ubiquitin residues (U)]. As a consequence of hormone perception, specific regulator proteins (AUXIN/INDOLE ACETIC ACID (Aux/IAAs) proteins for auxin and JASMONATE-ZIM-DOMAIN (JAZ) proteins for jasmonate signaling) associate to the complex and become polyubiquitinated and thereby targeted for degradation by the 26S proteasome. Gibberellin and strigolactone are perceived by a co-receptor (GIBBERELLIN INSENSITIVE DWARF1a,b and c (GID1a, b and c) and DWARF14 (D14), respectively) that associates to the $SCF^{F\text{-}Box}$ complex and a specific regulator protein (DELLA proteins for Gibberellin perception and SMXL proteins for strigolactone perception) which becomes polyubiquitinated and

degraded by the 26S proteasome. (B) Auxin perception. Auxin is perceived by TIR1 (or its homologs). Aux/IAA regulators associate to this complex and become polyubiquitinated and degraded by the 26S proteasome. (C) Biosensor design. A renilla luciferase (REN) is connected via a 2A peptide with an Aux/IAA sensor module fused to a firefly (FF) luciferase. The 2A peptide leads to the stoichiometric co-expression (by autocatalytic co-translational cleavage) of the renilla luciferase, as a normalization element, and the Aux/IAA-FF fusion. Upon hormone induction, the Aux/IAA-FF becomes polyubiquitinated and degraded by the 26S proteasome whereas REN expression remains constant resulting in a decrease in FF/REN ratio.

Application of the system

The genetically-encoded quantitative, luminescent and degradation-based biosensors show a high selectivity and sensitivity as well as high signal-to-noise ratios. These characteristics can be applied for phytohormone analyses on various levels such as phytohormone perception complex formation as well as downstream signaling levels. In addition, mutant protoplast can be utilized to quantitatively analyze the biosynthesis of phytohormones as well as other metabolic aspects such as their inactivation. This highly sensitive system allows the co-expression of for example putative transporters or enzymes. We have previously shown the establishment of short versions of Aux/IAA 17 only containing the core region of domain II to investigate the sensitivity towards IAA and NAA as well as transporter activities (Wend et al., 2013).

Here, we demonstrate the applicability of the biosensor platform to perform comparative, dynamic analyses of full-length Aux/IAAs.

Experimental design

In this protocol, *Arabidopsis* mesophyllic protoplasts were isolated and transformed with three different Aux/IAA-based biosensors (Aux/IAA 17, 31 and 34) and induced 20 h later with an IAA serial dilution (concentrations ranging from 100 pM to 1 µM). Luminescence was determined simultaneously in two microplate readers for firefly luciferase as a reporter, and renilla luciferase as a normalization element. Hormone induction and the subsequent measurements were performed with six replicates per hormone concentration. The determined values were evaluated by calculating the average for every replicate. Next, the FF/REN value for every replicate is determined and the average for the six replicates is calculated. In addition, the standard error of the mean is calculated.

2 Materials

2.1 Reagents, consumables and kits

2.1.1 DNA and plant material preparation

1) Plasmids cloned via AQUA cloning (Fig. 1 and Tab. 1):
    a. pPF105: P_{35S}-Renilla-2A-IAA34-Firefly-myc-pA
    b. pPF118: P_{35S}-Renilla-2A-IAA17-Firefly-myc-pA
    c. pPF126: P_{35S}-Renilla-2A-IAA31-Firefly-myc-pA
2) Ampicillin (Roth, cat. no. K029.2, stock solution 100 mg/ml)
3) Petri dish, plastic, 94 x 16 mm (Sarstedt, cat. no. 82.1473)
4) Scalpel
5) Filter paper (Macherey-Nagel, MN615)
6) Square, plastic petri dish (Greiner Bio-One, cat. no. 688102)
7) Calcium hypochlorite (Roth, cat. no. 5164)
8) Triton X-100 (Applichem, A1388)
9) Gamborg B5 basal salt powder with vitamins (bioWORLD, cat. no. 30630029)
10) $MgSO_4 \cdot 7H_2O$ (Applichem, cat. no. 131404)
11) Sucrose (Merck, cat. no. 573113)
12) Gamborg B5 Vitamin Mix (bioWORLD, cat. no. 30630027)
13) Phytoagar (Plantmedia, cat. no. 40100072)
14) Parafilm

Table 1: Amino acid sequences of the components of the StrigoQuant, CtrlQuant and D14-Receptor Sensors.

Renilla Luciferase	MTSKVYDPEQRKRMITGPQWWARCKQMNVLDSFINYYDSEKHAENAVIFLHGN AASSYLWRHVVPHIEPVARCIIPDLIGMGKSGKSGNGSYRLLDHYKYLTAWFELL NLPKKIIFVGHDWGACLAFHYSYEHQDKIKAIVHAESVVDVIESWDEWPDIEEDIA LIKSEEGEKMVLENNFFVETMPSKIMRKLEPEEFAAYLEPFKEKGEVRRPTLSWP REIPLVKGGKPDVVQIVRNYNAYLRASDDLPKMFIESDPGFFSNAIVEGAKKFPN TEFVKVKGLHFSQEDAPDEMGKYIKSFVERVLKNEQ	
2A peptide	VKQLLNFDLLKLAGDVESNPGP	
Sensor Module	**IAA34**	MYCSDPPHPLHLVASDKQQKDHKLILSWKKPTMDSDPLGVFPN SPKYHPYYSQTTEFGGVIDLGLSLRTIQHEIYHSSGQRYCSNEG YRRKWGYVKVTMDGLVVGRKVCVLDHGSYSTLAHQLEDMFGM QSVSGLRLFQMESEFCLVYRDEEGLWRNAGDVPWNEFIESVE RLRITRRNDAVLPF
	IAA17	MMGSVELNLRETELCLGLPGGDTVAPVTGNKRGFSETVDLKLN LNNEPANKEGSTTHDVVTFDSKEKSACPKDPAKPPAKAQVVG WPPVRSYRKNVMVSCQKSSGGPEAAAFVKVSMDGAPYLRKID LRMYKSYDELSNALSNMFSSFTMGKHGGEEGMIDFMNERKLM DLVNSWDYVPSYEDKDGDWMLVGDVPWPMFVDTCKRLRLMK GSDAIGLAPRAMEKCKSRA
	IAA31	MEVSNSCSSFSSSSVDSTKPSPSESSVNLSLSLTFPSTSPQREA RQDWPPIKSRLRDTLKGRRLLRRGDDTSLFVKVYMEGVPIGRK LDLCVFSGYESLLENLSHMFDTSIICGNRDRKHHVLTYEDKDGD WMMVGDIPWDMFLETVRRLKITRPERY

Firefly Luciferase	MEDAKNIKKGPAPFYPLEDGTAGEQLHKAMKRYALVPGTIAFTDAHIEVDITYAE YFEMSVRLAEAMKRYGLNTNHRIVVCSENSLQFFMPVLGALFIGVAVAPANDIYN ERELLNSMGISQPTVVFVSKKGLQKILNVQKKLPIIQKIIIMDSKTDYQGFQSMYTF VTSHLPPGFNEYDFVPESFDRDKTIALIMNSSGSTGLPKGVALPHRTACVRFSHA RDPIFGNQIIPDTAILSVVPFHHGFGMFTTLGYLICGFRVVLMYRFEEELFLRSLQ DYKIQSALLVPTLFSFFAKSTLIDKYDLSNLHEIASGGAPLSKEVGEAVAKRFHLP GIRQGYGLTETTSAILITPEGDDKPGAVGKVVPFFEAKVVDLDTGKTLGVNQRGE LCVRGPMIMSGYVNNPEATNALIDKDGWLHSGDIAYWDEDEHFFIVDRLKSLIKY KGYQVAPAELESILLQHPNIFDAGVAGLPDDDAGELPAAVVVLEHGKTMTEKEIV DYVASQVTTAKKLRGGVVFVDEVPKGLTGKLDARKIREILIKAKKGGKIAV

152

153 **2.1.2 Protoplast isolation and transformation**

154 1) MES monohydrate (Roth, cat. no. 6066)
155 2) $CaCl_2 \cdot 2H_2O$ (Acros organics, CAS: 10035-04-8)
156 3) D-Mannitol (Sigma-Aldrich, cat. no. M1902)
157 4) Cellulase “Onozuka” R10 (SERVA, cat no. 16419)
158 5) Macerozyme R10 (SERVA, cat. no. 28302)
159 6) PEG4000 (Sigma Aldrich, cat. no. 202398)
160 7) L-glutamine (Carbolution, CC10066)
161 8) Calcium-D(+)-pantothenate (Roth, cat. no. 3812)
162 9) Biotin (Sigma-Aldrich, B4501)
163 10) 70 µM pore size sieve (Greiner bio-one, cat. no. 542070)
164 11) Round bottom 15 ml reaction tubes (Greiner bio-one, cat. no. 186171)
165 12) Conic 50 ml reaction tubes (Sarstedt, cat. no. 62.547.254)
166 13) 200 µl and 1 ml large orifice pipette tips
167 14) Nontreated 6 well plates (Sarstedt, cat. no. 83.3920.005)

168

169 **2.1.3 Hormone induction and luminescence determination**

170 1) Indole-3-acetic acid (IAA, Olchemim, cat. no. 0031531)
171 2) 96 deep well storage plate (Sigma-Aldrich, cat. no. Z717274)
172 3) White 96-well assay plate (Corning, cat. no. CORN3912)
173 4) Coelenterazine (Roth, cat. no. 4094)
174 5) D-luciferin (Biosynth AG, cat. no. L-8230)
175 6) $EDTA \cdot 2H_2O$ (Acros organic, CAS: 6381-92-0)
176 7) 1,4-dithiothreitol (Roth, cat. no. 6908)
177 8) adenosine 5′-triphosphate (Sigma Aldrich, A2383)
178 9) acetyl-coenzyme A (Applichem, cat. no. A3753)
179 10) $MgCO_3 \cdot 5H_2O$ (Roth, cat. no. 3530)
180 11) NaOH (Applichem, CAS no. 1310-73)

181

2.2 Reagent setup

Use plant cell culture tested reagents for all solutions needed for plant material preparation and protoplast isolation/transformation. Store all reagents at 4 °C (unless indicated otherwise). The reagents are not autoclaved but sterilized by filtering!

2.2.1 SCA (seedling culture *Arabidopsis*) growth medium, (modified from Dovzhenko et al., 2003)

Dissolve 0.32% (w/v) Gamborg B5 basal salt powder with vitamins, 4 mM MgSO4·7H2O, 43.8 mM sucrose, 0.8% (w/v) phytoagar in ddH2O. Mix and adjust to pH 5.8 and afterwards autoclave. Add 0.1% (v/v) Gamborg B5 Vitamin Mix and 1:2,000 ampicillin and pour 50 ml in each 12 cm^2 plate.

2.2.2 Seed sterilization solution (modified from Luo and Koop, 1997)

Dissolve 5% (w/v) calcium hypochlorite and 0.02% (v/v) Triton X-100 in 80% (v/v) ethanol solution in a bottle, and mix it for some hours. Store the solution at 4°C. Let the formed precipitate settle and do not agitate the bottle before usage.

2.2.3 MMC (MES, Mannitol, Calcium) (Dovzhenko et al., 2003)

Dissolve 10 mM MES, 40 mM $CaCl2{\cdot}H_2O$ in ddH_2O and add mannitol until 550 mOsm is obtained. Adjust to pH 5.8 and filter sterilize the MMC.

2.2.4 Cellulase and Macerozyme stock solution

Mix 5 % cellulase Onozuka R10 and 5% macerozyme R10 in MMC. Sterilize by filtering the cellulose/macerozyme mix and make 2 ml aliquots. Store them at - 20°C.

2.2.5 MSC (MES, Sucrose, Calcium) (Dovzhenko et al., 2003)

Dissolve 10 mM MES, 0.4 M sucrose, 20 mM MgCl2·6H2O in ddH2O and supplement mannitol until an osmolarity of 550 mOsm is obtained. Adjust to pH 5.8 and sterilize by filtering the MSC.

2.2.6 MMM (MES, Mannitol, Magnesium) (Dovzhenko et al., 2003)

Dissolve 15 mM MgCl2, 5 mM MES and 550 mOsm with mannitol (pH 5.8) in ddH2O. Sterile filter the MMM.

2.2.7 W5

Dissolve 2 mM MES, 154 mM NaCl, 125 mM CaCl2·2H2O, 5 mM KCl and 5 mM glucose (pH 5.8) in ddH2O. Sterilize the W5 medium by filtering.

2.2.8 Polyethylene glycol (PEG) solution

Mix 2.5 ml of 0.8 M mannitol, 1ml of 1M$CaCl_2$, 4 g of PEG_{4000}, and 3 ml of ddH2O. The PEG solution has to be prepared fresh for every experiment. Place the tube at 37°C for PEG dissolution.

2.2.9 PCA (Protoplast Culture *Arabidopsis*) (modified from Dovzhenko et al., 2003)

Mix 0.32% (w/v) Gamborg B5 basal salt powder with vitamins, 2 mM $MgSO_4 \cdot 7H_2O$, 3.4 mM $CaCl_2 \cdot 2H_2O$, 5 mM MES, 0.342 mM L-glutamine, 58.4 mM sucrose, glucose 550 mOsm, 8.4 mM Ca-pantothenate, 2% (v/v) biotin from a biotin solution of 0.02% (w/v) in ddH2O, 0.1% (v/v) Gamborg B5 Vitamin Mix, and 1:2,000 ampicillin (100 mg/ml stock solution). Adjust to pH 5.8 and filter sterilize the PCA.

2.2.10 PBS

Dissolve 26.82 mM KCl, 14.7 mM KH_2PO_4, 80.34 mM $Na_2HPO_4 \cdot 2H_2O$ and 1.37 M NaCl in ddH_2O. Dilute the PBS to 1x, filter sterilize it.

2.2.11 Coelenterazine

Dissolve 472 mM coelenterazine stock solution in pre-cooled methanol and prepare 100 µl aliquots in pre-cooled, black 1.5 ml reaction tubes and freeze them at -80 °C. Dilute it directly before use, 1:15 in PBS.

2.2.12 Firefly substrate

Mix the reagents in the following order: 20 mM tricine, 2.67 mM $MgSO_4 \cdot 7H_2O$, 0.1 mM $EDTA \cdot 2H_2O$, 33.3 mM dithiothreitol, 0.52 mM adenosine 5′-triphosphate, 0.27 mM acetyl–coenzyme A, 0.47 mM D-luciferin, 5 mM NaOH and 264 mM $MgCO_3 \cdot 5H_2O$ in ddH_2O in a beaker. Adjust to pH 8 and aliquot the firefly substrate in pre-cooled, black 15 ml reaction tubes and freeze them at -80 °C.

2.3 Equipment

1) Biological safety cabinet (Thermo Scientific, HeraSafe S2020 1.8 cat. no. 104222784)
2) Plant growth chamber (Sanyo/Panasonic MLR-352-PE)
3) Fuchs-Rosenthal cell-counting chamber (Brand, cat. no. 719805)
4) Microplate reader (Berthold, Tristar^2 S LB 942 multimode plate reader and Centro XS^3 LB 960 microplate luminometer)
5) Multipette® M4 (Eppendorf, cat. no. 4982000012)
6) Multichannel pipette (Eppendorf Xplorer ®, cat. no. 4861000163)
7) Centrifuge (Eppendorf 5702, cat. no. 5702000010)

3 Methods

3.1 Plant material preparation • estimated duration: 0.5 h in the morning and 0.5 h in the afternoon (depending on the amount of plant material)

Seed sterilization should be made in a sterile working hood.

1) Place *A. thaliana* seeds in a 1.5 ml reaction tube (the 0.5 ml mark should not be exceeded) and rinse with 1 ml of 80% EtOH until all visible dirt is removed. Surface sterilize the seeds with 1 ml of sterilization solution for 10 min (either invert or vortex them). Remove the solution and wash the seeds twice with 1 ml 80% EtOH for 5 min and 2 min (under agitation). Finally, wash the seeds with 1 ml absolute EtOH for 1 min and remove all EtOH. Let them dry for some hours (approx. at least 4 h) until they are completely dry.
2) Prepare 12 cm^2 plates with 50 ml SCA growth medium. The plates do not need to be freshly prepared. Place two sterile filter paper stripes per plate. Add autoclaved water to the sterilized seeds and place them on the filter paper in a line (200-300 seeds/stripe) by pipetting. Seal the plates with parafilm. Finally, grow the seeds in a growth chamber with 16 h light/8 h dark regime and at 22 °C. After 2 weeks, harvest the plantlets for protoplast isolation.

.

3.2 Protoplast Isolation • estimated duration: 0.5 h – 1 h (day 1) and 3 – 3.5 h (day 2)

A. thaliana protoplast isolation via flotation and PEG-transformation are performed as described in (Dovzhenko et al., 2003) with some modifications. All pipetting steps should be done with wide open tips to prevent protoplast damage.

1) Dissect plant shoots with a sterile scalpel from the plates and cut them into small pieces in a 5 ml MMC containing petri dish.
2) Place the cut plant leaf material in another petri dish with a final volume of 10 ml MMC.
3) Supplement 1 ml 5% macerozyme + cellulase mix for the enzymatic digestion of the cut plant material. Seal the petri dish with parafilm.
4) Incubate the plant material in MMC overnight (approx. 16 h) in dark (e.g. wrapped in aluminum foil) at 22 °C in a growth chamber.
5) In the morning, homogenize the plant material by pipetting up and down with a 10 ml or 25 ml serological stripette to release the protoplasts. Filter the plant material through a 40 – 70 µM pore size sieve into a 50 ml reaction tube, and add up to 50 ml with MMC.

   NOTE: From now on work carefully and slowly. Protoplasts are fragile.
6) Sediment the protoplasts with a centrifugation step for 20 min at 100 *g*.

7) Afterwards, remove the supernatant and resuspend the pellet in 10 ml MSC. Transfer the suspension to a 15 ml round-bottom reaction tube and overlay it with 3 ml MMM.

NOTE: Pipette carefully and with a tip-in-tip technique to not mix MSC and MMM.

8) Isolation of protoplasts is performed via flotation in MSC solution. Therefore, centrifuge the samples for 10 min at 100 *g* and collect 1.5 ml of the protoplasts in the intermediate phase in 7 ml W5. Repeat this step and collect two more intermediate phases in one single W5 solution. Afterwards, determine the protoplast density with a Fuchs-Rosenthal cell-counting chamber.

3.3 Protoplast Transformation • estimated duration 1 h (day 2)

1) Prepare 20 µg of the biosensor construct adjusted with MMM solution to a total volume of 20 µl in the rim of a well of a six well plate culture plate.
2) Add 500,000 protoplasts in 100 µl MMM solution to the DNA, and gentle pipette up and down. Incubate for 5 min.
3) In the next step, add 120 µl of a PEG solution per well in a dropwise manner with a tip-in-tip technique and incubate for 8 – 9 min. Do not shake the plates.
4) Finally, supplement with 120 µl of MMM solution and immediately afterwards fill up to a total volume of 1.8 ml with PCA solution.

NOTE: Multiple transformation can be performed in parallel in this manner.

3.4 Hormone Induction • estimated duration 0.5 – 1 h and 2 – 6 h incubation time (day 3)

1) After approx. 20 h, pool the protoplasts in a round-bottom 15 ml reaction tube.
2) Pipette 960 µl aliquots of the protoplast suspension into the wells of a 2.2 ml deep-well storage plate for each concentration of IAA inducer substrate tested.
3) Prepare a serial dilution of IAA with a 11-fold concentration of the desired final experimental concentration in PCA solution. Add a volume of 96 µl to the 960 µl of protoplast suspension and carefully mix them by pipetting up and down.
4) Incubate for 2 h, 4 h and 6 h.

3.5 Luminescence Determination (day 3)

1) After hormone induction, transfer 80 µl per replicate (approx. 20,000 cells) of the (hormone-induced) protoplast suspensions in two separate white 96-well assay plates. Determination of firefly and renilla luminescence is performed in a simultaneous manner in two microplate readers.
2) Supplement either 20 µl of coelenterazine or firefly substrate, respectively.

3) Determine luminescence activities simultaneously in two microplate readers (20 min total measuring time with 0.1 s/well measuring time per well, per measuring round).

3.6 Statistical Analysis

1) Calculate the FF/REN ratio for every well, the average for all replicates and the the standard error of the mean (SEM).
2) Perform ordinary one-way ANOVAs and multiple comparisons (here performed with Prism 7 for Mac OS X)

4 Aux/IAAs show different sensitivities towards IAA

The above-described protocol was implemented to quantitatively analyze Aux/IAA stability in response to auxin. *A. thaliana* protoplasts were transformed with three different biosensor constructs, namely full-length Aux/IAA17 containing the full domain II core consensus sequence degron, Aux/IAA31 which comprises small deviations from this domain II core consensus sequence degron and Aux/IAA34 with large deviations from the core consensus sequence degron. The Aux/IAAs displayed different degradation behaviors in response to auxin treatment: i) Aux/IAA17 was already strongly degraded after 2 h, with no subsequent decrease after 4 h and 6 h, ii) Aux/IAA31 showed a slight decrease after 2 h (at high auxin concentrations), but a strong degradation (80 %) only after 4 h and 6 h and at high nM concentrations; and iii) Aux/IAA34 did not display any significant degradation at all. The results showed that the degradation responses of distinct Aux/IAAs depend on the composition of the DII domain. The high sensitivity and signal-to-noise ratio in protoplasts, as a plant system, allow for a comprehensive comparison of Aux/IAAs and open up new perspectives for auxin signaling analyses in a quantitative manner in a plant system such as in- and efflux-transporter activities, screening of molecules with auxin-like functions and metabolic analyses.

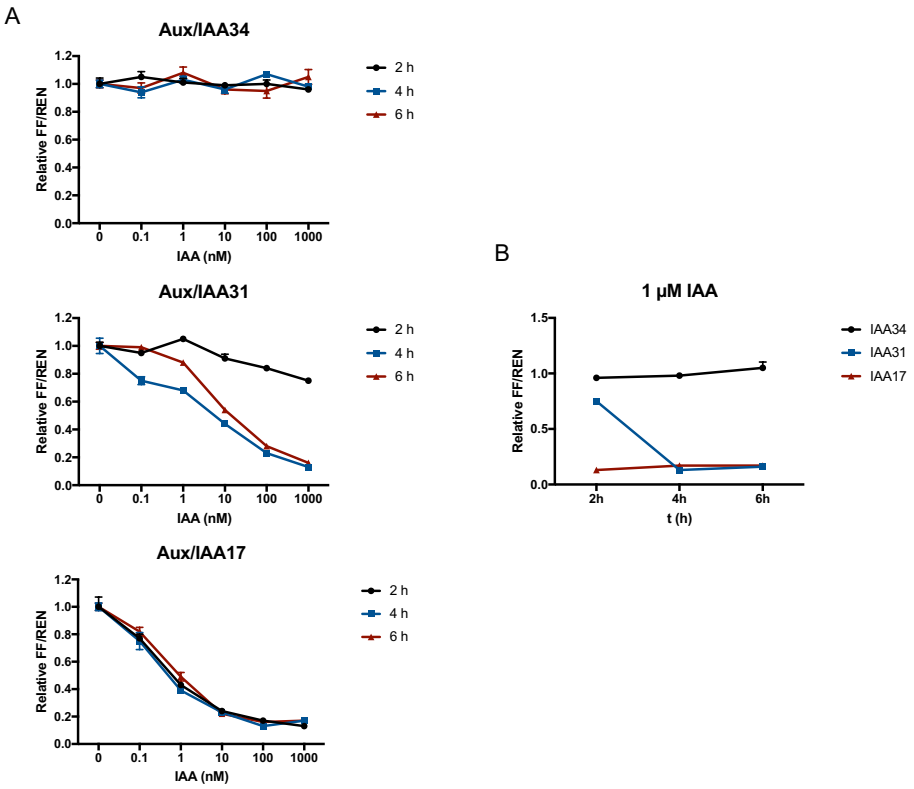

Figure 2: Sensitivity of auxin-induced degradation among three Aux/IAA family members. Biosensors incorporating Aux/IAA17, 31 and 34 as sensor modules were transiently expressed in *A. thaliana* mesenchymal protoplasts and 20 h post transformation induced with IAA (concentrations ranging from 100 pM to 1 µM) for 2 h, 4 h and 6 h. Firefly and renilla luciferase activities were determined and the averaged FF/REN ratios were calculated. The error bars represent the SEM for this individual experiment with *n*=6. (A) Degradation curves for Aux/IAA 17, 31 and 34 after 2 h, 4 h and 6 h IAA induction (concentrations ranging from 100 pM to 1 µM). (B) Degradation curves for Aux/IAA 17, 31 and 34 induced with 1 µM IAA for 2 h, 4 h and 6 h.

Notes

1) Work carefully and slowly in every step of the protoplast isolation and transformation to avoid damaging the protoplasts.
2) Prepare the SCA plates immediately after autoclaving, because the phytoagar does not dissolve after reheating.
3) The poorly soluble macerozyme and cellulase should not be inhaled. Work under a fume hood when preparing the enzyme solution and prewarm MMC.
4) Prepare tricine, DTT, ATP and acetyl-CoA freshly for the firefly substrate and work under a fume hood. The rest can be prepared in advance. D-luciferin is sensitive to light and heat. For these reasons, work in darkness and as fast as possible.
5) Prepare several 100 µl aliquots of the coelenterazine solved in methanol in darkness and at low temperatures (such as in a dark 4 °C room).
6) For a better separation of the phases, invert the tube before adding MMM on top of the MSC.
7) Protoplasts can be transformed with a maximum of 40 µg – 50 µg of total amounts of DNA. The total amount of DNA needs to be constant. When several plasmids are transformed, the amount of DNA needs to be adjusted proportionally.

Acknowledgements

We thank P.Fischbach, L. Koch and T. Blomeier for experimental support and fruitful discussions, and R. Wurm, M. Gerads and J. Müller for valuable experimental support.

Author contributions

JA and MDZ designed the system and performed the experiments, analyzed the data and wrote the protocol.

391 **References**

392 **Brunoud G, Wells DM, Oliva M, Larrieu A, Mirabet V, Burrow AH, Beeckman T,**
393 **Kepinski S, Traas J, Bennett MJ, et al** (2012) A novel sensor to map auxin response
394 and distribution at high spatio-temporal resolution. Nature **482**: 103–106
395 **Dovzhenko A, Dal Bosco C, Meurer J, Koop HU** (2003) Efficient regeneration from
396 cotyledon protoplasts in Arabidopsis thaliana. Protoplasma **222**: 107–111
397 **Jensen MK, Keasling JD** (2014) Recent applications of synthetic biology tools for yeast
398 metabolic engineering. FEMS Yeast Res **15**: n/a-n/a
399 **Jones AM, Danielson JÅ, ManojKumar SN, Lanquar V, Grossmann G, Frommer WB**
400 (2014) Abscisic acid dynamics in roots detected with genetically encoded FRET
401 sensors. Elife. doi: 10.7554/eLife.01741
402 **Khakhar A, Leydon AR, Lemmex AC, Klavins E, Nemhauser JL** (2018) Synthetic
403 hormone-responsive transcription factors can monitor and re-program plant
404 development. Elife. doi: 10.7554/eLife.34702
405 **Liu Z, Zhang J, Jin J, Geng Z, Qi Q, Liang Q** (2018) Programming Bacteria With Light-
406 Sensors and Applications in Synthetic Biology. Front Microbiol **9**: 2692
407 **Luo Y, Koop H-U** (1997) Somatic embryogenesis in cultured immature zygotic embryos and
408 leaf protoplasts of Arabidopsis thaliana ecotypes. Planta **202**: 387–396
409 **Okamoto M, Hanada A, Kamiya Y, Yamaguchi S, Nambara E** (2009) Measurement of
410 Abscisic Acid and Gibberellins by Gas Chromatography/Mass Spectrometry. Humana
411 Press, Totowa, NJ, pp 53–60
412 **Rizza A, Walia A, Lanquar V, Frommer WB, Jones AM** (2017) In vivo gibberellin gradients
413 visualized in rapidly elongating tissues. Nat Plants **3**: 803–813
414 **Salehin M, Bagchi R, Estelle M** (2015) SCFTIR1/AFB-based auxin perception: mechanism
415 and role in plant growth and development. Plant Cell **27**: 9–19
416 **Samodelov SL, Beyer HM, Guo X, Augustin M, Jia K-P, Baz L, Ebenhöh O, Beyer P,**
417 **Weber W, Al-Babili S, et al** (2016) StrigoQuant: A genetically encoded biosensor for
418 quantifying strigolactone activity and specificity. Sci Adv **2**: e1601266
419 **Samodelov SL, Zurbriggen MD** (2017) Quantitatively Understanding Plant Signaling: Novel
420 Theoretical–Experimental Approaches. Trends Plant Sci **22**: 685–704
421 **Santner A, Calderon-Villalobos LIA, Estelle M** (2009) Plant hormones are versatile
422 chemical regulators of plant growth. Nat Chem Biol **5**: 301–307
423 **Urbanová T, Tarkowská D, Novák O, Hedden P, Strnad M** (2013) Analysis of gibberellins
424 as free acids by ultra performance liquid chromatography–tandem mass spectrometry.
425 Talanta **112**: 85–94
426 **Wend S, Bosco CD, Kämpf MM, Ren F, Palme K, Weber W, Dovzhenko A, Zurbriggen**
427 **MD** (2013) A quantitative ratiometric sensor for time-resolved analysis of auxin

428 dynamics. Sci Rep **3**: 2052
429 **Xie M, Fussenegger M** (2018) Designing cell function: assembly of synthetic gene circuits
430 for cell biology applications. Nat Rev Mol Cell Biol **19**: 507–525
431